Functional Polymer Based Nanoparticles:

Development of Defined Complex Structures as Basis for *In Vitro* and *In Vivo* Applications

Dissertation zur Erlangung des Grades
„Doktor der Naturwissenschaften“
im Promotionsfach Chemie

am Fachbereich Chemie, Pharmazie und Geowissenschaften
der Johannes Gutenberg-Universität
in Mainz

Matthias Barz

geboren in Frankfurt am Main

Mainz, 2009

1. Berichterstatter:

2. Berichterstatter:

3. Berichterstatterin:

Datum der mündlichen Prüfung:

Erklärung

Hiermit versichere ich, dass ich die vorliegende Dissertation eigenständig verfasst und keine anderen als die angegebenen Hilfsmittel verwendet habe.

Die Dissertation habe ich weder als Arbeit für eine staatliche oder andere wissenschaftliche Prüfung eingereicht noch ist sie oder ein Teil dieser als Dissertation bei einer anderen Fakultät oder einem anderem Fachbereich eingereicht worden.

Mainz, Dezember 2009

This work is dedicated to my wonderful darling and my great parents.

Abstract

In this work a new synthesis pathway to a variety of functional polymeric architectures is described. The structures themselves are based on the clinical approved poly(N-(2-hydroxypropyl) methacrylamide) (PHPMA). In contrast to conventional systems the applied synthetic strategy is based on a combination of activated ester approach and reversible addition fragmentation chain transfer (RAFT) polymerization.

Furthermore, it was possible to use the RAFT polymerization method to create a new type of partially biodegradable block copolymer based on highly biocompatible polymeric blocks. In this respect, a well-defined polylactide was functionalized with a chain transfer agent (CTA) mediating the RAFT polymerization of the activated ester. Consequently, it was demonstrated that the reactive precursors were transferred into functional polymeric structures combining a targeting moiety (folate) and imaging agent (fluorescent dyes or β^+-emitters) enabling *in vitro* as well as *in vivo* investigations.

After all, these synthetic approaches have been applied to study the influence of polymer microstructure on aggregation using light scattering and fluorescence correlation spectroscopy. In conclusion, kinetics of cellular uptake are directly attributed to the aggregate properties. These findings underline the great importance of structure-property relationships, which have to be carefully considered in the development of polymer-based nanomedical devices.

In summary, in this work a new synthetic pathway to functional HPMA-based polymers was developed. This approach will allow the facile synthesis of various polymeric architectures. The concept can be considered as a promising tool in the development of new polymer-based therapeutics. Besides synthesis, this work clearly points out that polymer microstructure greatly influences aggregate formation and therefore determines interactions of synthetic polymers with biological systems.

Zusammenfassung der Arbeit:

In Rahmen der vorliegenden Arbeit wurde ein neuartiger Zugang zu einer Vielzahl von Polymerstrukturen auf Basis des klinisch zugelassenen Polymers Poly(N-(2-Hydroxypropyl)-methacrylamide) (PHPMA) entwickelt. Der synthetische Zugang beruht zum einen auf der Verwendung von Reaktivesterpolymeren und zum anderen auf der Reversible Addition Fragmentation Chain Transfer (RAFT) Polymerisationsmethode.

Durch Verwendung der RAFT Polymerisation war zum einen die Synthese von poly(HPMA)-block-poly(Lauryl Methacrylat) Blockcopolymeren möglich. Zum anderen konnten ebenfalls partiell bioabbaubare Blockcopolymere auf Basis von Polylactiden und HPMA hergestellt werden, indem ein Kettentransferreagenz (CTA) an ein wohl definiertes Polylactid gekoppelt wurde. Diese verschiedenen Strukturen wurden in ihrer Zusammensetzung variiert und mit Erkennungsstrukturen (Folaten) und markierenden Elementen (Fluoreszenzfarbstoffe und β^+-emittierenden Radionukleide) versehen und *in vitro* und *in vivo* evaluiert. Die entwickelten radioaktiven Markierungsstrategien für Polymere werden bei der weiteren Entwicklung von polymeren Medikamenten von großem Nutzen sein, denn sie erlauben eine genaue nichtinvasive Bestimmung der Biodistribution.

Es konnte der große Einfluss der Polymermikrostruktur auf das Aggregationsverhalten mittels Lichtstreuung und Fluoreszenzkorrelationsspektroskopie nachgewiesen werden. Erst diese Informationen über die Überstrukturbildung konnten eine plausible Erklärung für die Kinetik der Zellaufnahme liefern. Somit konnte die elementare Rolle von Strukturwirkungsbeziehungen in biologischen Systemen nachgewiesen werden.

Folglich konnte neben der Synthese, Charakterisierung und ersten biologischen Evaluierungen ein Beitrag zum besseren Verständnis der Interaktion von polymeren Partikeln mit biologischen Systemen geleistet werden.

Table of contents

1. Introduction:

2. Manuscripts and additional results:

1. Introduction

1.1 Basic ideas, biological rationality and development of polymer therapeutics and nanoparticles for medical applications

Whenever highly functional and complex systems are needed, nature has chosen to apply macromolecular structures. The most prominent example is the deoxyribonucleic acid (DNA) storing all information of life. Compared to nature synthetic macromolecules are less defined and less functional. But nevertheless artificial polymers can be synthesized and functionalized in a well-controlled manner. Especially in biological or medical application polymers have to mimic biological systems, combining functionalities to achieve selectivity. Therefore, the polymer itself has to be soluble in aqueous solution, non immunogenic and minimize unspecific interactions with biological membrane. For example, polyethylenglycol or poly(*N*-(2-hydroxypropyl) methacrylamide) PHPMA fulfill these requirements. During the last decades, this concept was applied to various systems [1-8], which can be separated into 5 main groups and summarized under the name polymer therapeutics (figure 1).

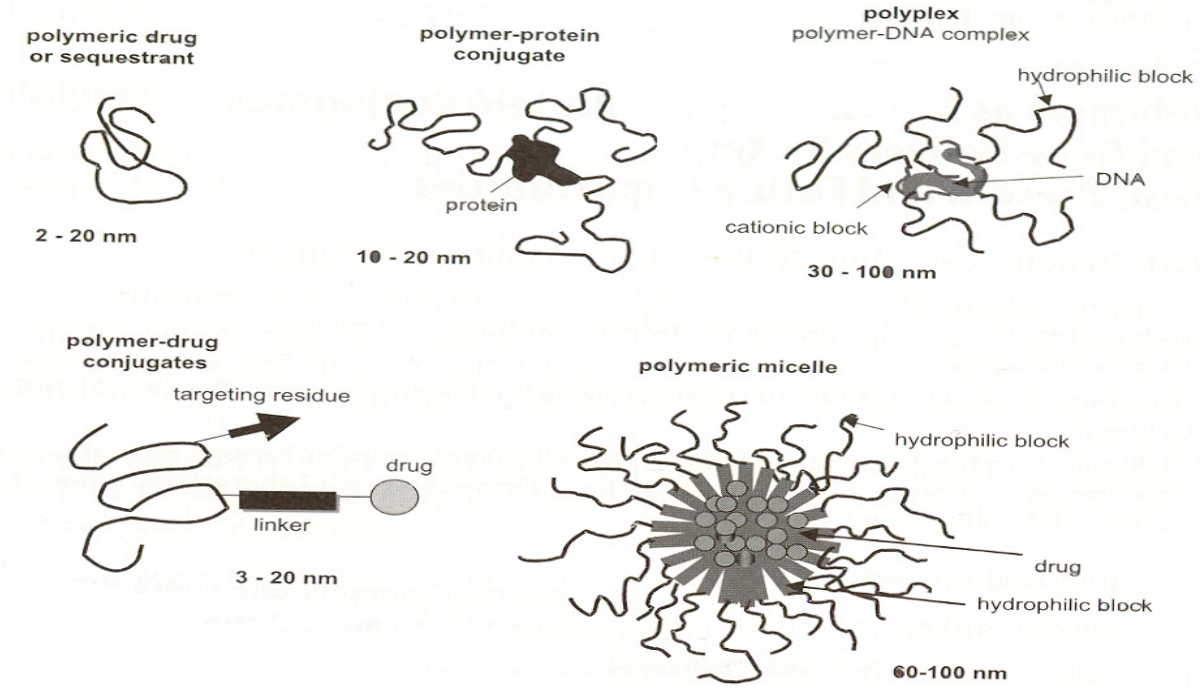

Figure 1. The different groups of therapeutic agents summarized as “Polymer therapeutics” [1]

The concept of polymer drug conjugates was first proposed be H. Ringsdorf et al. [9] in the 1970s and is directly related to Paul Ehrlich`s concept of the "magic bullet", which selectively targets the side of disease without affecting any other organ. It is based on a water-soluble polymer backbone, which carries a drug on a degradable spacer as well as a targeting moiety (homing device). This simple concept leads to the first polymers in clinical trail in the 1980s (PK1 and PK2) [10-12] and even today polymer drug conjugates are mainly based on this visionary concept.

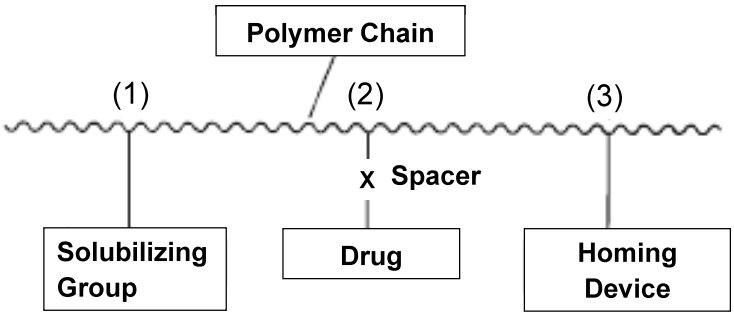

Figure 2. First model of a pharmacological active polymer by H. Ringsdorf et al. in the 1970s.

From the model mentioned above it is understandable that research on polymer drug conjugates has to concider all five aspects. First, the polymeric material itself has to be soluble as well as biocompatible. The polymer fulfilling those needs is poly(*N*-(2-hydroxypropyl) methacrylamide) (HPMA). [1,2,5,10,11,12] HPMA was originally developed as a material for contact lenses, by Kopecek et al. [13] and was successfully applied as a highly biocompatible polymeric material. It can be polymerized by radical polymerization with also offer the great opportunity to synthesize copolymers bearing activated ester units, which can be modified by polymer analogues reactions yielding multifunctional polymers. The direct polymerization of most bio-relevant structures is limited due to possible side reactions. In this respect, the activated ester approach developed by H. Ringsdorf et al. is a wonderful tool for functional polymeric architectures derived by any radical polymerization method. The activated ester undergoes a nucleophilic substitution reaction with good nucleophiles, e.g. amines or alcoholates. Additionally, the reactivity can be nicely tuned by the choice of activated ester. Until today many activated esters have been published in literature. [14-16]

Even today the research area based on H. Ringsdorf`s basic concept is rather large. The idea has mainly influenced the structure of polymer therapeutics and therefore it is still applied in various research areas. For example, polymer-protein conjugates, polymer drug conjugates for combination therapy and polymer-antibody conjugates become more and more important.

Beside the synthesis of polymer drug conjugates, these systems were also applied to the modification of inorganic nanoparticles. Inorganic nanopaticles, e.g. iron oxide, have gained increasing attention due to the possible application as MRI contrast agents. In this case the metal chelating catechols (Dopamin) can be introduced via postpolymerization reaction to the polymer. The aromatic hydroxyl groups bind multivalent to metal ions on the particle surface and are therefore a wonderful tool to modify the surface of any oxidic inorganic nanoparticle as shown by Meuer et al, Tahir et al. and Shukoor and coworkers. [17-25]

A second major research area among polymer therapeutics is based on polymeric micelles or more general on polymeric superstructures, e.g. micelles, compound micelles, polymersomes and more complex aggregates. The basic idea of micellar drug delivery systems was again proposed by Ringsdorf at al. in 1982. [26] Hörpel et al. reported the synthesis of micelle-forming copolymers by the reaction of palmitic acid with poly(ethylenimine), and by the copolymerization of polyethylene glycol and hydroxyethyl methacrylate. The fixation of stabilized but activated carboxydecylthiocyclo-phosphamide (I) to these polymers was carried out by reaction of the -OH or -NH2 groups of the polymers with acid group of the drug. In summary, block copolymers as well as random copolymers were prepared in which a drug was covalently linked to the polymer.

However, it was the group of Kazunori Kataoka, which investigated and developed these systems further for a number of medical applications. [27] The first PEG-based polymeric micelles under clinical investigations were based on the research of Kataoka et al. leading to clinical trails of polymeric micelles. [28, 29]

In general, one has to differenciate between two different types of block copolymer micelles for drug delivery. The main characteristic of the first group is that a hydrophobic drug is covalently linked to one block of the polymer inducing an amphiphilic character. Thus, the amphiphilic structure undergoes a self-organization process in a block selective solvent, which is usually aqueous for biomedical application. [30] A higher ordered structure, e.g. a micelle, is formed. In the second group a drug is entrapped into the hydrophobic core of the micelle. In this case the block copolymer acts like a surfactant and solubilizes the hydrophobic drug. In this respect, the second concept is much more versatile. But it has to face the problem of an unspecific release of the drug, because the polymeric micelle itself is not stable under all conditions. In addition, for slightly water-soluble drugs a continuous diffusion of the drug may occur. If the drug is covalently linked, the drug cannot defuse from the micelle or be released when the micellar structure is disrupted.

Besides encapsulation of drugs, micelles can be used to entrap bio-molecules, e.g. oligo- or poly-nucleotides, proteins or enzymes. [31] A cationic block within the block copolymer can efficiently complex the oligo-nucleotides, e.g. siRNA or DNA, while the other block can provide solubility, non-immunogenic character, stealth properties or further functionalities for controlled specific delivery within the body. [32] The same concept can be applied to the encapsulation of proteins [33] protecting them for degradation on the extracellular level. There are several proteins of great biomedical relevance, e.g. apoptosis proteins. These proteins delivered into certain types of tumor cells would induce apoptosis. [34-35]

However, one has to keep in mind that all the mentioned approaches are only possible by the use of micelles, polymersomes or even liposomes. In these cases the bio-molecule can be simply entrapped inside the hydrophilic center of the particle by either by sterical encapsulation as well as by electrostatic interactions. But once again the electrostatically stabilized complexes can be expected to be more efficient in terms of upload as well as in vivo stability. Thus, these systems may offer the higher potential for in vivo protein delivery.

The author is well aware that there are other promising systems used for biomedical application, e.g. polymeric particles synthesized by mini-emulsion techniques (e.g. Cyaonacrylate), various inorganic polymer functionalized nanoparticles, polymer-protein conjugates, modified natural proteins and viral carrier. However, they are beyond the scope of this work. In addition, these systems are not related to the results presented in this work. Nevertheless, most of these systems have certainly promising potential for specific applications. [36]

After the introduction of various polymeric systems, the biology has to be considered. How do synthetic polymers interact with biological membranes? How do cells internalize polymers? What is their intracellular fate? But most important, what do we know about the way of polymeric particles *in vivo*? These questions are essential to ask for further development of nanomedicine.

In general very little is known for polymers and their *in vitro* as well as *in vivo* fate. Only for some systems investigations are reported in literature and therefore will be discussed in the following paragraph or in chapter 1.2.

Whenever macromolecules are injected into the blood stream various interactions have to be considered. After the injections soluble particles may circulate a certain time. They can be eliminated from the blood stream by cellular uptake, renal clearence, the reticuloendothelial system (RES) or mononuclear phagocyte system (MPS). The celluar uptake does depend on the polymeric material itself as well as on targeting moieties on the structure and will be described later. The renal clearance is in first order related to the size of the macromolecule or particle. Additionally the renal clearance is influenced by the surface charge of the particle. Usually particles with a diameter below 5 nm in

diameter get cleared from the blood stream. For positive charged particles the limit in diameter can go up to 8-10 nm (dextrane particles). [37]

An enhanced uptake in the liver, spleen, and bone marrow is largely attributed to the macrophages residing in the tissues, which are responsible for clearing particulates and macromolecules circulating in the blood. When nanoparticles are i.v. injected a variety of serum proteins can bind to the surface of the nanoparticles, which are recognized by the scavenger receptor on the macrophage cell surface and internalized, leading to a significant loss of nanoparticles from the blood stream. The serum proteins binding on the nanoparticles are also termed “opsonins”, and the macrophages contributing the major loss of injected dose are also known as the reticuloendothelial system (RES) or mononuclear phagocyte system (MPS). Minimizing protein binding is a key point for developing long circulation nanoparticle formulations. These findings clearly underline the need for soluble, non-immunogenic and non-protein-adhesive polymers for in vivo application in diagnostics or drug delivery.

But even if a material fulfills all these needs an accumulation somewhere in the body can occur. The limited pore size of the endothelial wall in the tissue is the primary delivery barrier for nanoparticles but also allows selective accumulation in certain tissues. Unlike small molecule drugs that can diffuse through the capillary wall into the tissue, nanoparticles rely on the gaps between the endothelium to pass through the barrier. Tissues with a leaky endothelial wall usually contribute significant uptake of nanoparticles, including tumor, liver, spleen, and bone marrow. The increased rate of tumoral uptake of nanoparticles is based on a phenomenon termed the “enhanced permeability and retention” (EPR) effect (see figure 3) due to an increased capillary permeability in the tumor tissue and reduced lymphatic drainage. [38] The EPR effect is the basis of polymer or nanoparticle based cancer therapy, because it is the biological rational for passive accumulation of these structures within the tumor tissue.

However, a polymer can be used to modify *in vivo* distribution and can lead to a certain accumulation in a specific tissue. But it does not directly influence the cellular uptake. This process is based on polymer membrane or polymer-membrane protein interactions.

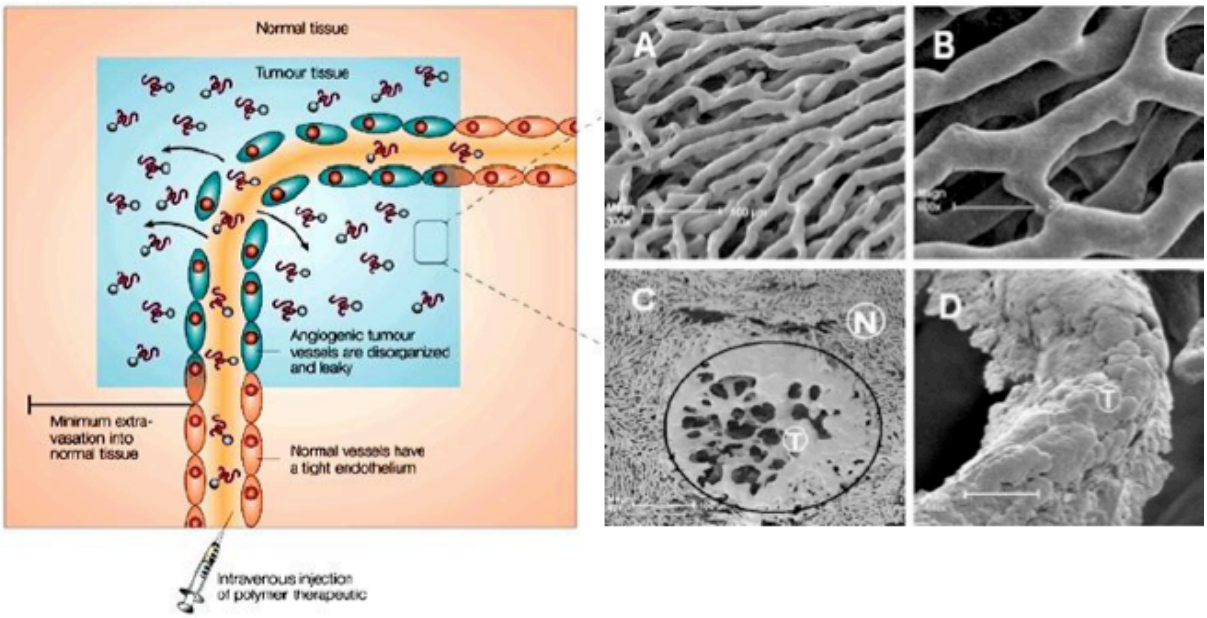

Figure 3. a) Schematic picture of the EPR-effect and b) electron-microscopy images of the healthy vasculature in the liver (A/B) and tumor vasculature (C/D)

Whenever a polymeric particle interacts with a cellular membrane endocytosis can occur, leading to internalization of macromolecules. [39-41] The endocytic and intracellular trafficking pathways are complex and highly regulated processes. The processe itself serves to help mediate cellular homeostatic control by initiating receptor mediated cell signaling, leading to organelle biogenesis. It has been realized that nano-sized delivery systems can hijack these physiological transport pathways to facilitate improved drug delivery. Eucaryotic cells are taking up fluids, small and large molecules continuously by a process called endocytosis. Some special cells (e.g. macrophages) are able to internalize larger particles or even other cells. A small portion of the plasma membrane encloses the material, which is taken up into the cell. In the first step of this process the membrane buds inward and then pinched off to form an intracellular endocytic vesicle. The material taken up by this vesicle is directly delivered to the lysosomes, where it is digested. The derived metabolites are directly transferred into the cytosol, where the cell can use them for various processes.

The process of endocytosis can be devided into two types. These types are distinguished on the basis of the size of the formed endocytic vesicle. Pinocytosis (“cellular drinking”) involves the uptake of fluid containing small vesicles with a diameter below 150 nm. In contrast the term phagocytosis (“cellular eating”) describes the ingestion of large particles via large vesicles with a diameter above 250 nm. A special case of phagocytosis can be observed when phagocytic cells, e.g. macrophages, are observed. These cells defend us against infections by ingesting invading microorganisms (see figure 4)

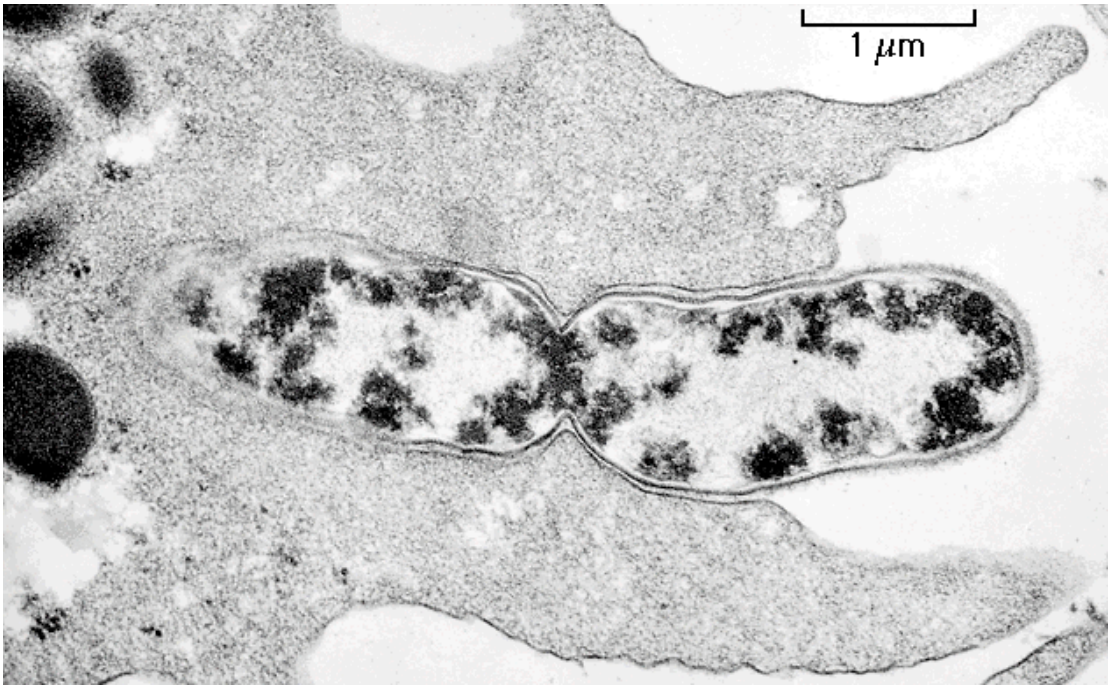

Figure 4. Phagocytosis of a bacterium by a white blood cell [42]

Phagocytic cells are also of great importance in scavenging dead and damaged cells and cellular debris. As an astonishing example, macrophages ingest more than 10^{11} of worn-out red blood cells every day.

But for polymeric particles pinocytosis is the more important process. Eucaryotic cells continually ingest parts of their plasma membrane in form of small vesicles that are later on returned to the membrane. This process is not only related to the uptake of nutrition it is also essential for the "renovation" of membrane bound proteins (e.g. receptors, ion channels or enzymes). The rate at which plasma membrane is internalized varies from cell type to cell type, but it is usually rather large. In this respect, it is understandable how polymers enter the cell or why poly-cations are potent transfection agents. They stick to the membrane proteins or lipids by electrostatic interactions and get internalized. Of course, there can be also active mechanisms involved, but the normal adsorption should not be underestimated.

Mainly pinocytosis is carried out by clathrin coated pits and vesicle formation (see figure 5). The protein clathrin assembles into basketlike network on the cytosolic surface of the membrane. Now the assembling process starts shaping the membrane into a vesicle.

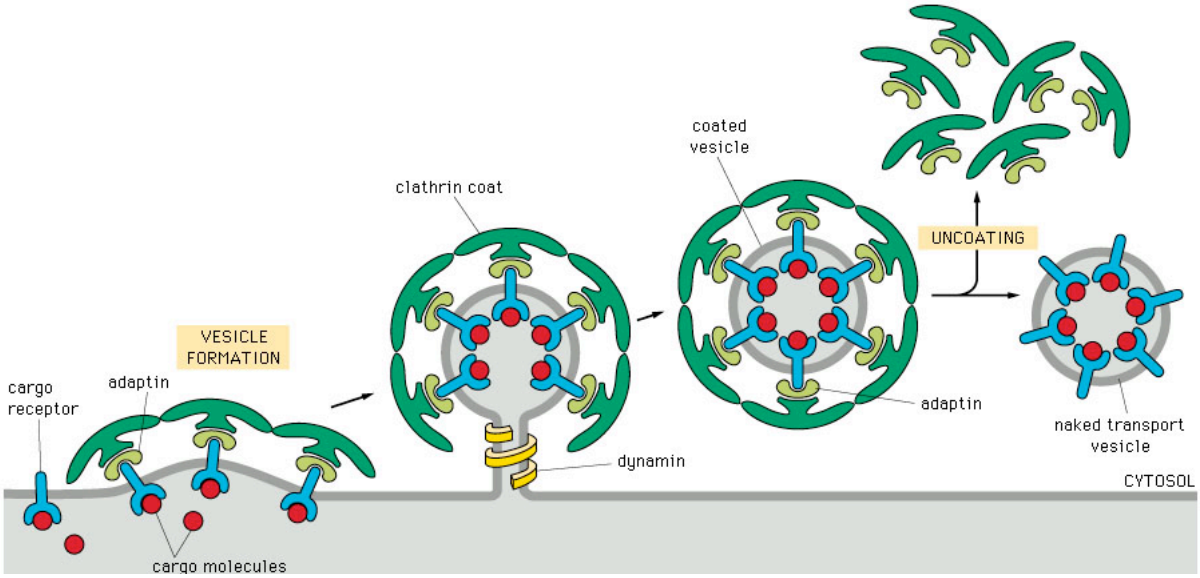

Figure 5. Selective transport mediated by clathrine-coated vesicles. [42]

A small GTP-binding protein named dynamin assembles as a ring around the neck of each deeply invaginated pit. The dynamin hydrolyses its GTP and the gained energy is used to constrict the ring, which leads to a pinching off of the vesicle from the membrane. The clathrin itself plays no part in capturing specific molecules for the intracellular transport, because it does not penetrate the membrane or bind to a membrane associated receptor. This is the role of the proteins named adaptins, which bind to transmembrane cargo receptors as well as to clathrines. They help to capture specific cargo molecules by trapping the cargo receptors that bind them. This is the process in which a new clathrin coated vesicle is formed. After the vesicle is pinched of the membrane, they rapidly shed their coat and fuse with an endosome. The receptor-mediated endocytosis by clathrin-coated vesicles is the major uptake route into animal or even human cells. There is a huge variety of cell surface receptors, which can be addressed for specific uptake including transferrin, asialoglycoprotein [43], epidermal growth factor (EGF) [44] and chemokine. [45] They serve as high affinity binding sites and have been investigated for their use in targeting to different cell types. In all cases, a ligand binds to specific cell surface receptors, signaling their directional movement towards clathrin coated pits in the membrane and the process described above occurs.

A second uptake route is cell adhesion molecule mediated endocytosis. A subfamily of immunoglobulins (IGs), namely cell adhesion molecules (CAMs) or L1, found in endothelial and neuronal cells, contain a signaling sequence, ArgSerLeuGlu, on the cytosolic domain which localizes these proteins to clathrincoated pits. Cell adhesion receptors, including integrin and cadherin, will

enter into the cell in this manner after binding cell adhesion peptides. Conformational changes of the integrin result in activation and ligand binding, which signals the complex to the coated pits. Peptides such as Arg–Gly–Asp (RGD) specifically bind to a cell adhesion receptor and have recently been used in targeted drug delivery systems for the treatment of cancer and autoimmune diseases. [46]

In contrast, clathrine independent uptake routes are known. Clathrin-independent internalization enables the intracellular accumulation of materials along a less destructive path as compared to clathrine-mediated endocytosis (see figure 6).

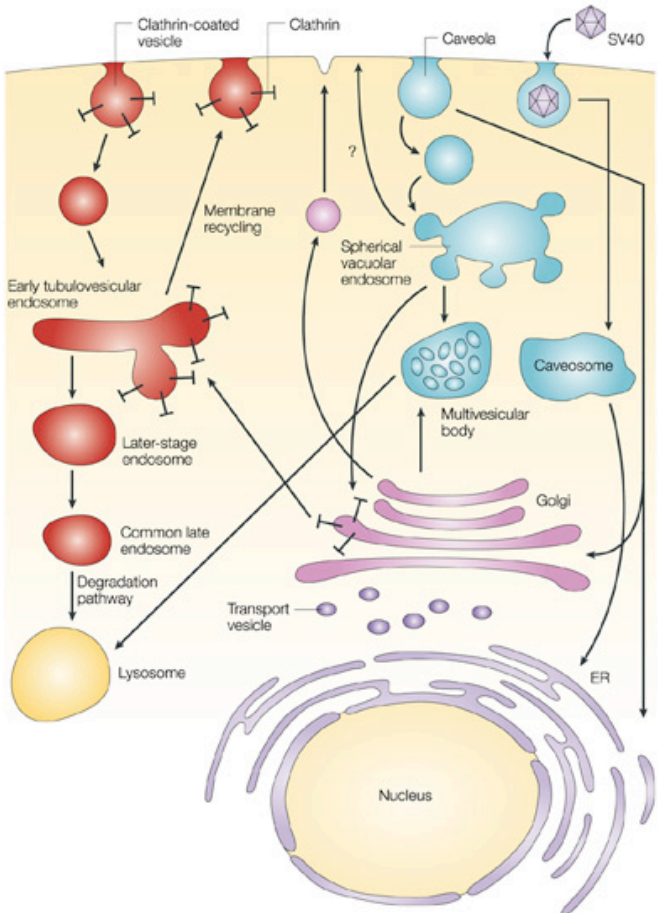

Figure 6. Intracellular trafficking pathways. [47]

The two major pathways include caveolae-mediated endocytosis (CvME) and the less characterized lipid raft internalization. Caveolae are flask-shaped invaginations, ranging from 50 to 100 nm in diameter, making up more than 10% of the plasma membrane for endothelial cells. Caveolar

morphology differs dramatically between cell types making it complicated to definitively infer on common structural features. These invaginations are held in place by underlying actin filaments in the cytoskeleton, where certain membrane proteins are found to concentrate. Unlike clathrin-mediated endocytosis, caveolae-assisted endocytosis is a triggered process that involves subsequent complex signaling. In general, molecules taken up by a clathrin-independent mechanism are localized to lipid rafts. [48] Small-interfering RNA (siRNA) strategies aim to investigate the importance of caveolin-1 for clathrin-independent internalization illustrated that this protein is not mandatory for internalization through lipid-rich membrane regions. Ligands internalized through receptor-dependent caveolae-mediated endocytosis include, folic acid [49], albumin and cholesterol. Folic acid, or vitamin B9, appears an especially attractive target for targeted drug delivery and therefore it is discussed in chapter 2.5. For example, folate targeted poly(ethylene glycol) (PEG)-coated nanoparticles are found to bind to folate receptors allowing for caveolae-assisted endocytosis, followed by the formation of intracellular vesicles. The uptake process can be visualized by confocal microscopy. [50]

After macromolecules have been taken up into cells they usually undergo intracellular digestion and if the polymer itself cannot be degraded, exocytosis will most likely occur. The three pathways to endosomal degradation are shown schematically in figure 7.

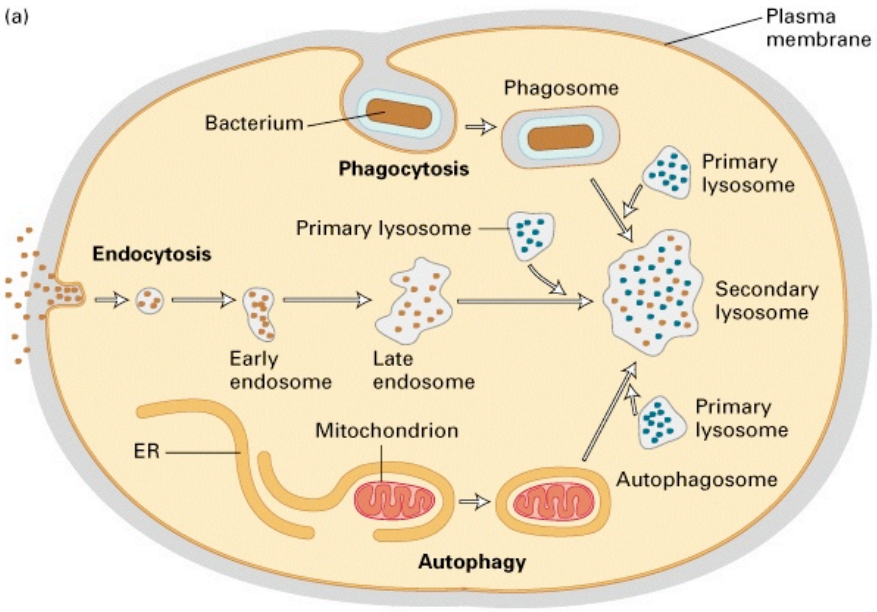

Figure 7. Three pathways to lysosomal degradation [42]

For many applications a lysosomal delivery of macromolecules is necessary, e.g. whenever an oligo-peptide-linked drug is used, degradation is mandatory for the release of the drug. [51]

In contrast, for protein and DNA delivery a transport to the lysosome has to be avoided. In this respect, an endosomal escape is discussed as a major need for efficient cytosolic delivery. [52] For that propose Kataoka at al. suggest polycationic block copolymers. [32] These systems take advantage of the pH gradient occurring during endocytosis. In the process of endocytosis the pH in the vesicle drops from 7.4 at the beginning down to 5-4 in the lysosome. It is reported that in the late endosome the pH level is between 6 to 5. Behr and others introduced the concept of the "proton sponge" and hypothesized, that polymers with buffering capacities between 7.2 and 5.0, such as polyethylenimine (PEI) or (meth)acrylates bearing tertiary amines in the side chain, could buffer the endosome and potentially induce its rupture. [53-55]

The proton sponge effect is for sure one of the most promising approaches for the delivery of proteins or nucleotides. [32,33] It may open up a new way to treat various deceases, e.g the delivery of apoptosis proteins into cancer cells, which are no longer able produce these apoptosis inducing proteins themselves leading to uncontrolled proliferation. In addition, these proteins are supposed to be not harmful to healthy cells. Thus, a biological way of targeted medication can be achieved.

In summary, it can be concluded that still little is known about the *in vivo* as well as *in vitro* fate of many polymer-based particles and polymer therapeutics. Only for some systems these subjects have been investigated to a certain extend (see chapter 1.2). In some cases biological processes are explored. However, many questions remain untouched. More research has to be carried out to understand the in vivo fate of polymeric carriers. We have to gain knowledge, essential for the development of more efficient drugs for a better treatment of patients.

Literature:

[1] Satchi-Fainaro R, Duncan R. Polymer Therapeutics I and II. Advances in Polymer Science, Springer Berlin/Heidelberg 2006;192 and 193.

[2] Ringsdorf H. Structure and properties of pharmacologically active polymers. J Polymer Sci Polym Symp 1975;51:135-153.

[3] Ferrari M. Cancer nanotechnology: opportunities and challenges. Nat Rev Cancer 2005;5:161-171.

[4] Duncan R. Polymer conjugates as anticancer nanomedicines. Nat Rev Cancer 2006;6:688-701.

[5] Haag R, Kratz F. Polymer Therapeutics: Concepts and Applications Angew Chem Int Ed 2006;45:1198-1215.

[6] Harris JM, Chess RB. Effect of pegylation on pharmaceuticals. Nat Rev Drug Discovery 2003;2:214-221.

[7] Gu, F., Karnik, R., Wang, A., Alexis, F., Levy-Nissenbaum, E., Seungpyo, H., Langer, R., Farokhzad, O., Targeted nanoparticles for cancer therapy, Nano Today 2007;2:14-21

[8] Duncan R. The dawning era of polymer therapeutics. Nat Rev Drug Discov 2003;2:347–60.

[9] Gros L, Schupp H, Ringsdorf H. Polymeric Antitumor Agents on a Molecular and on a Cellular Level? Angew. Chem. Int. Ed. 1981;20(4):305-325.

[10] Duncan R, Coatsworth JK, Burtles S. Preclinical toxicology of a novel polymeric antitumour agent: HPMA copolymer-Doxorubicin (PK1). Hum. Exp. Toxicol. 1998;17(2):93-104.

[11] Hopewell JW, Duncan R, Wilding D, Chakrabarti K. Preclinical evaluation of the cardiotoxicity of PK2: A novel HPMA copolymer–doxorubicin–galactosamine conjugate antitumour agent. Hum. Exp. Toxicol. 2001;20(9):461-470.

[12] Říhová B, Kovář M. Immunogenicity and immunomodulatory properties of HPMA-based polymers. Adv. Drug Del. Reviews. Article in Press

[13] Kopeček J, Bažilová H. Poly[N-(2-hydroxypropyl)methacrylamide]. I. Radical polymerization and copolymerization, Eur. Polym. J. 1973;9:7–14.

[14] Batz HG, Franzmann G, Ringsdorf H. Model Reactions for Synthesis of Pharmacologically Active Polymers by Way of Monomeric and Polymeric Reactive Esters. Angew Chem Int Ed 1972;11:1103-04.

[15] Gauthier MA, Gibson MI, Klok H-A. Synthesis of Functional Polymers by Post-Polymerization Modification. Angew. Chem. Int. Ed. 2009;48:48–58

[16] Theato P. Synthesis of well-defined polymeric activated esters. J Polym Sci Part A Polym Chem 2008;46:6677–6687.

[17] Meuer S, Oberle P, Theato P, Tremel W, Zentel R. Liquid crystalline phases from polymer functionalized TiO_2 nanorods. Adv. Mater. 2007;19(16): 2073-2078.

[18] Zorn M, Meuer S, Tahir MN, Khalavka Y, Sönnichsen C, Tremel W, Zentel R. Liquid crystalline phases from polymer functionalised semiconducting nanorods. J.Mater. Chem. 2008;18:3050-3058.

[19] Tahir MN, Therese HA, Shah MR, Berger R, Butt H-J, Theato P, Schröder HC, Müller WEG, Tremel W. Biofunctionalization of chalcogenide nanotubes. J. Am. Chem. Soc. 2008;130:12342–12347.

[20] Wang J, Kappl M, Tahir MN, Barz M, Theato P, Tremel W, Butt HJ. Influence of binding site density in wet bioadhesion. Adv. Mater. 2008;20:3872-3876.

[21] Tahir MN, Berger R, Barz M, P. Theato, Natalio F, Schröder HC, Müller WEG, Tremel W. Growth of Fibrous Aggregates of Silica Nanoparticles: Control of Fiber Growth by Mimicking The Biogenic Silica Patterning Processes Soft Matter 2009, in press

[22] Shukoor MI, Natoli F, Glube N, Tahir MN, Therese HA, Ksγenofontov V, Theato P, Langguth P, Boissel J-P, Schröder HC, Müller WEG, Tremel W. dsRNA Functionalized Multifunctional γ-Fe_2O_3 Nanocrystals: A Tool For Targeting Cell Surface Receptors. Angew. Chem. Int. Ed. 2008;47:4748-4752.

[23] Shukoor MI, Natalio F, Tahir MN, Wiens M, Tarantola M, Therese HA, Barz M, Weber S, Terekhov M, Schröder HC, Müller WEG, Janshoff A, Theato P, Zentel R, Schreiber LM, Tremel W. Pathogen-Mimicking MnO Nanoparticles for Selective Activation of the TLR9 Pathway and Imaging of Cancer Cells. Adv. Funct. Mater. 2009;19:1–9.

[24] Shukoor MI, Natalio F, Divekar M, Tahir MN, Metz N, Therese HA, Theato P, Ksenofontov V, Schröder HC, Müller WEG, Tremel W. Biomagnetic Separation of Recombinant Histidine Tagged Protein by Multifunctional Polymer Derivatized γ-Fe_2O_3 Nanocrystals. Magn. Magn. Mater. 2008;320:2339-2344.

[25] Shukoor MI, Natalio F, Krasko A, Schröder HC, Müller WEG, Tremel W. Multifunctional Magnetite Nanoparticles for Protein Separation. Chem. Commun. 2007;4677-4679.

[26] Pratten MK, Lloyd JB, Hörpel G, Ringsdorf H. Micelle-forming block copolymers: Pinocytosis by macrophages and interaction with model membranes. Makromol. Chem. 1985;186(4), 725-733.

[27] Matsumura Y, Kataoka K. Preclinical and clinical studies of anticancer agent-incorporating polymer micelles. Cancer Sci. 2009;100(4):572-579

[28] Kataoka K, Harada A, Nagasaki Y. Block copolymer micelles for drug delivery: design, characterization and biological significance, Adv. Drug Deliv. Rev. 2001;47:113-31.

[29] Kwon GS, Kataoka K. Block copolymer micelles as long-circulating drug vehicles. Adv. Drug. Delivery Rev. 1995;16:295-309.

[30] Nagarajan R, Ganesh K. Block copolymer self-assembly in selective solvents:theory of solubilization in spherical micelles. Macromolecules 1989;22:4312-4325.

[31] Kabanov AV, Batrakova EV, Alakhov VY. Pluronic block copolymers as novel polymer therapeutics for drug and gene delivery. J. Control. Release 2002;82:189-212.

[32] Lee Y, Miyata K, Oba M, Ishii T, Fukushima S, Han M, Koyama H, Nishiyama N, Kataoka K. Charge-conversion ternary polyplex with endosome disruption moiety: A technique for efficient and safe gene delivery. Angew. Chem. Int. Ed. 2008;47(28):5163-5166.

[33] Lee Y, Ishii T, Cabral H, Kim H-J, Seo J-H, Nishiyama N, Oshima H, Osada K, Kataoka K. Charge-conversional polyionic complex micelles-efficient nanocarriers for protein delivery into cytoplasm. Angew. Chem. Int. Ed. 2009;48(29):5309-5312.

[34] Thompson CB. Apoptosis in the pathogenesis and treatment of disease. Science 1995;267:1456–1462.

[35] Hay S, Kannourakis G. A time to kill: viral manipulation of the cell death program. J Gen Virol. 2002;83(7):1547–64.

[36] Mailänder V, Landfester K. Interaction of Nanoparticles with Cells. Biomacromolecules 2009;10:2379–2400.

[37] Thews G, Mutschler E, Vaupel P. Anatomie, Physiologie, Pathophysiologie des Menschen. Wissenschaftliche Verlagsges.; Auflage: 6., 2007

[38] Maeda H, Wu J, Sawa Y, Matsumura Y, Hori K. Tumor vascular permeability and the EPR effect in macromolecular therapeutics: a review. J. Controlled Release 2000;65:271-84.

[39] Bareford LM, Swaan PW. Endocytic mechanisms for targeted drug delivery. Adv. Drug Del. Rev. 2007;59:748–758.

[40] Marsh M, McMahon HT. The structural era of endocytosis. Science 1999;285:215-220.

[41] Miaczynska M, Stenmark H. Mechanisms and functions of endocytosis. The Journal of Cell Biology 2008;180(1): 7-11.

[42] Alberts B, Bray D, Johnson A, Lewis J, Raff M, Roberts K, Walter P. Essential Cell Biology: An Introduction to the Molecular Biology of the Cell. Garland Publishing, Inc. New York & London. 1998.

[43] Biessen EA, Vietsch H, Rump ET, Fluiter K, Kuiper J, Bijsterbosch MK, van Berkel TJ. Targeted delivery of oligodeoxynucleotides to parenchymal liver cells in vivo. Biochem. J. 1999;340(3):783-792.

[44] Mamot C, Drummond DC, Greiser U, Hong K, Kirpotin DB, Marks JD, Park JW. Epidermal growth factor receptor (EGFR)-targeted immunoliposomesmediate specific and efficient drug delivery to EGFR- and EGFRvIII overexpressing tumor cells, Cancer Res. 2003;63:3154-3161.

[45] Biragyn A, Ruffini PA, Coscia M, Harvey LK, Neelapu SS, Baskar S, Wang JM, Kwak LW. Chemokine receptor-mediated delivery directs self-tumor antigen efficiently into the class II processing pathway in vitro and induces protective immunity in vivo. Blood 2004;104:1961-1969.

[46] Dunehoo AL, Anderson M, Majumdar S, Kobayashi N, Berkland C, Siahaan TJ. Cell adhesion molecules for targeted drug delivery, J. Pharm. Sci. 2006;95:1856-1872.

[47] Carver LA, Schnitzer JE. Caveolae: mining little caves for new cancer targets. Nature Rev. Cancer 2003;3:571-581.

[48] Lamaze C, Dujeancourt A, Baba T, Lo CG, Benmerah A, Dautry-Varsat A. Interleukin 2 receptors and detergent-resistant membrane domains define a clathrin-independent endocytic pathway. Mol. Cell 2001;7:661-671.

[49] Chang WJ, Rothberg KG, Kamen BA, Anderson RG. Lowering the cholesterol content of MA104 cells inhibits receptor-mediated transport of folate, J. Cell Biol. 1992;118:63-69.

[50] Dauty E, Remy JS, Zuber G, Behr JP, Intracellular delivery of nanometric DNA particles via the folate receptor, Bioconjug. Chem. 2002;13:831-839.

[51] Duncan R, Cable HC, Lloyd JB, Rejmanová P, Kopecek J. Polymers containing enzymatically degradable bonds, 7. Design of oligopeptide side-chains in poly[N-(2-hydroxypropyl)methacrylamide] copolymers to promote efficient degradation by lysosomal enzymes. Makromol Chem 1983;184:1997-2008.

[52] Pack D, Putnam D, Langer R. Design of imidazole-containing endosomolytic biopolymers for gene delivery. Biotechnol. Bioeng. 2000;67:217–223.

[53] Behr J-P. The proton sponge: a trick to enter cells the viruses did not exploit. Chimica 1997;51:34–36.

[54] Boussif O, Lezoualch F, Zanta M A, Mergny M D, Scherman D, Demeneix B, Behr J-P A versatile vector for gene and oligonucleotide transfer into cells in culture and in vivo: polyethylenimine. Proc. Natl. Acad. Sci. 1995;92:7297–7301.

[55] Midoux P, Monsigny M. Efficient gene transfer by histidylated poly- lysine /pDNA complexes. Bioconjug. Chem. 1999;10:406–411.

1.1 Defined polymers for therapeutic applications:

From Structure-Property Relationships to better defined Therapeutics

Authors: **Barz M, Luxenhofer R, Zentel R, Vicent MJ.**

Journal: **Invited Review for Polymer Chemistry**

1. Introduction

Modern life as we know would be simply impossible without polymers. Natural and synthetic polymers are essential not only in our day-to-day life but also become increasingly important in biomedical applications. First use of polymers for therapeutic applications dates back several decades on the visionary work of H. Ringsdorf [1], but the terms polymer therapeutics and nanomedicine have come into use only recently.

While nature is preparing -and using- defined multifunctional polymers, i.e. polypeptides and polynucleotides since the dawn of biotic times, we humans have been consciously preparing polymers only for a couple of decades and relatively defined polymers are still playing only a minor role. This has probably two main reasons. First, the difficulty to prepare defined polymers and polymeric systems and secondly somehow resulting from the first reason: the lack of knowledge of the effects of polymer architecture, size, charge and charge distribution etc. *in vitro* and *in vivo*. These are factors, which can only be assessed when defined polymers are used. Furthermore many of the well-known properties of polymers are not related to their uniformity or are even based on their polydispersity. As mentioned above, in certain applications defined polymers are indispensable. Whenever polymers, especially non-degradable ones, are used for *in vivo* application as polymer drug conjugates [2,3], polymeric micelles [4,5], polymersomes [6,7], functional coating of inorganic nanoparticles [8,9] or nanogels [10,11], we need to know their *in vivo* fate. Are they cleared from the organism or do they accumulate somewhere, even if it is only a minor fraction of the used material? The renal exclusion limit as an example depends, among other factors, on the size of polymers in solution. Therefore

macromolecules having comparable sizes are mandatory to fine-tune the properties of the whole population.

In the last one or two decades, a multitude of new methods for the controlled polymerization has been established. Especially the controlled radical polymerization methods ATRP, RAFT and NMP have pushed the field enormously. In addition, the preparation of defined, synthetic polypeptides has made huge progress since the first reports by Deming and coworkers. [12] Poly(2-oxazoline)s are another type of polymer that has been accessible in a defined manner for quite a while but is only beginning to draw considerable attention for biomedical applications more recently. [13] In this short review, we will try to concentrate on these three types of methods to obtain well-defined polymers and their potential applications in the biomedical field.

However up to date, the most commonly used polymers in biomedical applications are polyethylenglycols (PEG) in various architectures. More recently, several reports show that under certain conditions PEG and PEG-containing polymers can illicit significant complement activation [14-15], and rapid clearance can occur after repeated injections of PEGylated liposomes. [16] Not only for this reason alternatives to PEG in biomedical applications are investigated. About PEG a huge number of reviews are available. [17-20] For this reason, this polymer will not be considered in more detail in this review.

Our second intention is to review the data and information obtained in recent years about the structure-property relationships of polymers and their behaviour *in vitro* and *in vivo*. Due to the tremendous advances of synthetic possibilities, various defined polymer architectures are accessible. So the key issue is what do we know about the influence of polymeric design and its influence on cellular fade of polymers? And what can we expect for medical applications?

2.1. Defined Structures from Polypeptides and Polypeptide Hybrids

Polypeptides are comprised of amino acids, natural building blocks that are readily available and non-toxic in doses of interest. Apart from proteins, i.e. well defined polypeptides with accurate structure control, only a very limited number of natural polypeptides, resembling less defined classic synthetic polymers are known. Poly-γ-glutamic acid produced from bacteria and cnidaria [21] is widely used for biomedical applications. [22,23] Synthetic polypeptides have been described first by Leuchs in 1908. [24] However, not until rather recently, the synthetic procedure was not controlled and it was not possible to obtain repeatable results, defined polymers or more complex polymer architectures such as block copolypeptides, star-like polypeptides or bottle-brushes. Deming was the first to describe defined polypeptides using transition metal catalysts. [24] Since then, a large number of researchers

dedicated efforts to find alternative ways towards defined polypeptides. Hadjichristidis and co-workers reported on the use of highly purified monomers, solvents and reagents as well as high vacuum techniques. [25] While this approach allows the preparation of very large polypeptides with high definition, it most likely will not become a common approach, as it is very challenging from the technological standpoint. In contrast, Schlaad and co-workers demonstrated a very facile method. [26] By the use of protonated amine initiators, side reactions and alternative polymerization routes are strongly reduced. Similar to controlled radical polymerization techniques, the nucleophilic amine terminus is transferred into a dormant (i.e. protonated) state. Thus, block copolymers and synthetic peptide hybrids have become available using a relatively easy method. More recently, Chen and co-workers have reported another facile approach. [27] Use of silylated amine initiators also allows the preparation of defined polypeptides. Since the trimethylsilyl residue is present at the polymer terminus, again, control over the polymerization is retained. Interestingly, in this approach the polymerization does not seem to be slowed down as the authors describe quantitative polymerization (degree of polymerization $\leq$ 300) at room temperature within 24h or less under atmospheric pressure. [28] In contrast, the protonated amines lead to a much slower propagation. Here elevated temperatures (40 - 80 °C) are applied and the polymerization proceeds for several days. [26,29] All previously mentioned methods of controlled polypeptide synthesis have been shown to give (multi)block copolypeptides [30], block and graft copolymers with other polymers such as, among others, polyisobutylene [31], poly(2-oxazoline)s [29], chitosan [32] or other interesting structures such as star [33] and brush-like polypeptides. [34] In several cases, these polymer architectures lead to further assembly of a higher hierarchy, such as polymer micelles [26], polymer vesicles (polymersome/peptosome) [35,36] or even peptide based nanofibres and nanotubes. [37] All these structures are of great interest for drug delivery or diagnostic applications, both after covalent attachment of drugs of therapeutic interest and for the transport of non-covalently bound active compounds. Polypeptides are also becoming increasingly interesting, as several polypeptides revealed stealth properties, i.e. their ability to evade the reticuloendotheliary system (RES). [35,36,38] In this respect, poly(sarcosine) is discussed as potential, biodegradable alternative to PEG. Similary, side chain modified polypeptides such as poly(hydroxyethyl l-glutamine) (PHEG) and poly(hydroxyethyl l-asparagine) (PHEA) have also been shown to allow the preparation of long circulating liposomes. [37,39]

Lu et al. reported recently on an interesting approach to obtain well-defined polypeptide brushes via combination of two controllable polymerization mechanisms. The ring-opening metathesis polymerization (ROMP) of norbornene derivatives and the TMS initiated NCA polymerization of l-glutamic acid, l-lysine and l-leucine. [27] In a one pot synthesis they were able to obtain very well defined polypeptide brushes with different backbone length and different side chain lengths. It was shown, that both polymerizations were very well controlled and the final products had polydispersity indices below 1.2 even for polymers with molar masses as high as 500 kg/mol. Kinetic investigations

showed that side chain NCA polymerization was efficient, at least when only approx. every fourth monomer served as an initiator. Whether this is enough to obtain rod-like molecular brushes remains to be elucidated. Nevertheless, such excellent control over the backbone and side chain lengths allows the preparation of a great variety of polymer structures from the same monomers. The great variety of natural and non-natural amino acids gives even more leverage to vary polymer structure and properties. Thus, such a system is very intriguing for the investigation of detailed structure property relationships in the near future.

It is well known that the size and steric demand of (polymer) amphiphiles has significant effect on the nature of aggregates formed in aqueous solution. Simple spherical micelles, polymersomes but also nanorods and nanotubes can be formed. Kimura and co-workers observed that the morphology of the molecular assemblies was tunable by suitable molecular design of the hydrophobic block, selection of chain length of the hydrophilic block, mixing two-type block peptides and processing. [37]

Deming and co-workers used block copolypeptides comprising of a water soluble poly(l-lysine) block and enantiopure as well as racemic hydrophobic blocks to investigate the difference of such polymers in stabilizing a hydrophilic/hydrophobic interface. Enantiopure l-leucine is well known to form α-helices, which are highly incompatible with most solvents. In contrast, for racemic oligo- or polyleucine the formation of a-helices is strongly suppressed and the block becomes readily soluble in non-polar solvents. This molecular difference manifests itself in a pronounced difference in the micro- and macroscopic behaviour of emulsions of silicon oil in water stabilized by a polymer system. In contrast to the enantiopure polypeptides, the racemic samples were able to stabilize double emulsions. To achieve this, the polymers must be able to stabilize both a convex as well as concave hydrophilic/hydrophobic interface at the same time. This is attributed by the authors to the possibility of interchain hydrogen bond formation between the racemic poly(*rac*-leucine) chains on one hand and the good solubility of the polymer in the hydrophobic solvent on the other hand. However, a considerable contribution of the polydispersity of the described polymers to the stabilization of either curvature cannot be ruled out. In any case, this report exemplifies the additional level of potential molecular design available for polypeptides in a concise way, the use of enantiopure and racemic monomers. Besides structural variation available in this way, it becomes immediately evident that biological parameters such as cellular uptake, clearance rates, metabolization and immunogenicity as well as pharmaceutical parameters such as aggregate stability and drug release rates can be affected in this way.

For a more detailed overview on chemistry and application of polypeptides from NCA polymerization, the reader is referred to three excellent and recent reviews by Kricheldorf [40], Deming [41] as well as Hajichristidis and coworkers. [42]

2.2. Poly(2-oxazoline)s

Previously, poly(2-oxazoline)s or poly(N-acylethylenimine) mainly were of interest for researchers in the drug delivery field as a convenient source for linear poly(ethylene imine) for gene delivery studies. However, more recently, several research groups divert considerable efforts towards the use of poly(2-oxazoline)s (POx) as a versatile building block of polymer therapeutics or drug delivery systems. POx are prepared by living cationic ring opening polymerization (LCROP) and are available with a large array of reactive (protected) and non-reactive side chains. POx can be seen as pseudo-polypepdtides as each repeating unit contains a peptide bond, albeit in the side chain instead of within the main chain. Depending on the nature of the pending side chains, these polymers are extremely hydrophilic, show amphiphilicity and thermoresponsiveness or are hydrophobic or fluorophilic. For reactive side chains, aldehydes, alkynes, carboxyls, thiols, amines, hydroxyls and others have been described and used for polymer analogous modifications. Moreover, lipopolymers are easily accessible using lipid initiators. Zalipsky and co-workers used lipoPOx for the decoration of liposomes and showed that hydrophilic POx can prolong the circulation of coated liposomes just as PEG does. [43] In contrast, low molecular weight hydrophilic POx are readily excreted via the kidneys and show no unspecific accumulation in any organ. [44]

POx-enzyme conjugates have been known for decades and it is well established that POx conjugation (POxylation) can solubilize enzymes in organic media and helps to retain enzyme activity therein. [45] Moreover, non-covalent encapsulation of enzymes in amphiphilic block coPOx has been described. [46] More recently, Mero et al. reported covalent attachment of trypsin and cytosine arabinose. [47] It was shown that the autolysis rate of polymer-conjugated trypsin was very comparable between PEGylated and POxylated trypsin. In contrast, the POxylated cytosine arabinose activity was shown to be somehow lower as compared to its PEGylated counterpart. This, however, was attributed by a slower drug release from the carrier polymer. Up to date, no significant cytotoxicity of POx has been reported, neither *in vitro* nor *in vivo*, albeit a lack of profound studies must be acknowledged. Since the polymer architecture is also an important parameter for the pharmacokinetic behaviour *in vivo*, recent developments by Jordan and co-workers are important in this aspect. Defined star-like POx as well as molecular brushes became accessible by the use of pluri- and polytriflate initiators. [48,49] In contrast to halogen-based multi-initiators [50], these give a much faster (and quantitative) initiation rate in comparison to the relatively slow polymerization. This is essential to obtain defined polymer structures.

Another point of interest in water-soluble polymers is the phenomenon of their change in water solubility in dependence of temperature. The lower critical solution temperature (LCST) can be observed for the majority of water-soluble polymers. Above a certain temperature, the polymers

become insoluble and precipitate. When used in networks such as hydrogels, the hydrogels collapse. Two points are especially of importance for applications of this phenomenon, i) being able to tune the temperature of the phase transition and ii) obtaining materials with very rapid and sharp transition when the respective temperature is reached. For specific applications, reversibility and lack of a hysteresis is also of great importance. As mentioned before, the side chain of POx strongly influences their character, in particular their water solubility. With methyl substituents, no LCST is observed and the polymer is highly water soluble, in fact hygroscopic. Also poly(2-ethyl-2-oxazoline)s are well soluble in water, however, this polymer already shows a LCST of 60 – 70 °C, depending on the polymer architecture and degree of polymerization. POx with isopropyl and n-propyl side chains show LCSTs of ~ 40 °C and 25 °C, respectively, while poly(2-butyl-2-oxazoline) is not water soluble any more. Further tuning of the LCST can be achieved by two means, copolymerization of different monomers and modification of polymer termini. [51-53] Thus, LCST values covering almost the entire range of liquid water have been achieved. In this context, the low polydispersity of the polymers is also of great importance. Since the LCST of polymers depends, among other factors, on the molar mass, samples with a higher polydispersity will naturally contain species with differing thermal behaviour. In order to achieve a rapid and complete phase transition in a narrow temperature interval, high polymer definition (i.e. low polydispersity) is indispensable.

Additionally, polymer analog modification of unsaturated side chains with hydrophilic and hydrophobic side chains also allowed LCST modification over a wide range. [54] Especially the latter method is interesting in the context of polymer conjugates for therapeutic applications. Therapeutics, which are covalently attached to water soluble polymers, are hydrophobic in the vast majority of cases. Therefore, researchers are advised to ensure that the formed conjugates do not become water-insoluble at 37 °C.

For a more detailed and recent overview on the potentials of POx the interested reader is referred to a review by Hoogenboom. [13] The general rather easy synthetic access to POx of complex structures with multiple and/or different chemical functionalities either along the side chain and/or the polymer termini makes this family of polymers a very interesting candidate for future applications in the field of drug delivery and nanomedicine.

2.3. Defined Polymers by controlled radical polymerization techniques

The development of controlled radical polymerization (CRP) techniques, sometimes also termed living radical polymerization (LRP) techniques, had a tremendous impact on synthetic polymer chemistry. Especially in the field of therapeutic application, defined polymers are mandatory because

molecular weight as well as polymeric structure determines interaction with biological tissue and therefore determine the *in vivo* fate of any polymer therapeutics.

The LRP have in common that all methods were developed to suppress termination as well as uncontrolled transfer of the created radical. These LRPs are divided into three subgroups, which are stable free radical polymerization (e.g. NMP), degenerative transfer polymerization (e.g. RAFT, MADIX) and metal mediated catalyzed polymerization (e.g. ATRP). Among these, ATRP and RAFT are the most commonly used and most versatile processes. There have been various reviews describing mechanism as well as recent developments of either RAFT [55,56] or ATRP [57,58]. Briefly, ATRP is a means of forming carbon-carbon bond through transition metal catalyst. As the name implies, the atom transfer step is the key step in the reaction and therefore it is responsible for uniform polymer chain growth. This is leading to polymers with rather low polydispersities, which is mainly related to the transition metal based catalyst. This catalyst provides an equilibrium between active polymer propagating the polymerization and an inactive form which is commonly described as the dormant form. Since the dormant state of the polymer is vastly preferred in this equilibrium, the concentration of propagating radicals is constantly low. Thus, side reactions, e.g. termination and recombination, are effectively suppressed and control over molecular weights can be achieved.

ATRP reactions are very tolerant of many functional groups like allyl, amino, epoxy, hydroxy and vinyl groups present in either the monomer or initiator. The ATRP method is also advantageous due to their ease of preparation and inexpensive commercially availability of catalysts (copper complexes), pyridine based ligands and initiators (alkyl halides). Only the copper content may influence biological systems even so it is usually below the upper limit of copper approved for medical application.

In contrast to ATRP, the RAFT polymerization technique does not require any metal catalyst. RAFT polymerization uses thiocarbonyl compounds, for instance dithioesters, dithiocarbamates, trithiocarbonates, and xanthates (MADIX) in order to mediate the polymerization via a reversible chain-transfer process. These reagents are called chain transfer agent (CTA). The mechanism itself is complex. It is based on two chain-transfer and two chain-propagation equilibriums. These chain transfer equilibriums offer control over the radical polymerization process. In this process, a growing polymer chain reacts with the chain transfer agent (CTA) yielding an intermediate radical. Due to the chemical structure of the CTA it can fragment in two different ways. This event leads to a new chain transfer agent and a free radical, which can propagate the polymerization. In this respect, the propagation probability is equally distributed over all polymer chains. This means that all polymer chains do have the same probability and time to grow, the reason for narrowly distributed polymers. Furthermore, the different equilibriums do lead to a tremendous reduction of free radicals. Thus, side reactions are successfully suppressed. In addition, it is important to point out that the average chain length is proportional to the concentration of the CTA as well as to the conversion of the polymerization itself.

During the last years, some reviews have already focused on the recent approaches on biological application of both techniques. [59-62] But these detailed and interesting reviews have focused much more on the synthesis of new polymers and polymer architectures, but less on biological or medical application of defined systems. In this respect, we would like to point out materials which can be expected to enrich the pool of building blocks for polymer therapeutics.

2.4. Defined polymers for biomedical application

During the last years not only polymerization methods have improved tremendously. In addition, a variety of novel biocompatible monomers were investigated. The number of these systems is rather high and a detailed description of developments is beyond the scope of this short review. Therefore we would like to focus on some old and new examples of polymeric materials, which have been already applied to biological investigations. Additionally, we would like to introduce useful synthetic approaches, which may open up a broad road to highly functional and biocompatible polymeric structures, e.g. the postpolymerization modification of reactive polymer precursors. [63-65]

These polymers belong mainly to the group of poly(meth)acrylates or poly(meth)acrylamides. In this respect we would like to start with polyacrylates and -methacrylates.

Among these monomers the group of (meth)acrylates bearing oligo(PEG) side chains, e.g. poly(OEGMA) or poly(DEGMA) are of an increasing interest. These systems have rather interesting properties such as high solubility in water, non-immunogenic and non-toxic character, lower critical solution temperature (LCST) and enhanced blood circulation times. [66-69] The LCST can be precisly tuned by copolymerization of both monomers. It was reported by Lutz et al. that the LCST can be adjusted from 26 °C to 90 °C by changing the ratio of OEGMA to DEGMA units within the copolymer. [70]

These systems have been either applied to ATRP as well as RAFT polymerization leading to well-defined homo, random, block or star polymers. [66] Additionally, the block copolymers prepared from these monomers have shown interesting super structure formation in solution. The formation and biomedical application of micelles [71,72] and polymersomes [73] has been reported during the last years. Especially after the safety of PEG for *in vivo* applications was claimed by Webster et al. as well as Eaton and coworkers [74,75] ethylene oxide based systems may offer various advantages. However, they have been under clinical research for quiet some years, which has to be considered as a major advantage in the approval of new therapeutics. But it has to be kept in mind, even so the new material might appear comparable to linear PEG, the biological properties of these (meth)acrylates have been found to be different. S. M. Ryan et al. reported that linear PEG grafted onto salmon

calcitonin enhances the serum half life time, while comb-shaped PEG displayed increasing resistance of the protein against intestinal enzymes, liver homogenate and serum. [76] Additionally Gao et al. reported also improved pharmacokinetics by conjugation of poly(oligo(ethylenglycol) methyl ether methacrylate) with the N-terminus of myoglobin. [77] The cytotoxicity was investigated in various cell lines, e.g. Caco-2, HT29-MTX-E12 or HepG2, ensuring nontoxic behaviour up to a polymer concentration of 5 mg/mL. [76,78]

Further interesting polymer systems are based on poly(2-(meth)acryloyloxyethyl phosphorcholine)s (PMPC). The monomer structure is highly bio-inspired, because the side chain contains the head group of the natural phospholipid phosphatidylethanolamine ensuring high biocompatibility. It was polymerized by ATRP [79-81] as well as RAFT [82-85] yielding various well-defined polymer architectures. Micelles [86-88] and polymersomes [89-91] have been reported during the last years. Polymersomes have been applied to study diffusion across oral epithelium and were used as transfection agents by Battaglia et al. [90,91] ensuring pronounced cellular uptake as well as non-toxic behaviour. In addition, PMPC was used for protein conjugation by Lewis and coworkers. [92] They have found a reduced tissue migration compared to similar PEG-protein conjugates of the same hydrodynamic volume. Thus, an improved depot effect in the tissue as well as subsequent longer elimination half-life lead to improved pharmacokinetics. These findings clearly underline the potential of PMPC based polymeric systems for further medical application.

Another group of polymers having high potential for medical applications are glycopolymers, which have been investigated by various groups regarding synthesis, physicochemical properties as well as first biological evaluations. [93-95] In nature glycosides or glycopeptides are the key to various processes in cell-cell interactions. The glycocalyx is involved in inflammations, viral infections, fertilization and signal transmission. Hence, glycopolymers can be expected to provide interesting properties in medical applications, [96] e.g. immunotherapy of cancer or treatment of auto-inflammatory diseases. [97] This natural glyco-code is highly complex and therefore structures mimicking or interacting with it are highly complex. For example the total synthesis of siaLe^x includes at least 26 steps [98] yielding a pure defined selectin ligand, which playes a major role in the inflammatory cascade [99] and can be expected to be a useful tool in the treatment of autoinflamatory diseases. But as mention above the structures are highly complex and therefore mimicking agent are desirable. In this respect, well-defined glycopolymers or glycoside-functionalized polymers are needed.

Deng et al. reported a non-toxic behaviour up to 5 mg/mL of gluconolactone derivate bearing block copolymers taken up by HeLa cells. [100] In addition, lectin-binding experiments were carried out by Granville et al. ensuring binding ability. Interestingly, the protein-carbohydrate binding is completely disrupted when the 6-carbon position is modified. [101]

Ayres et al. prepared polymer brushes containing sulfonated sugar repeat residues by ATRP. They compared these systems with the non-sulfonated analogues in vitro. The sulfonated brushes showed improved blood compatibility in terms of plasma recalcification, clotting times and complement activation. [102]

Furthermore, protein-glycopolymer conjugates have been prepared and evaluated *in vitro*. Shi et al have combined a near infrared (NIR) fluorescent dye with avidin employing the well-known avidin-biotin interaction or activated ester conjugating onto BSA. As expected, the higher NIRF dye content lead to enhanced optical properties compared to labelled proteins. [103] In general the binding essays are first hinds, but in vivo experiments have to be carried out to evaluate therapeutical potential, too. Glycopolymers may bind to targets, but the polymer has to prove their specificity *in vivo*. Why would nature use a complex structure, when a simple undefined motive would do the same job?

Further well-established polymers for therapeutic application have been applied to the new synthetic methods of LRP. During the last years many groups around the world have applied RAFT or ATRP to the synthesis of functional (N-(2-(hydroxypropyl) methacrylamide (HPMA) based polymers. [104-107] Some of these systems will be discussed in detail in the last chapter of this review.

Last but not least we would like to mention postpolymerization modification methods [63-65], which can be considered as an old but still promising approach to highly functional and complex structures based on well-established polymers. In this approach the final structure is not polymerized directly. Instead, a reactive precursor polymer is synthesized, which can be precisely characterised and afterwards easily transferred into a highly biocompatible system. The currently most prominent example of the postpolymerization modification is the Huisgen [2+3] cycloaddition, in which an azide reacts with an alkyne, typically under Cu(I) catalysis, forming a triazole derivative. [65] During the last years the number of publications has grown enormously and detailed description is beyond the scope of this short review. As an example, Geng et al. have applied this method to the synthesis of glycopolymers. [108,109] These glycopolymers were conjugated to BSA yielding artificial glycopeptides. Thus, the normally inert BSA showed innate immune system interaction properties. [109]

Among reactive polymers for polymer analogue reactions the activated ester offer some advantages: First of all, most of them have proven abilities in synthetic peptide chemistry. Second, they have already been applied to the synthesis of the first polymer therapeutics entering clinical trails (PK1 and PK2) at the end of the last century. [110,111] Additionally various activated ester are known in literature offering tuneable reactivities. However most important, they can be used to synthesize various acrylate or acrylamide based architectures from one polymer precursor. Thus, copolymerization parameters can be disregarded and amphiphilic block copolymers can be prepared from well-characterised non-polar polymers.

Taking advantage of the activated ester approach, the synthesis of a variety of HPMA based polymers was possible. Additionally, *in vitro* as well as *in vivo* studies were carried out. [112-116] Gibson et al. could demonstrate, that HPMA based homopolymers derived from poly(pentafluorophenyl methacrylate) (PPFMA) have comparable cell toxicity values. [113] Barz et al. reported nontoxic behavior of poly(HPMA)-block-poly(lauryl metacrylate) block copolymers up to a concentration of 3 mg/mL. [112] Moreover, Herth at al. used comparable polymers in preliminary *in vivo* experiments. [114] In this work a new radioactive labeling chemistry for positron emission tomography was introduced, monitoring non-invasively the body distribution of various polymeric architectures. Most important, the reactive precursor strategy offers the chance to synthesize functional systems from one precursor polymer as demonstrated by Barz et al. [115] and Brocchini and coworkers. [116] An important feature of this approach is the untouched degree of polymerization, although the functionalization is altered.

Finally most important, this technique can be applied to study structure property relationships among different polymers without changing the chain length of the polymer itself. [115] These structure-property relationships are essential for a more sophisticated design of polymer therapeutics and will therefore be discussed in the next paragraph.

2.5. Structure Property Relationship: Influencing cellular fate of polymer carriers and their cargo

In order to investigate structure-property relationships, the first step is to control the structure as exactly as possible. In case of free radical copolymerization this is typically hardly possible. If the copolymerization parameters are not matched, the composition of the copolymers will change during the polymerization. Accordingly, polymers obtained by this method suffer from three different problems, 1) molar mass distribution, 2) quantitative comonomer content distribution and 3) spatial comonomer distribution. Subsequent fractionation is typically only able to narrow the molar mass distribution. The latter two problems, however, are very difficult to address by postpolymerization techniques. However, the microstructure, i.e. the distribution of comonomers along the polymer chain has a major influence on endocytosis in mammalian cells, as recently shown by Barz and coworkes. [115]

In the case of different reactivities of the monomers employed, as is it very typically the case, the composition of a polymer prepared by free radical polymerization depends on the monomer conversion. Polymers formed at low monomer conversion will comprise different relative monomer molar fractions than polymers obtained at high monomer conversions. In contrast, polymers obtained

via controlled or living polymerization techniques grow at the same time and over the whole course of polymerization. Thus, while polymers theoretically obtained in early polymerization stages differ from those at latter stages, the polymers, and especially their relative comonomer contents eventually obtained, differ only very slighty, e.g. for controlled/living polymerisates. Thus, the LRP are of essential importance in the synthesis of defined polymers on which structure-properties relationships can be discussed.

The influence of other factors such as charge and charge density is more established and obvious. In these cases direct electrostatic interactions determine uptake and intracellular distribution.

The intracellular fate of any taken up material will depend strongly on the mechanism of entry. Sahay et al. recently reported on differential uptake mechanisms for polymer unimers and their micelles, respectively. [117] In this study, an amphiphilic triblock copolymer of PEG, poly(propylenoxide) and PEG, Pluronic P85 was investigated. The authors concluded that unimers entered the cells via caveolae-mediated endocytosis, while the polymer micelles were taken up via a clathrin-mediated route. At the same time, it was observed that P85 was able to inhibit caveolae-mediated endocytosis. It should be underlined that no ligand for specific cellular uptake was employed in this study. The authors suggested that the specific interaction with caveolae may be due to perturbation of these specialized structures by changing the membrane microviscosity or membrane curvature. Moreover, the same group recently reported on the endocytosis of nanogels formed by PEG-poly(methacrylate) block copolymers. [118] These crosslinked polymer micelles also enter the cells via caveolae in a highly specific manner and are then routed to lysosomes. Caveolae mediated endocytosis is highly regulated in epithelial cells and is typically strongly surpressed in cells forming tight junctions. Accordingly, high uptake of drug-loaded nanogels was observed in cancer cells (MCF7/ADR) and sub-confluent MDCK cells. In contrast, when the MDCK cells became confluent and thus, form tight junctions, uptake of the nanogels was practically abolished. Interestingly, Pluronic P85 and the nanogels share a similar PEG-based corona. Future studies using PEG and non-PEG based materials will hopefully show whether such specific cellular interactions of non-modified hydrophilic polymers are a more general feature that could be used for the facile preparation of materials with specific biological interactions. As for mass-production and for regulatory issues it will obviously be benefical, if the introduction of low molecular weight ligands should not be necessary in order to obtain specific cell-nanomaterial interactions. The same group very recently published more detailed investigation of the cellular uptake and subsequent subcellular distribution of Pluronic P85 in a variety of cells, including neurons and BBMEC. [119]

In general it has to be emphasized that these findings clearly point out the key role of aggregate properties, because they are essential for a more detailed understanding of the processes taking place whenever polymeric carriers interact with biological systems.

Kimura and co-workers are using amphiphilic polypeptides and polydepsipeptides to obtain self-assembled aggregates forming polymer micelles and vesicles, which they term peptosomes and lactosomes. In both cases poly(sarcosine) serves as the hydrophilic polymer. Long circulation times of 48 h and more were reported [36] and the RES was successfully avoided. Thus, it was possible to detect tumors in the liver. [35] Interestingly, a comparison of aggregates comprising either polypeptide block copolymer or polypeptide/poly lactide block copolymer revealed that the former showed much lower tumor to liver ratios. Both aggregates were of similar size (32 nm vs. 37 nm) but the poly(sarcosine) block length differed somehow (degree of polymerization 60 vs. 90). It remains uncertain whether the difference in the in vivo behavior could be attributed to the aggregate core material or to the minor differences in the hydrophilic corona. Unfortunately no details on the characterization of the polymers the polymers were reported. Thus, it is impossible to point out differences in microstructure leading to differences in aggregation behaviour.

Nemoto et al. demonstrated recently the effect of the polydispersity of star-like poly(N,N-dimethylaminopropylacrylamide) (PDMAPAAm) used as non-viral gene delivery systems on the transfection efficiency. [120] This work compares the crude polymer with a slightly higher polydispersity (PDI = 1.4) and fractions thereof with lower polydispersities (1.1-1.2). The authors report that not only the molar mass, but also the polydispersity have an influence on the transfection efficiency.

In addition, Callahan et al. have investigated the influence of molecular weight and charge of HPMA-based copolymers on their intracellular distribution after cytosolic microinjection. [121] Although the copolymers were synthesized by free radical polymerization surprisingly low polydispersities of 1.4-1.7 before and 1.0-1.2 after fractionation were obtained. However, fractionation cannot solve the problems of quantitative comonomer content distribution and spatial comonomer distribution. In this respect, the polymeric material is not really well defined. Nevertheless, the findings are interesting. All copolymers rapidly and evenly diffused throughout the cytoplasmic compartment after the microinjection took place. The smallest copolymer fractions also rapidly diffused into the nucleus. The exception of passive intracellular diffusion was the strongly cationic copolymer containing 20% of a quaternary amine in the side chain. This copolymer was found to localize specifically to microtubules from the cytoplasm. Nuclear entry from the cytoplasm was dictated by size-limited passive diffusion through the nuclear pore complexes, however, small but significant differences in rates of nuclear import were observed for polymers with sizes near the molecular weight exclusion limit as a function of the charge and hydrophobicity of the copolymers. Weak bases were found to have the highest nuclear uptake. These findings indicate a strong structure-property relationship, but an investigation of the aggregates would be interesting, too. Maybe differences in aggregation would help to gain a deeper inside. Furthermore the standard deviation of the performed measurements is rather high.

Richardson et al. found pronounced differences in the intracellular distribution of dextrine, HPMA and PEG based polymers [122] underlining the tremendous influence of the polymeric structure on the cellular fate of the particle.

In conclusion, structure-property relationships are surely interesting from the academic point of view, but, what is more, they are also of great importance for the development of polymer therapeutics.

3. Conclusion

Tremendous advances in polymer chemistry and macromolecular engineering offered accessibility for many new materials as well as remodelling old materials in a more defined way. Although detailed investigations of structure property relationship using highly defined polymers other than PEG is a relatively young field, it has already become clear that it is of major importance. This is not surprising at all, since similar trends have already been observed for other systems such as highly defined dendrimers. In order to completely use the potential of highly defined polymers and their effects on biological entities, polymer chemists need to work closely together with pharmacists, biologists and medical doctors.

4. References

[1] Ringsdorf, H. *J. Polym. Sci. Polym. Symp.* 1975, **51**, 135-153.

[2] R. Duncan. *Nat. Rev. Cancer* 2006, **6**, 688-701.

[3] R. Duncan. Nat. Rev. Drug Discovery 2003, **2**, 347-360.

[4] Y. Matsumura, K. Kataoka. *Cancer Sci.* 2009, **100**, 572-579.

[5] E.V. Batrakova, A.V. Kabanov. *J. Control. Release* 2008, **130**, 98-106.

[6] D. E. Discher, A. Eisenberg. Science 2002, 297, 967-973.

[7] A. Samad, Y. Sultana, M. Aqil. *Curr. Drug Deliv*. 2007, **4(4)**, 297-305.

[8] D. A. LaVan, T. McGuire, R. Langer. *Nat Biotechnol.* 2003, **21(10)**, 1184-1191.

[9] V. Mailänder, K. Landfester. *Biomacromolecules* 2009, **10(9)**, 2379-2400.

[10] A. V. Kabanov, S. V. Vinogradov. *Angew. Chem. Int. Ed*. 2009, **48(30)**, 5418-5429.

[11] J. Kopecek, J. Yang. *Polymer Int*. 2007, **56(9)**, 1078-1098

[12] T. J. Deming, *Nature*, 1997, **390**, 386-389.

[13] R. Hoogenboom, *Angew. Chem. Int. Ed.*, 2009, **48**, 7978-7994.

[14] I. Hamad, A. C. Hunter, J. Szebeni, S. M. Moghimi, *Mol. Immunol.*, 2008, **46**, 225-232.

[15] S. M. Moghimi, A. C. Hunter, C. M. Dadswell, S. Savay, C. R. Alving, J. Szebeni, *Biochim. Biophys. Acta*, 2004, **1689**, 103-113.

[16] T. Ishida, H. Kiwada, *Int. J. Pharm.*, 2008, **354**, 56-62.

[17] J. M. Harris, R. B. Chess. *Nat. Rev. Drug Discovery* 2003, **2**, 214-221.

[18] F. M. Veronese, G. Pasut. *DDT* 2005, **10**, 1451-1458.

[19] K. Kataoka, A. Harada, Y. Nagasaki, *Adv. Drug Deliv. Rev*. 2001, **47**, 113-31.

[20] C. S. Fishburn. J. Pharm. Sci. 2008, 97(10), 4167-4183.

[21] T. Candela, A. Fouet, *Mol. Microbiol.*, 2006, **60**, 1091-1098.

[22] M. H. Sung, C. Park, C. J. Kim, H. Poo, K. Soda, M. Ashiuchi. *Chem Rec.* 2005, **5(6)**, 352-366.

[23] C. Li. *Adv. Drug Del. Rev.* 2002, **54(5)**, 695-713.

[24] a) H. Leuchs, *Ber. Dtsch. Chem. Ges.*, 1906, **39**, 857-861. b) H. Leuchs, W. Manasse, *Ber. Dtsch. Chem. Ges.*, 1907, **40**, 3235-3249. c) H. Leuchs, W. Geiger, *Ber. Dtsch. Chem. Ges.*, 1908, **41**, 1721-1726.

[25] T. Aliferis, H. Iatrou, N. Hadjichristidis, *Biomacromolecules*, 2004, **5**, 1653-1656.

[26] I. Dimitrov, H. Schlaad, *Chem. Comm.*, 2003, 2944-2945.

[27] H. Lu, J. Cheng, *J. Am. Chem. Soc.*, 2007, **129**, 14114-14115.

[28] H. Lu, J. Cheng, *J. Am. Chem. Soc.*, 2008, **130**, 12562-12563.

[29] M. Meyer, H. Schlaad, *Macromolecules*, 2006, **39**, 3967-3970.

[30] T. Aliveris, H. Iatrou, N. Hadjichristidis, *J. Polym. Sci. A1*, 2005, **43**, 4670-4673.

[31] T. Higashihara, R. Faust, *React. Funct. Polym.*, 2009, **69**, 429-434.

[32] R. Nakamura, K. Aoi, M. Okada, *Macromol. Rapid Commun.*, 2006, **27**, 1725-1732.

[33] T. Aliferis, H. Iatrou, N. Hadjichristidis, J. Messman, J. Mays, *Macromol. Symp.*, 2006, **240**, 12-17.

[34] H. Lu, J. Wang, Y. Lin, J. Cheng, *J. Am. Chem. Soc.* 2009, **131**, 13582-13583.

[35] A. Makino, S. Kizaka-Kondoh, R. Yamahara, I. Hara, T. Kanzaki, E. Ozeki, M. Hiraoka, S. Kimura, *Biomaterials*, 2009, **30**, 5156-5160.

[36] H. Tanisaka, S. Kizaka-Kondoh, A. Makino, S. Tanaka, M. Hiraoka, S. Kimura, *Bioconj. Chem.*, 2008, **19**, 109-117.

[37] T. Kanzaki, Y. Horikawa, A. Makino, J. Sugiyama, S. Kimura, *Macromol. Biosci.*, 2008, **8**, 1026-1033.

[38] B. Romberg, J. M. Metselaar, L. Baranyi, C. J. Snel, R. Bünger, W. E. Hennink, J. Szebeni, G. Storm, *Int. J. Pharm.*, 2007, **331**, 186-189.

[39] J. M. Metselaar, P. Bruin, L. W. de Boer, T. de Vringer, C. Snel, C. Oussoren, M. H. Wauben, D. J. Crommelin, G. Storm, W. E. Hennink, *Bioconj. Chem.*, 2003, **14**, 1156-1164.

[40] H. R. Kricheldorf, *Angew. Chem.*, 2006, **45**, 5752-5784.

[41] T. J. Deming, *Prog. Polym. Sci.*, 2007, **32**, 858-875.

[42] N. Hadjichristidis, H. Iatrou, M. Pitsikalis, G. Sakellariou, *Chem. Rev.*, DOI 10.1021/cr900049t

[43] S. Zalipsky, C. B. Hansen, J. M. Oaks, T. M. Allen, *J. Pharm. Sci.*, 1996, **85**, 133-137.

[44] F. C. Gaertner, R. Luxenhofer, B. Blechert, R. Jordan, M. Essler, *J. Control. Release*, 2007, **119**, 291-300.

[45] M. Miyamoto, K. Naka, M. Shiozaki, Y. Chujo, T. Saegusa, *Macromolecules*, 1990, **23**, 3201-3205.

[46] a) K. Naka, A. Ohki, S. Maeda, *Chem. Lett.*, 1991, 1303. b) K. Naka, T. Nakamura, A. Ohki, S. Maeda, *Polym. J.*, 1995, **27**, 1071. c) A. Ohki, K. Naka, O. Ito, S. Maeda, *Chem. Lett.*, 1994, 1065. d) K. Naka, Y. Kubo, A. Ohki, S. Maeda, *Polym. J.*, 1994, **26**, 243-249. e) K. Naka, R. Yamashita, T. Nakamura, A. Ohki, S. Maeda, K. Aoi, K. Tsutsumiuchi, M. Okada, Macromol. Chem. Phys., 1997, **198**, 89-100.

[47] A. Mero, G. Pasut, L. Dalla Via, M. W. M. Fijten, U. S. Schubert, R. Hoogenboom, F. M. Veronese, *J. Controlled Release*, 2008, **125**, 87-95.

[48] R. Luxenhofer, M. Bezen, R. Jordan, *Macromol. Rapid Commun.*, 2008, **29**, 1509-1513.

[49] N. Zhang, A. Schulz, S. Huber, R. Luxenhofer, R. Jordan, *Macromolecules*, 2008, **42**, 2215-2221.

[50] S. Kobayashi, H. Uyama, Y. Narita, J. Ishiyama, *Macromolecules*, 1992, **25**, 3232-3236.

[51] S. Huber, R. Jordan, *Colloid Polym. Sci.*, 2007, **286**, 395-402.

[52] J. S. Park, K. Kataoka, *Macromolecules*, 2007, **40**, 3599-3609.

[53] S. Huber, N. Hutter, R. Jordan, *Colloid Polym. Sci.*, 2008, **286**, 1653-1661.

[54] C. Diehl, H. Schlaad, *Macromol. Biosci.*, 2009, **9**, 157-161.

[55] G. Moad, E. Rizzardo, S. H. Thang, *Aust J Chem*, 2005, **58**, 379-410.

[56] G. Moad, E. Rizzardo, S. H. Thang, *Polymer*, 2008, **49**, 1079-1131.

[57] K. Matyjaszewski, Y. Gnanou, L. Leibler, *Macromolecular Engineering Vol. 1.* Weinheim: Wiley-VCH; 2007.

[58] N. V. Tsarevsky, K. Matyjaszewski, *Chem. Rev.*, 2007, **107**, 2270-2299.

[59] M. Stenzel, *Chem. Commun.* 2008, 3486-3503.

[60] C. Boyer, V. Bulmus, T. P. Davis, V. Ladmiral, J. Liu, S. Perrier, *Chem. Rev.* 2009, 109, 5402–5436.

[61] N. V. Tsarevsky, K. Matyjaszewski. *Materials. Chem Rev*. 2007, **107**, 2270-2299.

[62] J. H. Oh, S. A. Bencherif, K. Matyjaszewski, *Polymer*, 2009, **50**, 4407-4423.

[63] M. A. Gauthier, M.I. Gibson, H.-A. Klok, *Angew. Chem. Int. Ed.*, 2009, **48**, 48–58.

[64] P. Theato, *J. Polym. Sci. Part A: Polym. Chem.* 2008, **46**, 6677-6687.

[65] W.H. Binder, R. Sachsenhofer, *Macromol. Rapid Commun.* 2008, **29**, 952-981.

[66] J.-F. Lutz, *J. Polym. Sci. Part A: Polym. Chem.* 2008, 46, 3459-3470.

[67] S. Han, M. Hagiwara, T. Ishizone, *Macromolecules*, 2003, **26**, 8312-8319.

[68] J.-F. Lutz, O. Akdemir, A. Hoth, *J. Am. Chem. Soc.*, 2006, **128**, 13046-13047.

[69] L. Tao, G. Mantonani, F. Lecolley, D. M. Haddelton, *J. Am. Chem. Soc.*, 2004, 126, 13220-13221.

[70] J.-F. Lutz, A. Hoth. *Macromolecules* 2006, **39**, 893–896.

[71] A. O. Saeed, S. Dey, S. M. Howdle, K. J. Thurecht, C. Alexander, *J. Mater. Chem.*, 2009, **19**, 4529-4535.

[72] L. Zhang, J. Bernard, T. P. Davis, C. Barner-Kowollik, M. H. Stenzel, *Macromol. Rapid Commun.*, 2008, **29**, 123.

[73] F. Ahmed, R. I. Paunlu, G. Srinivas, A. Brannan, F. Bates, M. L. Klein, T. Minko, D. E. Discher, *Mol. Pharm.*, 2006, **3**, 340-350.

[74] M. Eaton, *Nature Materials*, 2007, **6**, 251-253.

[75] R. Webster, E. Didier, P. Harris, N. Siegel, J. Stadler, L. Tilbury, D. Smith, *Drug Metab. Dispos.*, 2007, **35**(1), 9-16.

[76] S. M. Ryan, X. Wang, G. Mantovani, C. T. Sayers, D. M. Haddleton, D. J. Brayden, *J. Control. Release*, 2009, **135**, 51-59.

[77] W. Gao, W. Liu, J. A. Mackay, M. R. Zalutsky, E. J. Toone, A. Chilkoti, *Proc. Natl. Ac. Sci.*, 2009, **106**(36), 15231-15236.

[78] J.-F. Lutz, J. Andrieu, S. Üzgün, C. Rudolph, S. Agarwal, *Macromolecules*, **40**, 8540-8543.

[79] A. L. Lewis, *Encyclopedia of Biomaterials and Biomedical Engineering*, 2004, 1198-1211.

[80] E. J. Lobb, I. Ma, N. C. Billingham, S. P. Armes, *J. Am. Chem. Soc.*, 2001, **123**, 7913-7914.

[81] Y. Ma, Y. Tang, N. C. Billingham, S. P. Armes, A. L. Lewis, A. W. Lloyd,

J. P. Salvage, *Macromolecules*, 2003, **36**, 3475-3484.

[82] Du, Y. Tang, A. L. Lewis, S. P. Armes, *J. Am. Chem. Soc.*, 2005, **127**, 17982-17983.

[83] B. Yu, A. B. Lowe, K. Ishihara. *Biomacromolecules* 2009, **10**, 950–958.

[84] M. H. Stenzel, C. Barner-Kowollik, T. P. Davis, H. M. Dalton, *Macromol. Biosci.*, 2004, **4**, 445-453.

[85] M. Mertoglu, S. Garnier, A. Laschewsky, K. Skrabania, J. Storsberg, *Polymer*, 2005, **46**, 7726-7740.

[86] E. J. Lobb, I. Ma I, N. C. Billingham, S. P. Armes, A. L. Lewis, *J. Am. Chem. Soc.* 2001, **123**, 7913-7914.

[87] Y. Ma, Y. Tang, N. C. Billingham, S. P. Armes, A. L. Lewis, A. W. Lloyd, J. P. Salvage. *Macromolecules* 2003, **36**, 3475–3484.

[88] M. Licciardi, Y. Tang, N. C. Billingham, S. P. Armes, A. L. Lewis, *Biomacromolecules* **2005**, *6*, 1085–1098.

[89] G. Battaglia, A. Ryan, *J. Am. Chem. Soc.*, 2005, 127, 8757-8764.

[90] V. Hearnden, H. Lomas, S. MacNeil, M. Thornhill, C. Murdoch, A. Lewis, J. Madsen, A. Blanazs, S. Armes, G. Battaglia, *Pharm. Res.*, 2009, **26**(7), 1718-1728.

[91] H. Lomas, M. Massignani, K. A. Abdullah, I. Canton, C. L. Presti, S. MacNeil, J. Du, A. Blanazs, J. Madsen, S. P. Armes, A. L. Lewis, G. Battaglia, *Faraday Discuss.*, 2008, **139**, 142-159.

[92] A. Lewis, Y. Tang, S. Brocchini, J. Choi, A. Godwin, *Bioconjugate Chem.*, 2008, **19**(11), 2144-2155.

[93] V. Ladmiral, E. Melia, D. M. Haddleton, *Eur. Polym. J.*, 2004, **40**, 431-449.

[94] A. B. Lowe, B. S. Sumerlin, C. L. McCormick, *Polymer*, 2003, **44**, 6761-6765.

[95] Y. Miura, *J. Polym. Sci. Part A: Polym. Chem.*, 2007, **45**(22), 5031-5036.

[96] A. Varki, R. D. Cummings, J. D. Esko, H. Freeze, G. Hart, J. Marth, *Essentials of Glycobiology*, Cold Spring Harbor Laboratory Press, Cold Spring Harbor, New York, 1999.

[97] Q. Yao, D. E. Furst. *Rheumatology* 2008, **47**, 946-951.

[98] K. Baumann, D. Kowalczyk, T. Gutjahr, M. Pieczyk, C. Jones, M. K. Wild, D. Vestweber, H. Kunz, *Angew. Chem. Int. Ed.*, 2009, **48**, 3174 –3178.

[99] a) D. Vestweber, J. E. Blanks, *Physiol. Rev.*, 1999, **79**, 181-213; b) F. M. Unger, *Adv. Carbohydr. Chem. Biochem.*, 2001, **57**, 207-435; c) R. P. McEver, *Curr. Opin. Cell Biol.*, 2002, **14**, 581-586; d) M. Sperandio, *FEBS J.*, 2006, **273**, 4377-4389.

[100] Z. Deng, M. Ahmed, R. J. Narain, , *J. Polym. Sci. Part A: Polym. Chem.*, 2009, 47, 614-627.

[101] A. M. Granville, D. Quemener, T. P. Davis, C. Barner-Kowollik, M. H. Stenzel, *Macromol. Symp.*, 2007, **255**, 81-89.

[102] N. Ayres, D. J. Holt, C. F. Jones, L. E. Corum, D. W. Grainger, *J. Polym. Sci. Part A: Polym. Chem.*, 2008, **46**, 7713-7724.

[103] W. Shi, S. Dolai, S. Averick, S. S. Fernando, J. A. Saltos, W. L`Amoreaux, P. Banerjee, K. Raja, *Bioconjugate Chem.*, 2009, **20**, 1595-1601.

[104] Godwin, A.; Müller, A. H. E.; Brocchini, S. *Angew. Chem., Int. Ed.* ,2001, **40**, 594.

[105] C. W. Scales, F. Huang, N. Li, Y. A. Vasilieva, J. Ray, A. J. Convertine, C. L. McCormick, *Macromolecules*, 2006, **39**, 6871-6881.

[106] M. J. Yanjarappa, K. V.Gujraty, A. Joshi, A. Saraph, R. S. Kane, *Biomacromolecules* 2006, **7**, 1665-1670.

[107] C.-Y. Hong, C.-Y. Pan, *Macromolecules* 2006, **39**, 3517-3524.

[108] J. Geng, J. Lindqvist, G. Mantovani, G. Chen, C. T. Sayers, G. J. Clarkson, D. M. Haddleton, QSAR Comb. Sci, 2007, 26, 1220-1228.

[109] J. Geng, G. Mantovani, L. Tao, J. Nicolas, G. Chen, R. Wallis, D. A. Mitchell, B. R. G. Johnson, S. D. Evans, D. M. Haddleton, *J. Am. Chem. Soc.*, 2007, 129, 15156-15163.

[110] R. Duncan, J. K. Coatsworth, S. Burtles, *Hum. Exp. Toxicol.*, 1998, **17**, 93-104.

[111] J.W. Hopewell, R. Duncan, D. Wilding, K. Chakrabarti, *Hum. Exp. Toxicol.* 2001, **20**, 461-470.

[112] M. Barz, M. Tarantola, K. Fischer, M. Schmidt, R. Luxenhofer, A. Janshoff, P. Theato, R. Zentel, *Biomacromolecules*, 2008, **9**, 3114-3118.

[113] M. I. Gibson, E. Fröhlich, H.-A. Klok, *J. Polym. Sci. Part A: Polym. Chem.*, 2009, **47**, 4332–4345.

[114] M. Herth, M. Barz, D. Moderegger, M. Allmeroth, M. Jahn, O. Thews, R. Zentel, F. Rösch, *Biomacromolecules*, 2009, **10**, 1697–1703.

[115] M. Barz, R. Luxenhofer, R. Zentel, A. V. Kabanov, *Biomaterials* 2009, ***30***, 5682-5690.

[116] E. Pedone, X. Li, N. Koseva, O. Alpar, S. Brocchini. *J. Mater. Chem.* 2003, **13**, 2825-2837.

[117] G. Sahay, E. V. Batrakova, A. V. Kabanov. *Bioconj. Chem.* 2008, **19**, 2023-2029.

[118] G. Sahay, J. O. Kim, A. V. Kabanov, T. K. Bronich. *Biomaterials,* 2009, DOI: 10-1016/j.biomaterials.2009.09.101, *in print*.

[119] G. Sahay, V. Gautam, R. Luxenhofer, A. V. Kabanov. *Biomaterials*, DOI: 10.1016/j.biomaterials.2009.11.020, *in print*.

[120] Y. Nemoto, A. Borovkov, Y.-M. Zhou, Y. Takewa, E. Tatsumi, Y. Nakayama, *Bioconj. Chem.* 2009 DOI: 10.1021/bc900283h, *in print*.

[121] J. Callahan, P. Kopeckova, J. Kopecek. *Biomacromolecules* 2009, **10**, 1704-1714.

[122] S. W. C. Richardson, K-L Wallom, E. L. Ferguson, S. P. E. Deacon, M. W. Davies, A. J. Powell, R. C. Piper, R. Duncan. *J. Control. Release* 2008, **127**, 1-11.

1.3 Applied *in vitro* and *in vivo* Methods

Beside modern tools for polymer synthesis and post polymerization functionalization various techniques were applied in this work to study the physical, chemical and biological properties of the synthesized polymers. Those techniques are essential for a better understanding of structure property-relationships, which determine superstructure formation, aggregate stability as well as any biological biological interaction. These key issues are responsible for *in vivo* as and *in vitro* fate of polymeric systems and therefore determine the application in nanomedicine.

The intention of this paragraph is to introduce basic principles, advantages and applications of the applied techniques. However, it has to be mentioned that this introduction cannot be detailed and therefore some aspects remain untouched.

1.3.1 Dynamic and Static Light Scattering

Light scattering is a well-known phenomenon, which appears in our daily life, e.g. the color of the sky and the Tyndall effect are scattering phenomena. An electromagnetic wave can interact with matter in different ways. On one side the atoms or molecules, of which all materials are composed, absorb the energy (thermal movement, fluorescence or phosphorescence) or scatter the light. To describe the interaction the classical wave picture can be applied. In this respect, an electromagnetic wave will interact with the charges in a given molecule polarizing the molecule. An electric dipole is induced, which acts itself as an emitter of a new electromagnetic wave of the same wavelength as the incident one. The scattered light is diffracted from the original beam of light. Whenever the energy (wavelength, frequency) of the scattered light remains untouched the process is called elastic scattering, does the frequency chance inelastic scattering has occurred. The elastic scattering of light can be used to gain much information about the scattering particle itself.

For all light scattering experiments a high intensity monochromatic light source, usually a laser, is launched in a solution containing the larger molecules, aggregates or nanoparticles and the intensity of scattered light is measured.

1.3.1.1 Static Light Scattering

Static light scattering can be used to obtain the absolute weight average molecular weight M_W of a macromolecule, the root mean square radius, also called the radius of gyration R_g. In addition, by measuring the scattering intensity for many samples of various concentrations, the second virial coefficient A_2, can be calculated.

The particle form factor P(q) is found to be:

$$P(q) = 1 - \frac{1}{3}q^2 s^2 + \ldots \qquad (1)$$

From the describtion of very small particles (scattering intensity is independent from the scattering angle) in dilute solution the basic equation for static light scattering experiments it is know to be:

$$\frac{Kc}{R} = \frac{1}{M} + 2A_2 c + \ldots \qquad (2)$$

For the larger particles treated in this paragraph, the normalized absolute scattering intensity R depends as well on the particle form factor P(q):

$$\frac{Kc}{R} = \frac{1}{M \cdot P(q)} + 2A_2c + ... \quad (3)$$

When definition of P(q) (1) is inserted into (3) the very important Zimm equation is derived:

$$\frac{Kc}{R} = \frac{1}{M}\left(1 + \frac{1}{3}s^2q^2\right) + 2A_2c \quad (4)$$

This equation provides the basis for analyzing the scattered intensity from comparatively small particles ($s^2q^2 << 1$, in case of light scattering: 10 nm < particle radius <50 nm) to determine the molar mass, the radius of gyration and the second Virial coefficient A_2, the latter providing a quantitative measure for the solute particle-solvent interactions. From this equation the Zimm plot can be derived, while at light scattering experiments are performed at several angles and at least 4 concentrations. From the Zimm plot a double extrapolation to zero angle and zero concentration can be performed yielding the mass average of the molecular weight of the polymeric sample.

1.3.1.2 Dynamic Light Scattering

In dynamic light scattering time-dependent fluctuation in the scattering intensity are used, which are due to the fact that the small molecules in solutions are undergoing Brownian molecular motion. This motion leads to constant changes in the distance between the scatterers in the solution within the experimental time. This scattered light can undergo either constructive or destructive interference by the surrounding particles and within this intensity fluctuations, information is contained about the time scale of movement (diffusion in solution) of the scatterers.

These dynamic information of the particles is derived from an autocorrelation of the intensity trace. The second order autocorrelation curve can be generated from the intensity trace:

$$g_2(q,\tau) = \frac{\langle I(q,t)I(q,t+\tau)\rangle}{\langle I(q,t)^2\rangle} \quad (5)$$

$g_2(q,\tau)$ is the autocorrelation function at a particular wave vector q, and delay time τ, and I is the intensity. At short observation times, the correlation is high due to the simple fact, that the particles do

not have a proper chance to move to a great extent from their initial state. The two signals are thus essentially the same when compared after only a very short time interval. As the time intervals get longer, the autocorrelation function starts to decay to zero exponentially, which means that after a long time period no longer any correlation between the scattered intensity of the initial and final states can be observed. This exponential decay is related to the diffusion of the particles, which is described by the diffusion coefficient. To fit the decay by the autocorrelation function, numerical methods are used, based on calculations of assumed distributions. If the sample is monodisperse then the decay is simply a single exponential. The Siegert equation relates the second order autocorrelation function with the first order autocorrelation function $g_1(q,\tau)$:

$$g_2(q,\tau) = 1 + \beta(g_1(q,\tau))^2 \tag{6}$$

where the parameter β is a correction factor that depends on the geometry and alignment of the laser beam in the light scattering setup. The most important use of the autocorrelation function is its use for size determination. Once the autocorrelation data has been generated, different mathematical approaches can be employed to determine the particle size from it. The analysis of the scattering is facilitated when particles collisions or electrostatic forces between ions are absent. Particle-particle collisions can be successfully suppressed by dilution, and charge effects are reduced by the use of salts to collapse the electrical double layer.

The simplest approach is to treat the first order autocorrelation function as a single exponential decay.

$$g_1(q,\tau) = \exp(-\Gamma\tau) \tag{7}$$

This is appropriate assumption for a monodisperse population of particles, where Γ is the decay rate. The translational diffusion coefficient D_s can be easily derived at a single angle or even better at a range of angles depending on the wave vector q.

$$\Gamma = D_s q^2 \qquad \text{with} \qquad q = \frac{4\pi n_0}{\lambda}\sin\left(\frac{\theta}{2}\right) \tag{8}$$

In here λ is the incident laser wavelength, n_0 is the refractive index of the sample and θ is angle at which the detector is located with respect to the sample cell.

Depending on the anisotropy and polydispersity of the system, a resulting plot of Γ/q^2 vs. q^2 may or may not show an angular dependence. Small spherical particles will not show any angular dependence, which means no anisotropy can be observed. A plot of Γ/q^2 vs. q^2 will result in a horizontal line. Particles with a shape other than a sphere will show anisotropy and thus an angular dependence when

plotting of Γ/q^2 vs. q^2. This will be in any case the translational diffusion coefficient. D_s can now be used to calculate the hydrodynamic radius of a particle through the Stokes-Einstein equation under the assumption that the particle itself is spherical.

$$D_s = \frac{kT}{6\pi\eta R_H} \tag{9}$$

It is important to note that the size determined by dynamic light scattering is the size of a sphere that moves in the same manner as the scatterer. So, for example, if the scatterer is a random coil polymer, the determined size is not the same as the radius of gyration determined by static light scattering. It is also useful to point out that the obtained size will include any other molecules or solvent molecules that move with the particle. So, for example particle with water attracted by its hydrophilic corona will appear larger by dynamic light scattering, which includes the layer of water molecules, than by transmission electron microscopy, which does not visualize the layer. So in many cases the particle diameter determined by cryo-TEM images is smaller than the hydrodynamic diameter from dynamic light scattering.

In almost all cases, polymer samples are polydisperse. In this respect, the autocorrelation function is a sum of the exponential decays corresponding to each of group of particles with in a certain narrow size range in the observed population.

$$g_1(q,t) = \sum_{i=1}^{n} G_i(\Gamma_i)\exp(-\Gamma_i\tau) = \int G(\Gamma)\exp(-\Gamma\tau)d\Gamma \tag{10}$$

It is tempting to obtain data for $g_1(q,\tau)$ and attempt to invert the above to extract $G(\Gamma)$. Since $G(\Gamma)$ is proportional to the relative scattering from each species, it contains information on the distribution of sizes. The following method has been developed among others to gain as much useful information as possible from an autocorrelation function.

This most common used method is the cumulant method, from which in addition to the sum of the exponentials above, more information can be derived about the variance of the system as follows:

$$g_1(q,t) = \exp(-\bar{\Gamma}\tau)\cdot\left(1 + \frac{\mu_2}{2!}\tau^2 - \frac{\mu_3}{3!}\tau^3 + \ldots\right) \tag{11}$$

where $\bar{\Gamma}$ is the average decay rate. The average translational diffusion coefficient $\langle D_s \rangle$ may be derived at a single angle or at various angles depending on the wave vector q.

$$\bar{\Gamma} = d^2 \langle D_s \rangle \tag{12}$$

One must note that the cumulant method is valid for small τ and sufficiently narrow G(Γ). Nevertheless this method can be applied to determine an average diffusion coefficient, which can be transferred into an average hydrodynamic radius using the Stokes-Einstein equation (9).

In addition the r-ratio will be mentioned in this work. This ratio is an experimental quantity, which provides important information about the topology of the scattering particle. This information is especially valuable for small particles, where a detailed analysis of the particle form factor is not possible. This r-ratio can be calculated from the experimentally derived hydrodynamic radius and the radius of gyration. It is defined as:

$$\rho = \frac{R_g}{R_H} \tag{13}$$

For example, the ratio is 0.78 for a homogeneous spherical particle, 1 for a hollow sphere and 1.51 for a random polymer coil.

Literature:

[1] Schärtl W. Light Scattering from Polymer Solutions and Nanoparticle Dispersions. Springer-Verlag Berlin Heidelberg 2007.

1.3.2 Fluorescence Correlation Spectroscopy

Fluorescence correlation spectroscopy (FCS) is a common technique to characterize dynamics of fluorescent species, e.g. single fluorescent dye molecules, fluorescent proteins in living cells or polymeric nanoparticles either in buffer or in living cells. FCS is in a way the fluorescent counterpart to dynamic light scattering affording coherent light scattering instead of (incoherent) fluorescence. The term spectroscopy may sound a little bit odd, because it is commonly used for a method providing a frequency spectrum. The autocorrelation is a form of spectrum. It is the time-spectrum generated from the power spectrum via an inverse Fourier transformation.

The FCS setup is usually comparable to the one used in optical microscopy, in particular confocal or two photon microscopy. In these techniques light is focused on a sample and the measured fluorescence intensity fluctuations, as mentioned in the DLS paragraph due to diffusion (Brownian Motion), physical or chemical reactions or aggregation, are analyzed. Thus, a temporal autocorrelation function can be derived. Since the measured fluorescence is essentially related to the magnitude and the number of fluctuations, there is an optimum measurement regime at the level when individual species enter or exit the observation volume. When too many entities are measured at the same time the overall fluctuations are small compared to the total signal and may not be resolvable or the overall intensity of fluorescent light is to high and may cause problems with the detectors. But of course filters can solve this problem to a certain point. In the other direction, if the individual fluctuation-events are too sparse in time, one measurement may take too long. With the development of sensitive detectors, e.g. avalanche photodiodes, the detection of the fluorescence signal coming from individual molecules in highly dilute samples has become practical.

When an appropriate model can be applied, FCS can be used to obtain quantitative information, for excample diffusion coefficients, hydrodynamic radii or average concentrations.

One major advantage of FCS is its specificity in investigating fluorescent species only. Fluorescent markers are available in a variety of colors and can be covalently or electrostatically bound to a particle or even simply encapsulated inside. Thus, it is possible to study the behavior of each individual particle in solutions as each dye can be excited separately. One limitation is the penetration depth of light but these limits are similar to in fluorescence microscopy enabling investigations on a cellular level.

The typical FCS setup consists of a laser emitting light of wavelengths ranging typically from 405 - 633 nm, which is reflected into a microscope objective by a dichroic mirror. The laser beam is focused in the sample, which contains the fluorescent particles highly diluted. Ths, only 1 - 100 particles are within the focal spot (≈1 femtoliter). When the particles cross the focal volume, they fluoresce. This

light is collected by the same objective and, because it is red-shifted with respect to the excitation light, it passes the dichroic filter reaching a detector, typically a photomultiplier tube or avalanche photodiode detector. The resulting electronic signal can be used either directly as intensity versus time trace to be analyzed at a later point, or Fourier-transformed to generate the autocorrelation directly (see figure 7).

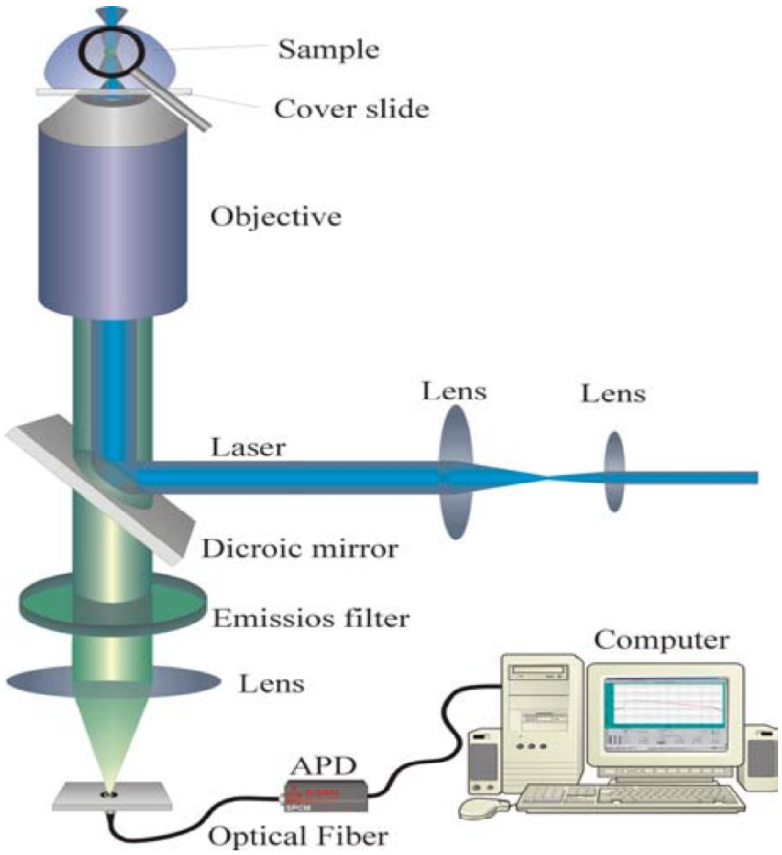

Figure 8. Schematic setup of a fluorescence correlation spectroscopy (FCS) experiment [1]

The autocorrelation function for one freely diffusing species of particles is found to be:

$$G(\tau) = \frac{1}{V_{ef} f \langle C \rangle} \cdot \frac{1}{\left(1 + \frac{\tau}{\tau_D}\right)} \cdot \frac{1}{\sqrt{1 + \left(\frac{r_0}{z_0}\right) \cdot \frac{\tau}{\tau_0}}} \tag{12}$$

When the focal volume is known from a calibration measurement, the local concentration of fluorescent molecules can be determined from the amplitude G(0) of the autocorrelation curve. For multiparticle systems the equation turns out to be much more complicated. The calibration of the

confocal volume can be done using a reference standard with known diffusion coefficient. A common dye applied to calibration is rhodamine.

$$\langle C \rangle = \frac{1}{V_{eff} \cdot G(0)} \tag{13}$$

As mentioned above, the diffusion time τ_D is related to the diffusion coefficient D of the species through $D = r_0^2/4\tau_D$. When the diffusion coefficient is known, the hydrodynamic radius of the particle can be calculated using the Stokes-Einstein equation: $R_h = k_B T/6\Pi\eta D$, where k_B is the Boltzmann constant, T is the temperature, and η is the viscosity of the solution. Similarily to DLS, the radius determined by FCS is the hydrodynamic radius.

Literature

[1] Schwille P. Fluorescence correlation spectroscopy. Theory and applications, Elson EL, Rigler R, Eds., Springer, Berlin, 2001;360

[2] Thomson NL. Topics in Flourescence Spectroscopy. J. Jakowicz Ed., Plenum Press, New York, 1991;1:337

1.3.3 Pyrene Fluorescence Spectroscopy

The pyrene fluorescenc spectroscopy can be used to investigate the local polarity around an individual pyrene molecule. Thus, it can be used to determine critical micelle concentration (CMC) of polymers. It has to be mentioned, that the CMC can also be determined by light scattering or fluorescence correlation spectroscopy (FCS). However, both methods are limited to a certain range of concentrations. In addition, a complex experimental setup is needed. The pyrene spectroscopy is based on the emission spectra of pyrene depending on the polarity of the pyrene surrounding. Pyrene has a very low solubility in water and upon formation of micelles, the molecules are transfered preferentially into their hydrophobic cores. This is accompanied by a red shift in the pyrene fluorescence spectrum and changes in relative peak intensities of the spectrum's vibrational fine structure. [1,2] To determine the onset of the micelle formation the pyrene emission spectra as reported previously by Müller et al. [3] as well as by Winnik [4] and coworkers has to be analyzed. The method is based on changes in the intensity of the vibrational bands of pyrene solubilized in water and in micellar medium.

a) b)

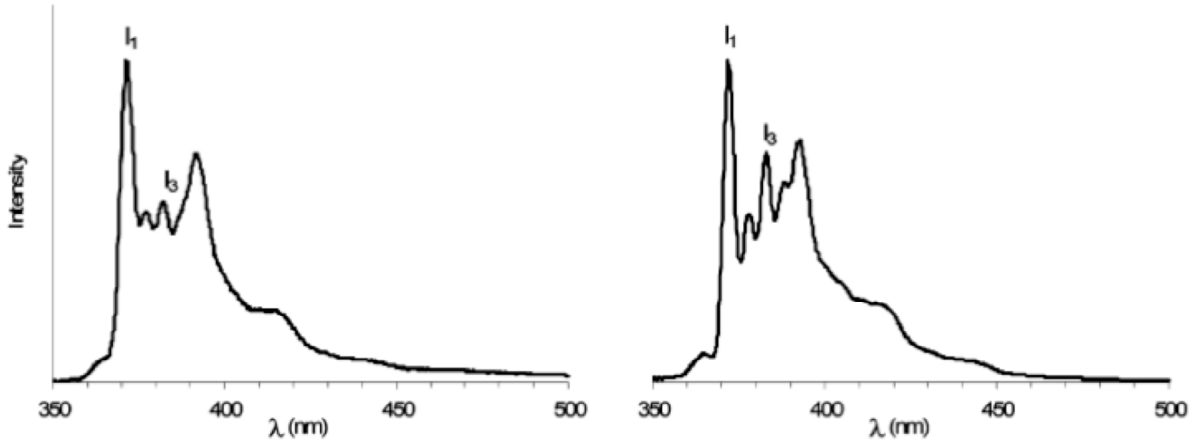

Figure 9. Pyrene emission spectra of a solution containing an amphiphilic block copolymer (surfactant) at concentrations a) below and b) above the CMC. [1]

Figure 9 clearly reveals the vibrational structure of fluorescence spectra depending on the block copolymer concentration. The ratio of the first vibrational band (372 nm), the highest energy vibrational band, to the fluorescence intensity of the third vibrational band (385 nm) has been shown

to correlate with solvent polarity [2]. For example, the ratio I1/I3 is 0.6 in hydrocarbon solvent and 1.6-1.8 in water.

It is well established that in block copolymer solutions the plot of I1/I3 versus polymer concentration shows a typical sigmoid shape. Figure 10 shows the results found for poly(HPMA)-block-poly(lauryl methacrylate) copolymers.

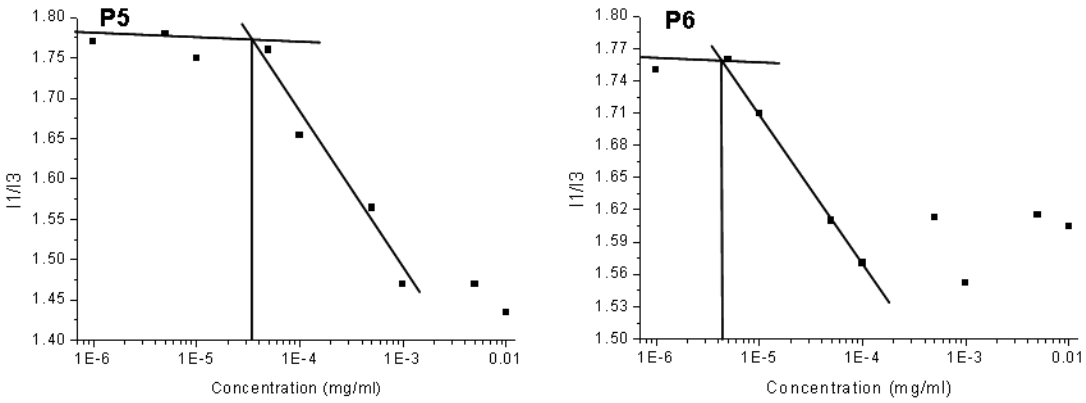

Figure 10. CMC-determination of poly(HPMA)-block-poly(lauryl methacrylate) **P5** and **P6** copolymers. The I1/I3 ratios are plotted versus the blockcopolymer concentrations. [5]

Below the CMC the I1/I3 ratio corresponds to its polar microenvironment. When the polymer concentration increases the ratio decreases rapidly as a consequence of the more hydrophobic environment of pyrene. Above the CMC the I1/I3 ratio reaches a constant value due to the incorporation of pyrene into the hydrophobic region of the micelle [6]. The CMC is obtained from the interception of the horizontal and the steep parts of the curve.

Literature

[1] Kalyanasundaram K, Thomas JK. J. Am. Chem. Soc. 1977;99:2039-44

[2] Kalyanasundaram K, Thomas JK. J. Phys. Chem. 1977;81:2176-80

[3] Colombani O, Ruppel M, Schubert F, Zettl H, Pergushov DV, Müller AHE. Macromolecules 2007;40:4338-50.

[4] Wilhelm M, Zhao CL, Wang Y, Xu R, Winnik MA, Mura JL et al. Macromolecules 1991;24:1033-40.

[5] Barz M, Luxenhofer R, Zentel R, Kabanov AV. Biomaterials 2009;30:5682-90

[6] Ananthapadmanabhan KP, Goddard ED, Turro NJ, Kuo PL. Langmuir 1985;1:352-5

1.3.4 Confocal Fluorescence Microscopy

Whenever intracellular localization of polymeric nanoparticles is under investigation confocal microscopy techniques are essential. Confocal laser scanning microscopy (CLSM or LSCM) is a technique for obtaining high-resolution optical images with depth selectivity. [1] The key feature of confocal microscopy is its ability to acquire in-focus images from selected depths. Slices in z range can be obtained. Images are acquired point-by-point and reconstructed with a computer, allowing the reconstruction of three-dimensional images of the observed objects.

A conventional microscope "looks" as far into the specimen as the light can penetrate, while a confocal microscope only images one z-level at a time. Effectively, the CLSM achieves a controlled and highly limited depth of focus, which allows to precisely locate the nanoparticles inside a cell. Since its development in the 1960s it has taken another thirty years untill the development of lasers for CLSM has become a standard technique in biological, medical as well as materials science. [1]

In a confocal laser scanning microscope (see figure1), a laser beam passes through a light source aperture and is then focused by an objective lens into a small focal volume within or on the surface of an object.

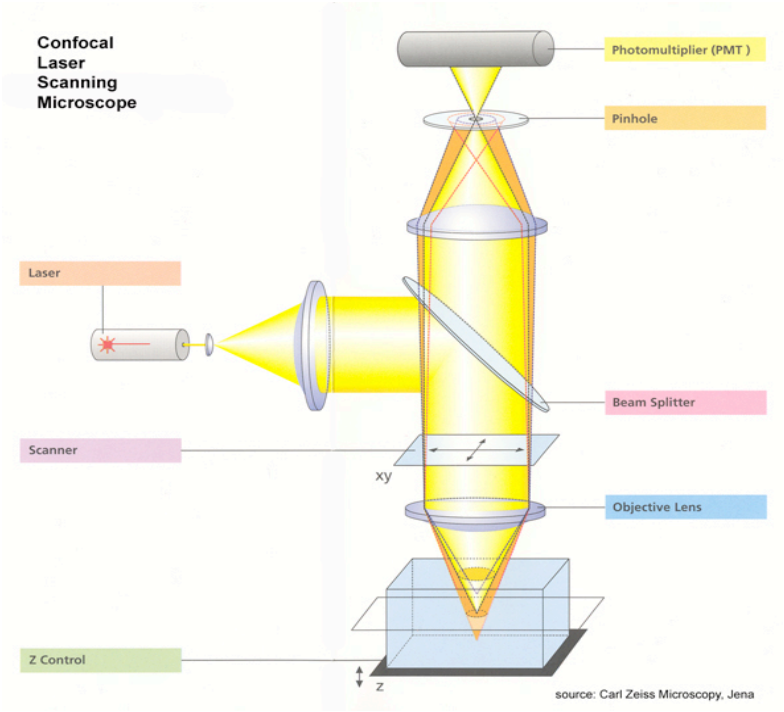

Figure 11. Scheme of the essential parts of a confocal laser scanning microscope (CLSM)

Especially in biological applications, the specimen may be fluorescent and within a cellular compartment. Scattered and reflected laser light as well as any fluorescent light from the illuminated spot is afterwards re-collected by the objective lens. A beam splitter separates off some portion of the light into the detection apparatus, which in fluorescence confocal microscopy will also have a filter that selectively passes the fluorescent wavelengths while blocking the original excitation wavelength. After passing a pinhole, the light intensity is usually detected by a photomultiplier tube (PMT) or avalanche photodiode, transforming the light signal into an electrical that is recorded by a computer. [2]

The out-of-focus light is suppressed: most of the returning light is blocked by the pinhole, which results in sharper images than those from conventional fluorescence microscopy techniques and allows to obtain z stacks images at various depths within the sample. [1]

Confocal microscopy provides the capacity for direct, noninvasive, cellular imaging with a minimum of sample preparation as well as a marginal improvement in lateral resolution. [2] Biological samples are often treated with fluorescent dyes to make selected objects visible. In this work the CLSM is used to explore the intracellular colocalization of fluorescently labeled polymeric nanoparticles. Fluorescent markers for cellular compartments, e.g. DRAQ5 (nucleus marker) or dextrane texas red (lysosomal maker), were applied to the confocal experiments. Whenever colocalization of the nanoparticle fluorescence with the compartment label occurred, the position of the macromolecule was detected.

To this respect, confocal laser scanning microscopy is the method of choice for studies concerning the precise intracellular localization of labeled particles.

Literature:

[1] Pawley JB. Handbook of Biological Confocal Microscopy (3rd ed.). Springer, Berlin. 2006.

[2] Walla PJ. Modern Biophysical Chemistry: Detection and Analysis of Biomolecules. Wiley-VCH, Weinheim, 2009.

1.3.5 Fluorescence Activated Cell Sorting (FACS)

Fluorescence activated cell sorting (FACS) is usually done using a commercial flow cytometer. [1] The flow cytometry developed in the 1960s is a technique, which is commonly applied for counting and examining cells or chromosomes, by suspending them in a solution and passing them through an optical detector. It allows simultaneous multiparametric analysis of the physical as well as chemical characteristics of up to thousands of particles per second. Flow cytometry is widely used in diagnosis of health disorders, especially blood cancers. In addition, it has many other applications in both research and clinical practice. A second slightly different approach is to physically sort particles based on their properties, thus purifying populations of interest.

The flow cytometer is based on five main components: a flow cell, an optical system (a laser), a detector and analogue-to-digital conversion (ADC) system - which converts signals from light into electrical signals that can be processed by a amplification system and a computer for analysis of the signals (see figure 1). In fluorescence activated cell sorting an additional unit for the sorting of cell is attached. In this unit the cells are separated into different containers.

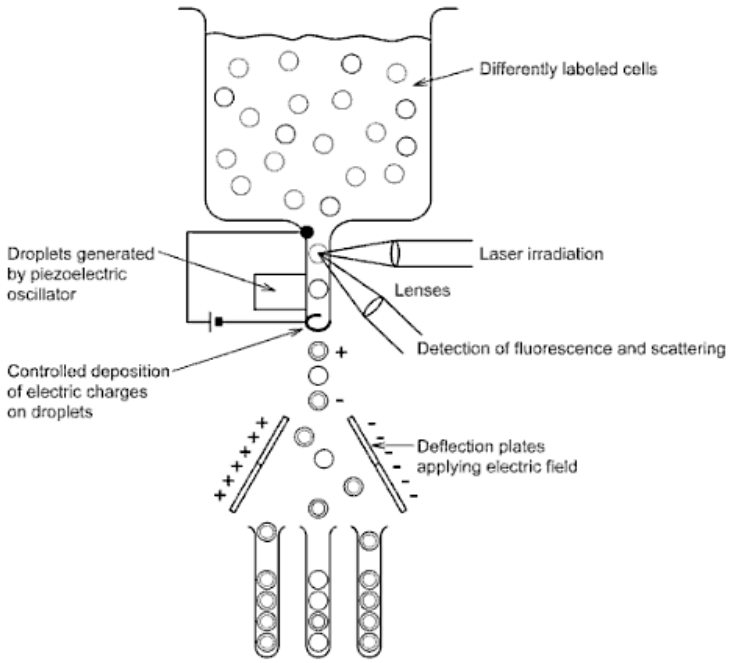

Figure 12. Schematic sketch of a flow cytometer for fluorescence activated cell sorting (FACS).

Usually a beam of laser light of a single wavelength is directed onto a focused stream of fluid. A number of detectors are aimed at the point where the stream passes through the light beam. One

detector is in line with the light beam (Forward Scatter or FSC) and several others are perpendicular attached to it (Side Scatter (SSC) and one or more fluorescent detectors). Each suspended particle from 0.2 to 150 micrometers passing through the beam scatters light, and fluorescent chemicals found in the particle or attached to the particle may be excited into emitting light at a higher wavelength than the light source. The combination of scattered and fluorescent light is detected by the detectors inside the flow cytometer. In real time, a computer analyses fluctuations in brightness at each detector. Thus, it is possible to derive various types of information about the physical and chemical structure of each individual particle. FSC correlates with the cell volume and SSC depends on the inner complexity of the particle. When the detected particles have to be separated from the population a certain process has to be applied. For cell sorting the flow has to be arranged in a way that large separation between cells relative to their diameter is possible. A vibrating mechanism causes the stream of cells to break into individual droplets. The system is adjusted, as there is a low probability of more than one cell per droplet. Just before the stream breaks into droplets, the flow passes through a fluorescence measuring station where the fluorescent character of interest of each cell is measured. An electrical charging ring is placed just at the point where the stream breaks into droplets. A charge is placed on the ring based just after fluorescence measurement, and the opposite charge is trapped on the droplet as it breaks from the stream. The charged droplets then fall through an electrostatic deflection system diverting the droplets into containers based upon their charge. In some systems, the charge is applied directly to the stream, and the droplet breaking off retains charge of the same sign as the stream.

In our experiments the flow cytometer was used to study the uptake kinetics of polymeric particles. In the experiments mentioned in this work a separation of cells was not necessary. In order to apply the flow cytometry, the polymers were fluorescently labeled and incubated with adherent cells. After different incubation times and temperatures the cells were removed from the plates and transferred into the vials of the flow cytometer, which separated the cells into specimen with and without polymer-associated fluorescence. In addition, the mean cell associated fluorescence was derived offering a certain value for internalization efficiency.

Literature:

[1] Walla PJ. Modern Biophysical Chemistry: Detection and Analysis of Biomolecules. Wiley-VCH, Weinheim, 2009.

1.3.6 Electrical Cell-Substrate Impedance Sensing (ECIS)

Electric Cell-substrate Impedance Sensing (ECIS) provides a method to perform real time cell monitoring without the use of biological markers. The principle of ECIS is the measurement of changes in impedance of a small electrode in alternating current (AC) fields. The impedance is defined as the ratio of the voltage to the electric current at the test cell. It is the analogue to the resistance in a direct current (DC) field. The measurement unit is a specialized slide that has individual wells, where cells can be easily cultured (see figure 1a). The bottom of the slide has an array of gold film electrodes connecting the ECIS electronics to each of the wells.

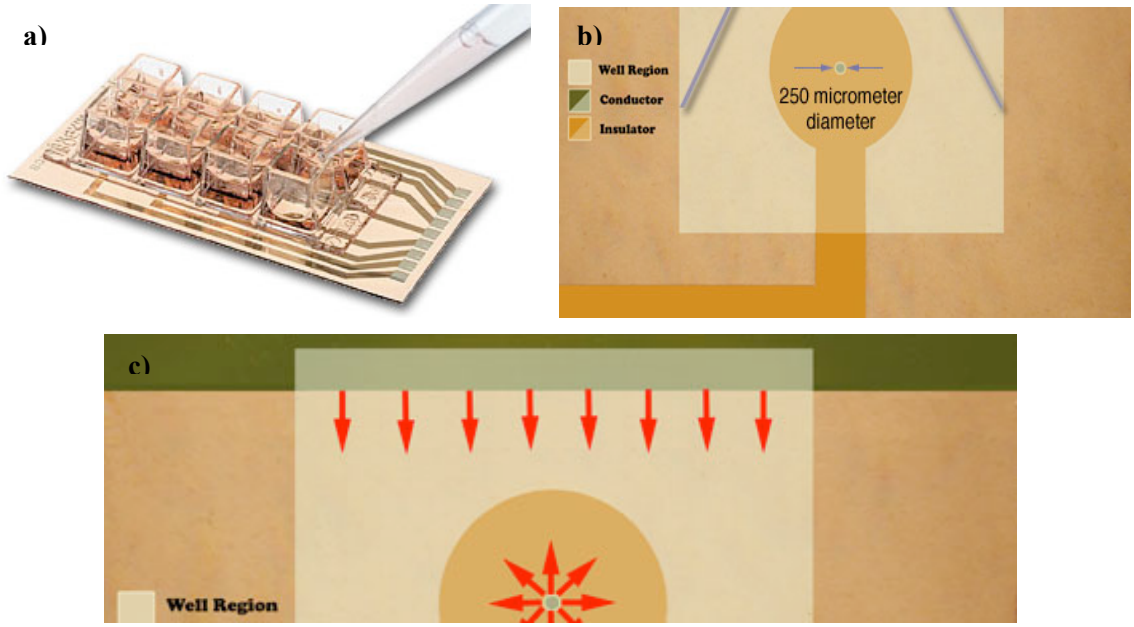

Figure 13. a) Commercially ECIS 8 well array. b) Top view onto the 250 µm diameter electrode after the wells have been removed c) top view on the electrode indicating the current flow between the small active electrode and the counter electrode (images taken from Applied BioPhysics).

The principle of all ECIS measurements can be described as follows [1]: Without adherent cells attached onto the electrode, the current flows unrestrained from the surface of the electrodes. The cell medium acts as a conducting electrolyte due to it`s pronounced ion content. In the presence of adherent cells on the active electrode, their insulating plasma membranes constrain the electrical

current and limit it to regions beneath and between the cells. The isolating character of cell membranes is essential for living cells. It allows building up a concentration gradient between the intracellular and extracellular space. As an example lipid bilayers are 10^9 times more permeable to water than to even small ions such as Na^+ or K^+. The strong electrical interaction of ions and water leads to the formation of a corona of water molecules surrounding an ion, which inhibit them from passing through the hydrocarbon phase of the lipid membrane. [2] The convoluted current path due to the isolating character of the cell membrane causes large changes in the measured impedance. Although this is taking place at both the small electrode as well as at the counter electrode, the impedance of the small electrode is several hundred times larger, and consequently the contribution of the large counter electrode is a fraction of a percent and can be ignored.

As an example, the impedance is about 2000 ohms when no cells are attached. But when adherent cells are attached to the electrode it easily can reach to a 5 - 7 times higher value. To this respect, the measurements are directly related to the isolating properties of the cellular membrane. When cells are exposed to a substance, e.g. polymeric particles, cell-particle interactions will occur. The particle may influence membrane properties or directly cell viability at a certain concentration. Usually in the case of adherent cells, a reduced cell viability will lead to a reduced amount of cells on the electrode and a decreasing impedance can be observed. Thus, ECIS can be used to study changes in the cell membrane resistance, most likely related to it`s fluidity. In addition, the level of impedance can be correlated to the cell viability and therefore provides an alternative method to determine cell toxicity of various substances. [3,4]

Literature:

[1] Giaever I, Keese CR. A morphological biosensor for mammalian cells, Nature 1993;366:591-592.

[2] Alberts B, Bray D, Johnson A, Lewis J, Raff M, Roberts K, Walter P. Essential Cell Biology: An Introduction to the Molecular Biology of the Cell. Garland Publishing. New York & London. 1998.

[3] Giaever I, Keese C. Use of Electric Fields to Monitor the Dynamical Aspect of Cell Behavior in Tissue Culture. IEEE Trans. Biomed. Eng. 1986;33:242-247.

[4] Sapper A, Wegener J, Janshoff A. Biological activity of cells probed by noise analysis of thickness shear mode resonators: a new means to measure vertical cell motility. Anal. Chem. 2006;78:5184-5191.

1.3.7 Positron Emission Tomography (PET)

The positron emission tomography (PET) is an imaging technique in radiopharmacy and nuclear medicine, which allows three- dimensional *in vivo,* non-invasive, quantitative, kinetic and repetitive imaging of processes within living bodies. Especially, *in vivo* biodistribution of drugs or polymeric nanoparticles can be evaluated in PET studies by applying β^+-emitting radioactive analogues. Common β^+-emitting elements are carbon-11 ^{11}C(~20 min), nitrogen-13 (^{13}N, $t_{1/2}$ ~10 min), oxygen-15 (^{15}O, $t_{1/2}$ ~2 min), and fluorine-18 (^{18}F, $t_{1/2}$ ~110 min). PET offers a great opportunity to study the *in vivo* fate of injected particles and therefore it has to be considered as a key technique in the development of future polymer therapeutics. Thus, it is possible to derive useful information regarding to circulation, accumulation and elimination kinetics. This knowledge will greatly influence the further development of nanomedical devices. In addition, PET has already become a widely accepted tool for molecular imaging. It is clinically accepted for diagnostic use in patients with certain brain or heart diseases as well as various cancer subtypes.

PET imaging principle makes use of the unique decay characteristics of a number of positron emitting radionuclides. The scheme of a PET scanner is shown in figure 1.

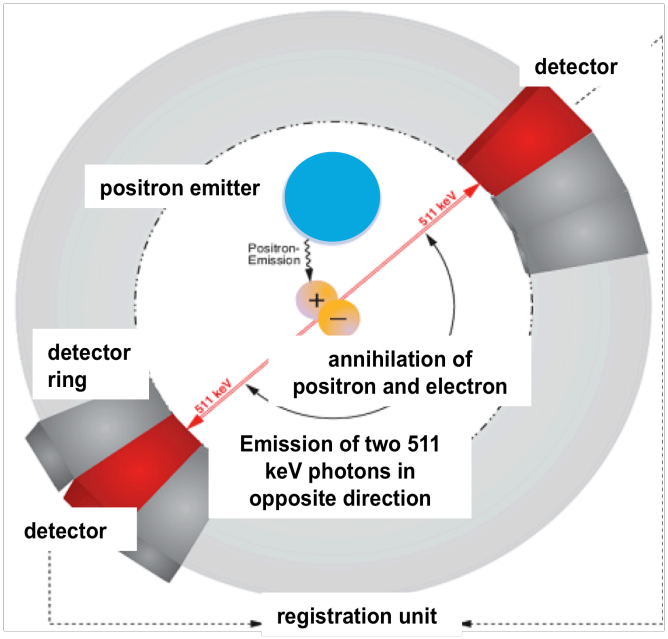

Figure 14. Schematic image of the annihilation detection process in positron emission tomography (PET) (modified from [1])

A neutron-deficient isotope inside its atomic nucleus converts a proton into a neutron with subsequent emission of a positron, a particle with the opposite charge of an electron, from the nucleus. The positron annihilates an electron and a pair of gamma rays is emitted. The most significant fraction of electron-positron decays result in two 511 keV gamma photons being emitted at almost 180 degrees to each other; hence it is possible to localize their source along a straight line of coincidence (also formally called the line of response or LOR). The PET scanner is able to detect these gamma rays.

The signal intensity in each of the image voxels is proportional to the amount of radiotracer therein and thus can be used for quantitative analyses. By measuring tissue concentration of radiotracers in a time sequence the biodistribution kinetics of macromolecules can be determined and there of mathematical modeling can be applied. As for the preliminary data presented in this work, a more detailed discussion is not necessary.

In contrast to magnetic resonance imaging (MRI) or computed tomography (CT), which mainly provide anatomic information, PET enables functional, diagnostic imaging. In addition, PET and also SPECT (Single Photon Emission Computed Tomography) offer advantages of high sensitivity. An average amount 10^{-12} M tracer is needed for the imaging process. The small amount of radioactive marker can be expected to hardly influence the structure and aggregation of the polymer aggregate itself and therefore does not change it`s character. A further advantage is the isotropism (*i.e.*, ability to detect expression accurately, regardless of tissue depth) of PET, which provides reliability for *in vivo* quantitative imaging analyses.

In the work presented in paragraph 2.8 and 2.9 we have applied ^{18}F and $^{72/74}$As as a positron emitter. While ^{18}F has a half-life time ($t_{1/2}$) of 110 min, arsenic offers half-life times depending on the isotope from 26 h (^{72}As) to 17,7 days (^{74}As). The labeling strategy differs for both emitting elements. In the case of arsenic free thiol groups can be used to bind arsenic to the polymeric structure as described in chapter 2.9.

In contrast a direct fluorination of polymers using ^{18}F is rather difficult. To this respect, a radioactive synthon was prepared. In an automated synthesis the radioactive fluoride undergoes a nucleophilic substitution reaction with ethylene di(p-toluenesulfonate) yielding fluoroethyltosylat ([^{18}F]FETos). [^{18}F]FETos can be used in the next step to label nucleophilic groups within the polymer. During the presented research in this work we were able to establish the first ^{18}F labeling strategy for polymers (see chapter 2.8), which is until today one of the very approaches for the labeling of polymers with β^+-emitters. The labeled polymers could be nicely monitored in vivo in a Kopenhagen rat model.

In summary, PET offers a powerful tool for in vivo imaging of polymeric particles. Due to the characteristics of polymers themselves even macromolecular imaging agents may enter clinical practice. And maybe in future highly specific imaging of various disfunctions or diseases may improve medical diagnostic and treatment.

Literature:

[1] Herzog H, Rösch F. Pharm. unserer Zeit 2005;34:468-73

[2] Saha GB, Basics of PET Imaging: Physics, Chemistry, and Regulations. 1 ed. Springer. Berlin. 2004.

1.4 Motivation and Aim of Research

Until today Paul Ehrlich`s concept of selective therapeutic has not been realized yet, however, the concept involved is still the basic idea of research among different disciplines of science. At least, the selective delivery to the side of a disease could be identified as highly complex. To this respect, it seems reasonable to use multifunctional systems, which are most likely polymers as first proposed by H. Ringsdorf in the 1970s.

After all, the concept itself is rather simple, the translation into polymer therapeutics is much more complicated. Nevertheless some polymer-based drugs have shown a certain potential and could therefore enter clinical trials. These systems offer some advantages compared to low molecular weight therapeutics, although they do not act as a “magic bullet”. In chemotherapy, as a prominent example, polymer-drug conjugates help to reduce side-effects by a more selective delivery of a cytotoxic drug. The enhanced selectivity is related to the properties of the polymer itself, e.g size, charge, polarity and immunogenic properties. In addition, targeting moieties can be used to tune to *in vivo* distribution. Thus, there is need for polymeric systems, which can be synthesized and functionalized in a controlled way. The size of the particle is related to the molecular weight of the polymer, as long as aggregation does not occur. On the other hand aggregation can be used to create superstructures such as micelles, polymersomes or compound micelles. The aggregates have molecular weights up to millions and sizes in up to some hundred nanometers consisting of single amphiphilic polymers. These systems are rather interesting for therapeutic applications. On the one hand, they will avoid renal clearance and even other therapeutic agents can be conjugated as well as encapsulated. Since more important for polymers with non-degradable backbones, their molecular weight (chain length) of the individual polymer can be kept below the renal exclusion limit. If the polymer can be degraded yielding a hydrophilic polymer, most likely no aggregation occurs and the single non-degradable parts can be eliminated from the body.

This approach was already used extensively by K. Kataoka et al. in PEG-based block copolymers, but these systems are only mono- or bifunctional, which can be a drawback in the creation of multifunctional carriers. As for desired multifunctional systems, functional polymers are mandatory. These systems are based on H. Ringsdorfs concept and have lead into clinical trail of PK1 and PK2 by R. Duncan and coworkers. Thus, it would be rather interesting to combine both approaches, as it is possible nowadays by the use of controlled/living radical polymerization.

After developing a synthetic pathway to these structures, these systems have to be applied to *in vitro* and *in vivo* experiments evaluating the potential of these new type of polymers, which essentially combine the idea of aggregates with multifunctional polymers. However, as for *in vitro* and *in vivo* experiments imaging agents have to be conjugated as well, especially for *in vivo* evaluations new markers may appear reasonable to understand the fate of the complex architectures.

The motivation of this work was to derive these systems and to explore their properties in *in vitro* as well as *in vivo* applications with a view towards better polymer based therapeutics. But besides developing concepts for new nanomedical devices, it would be rather interesting to explore structure-property relationships of these systems. For the first time it should be possible to combine the structural freedom of controlled radical polymerization techniques with biological or medical needs.

Of course, this work cannot be used to answer all the points mentioned, but maybe it offers a small contribution to a promising concept, which may one day fulfill to the dream of a “magic bullet”.

2.1. Synthesis and postpolymerization mocification of Polypentafluorophenyl methacrylates (PPFMA): A promising plattform for functional N-(2-hydroxypropyl)-methacrylamide (HPMA) polymers

unpublished results

Author: Matthias Barz[1], R. Forst[1], R. Zentel[1]

Address: [1]Institute of Organic Chemistry, Johannes Gutenberg-University Mainz, Duesbergweg 10-14, 55099 Mainz, Germany

Abstract

In this work we report the synthesis of well-defined pentafluorophenyl methacrylate (PFMA) polymers by the use of the reversible addition fragmentation chain transfer (RAFT) polymerization method. In addition, their postpolymerization modification yielding functional N-(2-hydroxypropyl)-methacrylamide (HPMA) polymers is described in detail. Various activated ester polymers have been synthesized. The molecular weights were in the range of 15 kDa to 121 kDa with a polydispersity index from 1.2-1.3 determined by gel permeation chromatography (GPC). The reactive polymers were transferred into HPMA-based systems by a postpolymerization modification using 2-hydroxypropylamine. The conversion kinetics of the PPFMA were monitored using ^{19}F NMR at 30, 60 and 90 °C temperatures. Complete conversion of the activated ester was observed after 90 min at 90 °C and 8 h at 60 °C. In contrast, the reaction needed 48 h reaction time at 30 °C and additional quenching until all PPFMA was converted. In addition, the polymer analogous reaction was performed with a *t*-Boc protected 2-hydroxypropylamine to investigate the reactivity of the hydroxyl group against the activated ester. At temperatures up to 70 °C no conversion of the PPFMA could be observed indication chemical stability of the activated ester towards the hydroxyl functionality.

Furthermor, we could ensure non-toxic behavior of the PHPMA polymer derived from the PPFMA activated ester up to a concentration of 3mg/mL in human cervix adenocarcinoma (HeLa) cells. In this respect, PPFMA activated ester can be used as a suitable precursor system in the preparation of various HPMA-based polymer architectures.

1. Introduction

During the last years tremendous improvements have been made in the free radical synthesis as well as in the field of activated ester polymers. The development of the living free radical polymerization (LRP) methods such as ATRP [1-4], NMP [5,6] and RAFT [7-10] has pushed the radical polymerization into a new age. These methods allow for precise control of molecular weight, composition, architecture, as well as end group functionality. Well-defined functional polymers can be easily synthesized in suitable amounts and time, which are not accessible by anionic or cationic polymerization techniques. For the preparation of these functional polymers, direct polymerization of the corresponding monomer is clearly the most convenient way. But there is still a variety of monomers that cannot be polymerized directly via the LRP methods. These polymers have to protected during the polymerization and deprotected afterwards. In addition, the synthesis of polymer libraries with identical chain lengths and chain-length distributions but variable side-chain functionality is enabled. Such polymer libraries are powerful tools to establish structure–property relationships as reported by Barz et al. for functional P(N-(2-hydroxypropyl)-methacrylamide)-block-P(lauryl methacrylate) copolymers and Brocchini et al for various acrylamides. [11,12] In this respect, the use of activated ester proposed by Ringsdorf et al. in the early 70s of the last century is elegant way. [12-14] Compared to the [1,3] dipolar Huisgen cycloaddition [15,16,17] it has the major advantage that no cupper catalyst is needed during the reaction, which has to be removed afterwards. In addition the activated ester approach can be used to derive acrylamide based structures such as the Food and Drug Administration (FDA) approved N-(2-hydroxypropyl)-methacrylamide (HPMA), which is a great advantage for further development of nanomedical devices. On the other hand activated ester polymers have been used in polymer therapeutics for linking a drug or targeting moiety to a polymer. The most prominent examples are the first polymer drug conjugates undergoing clinical trails in the end of the last century. [18-20]

Beside the well-established poly(N-acryloxy-succinimide) (PNAS) the number of activated ester polymers has increased offering tunable reactivity. [14] Among these systems the pentafluorophenyl methacrylate PPFMA has to be mentioned in detail. [21] This activated ester can be easily polymerized using the RAFT polymerization method and additionally it has the great benefit that the reaction kinetics can be directly monitored by ^{19}F NMR. [22] The PPFMA was already used to create functional HPMA-based structures by either Barz et al. as well as Klok and coworkers. [23-28]

In this work we would like to focus on the conversion kinetics of the polymeric activated ester with 2-hydroxypropylamine at various temperatures. In addition, we have investigated the stability of PPFMA against to hydroxyl group of the amine by protection the amino functionality, in order to exclude side reactions. All these mentioned studies have been performed by use of ^{19}F NMR.

2. Materials and Methods.

2.1 Materials.

All chemicals were reagent grade and obtained from Aldrich. The chemicals were used without further purification unless otherwise indicated. The Oregon green 488 cadaverine was obtained from Invitrogen. Dioxane used in the synthesis was freshly distilled from a sodium/potassium mixture. 2,2'-Azobis(isobutyronitrile) (AIBN) was recrystallized from diethyl ether and stored at -7°C.

2.2 Characterization.

^{1}H- and ^{19}F-NMR spectra were obtained at 400 MHz using a FT-spectrometer from Bruker and analyzed using the ACDLabs 6.0 software. The polymers were dried at 40 °C over night under vacuum and afterwards submitted to gel permeation chromatography (GPC). GPC was performed in tetrahydrofurane (THF) as solvent and with following parts: pump PU 1580, auto sampler AS 1555, UV-detector UV 1575, RI-detector RI 1530 from Jasco and miniDAWN Tristar light scattering detector from Wyatt. Columns were used from MZ-Analysentechnik: MZ-Gel SDplus 10^2 Å, MZ-Gel SDplus 10^4 Å and MZ-Gel SDplus 10^6 Å. The elution diagrams were analysed using the ASTRA 4.73.04 software from Wyatt Technology. Calibration was done using polystyrene standards. The flow rate was 1 mL/min at a temperature of 25 °C.

2.3 Synthesis of *t*-Boc-N-2-hydroxypropylamine

The *t*-Boc-N-2-hydroxypropylamine was synthesized according to the literature. [29] In the first step 5.8 g (6.1 mL, 26.6 mmol) di-tert-butyldicarbonate were dissolved in 100 mL acetonitrile at room temperature. Afterwards a solution of 2 g 2-hydroxypropylamine (26.6 mmol) in 50 mL acetonitrile was added drop-wise. The reaction was allowed to proceed for 3 h at room temperature. Finally the solved was removed and the product was dried under high vacuum. A colourless viscose liquid was obtained. Yield: 4.64 g (26.2 mmol) 98 %. ^{1}H NMR ($CDCl_3$): δ [ppm] 1.12 (d, 3H), 1.40 (s, 9H), 2.90 (m, lH), 3.20 (m, IH), 3.38 (b, lH), 3.82, (m, lH), 5.22 (s, 1H)

2.4 Synthesis of 4-cyano-4-((thiobenzoyl)sulfanyl)pentanoic acid.

The 4-cyano-4-((thiobenzoyl) sulfanyl)pentanoic acid was used as the CTA and synthesized in a 3 step reaction according to the literature. [30]

2.5 Synthesis of pentafluoro-phenyl methacrylate (PFMA).

PFMA was prepared according to the literature. [21]

2.6 General synthesis of the PPFMA.

The macro-CTA was prepared according to the literature. [22] The RAFT polymerizations of the PFMA using 4-cyano-4-((thiobenzoyl) sulfanyl) pentanoic acid were performed in a schlenk tube. The reaction vessel was loaded with 2,2'-azobis(isobutyronitrile (AIBN), 4-cyano-4-((thiobenzoyl)-sulfanyl)pentanoic acid (CTA) (molar ratio of AIBN/CTA = 1:8) and 15 g of PFMA in 20 mL of dioxane. Following three freeze–vaccum–thaw cycles, the tube was immersed in an oil bath at 70 °C. Afterwards the polymer poly(PFMA) was 3 times precipitated into hexane, isolated by centrifugation and dried for 12 hours at 30 °C under vacuum. In the end a slightly red powder was obtained. Yield: 8.9 g (59 %). ^{1}H NMR ($CDCl_3$): 1.6-2.2 (br), 0.9-1.5 (br) δ [ppm] ^{19}F NMR ($CDCl_3$): δ [ppm] -165.1 (br), -159.8 (br), -154.4 (br), -153.1 (br)

2.7 Removal of dithioester end groups.

The dithiobenzoate end group was removed according to the procedure reported by Perrier et al. [31] Typically 200 mg of polymer, (Mn = 25.000 g/mol), and 50 mg of AIBN (30 times excess in relation to the polymer endgroup) were dissolved in 3 mL of anhydrous dioxane/DMSO (4:1). The solution was heated at 80 °C for 2 h. Finally the copolymer was precipitated 3 times in 100 mL of diethyl ether and collected by centrifugation. In the case of the block copolymer the crude product was first precipitated in EtOH 2 times and than 1 time in diethyl ether. The copolymer was dried under vacuum for a period of 24 h and a colourless product was obtained (yield: 92 %). The absence of the dithiobenzoate end group was confirmed by UV-Vis spectroscopy by the absence of the peak at a wavelength of 302 nm.

2.8 Postpolymerization reactions of PPFMA

In a typical reaction 300 mg of PPFMA without ditihioester end group were dissolved in 4 mL abs. dioxane and 1 mL abs. DMSO. A colourless solution was obtained. 200 mg of 2-hydroxypropylamine and 200 mg triethylamine were added. The reaction was allowed to proceed under at temperatures from 30 to 90 °C. The solution was concentrated in vacuum and introduced to a column filtration using Sephadex^{TM} LH-20 in dioxane and precipitated in diethyl ether, removed by centrifugation and dried in vacuum at 30 °C for 14 hours. Yield: (86 %). ^{1}H NMR (DMSO-d_6): δ [ppm] 3.4-3.9 (br), 2.6-3.0, 0.9-1.5 (br)

2.9 Kinetics of the postpolymerization reaction

For kinetic measurements by ^{19}F NMR 20 mg of the PPFMA polymer were dissolved in dioxane-d_4 and DMSO-d_6 (4:1). Afterwards 15 mg 2-hydroxypropylamine or 18 mg *t*-Boc-N-2-hydroxypropylamine and 15 mg triethylamine were added and the nmr tube was placed into the 400 MHz FT-spectrometer from Bruker, which was already set on a constant temperatur. The measurements have been carried out at 30, 60 and 90 °C and the conversion was monitored by the

ratio of the signals of polymer bound and free pentafluorophenol. The chemical shift in the ^{19}F NMR for polymer bound pentafluorophenol is δ [ppm] -165.0 (br), -159.7 (br), -154.5 (br), -153.1 (br), while the signal of the free one are located at δ [ppm] 167.3, 167.6 and 171.4.

2.10 Cell cultures

HeLa (human cervix adenocarcinoma cells) were grown in DMEM medium supplemented with 10% v/v of heat-inactivated fetal bovine serum (FBS). Cells were maintained at 37°C in an atmosphere of 5% carbon dioxide and 95% air and underwent passage twice weekly.

2.11 Cells viability assay

The cytotoxicity of the conjugates synthesized was evaluated using the MTT (3-(4,5-dimethyltiazol-2-yl)-2,5-diphenyl-tetrazolium bromide) cell viability assay (72 h incubation) with HeLA cells. Cells were seeded into sterile 96-well microtitre plates (seeding density $2.2x10^4$ cell/mL). Cells were allowed to settle for 24 h before the unlabeled polymer P1 (0.2 µm filter-sterilized) was added. A series of stock solutions of conjugates dissolved in DMSO, with different concentrations ranging from 1 mg/mL to 300 mg/mL, were prepared and the cells were treated with 1 µL of each stock solution, in such a manner that the final polymer concentrations range from 0,01 mg/mL to 3 mg/mL with a final DMSO concentration of 1% (v/v). As control, cells were treated with the same percentage of DMSO, in absence of conjugates to evaluate solvent toxicity. 100% cell viability was assigned to control cells with 1% DMSO. After a further 68 h incubation, MTT (20 µL of a 5 mg/mL solution in PBS) was added to each well, and the cells were incubated for 4 h. After removal of the medium, the precipitated formazan crystals were dissolved in optical grade DMSO (100 µL), and the plates were read spectrophotometrically at 570 nm after 30 min using a Victor^2 Wallac plate reader.

3. Results and Discussion

The reactive PPFMA precursors that were investigated as precursor for postpolymerization modification were prepared via RAFT polymerization of PFMA using the procedure reported by Eberhardt and Theato (Scheme 1). [22]

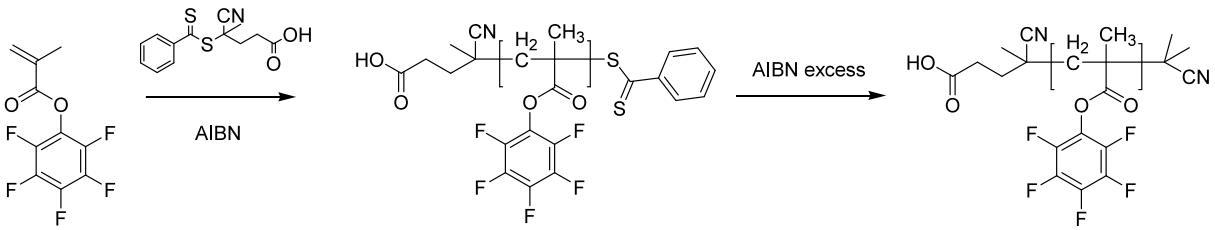

Scheme 1. Synthesis of poly(pentafluorophenyl methacrylate) polymers by the RAFT polymerization method

We were able to prepare various polymers with molecular weights ranging from 15 to 120 kDa. The polydipersity index was between 1.2-1.3 and only a slight influence of the molecular weight on the polydisperity was observed, indication a slightly broader molecular weight distribution for the higher molecular weight polymers (see table 1). The kinetics of the RAFT polymerization are in accordance to the data published by Eberhardt et al. and Gibson et al. [22,24] and therefore a detailed description is not necessary.

Table 1. Characteristics of synthesized PPFMA polymers

polymers	M_N (kg/mol) [a)]	M_W (kg/mol) [a)]	PDI [a)]
P1	13	16	1.20
P2	21	25	1.19
P3	32	39	1.23
P4	50	61	1.21
P5	104	134	1.29
P6	135	178	1.32

[a)] determined by GPC using THF as solvent

To explore the potential of PPFMA as a precursor polymer for a library of functional HPMA-based polymers, the postpolymerization modification of PPFMA precursors polymers with 2-hydroxypropylamine was carried out (see scheme 2). Before the aminolysis of the activated ester was performed the dithiobenzoate end group was removed according to the method reported by Perrier and coworkers. [31] An excess of AIBN was used to substitute the dithioester. Full conversion of the end group was monitored by the disappearance of the characteristic band at a wavelength of 302 nm in the UV-Vis spectra.

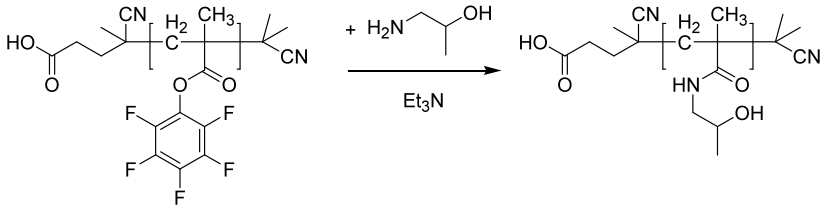

Scheme 2. Postpolymerization modification of PPFMA using 2-hydroxypropylamine

The reaction was carried out at 3 temperatures (30, 60, 90 °C). The conversion of the activated ester can be precisely studied by ^{19}F NMR, because the signals of polymer bound pentafluorophenol are well separated from the free fluorinated phenol (see figure 1 a, b). In addition this method can be used to monitor the successful workup after the polymer analogous reaction (see figure 1 c).

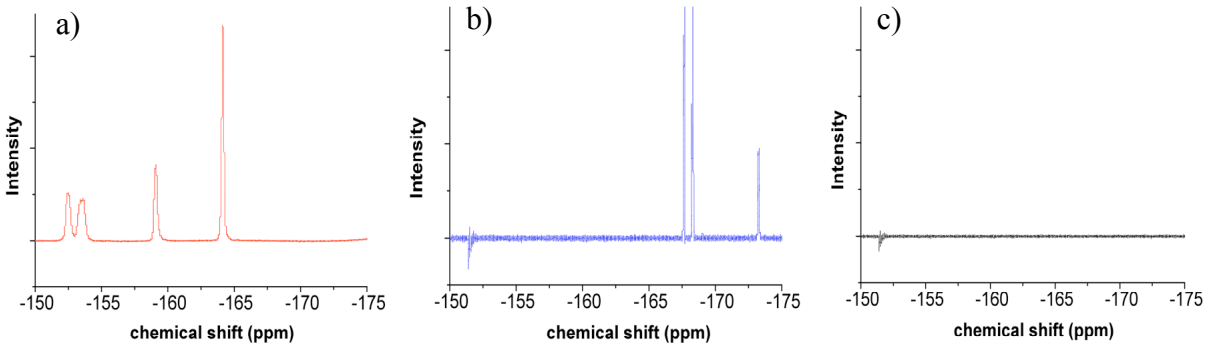

Figure 1. ^{19}F NMR spectra of a) PPFMA, b) pentafluorphenol and c) after purification

In addition, the derived peak integrals are reliable due to the lack of a nuclear Overhauser effect and therefore the conversion of the activated ester can be calculated by the peak integral ratio of free to polymer bound pentafluorophenol. For these experiments the postpolymerization modification was carried out in an NMR tube. The NMR tube was inserted into the NMR spectrometer, which was preheated to the temperature at which the reaction kinetics were investigated. The results of the temperature depended postpoly-merization modifications are presented in figure 2.

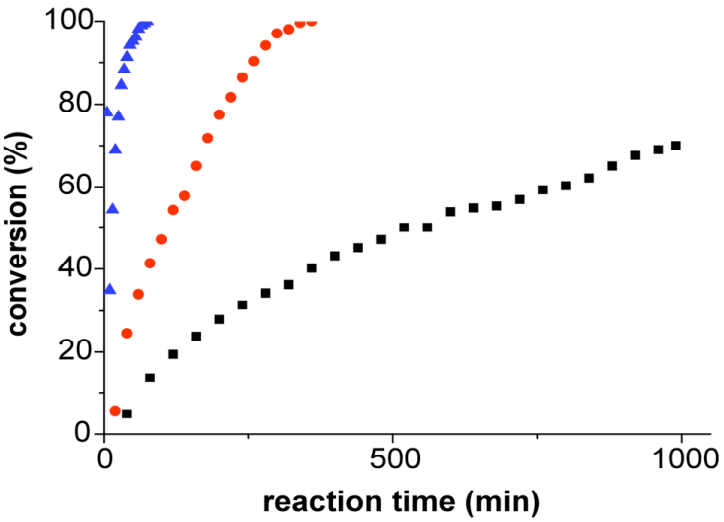

Figure 2. Temperature depended postpolymerization modification of PPFMA using 2-hydroxypropylamine (▲ T= 90 °C, ● T= 60 °C and ■ T= 30 °C)

As expected the conversion of the activated ester is highly temperature depended. At 30 ° C the conversion is rather slow and in after 16 h around 60-70 % of the activated ester are converted and a full conversion is reached after additional quenching of the activated ester is necessary. But even in this case full conversion can be achieved after a maximal reaction time of 48 h. At 60 °C full conversion was already observed after 8h and after 90 minutes at 90 °C.

For the rather tiny molecule 2-hydroxypropylamine no influence of the precursor molecular weight on the conversion was detected but detailed kinetic studies were not performed.

After monitoring the conversion of the activated ester the following question remains. Was the PPFMA successfully converted into HPMA or did side reactions occur. Gibson et al. have used conventional ^{1}H NMR to answer this question, but it is really difficult to obtain reliable information due to signal broadening and signal overlap. In this respect we have chosen ^{19}F NMR to investigate possible side reactions, e.g. hydrolysis of the activated ester by the hydroxyl group of the amine or remaining impurities of the compounds or solvents. For this purpose the amino group of the 2-hydroxypropylamine was protected using di-tert-butyl-dicarbonate. The resulting *t*-Boc-2-hydroxypropylamine was applied to the normal reaction conditions of the postpolymerization of PPFMA as mentioned above. The conversion of the activated ester was studied up to 70 °C and a reaction time of 18 h. For most postpolymerization modifications the applied temperatures are below this temperature.

The spectra after 3 minutes and the spectra after 16 h are shown in figure 3. I can be nicely seen that no conversion of the activated ester took place after 16 h. In this respect, we can conclude that only the primary amine can react with the activated ester. In contrast neither impurities nor the free hydroxyl group can under go a reaction with the PPFMA polymer.

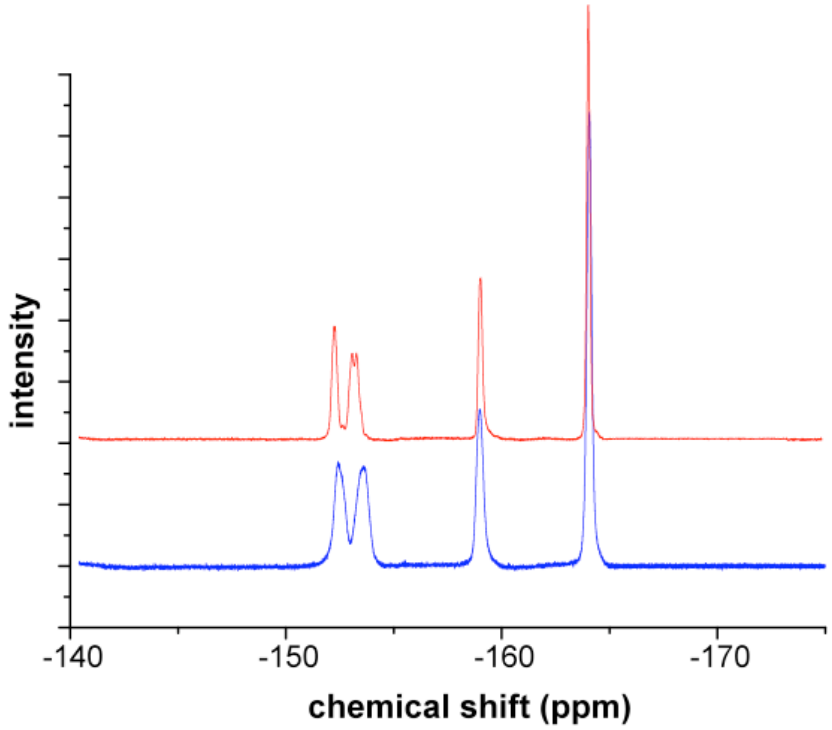

Figure 3. ^{19}F NMR spectra of the postpolymerization reaction mixture after 3 min (—) and 16 h (—) at 70 °C underlining the stability of the activated ester when the amine functionality is protected

These findings clearly point out that the ^{19}F NMR can be used to study the conversion of the activated ester. In addition, the disappearance of the signal related to polymer bound pentafluorophenol is directly and exclusively related to a reaction of the primary amine of 2-hydroxypropylamine. In this respect, PPFMA can be used to synthesize HPMA-based polymers.

Of course, for all NMR studies we are restricted to the detection limit of NMR and therefore it has to be ensured that the derived compounds are not cell toxic. Gibson et al. have nicely shown that the cell toxicity values of conventional HPMA are comparable to the one derived from an activated ester (PFPMA). We have performed additional cell toxicity experiments (MTT test) using human cervix adenocarcinoma (HeLa) cells. In these experiments we did not observe any polymer-associated toxicity up to a concentration of 3 mg/mL. In addition, no influence of the molecular weight was observed.

In summary, it can be concluded that PPFMA polymers can be used as a suitable base to create libraries of functional polymers having the same degree of polymerization. These systems can be expected to be a promising base for the development of various multifunctional and highly biocompatible polymeric architectures. But more important these systems will offer the great opportunity to study structure-property relationships. These findings will help to understand the influence of polymer structure on the in vitro as well as in vivo fate of polymer therapeutics.

4. Conclusion

In this work we have described the synthesis of activated ester polymers using the RAFT polymerization method. The PPFMA polymers had molecular weight from 15 up to 120 kDa. In all cases the PDI was around 1.3 ensuring well-defined polymers. Furthermore the ^{19}F NMR was successful applied to study the conversion of the reactive precursor polymers into HPMA-based systems. The HPMA-based polymers were achieved by postpolymerization modification of PPFMA with 2-hydroxypropylamine. As expected the reaction kinetics were temperature depended. But in all cases full conversion could be achieved. Additionally, it has been demonstrated that the activated ester is stable against hydrolysis when the t-Boc-2-hydroxypropylamine is used. Therefore possible side reactions could be excluded. With a view towards the use in biomedical applications the toxicity of the PHPMA polymers derived by the activated ester approach was evaluated. The MTT toxicity test ensured non-toxic behavior up to a concentration of 3 mg/mL in human cervix adenocarcinoma (HeLa) cells. These findings clearly underline that PPFMA based systems are a suitable basis for the development of various multifunctional and highly biocompatible polymeric architectures.

5. Acknowledgement

The authors would like to thank B. Mattiasch for the time and temperature dependent 19F-nmr measurements and Prof. Helmut Ringsdorf for his helpful advice. The authors also thank the graduate school of excellence MAINZ, COMATT and particularly the cluster of excellence SAMT of Rhineland-Palatina for support and funding.

6. References

[1] Matyjaszewski K, Xia J. Atom Transfer Radical Polymerization. Chem Rev 2001;101:2921-90.

[2] Matyjaszewski K, Gnanou Y, Leibler L. Macromolecular Engineering, Wiley-VCH; Weinheim; Germany 2007, Vol. 1.

[3] Tsarevsky NV, Matyjaszewski K. “Green” Atom Transfer Radical Polymerization: From Process Design to Preparation of Well-Defined Environmentally Friendly Polymeric Materials. Chem Rev 2007;107:2270-99.

[4] Matyjaszewski K, Jo SM, Paik HJ, Gaynor SG. Synthesis of Well-Defined Polyacrylonitrile by Atom Transfer Radical Polymerization. Macromolecules 1997;30:6398.

[5] Hawker CJ, Bosman AW, Harth E. New Polymer Synthesis by Nitroxide Mediated Living Radical Polymerizations. Chem Rev 2001;101:3661-3688.

[6] Schork FJ, Smulders YL, Russum JP, Butte A, Fontenot K. Miniemulsion Polymerization. Adv. Polym. Sci. 2005;175: 129-255.

[7] Barner-Kowollik C. Handbook of RAFT Polymerization. Wiley-VCH; Weinheim; Germany 2008.

[8] Moad G, Rizzardo E, Thang SH. Living Radical Polymerization by the RAFT Process. Aust J Chem 2005;58:379-410.

[9] Moad G, Rizzardo E, Thang SH. Radical addition–fragmentation chemistry in polymer synthesis. Polymer 2008;49:1079-1131.

[10] Stenzel MH. RAFT polymerization: an avenue to functional polymeric micelles for drug delivery, Chem. Commun. 2008;30:3486-503.

[11] Barz M, Luxenhofer R, Zentel R, Kabanov AV. The uptake of N-(2-hydorxypropyl)methacryl-amide based homo, random and block copolymers by human multi-drug resistant breast adenocarcinoma cells. Biomaterials 2009;30:5682-5690.

[12] Pedone E, Li X, Koseva N, Alpar O, Brocchini S. J. An information rich biomedical polymer library. Mater. Chem. 2003;13: 2825–2837.

[13] Batz HG, Franzmann G, Ringsdorf H. Model Reactions for Synthesis of Pharmacologically Active Polymers by Way of Monomeric and Polymeric Reactive Esters. Angew Chem Int Ed 1972;11:1103-04.

[14] Gauthier MA, Gibson MI, Klok H-A. Synthesis of Functional Polymers by Post-Polymerization Modification. Angew. Chem. Int. Ed. 2009;48:48–58

[15] Theato P. Synthesis of well-defined polymeric activated esters. J Polym Sci Part A Polym Chem 2008;46:6677–6687.

[16] Fournier D, Hoogenboom R, Schubert US. Clicking Polymers: a straightforward approach to novel macromolecular architectures. Chem Soc Rev 2007;36:1369–1380.

[17] Lutz J-F, Z. Zarafshani, Efficient Construction of Therapeutics, Bioconjugates, Biomaterials and Bioactive Surfaces using Azide-Alkyne »click« Chemistry. Adv. Drug Del. Rev. 2008;60:958-970.

[18] Binder WH, Sachsenhofer R. “Click” Chemistry in polymer and Material Science: An Update. Macromol. Rapid Commun. 2008;29:952-981.

[19] Duncan R. Polymer conjugates as anticancer nanomedicines. Nat Rev Cancer 2006;6:688-701.

[20] Duncan R, Coatsworth JK, Burtles S. Preclinical toxicology of a novel polymeric antitumour agent: HPMA copolymer-Doxorubicin (PK1). Hum. Exp. Toxicol. 1998;17(2):93-104.

[21] Hopewell JW, Duncan R, Wilding D, Chakrabarti K. Preclinical evaluation of the cardiotoxicity of PK2: A novel HPMA copolymer–doxorubicin–galactosamine conjugate antitumour agent. Hum. Exp. Toxicol. 2001;20(9):461-470.

[22] Eberhardt M, Mruk R, Zentel R, Theato P. New precursor polymers for the synthesis of multifunctional materials. Eur Polym J 2005;41:1569–75.

[23] Eberhardt M, Theato P. RAFT polymerization of pentafluorophenyl methacrylate: Preparation of reactive linear diblock copolymers. Macromol Rapid Commun 2005; 26:1488-93.

[24] Barz M, Tarantola M, Fischer K, Schmidt M, Luxenhofer R, Janshoff A, Theato P, Zentel R. From Defined Reactive Diblock Copolymers to Functional HPMA-Based Self-Assembled Nanoaggregates. Biomacromolecules 2008;9:3114-3118.

[25] Gibson MI, Fröhlich E, Klok H-A, Postpolymerization Modification of Poly(Pentafluorophenyl methacrylate): Synthesis of a Diverse Water-Soluble Polymer Library. Journal of Polymer Science: Part A: Polymer Chemistry 2009; 47:4332–4345.

[26] Herth M, Barz M, Moderegger D, Allmeroth M, Jahn M, Thews O, et al. Radioactive labeling of defined HPMA-based polymeric structures using [18F]FETos for in vivo imaging by positron emission tomography. Biomacromolecules 2009;10,1697–1703.

[27] Barz M, Canal F, Koynov K, Zentel R, Vicent MJ. Synthesis and in vitro evaluation of defined HPMA folate conjugates: Influence of aggregation on folate receptor (FR) mediated cellular uptake. Submitted.

[28] Barz M, Wolf F, Canal F, Koynov K, Vicent MJ, Frey H, Zentel R. Synthesis, Characterization and Evaluation of poly(HPMA)-*block*-poly(L-Lactide) copolymers: A new type of functional biocompatible block copolymers. Submitted.

[29] Zhong B, Lu X, Silverman RB. Syntheses of Amino Nitrones. Potential Intramolecular Traps for Radical Intermediates in Monoamine Oxidase-catalyzed Reactions. Bioorg. Med. Chem. 1998;6:2405-2419.

[30] Chong YK, Moad G, Rizzardo E, Tang SH. A More Versatile Route to Block Copolymers and other Polymers of Complex Architecture by Living Radical Polymerization: The RAFT Process. Macromolecules 1999;*32*:2071-2074.

[31] Perrier S, Takolpuckdee P, Mars CA. Reversible addition–fragmentation chain transfer polymerization: end group modification for functionalized polymers and chain transfer agent recovery. Macromolecules 2005;38:2033–6.

2.2 From Defined Reactive Diblock Copolymers to Functional HPMA-Based Self-Assembled Nanoaggregates

Biomacromolecules **2008**, *9,* 3114–3118

Authors: M. Barz[1], M. Tarantola[2], K. Fischer[2], M. Schmidt[2], R. Luxenhofer[3], A. Janshoff[2], P. Theato[1] and R. Zentel[1]

Address: [1]Institute of Organic Chemistry, Johannes Gutenberg-University Mainz, Duesbergweg 10-14, 55099 Mainz, Germany

[2]Institute of Physical Chemistry, Johannes Gutenberg-University Mainz,

Welderweg 11, 55099 Mainz, Germany,

[3]Department of Pharmaceutical Sciences and Center for Drug Delivery and Nanomedicine, College of Pharmacy, University of Nebraska Medical Center,

Omaha, Nebraska 68198-5830, USA

Abstract

This paper describes the synthesis of functional amphiphilic poly(*N*-(2-hydroxypropyl) methacrylamide)-blockpoly(lauryl methacrylate) copolymers by RAFT polymerization via the intermediate step of activated ester blockcopolymers (pentafluoro-phenyl methacrylate). Block copolymers with molecular weights from 12000-28000g/mol and PDIs of about 1.2 have been obtained. The amphiphilic diblock copolymers form stable super structures (nanoaggregates) by self-organization in aqueous solution. The diameters of these particles are between 100 and 200 nm and depend directly on the molecular weight of the block copolymer. Furthermore, we investigated the impact of these nanoaggregates on cell viability and on the motility of adherent cells. Cytotoxicity was investigated by the MTS test and the fluctuation in cell shape was monitored employing ECIS (electrical cell-substrate impedance sensing). In these investigations, the formed particles are not cell toxic up to a concentration of 2 mg/mL. Thus, our polymeric particles offer potential as polymer therapeutics.

1. Introduction

During the recent years, there has been a growing interest in the use of nanosized particles (copolymers, liposomes, micelles) for pharmaceutical applications. [1] Such particles offer the possibility to tune the body distribution either by size, for example, via the EPR-effect [2,3] or by attachment of selective targeting vectors (specific proteins or polysaccharides). [4] In addition, nanosized particles allow the introduction of different kinds of drugs for therapeutic use at once.The concept of polymer therapeutics for pharmaceutical applications was originally developed by Ringsdorf and Duncan [5] for statistic copolymers and was later extended to include selfassembled structures such as nanoaggregates, polymersomes [6], and micelles. [7] Besides lipids, especially amphiphilic block copolymers are known to form self-assembled structures by micellization in water and, accordingly, diblock copolymer-based systems have been widely explored as polymer therapeutics. [8-11] The original statistical copolymers described by Ringsdorf, Duncan, and Kopecec [12,13] were based on the nonimmunogenic poly(*N*-(2-hydroxypropyl)methacrylamide) (PHPMA) and polymeric-activated ester, which allowed the functionalization with amine-terminated targeting vectors and drugs. [1,12,13] Even nowadays, there have been various studies concerning targeting vectors, degradable linkers and therapeutics. [14] However, because these copolymers were prepared by free radical polymerization, their molecular weight distribution was rather broad. PHPMAbased copolymers with a narrow molecular weight distribution and block copolymers have been recently prepared by ATRP. [15,16] However, this polymerization technique requires the use of copper complexes, which are expected to be cell-toxic. Besides ATRP [17] and NMP [18], the reversible addition-fragmentation chain transfer (RAFT) polymerization is one of the most frequently used controlled radical polymerization methods. It allows the synthesis of narrowly distributed polymers and block copolymer [19,20] and it does not require any heavy metal catalyst. There is only a need for a chain transfer agent, which is, in our study, the 4-cyano-4-((thiobenzoyl)sulfanyl)pentanoic acid (CTA). Further, the RAFT polymerization is very tolerant to various monomers and solvents. Thus, it has been possible to synthesize reactive block copolymers, which can be first precisely characterized and afterward functionalized by polymer analogous reactions. [21] Therefore, it has been possible to prepare a series of multifunctional block copolymers from one precursor block copolymer. Copolymers and especially block copolymers featuring activated ester units attached to the polymer backbone are ideal for the preparation of multifunctional poly(acrylamides) [22-24], such as PHPMA, if a good solubility of the reactive precursor polymer in various solvents can be achieved. This is, however, not the case for the well-known succinimide based activated ester monomers. [21] In contrast, polymers based on pentafluorophenyl methacrylate, first described by Theato et al. [21,25], fulfill this requirement. In this work, we use this concept to synthesize amphiphilic poly(*N*-(2-hydroxypropyl) methacrylamide)-*block*-poly(lauryl methacrylate) copolymers, which self-assemble in

water. Using the activated ester in the synthesis offers a great flexibility for the incorporation of possible targeting vectors and fluorescent dyes that can be used for detection. Furthermore, we investigated the impact of these self-assembled structures on the motility of adherent cells and the organization of their cytoskeleton using fluorescence microscopy. Micromotion was monitored employing ECIS (electrical cell-substrate impedance sensing). [30-33] This approach provides a good time resolution to monitor electrical changes of adherent cells on small substrate-integrated goldelectrodes in real-time under culture conditions. A lock-in amplifier is monitoring the impedance, which is modulated by the shape of the attached cells as they act as insulating particles to the current flow from the small detecting electrode to the large counter electrode. Electrical characterization of adhesional, morphological, and motional cellular processes achieved by the ECIS-method was pioneered in 1984 by Giaever and Keese. [25] Fluctuations in the real part of the impedance, after being Fourier transformed, are analyzed in frequency regimes known for cell motility and serve as a measure for their viability. [26] Finally,the method is validated by conventional MTS cytotoxicity test.

2. Experimental Section

2.1. Materials

All chemicals were reagent grade and obtained from Aldrich. The chemicals were used without further purification unless otherwise indicated. Dioxane used in the synthesis was freshly destilled from a sodium/potassium mixture. 2,2'-Azobis(isobutyronitrile) (AIBN) was recrystallized from diethyl ether and stored at -7°C. Lauryl methacrylate was distilled and kept at -7°C.

2.2. Characterization

^{1}H-, ^{13}C- and ^{19}F-NMR spectra were obtained at 300 or 400 MHz using a FT-spectrometer from Bruker and analyzed using the ACDLabs 6.0 software. The polymers were dried at 40 °C over night under vacuum and afterwards submitted to gel permeation chromatography (GPC). Gel permeation chromatography (GPC) was performed in tetrahydrofurane (THF) as solvent and with following parts: pump PU 1580, auto sampler AS 1555, UV-detector UV 1575, RI-detector RI 1530 from Jasco and miniDAWN Tristar light scattering detector from Wyatt. Columns were used from MZ-Analysentechnik: MZ-Gel SDplus 10^{2}Å, MZ-Gel SDplus 10^{4}Å and MZ-Gel SDplus 10^{6} Å. The elution diagrams were analysed using the ASTRA 4.73.04 software from Wyatt Technology. Calibration was done using polystyrene standards. The flow rate was 1 ml/min at a T = 25 °C.

2.3. Synthesis of 4-cyano-4-((thiobenzoyl)sulfanyl)pentanoic acid (CTA)

The 4-cyano-4-((thiobenzoyl)sulfanyl)pentanoic acid was synthesized according to the literature. [20]

2.4. Synthesis of pentafluoro-phenyl methacrylate (PFMA)

Pentafluorophenyl methacrylate (PFMA) was prepared according to the literature. [19]

2.5. General synthesis of the macro-CTAs

RAFT polymerizations of PFMA using 4-cyano-4-((thiobenzoyl)sulfanyl)pentanoic acid were performed in a schlenk tube. The reaction vessel was loaded with 2,2'-azobis(isobutyronitrile (AIBN), 4-cyano-4-((thiobenzoyl)sulfanyl)pentanoic acid (CTA) (molar ratio of AIBN/CTA = 1:8) and 15 g of PFMA in 20 mL of dioxane. Following three freeze–vaccum–thaw cycles, the tube was immersed in an oil bath at 70 °C. Afterwards the polymer poly(PFMA) was 3 times precipitated into hexane, isolated by centrifugation and dried for 12 hours at 30 °C under vacuum. In the end a slightly red powder was obtained. Yield: (59 %). ^{1}H NMR ($CDCl_3$): 1.6-2.2 (br), 0.9-1.5 (br) δ [ppm] ^{19}F NMR ($CDCl_3$): δ [ppm] -165.1 (br), -159.8 (br), -154.4 (br), -153.1 (br)

2.6. General synthesis of block copolymers

The macro CTA obtained in the above mentioned polymerization was dissolved in dioxane and AIBN was added. Following three freeze–vaccum–thaw cycles, the tube was immersed in an oil bath at 70 °C. After 12 h polymerization time the solution was slightly concentrated and precipitated twice in ethanol and diethyl ether, removed by centrifugation and dried overnight at 30°C in vacuum. A slightly red powder was obtained. Yield: (89 %). ^{1}H NMR ($CDCl_3$): δ [ppm] 1.6-2.2 (br), 0.9-1.5 (br), 0.8-0.9 (br t) ^{19}F NMR ($CDCl_3$): δ [ppm] -165.1 (br), -159.8 (br), -154.4 (br), -153.1 (br)

2.7. Polymer analogous reactions

a) In this experiment typically 300 mg of poly(PFMA)-block-poly(lauryl methacrylate) were dissolved in abs. dioxane. A slightly red solution was obtained. To this solution 200 mg of triethylamine and 150 mg of hydroxypropylamine were added. The solution was kept at 60°C under nitrogen for 14 hours to ensure quantitative conversion. The solution was concentrated in vacuum and introduced to a column filtration using Sephadex^{TM} LH-20 in dioxane and precipitated in diethyl ether, removed by centrifugation and dried in vacuum at 30 °C for 14 hours.

b) In a typical reaction 300 mg of poly(PFMA)-block-poly(Lauryl methacrylate) were dissolved in 4 ml abs. dioxane and 1 ml abs. dimethylsulfoxide (DMSO). Once again a slightly red solution was obtained. After the addition of 20 mg hydroxypropylamine and 40 mg triethylamine the solution was stirred under nitrogen at 50 °C for 10 min. In the next step 4 mg of 4-nitro-7-(piperazin-1-yl)benzo[c][1,2,5]oxadiazole (NBD) and 20 mg of triethylamine were added. The mixture was kept at

60 °C for 2 hours. In the end 120 mg of hydroxypropylamine and 140 mg triethylamine were added. The reaction was allowed to go on under the above-mentioned conditions over night. The solution was concentrated in vacuum and introduced to a column filtration using Sephadex™ LH-20 in dioxane and precipitated in diethyl ether, removed by centrifugation and dried in vacuum at 30 °C for 14 hours. Yield: (81%). ^{1}H NMR (DMSO-*d*6): δ [ppm] 3.4-3.9 (br), 2.6-3.0 (br), 0.9-1.5 (br), 0.8-0.9 (br t)

2.8. Preparation and analytics of nano-aggregates

10 mg of the poly(HPMA)-*block*-poly(lauryl methacrylate) polymer were dissolved over night in 10 ml of $1*10^{-3}$ M solution of Lithium trifluoroacetate in hexafluorisopropanol (HFIP). The solution was filtered with an anatop 20nm filter. 40 mg of the block copolymer solution (c = 1 mg/ml) were added dropwise to $2.2*10^3$ mg of an aqueous solution of sodium bromide (NaBr) ($1*10^{-3}$ M). Under this condition the influence of the solvent (HFIP) can be disregarded. The aggregates were analyzed right after the preparation and 12 to 16 hours later by dynamic and static light scattering. Static light scattering (SLS) measurements were performed with an ALV-SP86 goniometer, an ALV-3000 correlator, a Uniphase HeNe Laser (25 mW output power at λ = 632.8 nm wavelength) and ALV/High QE APD avalanche diode fiber optic detection system. For dynamic light scattering (DLS) an ALV-SP125 goniometer, an ALV-5000 correlator, a Spectra Physics 2060 Argon ion laser (500 mW output power at λ = 514.5 nm wavelength) were utilized. The scattered intensity was divided by a beam splitter (approximately 50:50), each portion of which was detected by a photomultiplier. The two signals were cross-correlated in order to eliminate non-random electronic noise. The complex solutions were typically measured from 30°-150° in steps of 5° (SLS) or in steps of 10° (DLS). The static scattering intensities were analyzed according to standard procedures in order to yield the weight average molar mass, M_w, and the mean square radius of gyration. The correlation functions showed a monomodal decay and were fitted by a sum of two exponentials, from which the first cumulant Γ was calculated. The z-average diffusion coefficient D_z was obtained by extrapolation of Γ/q^2 for to q = 0 leading to the inverse z-average hydrodynamic radius by formal application of Stokes law.

2.9. Cell culture conditions and measurement procedures

For subculture, MDCKII cells were maintained in Earle's minimum essential medium supplemented with 4 mM glutamine, 100 µg/ml of both penicillin and streptomycin (purchased by Biochrom, Berlin, Germany), 10% (v/v) fetal calf serum (PAA Laboratories GmbH, Cölbe, Germany). For the measurements, cells were transferred to the ECIS setup located in an incubator (CO_2Cell, MMM, Germany) set to 37°C and 5% CO_2 environmental parameters. ECIS-wells were filled with an inoculum size of 600000 cells to reach confluence upon adhesion or filled with an equal amount of medium only. Exchange of medium containing the nanoparticles was carried out 15-24 hours later allowing tight-junctions to be established.

2.10. Immunochemistry and fluorescence microscopy

Immunostaining and fluorescence microscopy was applied to monitor alterations in the actin-cytoskeleton of the confluent cells. Therefore, confluent MDCKII cells were incubated with the nanoparticles for 24 or 48 h. After washing with PBS, fixation was carried out by immersing the cells in a -20°C cold acetone/methanol mixture (1:1 vol %) for 10 min. The cells were imaged with an upright epifluorescence microscope (Olympus BX51, Münster, Germany), equipped with a 3 MP colour camera.

2.11. ECIS cytotoxicity assay

A home-built ECIS-system was employed, consisting of a lock-in amplifier (SR830, SRS, Inc., Sunnyvale, CA) with an internal oscillator and a home-made multiplexer with analogue switches for automatic, step by step connection of multiple wells on the sensor chip. The chip consists of eight separate wells with gold electrodes, the diameter of 250 µm, integrated in the bottom and a large (7×46 mm^2) common counter electrode. In this setup, a 1 V AC signal with a 1 MΩ series resistor is applied and in- and out-of-phase voltages are recorded at 4 kHz with a sampling of 550 points at 1 Hz. The applied 1 µA current amplitudes are non-invasive to the cells layer; the voltages are proportional to the real (resistance) and imaginary (capacitive reactance) parts of the impedance and modified by the motility of adherent cells onto the circular gold electrodes. Noise analysis of time series of resistance fluctuations was carried out by Fast-Fourier-transformation (FFT). Linear fitting in the regime form $10^{-0,5}$ to $10^{-1,5}$ Hz, as describe by Giaever *et al.* yields a slope of -2.1 to -3 s^{-2} for fully motile epithelial cells exhibiting 100% micromotion and 0 to -1 for bare electrodes as well as fixed cells immersed in buffer. Time courses of the slopes have then been recorded for the application of various nanoparticles and ECIS.

2.12. Cytotoxicity assay

The applied MTS-cytotoxicity (3-(4,5-dimethylthiazol-2-yl)-5-(3-carboxymethoxyphenyl)-2- (4-sulfophenyl)-2H-tetrazolium, inner salt (MTS)) test has been adopted applying the manufacturer`s protocol. In brief, cells are grown to a predetermined optimal number on a 96 well-plate and afterwards incubated with nanoparticles for 24h. Washing is carried out three times with PBS^{++} and full medium before adding the MTS-agent to remove air bubbles that might disturb the photometric assay. Control experiments were carried using empty wells and fully vital cells. Incubation with the tetrazolium educt is carried out for 45 minutes. Absorbance is determined using a 96-well-plate photometer. The colour change is a direct measure of the cell's metabolic activity due to the reduction to formazan product by mitochondrial dehydrogenase enzymes or cytosolic NADH.

3. Results and Discussion

It was the aim of this work to develop a flexible synthetic route to biocompatible polymers based on clinically approved poly(N-(2-hydroxypropyl)methacrylamide) (PHPMA), which fulfils two side conditions (i) it should be easy to incorporate functional groups (e.g. dyes or targeting vectors) into the water soluble PHPMA and (ii) a hydrophobic block should allow the preparation of self-assembled structures in aqueous media. Thereby, adjusting the size of the self-assembled polymer structures should allow it to control their distribution within the body.

To reach this goal a synthetic route was developed (see scheme 1), which is based on the preparation of block copolymers from pentafluorophenyl methacrylate (PFMA) and lauryl methacrylate (LMA) by RAFT polymerization using 4-cyano-4-((thiobenzoyl)sulfanyl)-pentanoic acid as a chain transfer agent (CTA) and the subsequent aminolysis with 2-hydroxypropyl amine yielding PHPMA. The synthesis of the final block copolymer via a polymeric activated ester intermediate offered two advantages. First, the soluble PFMA block copolymers could be characterized in detail, which allowed it to control and optimize the RAFT-process easily. Second, the aminolysis of the activated ester units offered an easy way to introduce additional functional groups, such as dyes (see scheme 1).

Scheme 1. Synthetic pathway for the RAFT polymerization of functional block copolymers

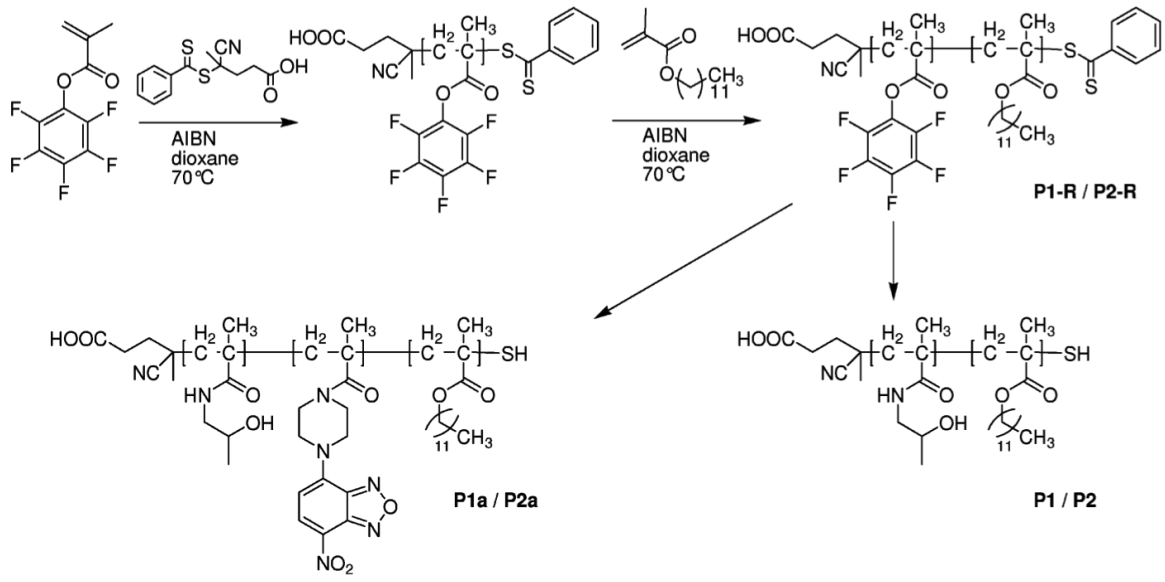

In general, block copolymers with adjustable molecular weights and narrow molecular weight distributions (Mw/Mn ~ 1.2) could be prepared. A list of synthesized block copolymers and their characterization data is compiled in table 1.

The CTA to PFMA ratio and the block ratio was adjusted to tailor a molecular weight of poly(PFMA)-*block*-poly(LMA) of around 25000 and 50000 g/mol in respect to the conversion of PFMA known in literature. [27] The block ratio of PFMA to LMA was set to be 80:20 for the low molecular weight polymers and 90:10 for the high molecular weight polymers, respectively. The calculated molecular weights and block ratios were in good accordance with the experimental data obtained by GPC and ^{1}H-NMR.

Table 1. Characterization of block copolymers from poly(pentafluoro-phenyl methacrylate)-block-poly(lauryl methacrylate) **P1-R** and **P2-R** and poly(N-(2-hydroxypropyl) methacrylamide)-block-poly(lauryl methacrylate) **P1** and **P2**.

polymer	block ratio$_{(calc)}$	block ratio[a]	ratio of fluorescent dye at the polymer %	M_n[b]	M_w[b]	PDI[b]	R_h (nm)[c]
P1-R	80:20	79:21	-	22680	27920	1.25	-
P1	80:20	79:21	-	12470[d)]	15350[d)]	1.25	2.0
P1a	80:20	79:21	1	12640	15520	1.25	-
P2-R	90:10	87:13	-	54840	64440	1.18	4.4
P2	90:10	87:13	-	27650[d)]	32480[d)]	1.18	3.8
P2a	90:10	87:13	0.5	27820	32650	1.18	-

a) As determined by ^{1}H NMR spectroscopy after aminolysis with hydroxypropylamine yielding **P1** and **P2**

b) As determined by GPC in THF as solvent for the activated ester polymers **P1-R** and **P2-R**. The value for **P1** and **P2** is recalculated from the molecular structure

c) Hydrodynamic radius obtained for **P1** and **P2** from dynamic light scattering in hexafluoroisopropanol (HFIP)

d) Calculated from the block ratio obtained by ^{1}H NMR and GPC data of **P1-R** and **P2-R**

The conversion of the activated ester polymers **P1-R** and **P2-R** with 2-hydroxypropylamine was monitored by ^{19}F-NMR spectroscopy. It proceeded quantitatively (see Ref. 20 for comparison) and fast, if the reaction was run at higher temperatures (100% conversion after 1 hour at 95 °C). But even at lower temperatures a quantitative conversion could be observed, if reaction time was elongated to 24 hours. ^{19}F-NMR spectroscopy offers also the possibility to characterize the purity of the reacted polymer by detecting unreacted PFMA groups. Thus, we could ensure that after work up the obtained polymer did not contain unreacted pentafluorophenyl esters. The block copolymers **P1** and **P2** were analized by ^{1}H-NMR in dioxane at higher temperature and the block lengths and the block ratio. Under these conditions no aggregation of the block copolymers was detected. In general, the recovery of the polymer after aminolysis was between 85 and 90%.

The block copolymers **P1** and **P2** dissolved homogenously in dioxane (see NMR investigations discussed above) and in hexafluoroisopropanol (HFIP), but they formed self-assembled structures in aqueous solutions, as expected for amphiphilic block copolymers. These self-assembled structures were investigated by light scattering. First, poly(HPMA)-*block*-poly(LMA) **P1** and **P2** were studied at a concentration of 1 mg/mL in a solution of $1*10^{-3}$ M of lithium trifluoroacetate in hexafluoroisopropanol (HFIP) by dynamic light scattering. In this solution we observed molecularly dissolved polymers with dimensions in the range of 2-4 nm (see table 1).

To induce the formation of self-assembled structures, polymer solutions in HFIP were added drop wise to an aqueous solution of NaBr ($1*10^{-3}$ M) leading to a polymer concentration of 0.01 mg/ml. The resulting aggregates were analyzed right after the preparation and one day later by dynamic and static light scattering. The results are listed in table 2.

Table 2. Characterization of aggregates from **P1** and **P2** in aqueous NaBr ($1*10^{-3}$ M) solution

Polymer	R_h (nm)	$\langle R_g^2 \rangle_{q1/2}$ (nm)	m_2	$\langle R_g^2 \rangle_{q1/2}/R_h$
P1	47.9	-	0.10	-
P1 (16h)	55.7	52.2	0.08	0.94
P2	106	85.0	0.07	0.80
P2 (14h)	112	88.0	0.08	0.79

The data show that both polymers **P1** and **P2** formed aggregates of moderate to low polydispersity in aqueous solution as revealed by the magnitude of the normalized second cumulant, $m_2 < 0.1$. The diameters of the aggregates were in the range of 100 nm for the low molecular weight block polymer **P1** and in the range of 200 nm for the high molecular weight block copolymer **P2**. The aggregates were stable, since only slight changes in the dimensions were observed within 12 hours. Spherical structures of similar size were also observed by cryo-TEM measurements (see Figure 1a), which also give an impression of the size distribution of the particles in qualitative agreement with the DLS results.

However, the size of these structures is definitely too small for simple spherical micelles, considering the radii of 2 to 4 nm for the individual block copolymers. From the light scattering results the detailed structure of the aggregates remains uncertain. For vesicles or polymersomes the ratio R_g/R_h is estimated to be in the order of 1 – 1.1 considering the polydispersity and the finite shell thickness. The experimental values lie significantly below 1, which is expected for full spheres of moderate polydispersity.

Fig. 1. Polymeric aggregates and their interaction with living cells (MDCK II)

a) Cryo-TEM image of polymer micelles from **P2** in aqueous solution (see Tab. 2)
b) Fluorescence image of the NBD labelled **P2a** in isotonic solution.
c) Living MDCKII cells with poly(HPMA)-block-poly(lauryl methacrylate) particles **P2a** (0.01 mg/ml) after 24 h incubation. The green fluorescence shows the presence of the polymer particles within in the cells. Particles do not penetrate the nucleus.

It is well known that so called “compound micelles” may form which resemble structures consisting of aggregated spherical micelles. Although the driving force for aggregation and the reason for the finite size are not clear, sometimes amazingly monodisperse spherical structures are reported. [28,29]

In addition the incorporation of a hydrophilic dye (bengal rosa B) was investigated. The dye and the block copolymer were dissolved in HFIP and dropped to an aqueous solution according to the procedure described for the light scattering experiment. Even after 8 days of dialysis against water, it was not possible to remove the dye from solution. In contrast, the control experiment with only the dye dissolved in water leads to a colourless solution after dialysis. Obviously, structures with a hydrophilic core that are capable of encapsulating the dye must have been formed, a finding compatible with both, vesicles, multi-shell vesicles and compound micelles. For the present purpose, the detailed internal structure of the aggregates is not of fundamental importance for biological applications presented below.

P1a and **P2a** can be functionalized additionally with a fluorescence dye (NBD) that has been covalently attached to the hydrophilic part of the diblock copolymer. A ratio of 0.5-1 % of dye per polymer backbone turned out to be enough to detect the self-assembled polymeric structures using a fluorescence microscope (see figure 1b). This small amount of dye will –in all probability- not effect the aggregation behaviour during liposome formation but it offers the possibility to detect the cell uptake of nano-aggregates (see figure 1c).

Based on earlier work related to PHPMA, which showed the biocompatible and non-immunogenic properties of this polymer, it was obvious to test the poly(HPMA)-*block*-poly(LMA) polymers in cell experiments to ensure biocompatibility. In this respect, we have chosen the MTT test to ensure non toxicity. The MTS test was performed using a mammalian, monolayer-forming epithelial cell model, the MDCKII cell line. The polymeric structures did not show any cell toxicity during 24 h up to a concentration of 2 mg/ml. In addition we chose a biocompatibility test based on detecting cell shape fluctuations of cells cultured in a continuous layer on small gold electrodes of 250 µm diameter. This assay is ideally suited to address cytotoxicity in a label-free and time-resolved manner, as shown in literature. [30,31] Fluctuations in the real part of the impedance were recorded and transformed into the frequency domain by means of Fast Fourier-transformation. The resulting power spectra are a direct measure for the cells viability and reflect the so-called micromotion, which can be correlated in a dose and time dependent fashion to the nanoparticles` cytotoxic effect. [32] Giaever and co-workers, the inventors of this technique, refer to biologically active cells if the slope in the low frequency part of the power spectrum is higher than -2.0, usually -2.1 to -3. [33] Hence, we use the term biological activity and micromotion synonymously. We determined micromotion after 24 and 48 h incubation of the adherent MDCK II cells grown to confluency with **P1a** and **P2a** polymer-nanoparticles (polymer vesicles, for size see Tab. 2) in three different concentrations (see table 3). Additionally, the time needed to reach half-inhibition of motility t_{IC50} was determined by fitting a sigmoidal function to the

data (micromotion (%) as a function of time). Addition of **P1a** and **P2a** particles at a fairly high concentration (0.1 mg/ml) produced a similar t_{IC50} (table 3) for both particle populations.

Table 3. Micromotion (% vitality) of adherent MDCK II cells exposed to polymers

Polymer (mg/ml)	IC_{50}(24h) from MTS[a] C_{max}= 2mg/ml	t_{IC50}[b] (min.) ± S.D. in %(n=3)	Micromotion[c] (%) ± S.D. in % after 24 h (n=3)	Micromotion[c] (%) ± S.D. in % after 48 h (n=3)
P1a 0.1		2600 ± 6	93 ± 10	54 ± 29
P1a 0.01	Not reached	-	117 ± 6	89 ± 2
P1a 0.001		-	112 ± 6	94 ± 1
P2a 0.1		2665 ± 11	74 ± 18	47 ± 36
P2a 0.01	Not reached	1405 ± 6	57 ± 25	51 ± 33
P2a 0.001		1632 ± 6	66 ± 2	35 ± 5

a) Viability vs. concentration plots in the regimes 0,001-2 mg/ml for the particles for MDCKII cells

b) Extracted from ECIS-micromotion vs.time plots.

c) Normalized to 100 % micromotion that has been reached at quasi-steady-state situation upon confluency and standardized to controls with living cells in pure culture medium

At lower particle concentration, however, we found that the vitality of cells remained at a very high level in the case of **P1a** (diameter about 100 nm), while for **P2a** vesicles (diameter about 200 nm) a drop of vitality was observed. After addition of **P1a** vesicles, micromotion persisted at high level up to 48 h.

Moreover, we found -to our surprise-, an increased activity of the cells within the 24 h interval, as indicated by increased micromotion values in comparison to controls with cells that were not in contact to nanoparticles.

Fluorescence images of living cells (Fig. 1 c) exposed to **P2a** show the uptake of vesicles and their perinuclear arrangement together with some brightly emitting aggregates within the cells.

Thus, from the MTS test and the ECIS investigations, which detect changes in the cell activity sensitively (long before the final death of the cell) we can conclude that cells could tolerate high concentrations of our polymeric aggregates with its PHPMA corona. Nano-aggregates in concentrations of 2 mg/ml and below, which are reasonable concentrations for polymeric therapeutics or imaging agents, are not cell toxic. But we have to conclude as well that the nano-aggregates may modify the micromotion in a, not yet understood way. Moreover, from our fluorescence measurements, we conclude that a considerable uptake of particles by cells takes place.

4. Conclusion

We have introduced a new synthetic route for the synthesis of functional nano-aggregates, which are based on the carefully investigated HPMA. Our new systems offer the possibility to vary the size of PHPMA based particles from some nanometres for well-known statistic copolymers to 200 nm for the largers nano-aggregates.

We have proven by MTS test that the structures are not cell toxic up to a concentration of 2 mg/ml. But the ECIS experiments show that the larger nano-aggregate modify the micromotion. Based on the high functionality and biocompatibility our polymeric particles offer the potential to be used as drug carriers or imaging agents. Especially, in combination with the introduction of targeting vectors, a directed distribution of the aggregates in the body may be achieved. In addition the differences in biological activity between nano-aggregates of different size (from **P1** and **P2**) show the potential of polymeric self-assembled structures that take advantage of the EPR effect. But further on the size is an additional parameter -besides targeting vectors- body distribution, cell uptake and biological function.

5. Acknowledgement

We gratefully acknowledge the flow Cell Analysis Facility at the University of Nebraska Medical Center for their skilful assistance und the Graduate School of Excellence (MAINZ) for financial support. We would like to thank Prof. H. Ringsdorf for stimulating discussions.

References

[1] Duncan, R. *Nature Rev. Cancer* **2006**, *6* (9), 688.

[2] Matsumura, Y.; Maeda, H. *Cancer Res.* **1986**, *46*, 6387.

[3] Maeda, H.; Greish, K.; Fang, J. *Ad*V. *Polym. Sci.* **2006**, *193*, 103.

[4] Haag, R.; Kratz, F. *Angew. Chem., Int. Ed.* **2006**, *45*, 1198.

[5] Ringsdorf, H. *J. Polym. Sci. Polym. Symp.* **1975**, *51*, 135.

[6] Yu, K. H.; Eisenberg, A. *Macromolecules* **1998**, *31*, 3509.

[7] Schlerb, B.; Venzmer, J.; Ringsdorf, H. *Angew. Chem., Int. Ed.* **1988**, *100*, 117.

[8] Maeda, H. *Ad*V. *Drug. Deli*V. *Re*V **1991**, *6*, 181.

[9] Maeda, H.; Sawa, T.; Konno, T. *J. Controlled Release* **2001**, *74*, 47.

[10] Yamamoto, Y.; Harada, A.; Nagasaki, Y.; Katuoka, K. *J. Controlled Release* **2002**, *82*, 359.

[11] Kataoka, K.; Kwon, G. S.; Yokoyama, M.; Sakurai, Y. *J. Controlled Release* **1993**, *24*, 119.

[12] Duncan, R. *Makromol. Chem.* **1983**, *184*, 1997.

[13] Kopecek, J.; Rejmanova, P. *Controlled Drug Deli*V*ery*; CRC Press: Boca Raton, FL, 1983; Vol. 1, p 81.

[14] Subr, V.; Ullbrich, K. *React. Funct. Polym.* **2006**, *66*, 1525.

[15] Godwin, A.; Müller, A. H. E.; Brocchini, S. *Angew. Chem., Int. Ed.* **2001**, *40*, 594.

[16] Konak, C.; Matyjaszewski, K.; Kopeckova, P.; Kopecek, J. *Polymer* **2002**, *43*, 3735.

[17] Matjyjaszewski, K.; Xia, J. *Chem. Rev.* **2001**, *101*, 2921–2990.

[18] Benoit, D.; Harth, E.; Fox, P.; Waymouth, R. M.; Hawker, C. J. *Macromolecules* **2000**, 33, 363-370.

[19] Moad, G.; Rizzardo, E.; Thang, S. H. *Aust. J. Chem.* **2005**, *58*, 379.

[20] Chong, Y. K.; Moad, G.; Rizzardo, E.; Tang, S. H. *Macromolecules* **1999**, *32*, 2071.

[21] Eberhardt, M.; Mruk, R.; Zentel, R.; Theato, P. *Eur. Polym. J.* **2005**, *41*, 1569.

[22] Hong, C. Y.; Pan, C. Y. *Macromolecules* **2006**, *39*, 3517.

[23] Yanjarappa, M. J.; Joshi, A.; Saraph, A.; Kane, R. *S Biomacromolecules* **2006**, *7*, 1665.

[24] York, A. W.; Scales, C. W.; Huang, F.; McCormick, C. L. *Biomacromolecules* **2007**, *8*, 2337.

[25] Giaever, I.; Keese, C. *Proc. Natl. Acad. Sci. U.S.A.* **1984**, *81*, 3761–3764.

[26] Lo, C.-M.; Keese, C. R.; Giaever, I. *Exp. Cell Res.* **1993**, *204*, 102–109.

[27] Eberhardt, M.; Theato, P. *Macromol. Rapid Commun.* **2005**, *26*, 1488.

[28] Shen, H.; Zhang, L.; Eisenberg, A. *J. Am. Chem. Soc.* **1999**, *121*, 2728.

[29] Zhang, L.; Eisenberg, A. *J. Am. Chem. Soc.* **1996**, *118*, 3168.

[30] Hug, T. S. *Assay Drug De*V. *Technol.* **2003**, *1* (3), 479.

[31] Fareid Asphahani, F.; Zhang, M. *Analyst* **2007**, *132*, 835.

[32] Giaever, I.; Keese, C. *IEEE Trans. Biomed. Eng.* **1986**, *33*, 242.

[33] Sapper, A.; Wegener, J.; Janshoff, A. *Anal. Chem.* **2006**, *78*, 5184.

2.3 The uptake of N-(2-hydroxypropyl) methacrylamide based homo, random and block copolymers by human multi-drug resistant breast adenocarcinoma cells

Biomaterials **2009**, 30, 5682-5690

Authors: Matthias Barz[1#], Robert Luxenhofer[2#†], Rudolf Zentel[1], Alexander V. Kabanov[2]

Address: [1]Institute of Organic Chemistry, Johannes Gutenberg-University Mainz, Duesbergweg 10-14, 55099 Mainz, Germany

[2]Department of Pharmaceutical Sciences and Center for Drug Delivery and Nanomedicine, College of Pharmacy, University of Nebraska Medical Center,

Omaha, Nebraska 68198-5830, USA

[#] Both authors have equally contributed

Abstract

A series of well defined, fluorescently labelled homopolymers, random and block copolymers based on N-(2-hydroxypropyl)-methacrylamide was prepared by reversible addition-fragmentation chain transfer polymerization (RAFT-polymerization). The polydispersity indexes for all polymers were in the range of 1.2 to 1.3 and the number average of the molar mass (M_n) for each polymer was set to be in the range of 15 kDa to 30 kDa. The cellular uptake of these polymers was investigated in the human multi-drug resistant breast adenocarcinoma cell line MCF7/ADR. The uptake greatly depended on the polymer molecular mass and structure. Specifically, smaller polymers (approx. 15 kDa) were taken up by the cells at much lower concentrations than larger polymers (approx. 30 kDa). Furthermore, for polymers of the same molar mass, the random copolymers were more easily internalized in cells than block copolymers or homopolymers. This is attributed to the fact that random copolymers form micelle-like aggregates by intra- and interchain interactions, which are smaller and less stable than the block copolymer structures in which the hydrophobic domain is buried and thus prevented from unspecific interaction with the cell membrane. Our findings underline the need for highly defined polymeric carriers and excipients for future applications in the field of nanomedicine.

1. Introduction

The last decades have seen a steady increase of interest in polymer therapeutics and nanomedicines [1] such as conjugates of drugs or proteins with synthetic polymers as well as drugs incorporated in dendrimers, polymeric micelles or vesicles of different structure.[1-5] Various systems have reached clinical trials and some have been approved for the human use. [6-14]

It is widely recognized that the interactions of nanomaterials with cells define the toxicity, endocytosis and intracellular localization of such materials and altogether are critically important for the material performance in drug delivery. Studies by numerous groups found that the cellular interactions of nanomaterials in the absence of ligands for specific receptors can be affected by virtually any aspect of the nanomaterial structure and chemistry. In particular, the cellular uptake and even route of endocytosis of various polymers and nanoparticles depend on their size [15], architecture [16], surface charge [17], charge density [18], surface structure [18], and hydrophilic-lipophilic balance. [19] For the members of the family of poly(ethylene oxide)-poly(propylene oxide)-poly(ethylene oxide) amphiphilic triblock copolymers (Pluronic) the structural effects on the interaction with cell membranes have been investigated in great detail. Recently Sahay et al. reported that the uptake route of Pluronic P85 switches from caveolae mediated endocytosis to uptake through clathrin coated pits when the concentration of the copolymer is increased from below to above the critical micelle concentration (cmc). [20] Another material of considerable interest in the nanomedicine and drug delivery fields is poly(*N*-(2-hydroxypropyl) methacrylamide) (pHPMA), which has been extensively used in polymer-drug conjugates and various block copolymer-based systems. [21-24] In this study we investigate the differences in cellular uptake between the aggregate forming HPMA-based amphiphilic block copolymers and random copolymers having the same monomer composition but different polymer architecture. Such structure-property relationships could only be reasonably obtained with polymers that are structurally and chemically well defined. HPMA is typically polymerized by free radical polymerization with functional comonomers. However, this method results in a broad molar mass distribution of the copolymer, and is further complicated by a dependence of the copolymer composition on the conversion of the reaction, which is observed when reactivities of different monomers are not perfectly matched. Furthermore, the precise molar mass determination of amphiphilic copolymers by gel permeation chromatography (GPC) or nuclear magnetic resonance (NMR) is often complicated by the aggregation of these copolymers in solution. [25-27] Recent advances in controlled radical polymerization techniques including the atom transfer radical (ATRP) polymerization [28-30] and the reversible addition-fragmentation chain transfer (RAFT) polymerization [31-33] can produce well-defined polymers. Using these techniques it is possible to synthesize random copolymers as well as block copolymers. Furthermore, functional polymers can also be synthesized by these methods using functional monomers such as active esters established by

Ringsdorf et al. [34-37] This synthetic pathway has two main advantages. First, it can produce random copolymers by polymer-analogue transformation of precisely characterized functional homopolymer precursors. Second, amphiphilic block copolymers can be produced from functional precursors, which consist only of hydrophobic blocks and can be precisely characterized by GPC in solvents such as tetrahydrofuran, dioxane or hexafluoroisopropanol.

Here, we employ RAFT polymerization to produce defined HPMA homopolymers as well as random and block copolymers of HPMA and laurylmethacrylate of comparable molar mass. By this approach it was possible to compare the cellular uptake of various polymer architectures based on identical monomers. In the following article we invastigate the influence of molar mass and polymer architecture on the endocytosis of the HPMA-based polymers in the multi-drug resistant (MDR) breast cancer cell line MCF7/ADR. This study underscores a need for highly defined polymers for applications in the field of nanomedicine.

2. Experimental Section

2.1 Materials

All chemicals were reagent grade and obtained from Aldrich. The chemicals were used without further purification unless otherwise indicated. The Oregon green 488 cadaverine was obtained from Invitrogen. Dioxane used in the synthesis was freshly distilled from a sodium/potassium mixture. 2,2'-Azobis(isobutyronitrile) (AIBN) was recrystallized from diethyl ether and stored at -7°C. Lauryl methacrylate was distilled and kept at -7°C.

2.2 Characterization

^{1}H-, ^{13}C- and ^{19}F-NMR spectra were obtained at 300 or 400 MHz using a FT-spectrometer from Bruker and analyzed using the ACDLabs 6.0 software. The polymers were dried at 40 °C over night under vacuum and afterwards submitted to gel permeation chromatography (GPC). GPC was performed in tetrahydrofurane (THF) as solvent and with following parts: pump PU 1580, auto sampler AS 1555, UV-detector UV 1575, RI-detector RI 1530 from Jasco and miniDAWN Tristar light scattering detector from Wyatt. Columns were used from MZ-Analysentechnik: MZ-Gel SDplus 10^{2} Å, MZ-Gel SDplus 10^{4} Å and MZ-Gel SDplus 10^{6} Å. The elution diagrams were analysed using the ASTRA 4.73.04 software from Wyatt Technology. Calibration was done using polystyrene standards. The flow rate was 1 mL/min at a temperature of 25 °C.

2.3 Synthesis of 4-cyano-4-((thiobenzoyl)sulfanyl)pentanoic acid

The 4-cyano-4-((thiobenzoyl) sulfanyl)pentanoic acid was used as the CTA and synthesized according to the literature. [32]

2.4 Synthesis of pentafluoro-phenyl methacrylate (PFMA)

PFMA was prepared according to the literature. [36]

2.5 General synthesis of the macro-CTA

The macro-CTA was prepared according to the literature. [37] The RAFT polymerizations of the PFMA using 4-cyano-4-((thiobenzoyl) sulfanyl) pentanoic acid were performed in a schlenk tube. The reaction vessel was loaded with 2,2'-azobis(isobutyronitrile (AIBN), 4-cyano-4-((thiobenzoyl)-sulfanyl)pentanoic acid (CTA) (molar ratio of AIBN/CTA = 1:8) and 15 g of PFMA in 20 mL of dioxane. Following three freeze–vaccum–thaw cycles, the tube was immersed in an oil bath at 70 °C. Afterwards the polymer poly(PFMA) was 3 times precipitated into hexane, isolated by centrifugation and dried for 12 hours at 30 °C under vacuum. In the end a slightly red powder was obtained. Yield: (59 %). ^{1}H NMR ($CDCl_3$): δ [ppm] 1.6-2.2 (br), 0.9-1.5 (br) ^{19}F NMR ($CDCl_3$): δ [ppm] -165.1 (br), -159.8 (br), -154.4 (br), -153.1 (br).

2.5 General synthesis of the random copolymers

The RAFT polymerizations of the PFMA using CTA were performed in a schlenk tube. The reaction vessel was loaded with AIBN, CTA (molar ratio of AIBN/CTA = 1:8) and 15 g of PFMA in 20 mL of dioxane. Following three freeze–vaccum–thaw cycles, the tube was immersed in an oil bath at 70 °C. Afterwards the polymer poly(PFMA) was 3 times precipitated into hexane, isolated by centrifugation and dried for 12 hours at 30 °C under vacuum. In the end a slightly red powder was obtained. Yield: (67 %). ^{1}H NMR ($CDCl_3$): δ [ppm] 1.6-2.2 (br), 0.9-1.5 (br), 0.8-0.9 (br t) ^{19}F NMR ($CDCl_3$): δ [ppm] -165.1 (br), -159.8 (br), -154.4 (br), -153.1 (br).

2.7 General synthesis of block copolymers

The block copolymer was prepared according to the literature. [26] The macro CTA obtained in the above-mentioned polymerization was dissolved in dioxane and AIBN was added. Nitrogen was bubbled through the solution and three freeze-vacuum-thaw cycles were applied. Afterwards the tube was immersed in an oil bath at 70 °C. After polymerization time of 12 h, the solution was slightly concentrated and precipitated twice in ethanol and diethyl ether, removed by centrifugation, and dried overnight at 30 °C in vacuum. A slightly red powder was obtained. Yield: (89 %). ^{1}H NMR ($CDCl_3$): δ [ppm] 1.6-2.2 (br), 0.9-1.5 (br), 0.8-0.9 (br t) ^{19}F NMR ($CDCl_3$): δ [ppm] -165.1 (br), -159.8 (br), -154.4 (br), -153.1 (br).

2.8 Removal of dithioester end groups

The dithiobenzoate end group was removed according to the procedure reported by Perrier et al. [38] Typically 200 mg of polymer, (Mn = 25.000 g/mol), and 50 mg of AIBN (30 times excess in relation to the polymer endgroup) were dissolved in 3 mL of anhydrous dioxane/DMSO (4:1). The solution was heated at 80 °C for 2 h. Finally the copolymer was precipitated 3 times in 100 mL of diethyl ether and collected by centrifugation. In the case of the block copolymer the crude product was first precipitated in EtOH 2 times and than 1 time in diethyl ether. The copolymer was dried under vacuum for a period of 24 h and a colourless product was obtained (yield: 92 %). The absence of the dithiobenzoate end group was confirmed by UV-Vis spectroscopy.

2.9 Polymer analogous reactions of homopolymers

In a typical reaction 300 mg of PPFMA without ditihioester endgroup were dissolved in 4 mL abs. dioxane and 1 mL abs. DMSO. A colorless solution was obtained. In a typical reaction 2.5 mg for the 50000 g/mol precursor and 5 mg for the 25000 g/mol precursor of Oregon green 488 cadaverine and 20 mg of triethylamine were added. The mixture was kept at 25 °C for 4 h and finally 200 mg of hydroxypropylamine and 200 mg triethylamine were added. The reaction was allowed to proceed under the above-mentioned conditions over night. The solution was concentrated in vacuum and introduced to a column filtration using Sephadex^{TM} LH-20 in dioxane and precipitated in diethyl ether, removed by centrifugation and dried in vacuum at 30 °C for 14 hours. Yield: (86 %). ^{1}H NMR (DMSO-*d*6): δ [ppm] 3.4-3.9 (br), 2.6-3.0, 0.9-1.5 (br).

2.10 Polymer analogous reactions of random copolymers

In a typical reaction 300 mg of PPFMA without ditihioester endgroup were dissolved in 4 mL abs. dioxane and 1 mL abs. DMSO. A colorless solution was obtained. In a typical reaction 2.5 mg for the 50000 g/mol precursor and 5 mg for the 25000 g/mol precursor of Oregon green 488 cadaverine and 20 mg of triethylamine were added. The mixture was kept at 25 °C for 4 hours and finally 200 mg of hydroxypropylamine and 200 mg triethylamine were added. The reaction was allowed to proceed under the above-mentioned conditions over night. The solution was concentrated in vacuum and introduced to a column filtration using Sephadex^{TM} LH-20 in dioxane and precipitated in diethyl ether, removed by centrifugation and dried in vacuum at 30 °C for 14 hours. Yield: (79 %). ^{1}H NMR (DMSO-*d*6): δ [ppm] 3.4-3.9 (br), 2.6-3.0 (br), 0.9-1.5 (br), 0.8-0.9 (br t).

2.11 Polymer analogous reactions of block copolymers

In a typical reaction 300 mg of poly(PFMA)-block-poly(lauryl methacrylate) were dissolved in 4 ml abs. dioxane and 1 ml abs. DMSO. A colourless solution was obtained. In a typical reaction 5 mg of Oregon green 488 cadaverin and 20 mg of triethylamine were added. The mixture was kept at 25 °C for 4 hours. In the end 200 mg of hydroxypropylamine and 200 mg triethylamine were added. The

reaction was allowed to go on under the above-mentioned conditions over night. The solution was concentrated in vacuum and introduced to a column filtration using Sephadex^{TM} LH-20 in dioxane/DMSO (4:1) and precipitated in diethyl ether, removed by centrifugation and dried in vacuum at 30 °C for 14 hours. Yield: (81%). ^{1}H NMR (DMSO-*d*6): δ [ppm] 3.4-3.9 (br), 2.6-3.0 (br), 0.9-1.5 (br), 0.8-0.9 (br t).

2.12 Characterization in Solution

The aqueous solutions were prepared using Millipore water (deionized water, resistance >18 MW) and abs. DMSO. Pyrene (Aldrich, 98%) was used as fluorescent probe without further purification.

2.13. Pyrene Fluorescence Spectroscopy [39-41]

A stock solution of each block copolymer was prepared at a concentration of 0.1 g/L by dissolving the polymer in DMSO. The polymer stock solution was then diluted to 10 different concentrations down to 1×10^{-6} g/L using an aqueous NaCl solution. Each sample was then prepared by dropping carefully 40 mL of a pyrene solution (2.5×10^{-5} mol/L in acetone) into an empty vial, evaporating the acetone by gentle heating at 50-60 °C, adding 2 mL of one of the polymer solutions, and stirring the closed and light-protected vials 48-72 h at 50-60 °C. The final concentration of pyrene in water thus reached 5.0×10^{-7} mol/L, which is slightly below the pyrene saturation concentration in water at 22 °C. Steady-state fluorescence spectra of the air-equilibrated samples were recorded using a Perkin Elmer Luminescence Spectrometer LS 50 B spectrofluorophotometer (right angle geometry, 1 cm × 1 cm quartz cell) using the following conditions: excitation at 333 nm, slit width 10 nm for the excitation, and 2.5 nm for the emission. The intensities of the bands I1 at 372 nm and I3 at 383 nm were then evaluated, and their ratio was plotted vs the polymer concentration.

2.14. Light scattering experiments of Nanoaggregates

A total of 10 mg of the poly(HPMA)-*block*-poly(lauryl methacrylate) polymer were dissolved overnight in 10 mL of 1×10^{-3} M solution of lithium trifluoroacetate in hexafluorisopropanol (HFIP). The solution was filtered with an anatop 20 nm filter. A total of 40 mg of the block copolymer solution (*c*) 1 mg/ml) were added drop wise to 2.2×10^{-3} mg of an aqueous solution of sodium bromide (NaBr; 1 × 10-3 M). Under this condition, the influence of the solvent (HFIP) can be disregarded. The aggregates were analyzed right after the preparation by dynamic light scattering. For dynamic light scattering (DLS), an ALV-SP125 goniometer, an ALV-5000 correlator, a Spectra Physics 2060 Argon ion laser (500 mW output power at λ) 514.5 nm wavelength) were utilized. The scattered intensity was divided by a beam splitter (approximately 50:50), each portion of which was detected by a photomultiplier. The two signals were cross-correlated to eliminate nonrandom electronic noise. The complex solutions were typically measured from 30-150° in steps of 10° (DLS).

The correlation functions showed a monomodal decay and were fitted by a sum of two exponentials, from which the first cumulant Γ was calculated. The *z*-average diffusion coefficient D_z was obtained by extrapolation of $\Gamma/q2$ to $q = 0$, leading to the inverse *z*-average hydrodynamic radius $R_h = \langle R_h^{-1} \rangle_z^{-1}$ by formal application of Stokes law.

2.14. Cell culture

MCF7-ADR cells (derived from human breast carcinoma cell line, MCF7 (ATCC HT-B22) by selection with Doxorubicin, was kindly presented by Y.L. Lee (William Beaumont Hospital, Royal Oak, MI) and were maintained in Dulbecco´s Modified Eagle´s Medium (DMEM), containing 10% heat inactivated fetal bovine serum (FBS) and 1% penicillin/streptomycin as described elsewhere.[46] All tissue material media was obtained from Gibco Life Technologies, Inc. (Grand Island, NY). Cells were used 2 days after plated unless otherwise stated.

2.15. Evaluation of cytotoxicity of Polymers; MTT assay

MCF7/ADR were seeded in 96 well plates (10^4 cells per well) and were allowed to reattach for 24 h. Treatment solutions were prepared from a 1 mg/mL polymer stock solution in assay buffer (containing 122 mM NaCl, 25 mM $NaHCO_3$, 10 mM glucose, 10 mM HEPES, 3 mM KCl, 1.2 mM $MgSO_4$, 1.4 mM $CaCl_2$, and 0.4 mM K_2HPO_4, pH 7.4) by appropriate dilution with media (Dulbecco´s Modified Eagle´s Medium (DMEM), supplemented with 10% fetal bovine serum (FBS), 25 mM HEPES and penicillin/streptomycin). The cells were incubated for 48 h with 200 µL of treatment solution. After discarding the treatment solution, cells were washed thrice with PBS. FBS-free DMEM (100 µL/well) as well as 25 µL of a 5 mg/mL solution of 3-(4,5-dimethylthiazol-2-yl)-2,5-diphenyltetrazolium bromide (MTT, Invitrogen, Eugene, Oregon) in PBS were added and the cells incubated at 37 °C for 2 hours. The media was discarded subsequently and replaced with 100 µL of solvent (25% v/v DMF, 20% w/v SDS in H2O). The purple formazan product was allowed to dissolve over night and the absorbance at 570 nm was obtained using a plate reader (SpectraMax M5, Molecular Devices). Positive control cells were treated with media alone, negative controls were wells without cells. Each concentration was repeated in four wells, results are expressed as mean ± SEM.

2.16. Flow cytometry

For the analysis of cellular uptake by flow cytometry, MCF7/ADR cells were plated in 24 well plates (7.5×10^4 per well) two days prior to the experiment. Cells were treated with 200 µL of polymer solutions in FBS free media or assay buffer. In the case of experiment performed at 4 °C, the cells were pre-washed 3 times with ice cold PBS and incubated with ice-cold polymer solution. Cells were incubated for 60 min or the indicated time at 37 °C/5% CO_2 or 4°C, washed subsequently thrice with ice-cold PBS, trypsinized and centrifuged. The cell pellet was resuspended in 400 µL PBS with 1%

bovine serum albumin, split in two aliquots and analyzed using flow cytometry. Each data point was performed in triplicate. The mean fluorescence intensity was analyzed using Becton Dickinson FACStarPlus flow cytometer operating under Lysis II (San Jose, CA) equipped with an argon ion laser. Data were acquired in linear mode and visualized in logarithmic mode. Approximately 10,000 digital list mode events were collected and the data gated on forward and side-scatter parameters to exclude debris and dead cells. Control cells without labelled polymers were used as the negative control for autofluorescence. Data analysis was performed using DiVa software.

2.17. Confocal fluorescence microscopy

For live cell confocal microscopy (Carl Zeiss LSM 510 Meta, Peabody, MA) MCF7/ADR cells (4×10^4) were plated in Lab-Tek Chambered Cover Glasses dishes (Fischer Scientific, Waltham, MA) and after two days (37 °C, 5% CO_2) were exposed for 60 min to Oregon green labelled polymer solutions in FBS free media. Subsequently, cells were washed (3x PBS) and kept in complete media for imaging using the confocal microscope.

3. Results and Discussion

In order to investigate the influence of polymer architecture on the cellular uptake we synthesized by RAFT polymerization a series of fluorescently labelled HPMA-based homopolymers, random copolymers and block copolymers of different molar mass. The synthesis reactions are shown in scheme 1.

First, the active ester polymer precursors **P1R** to **P6R** were synthesized using an approach proposed by Ringsdorf group. [34-37] Second, these functional precursors were transformed by aminolysis into final HPMA based polymers **P1** to **P6**.

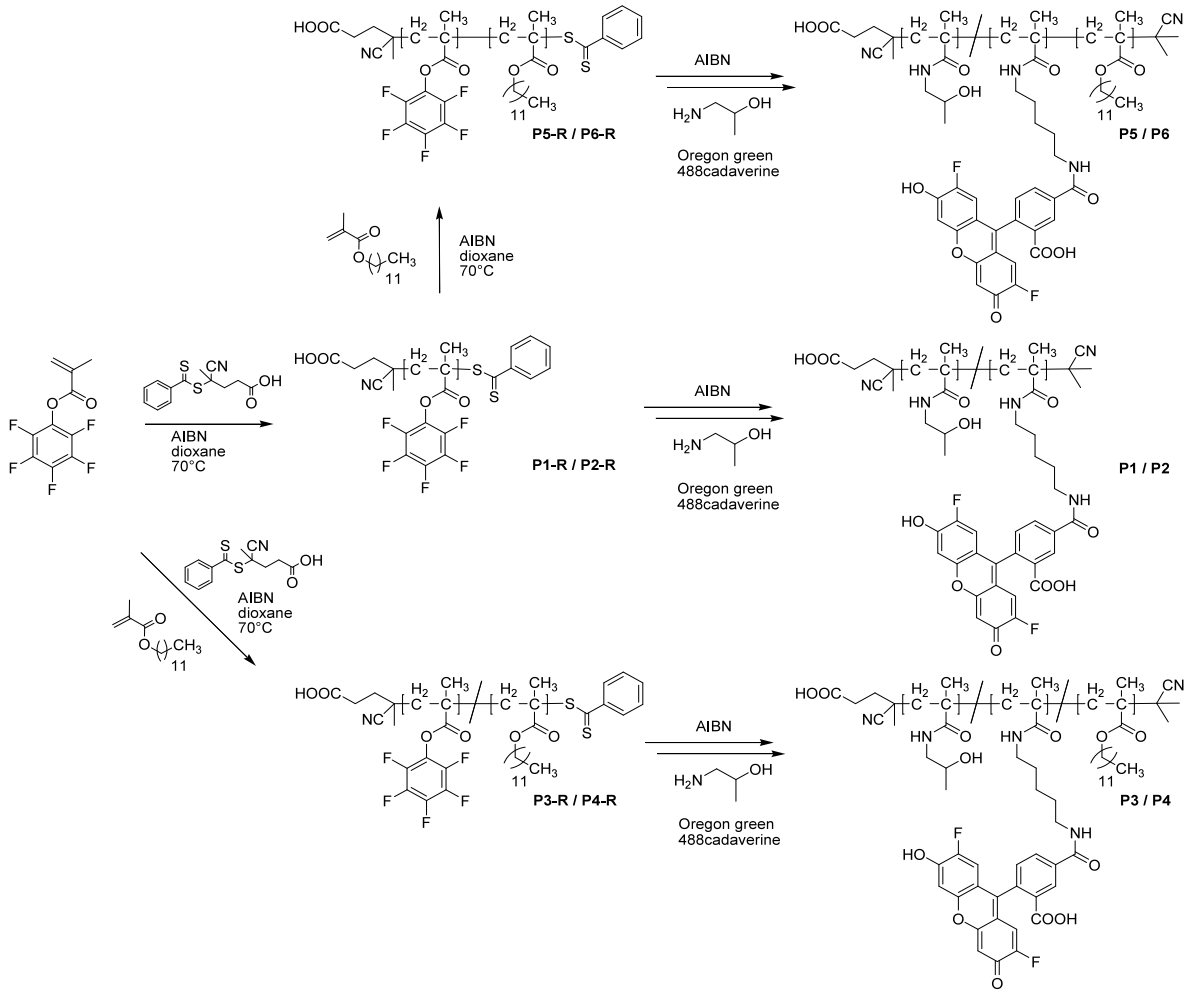

Scheme 1. Synthetic pathway to fluorescently labelled homopolymers, random copolymers and block copolymers based on pHPMA using the active ester approach.

Second, these functional precursors were transformed by aminolysis into final HPMA based polymers **P1** to **P6**. To obtain fluorescently labelled polymers the reactive precursor polymers were aminolysed in the presence of Oregon green 488 cadaverin and 2-hydroxy isopropan-1-ol. In average each polymer chain was labelled with one molecule of dye. For all polymer samples the conversion of the pentafluorophenyl-derivative to the HPMA was full as determined by a complete disappearance of the ^{19}F signal in the ^{19}F NMR spectra of the final polymers. Due to the use of dithiobenzoate derivatives as chain transfer agents (CTA) the end groups of the synthesized polymers represented a dithiobenzoic ester, which can undergo side reactions during the aminolysis of the pentafluorophenyl ester. [38] In order to avoid these side reactions the end group was removed prior to the aminolysis by large excess of AIBN.

For each polymer architecture two samples with different molar mass were synthesized. The molar masses and polydispersity indexes (PDI) of the precursor polymers **P1R** to **P6R** were determined by GPC. The molar mass and PDI of the precursors and final polymers are listed in Tables 1 and 2, respectively.

Table 1. Characteristics of reactive homopolymers (**P1R**, **P2R**), copolymers (**P3R**, **P4R**) and block copolymers (**P5R**, **P6R**)

	structure	monomer ratio [a]	M_n [b]	M_w [b]	PDI [b]
P1R	homopolymer	100:0	21.1	25.1	1.19
P2R	homopolymer	100:0	50.2	60.8	1.21
P3R	random copolymer	80:20	22.3	27.4	1.23
P4R	random copolymer	80:20	50.0	59.8	1.20
P5R	block copolymer	80:20	24.7	28.6	1.20
P6R	block copolymer	90:10	52.2	65.8	1.26

[a] Calculated monomer ratio

[b] kg/mol, determined by GPC in THF as solvent for the activated ester polymers P1R to P6R

Table 2. Characteristics of HPMA based random copolymers (**P1**,**P2**,**P3**,**P4**) and block copolymers (**P5**,**P6**).

	structure	HPMA/LMAunit ratio [a]	M_n [b]	M_w [b]	PDI [b]
P1	homopolymer	100:0	12.2	14.3	1.19
P2	homopolymer	100:0	28.7	40.0	1.21
P3	random copolymer	78:22	14.6	20.2	1.23
P4	random copolymer	81:19	32.8	39.3	1.20
P5	block copolymer	79:21	12.5	15.4	1.20
P6	block copolymer	88:12	27.7	32.5	1.26

[a] As determined by ^{1}H NMR spectroscopy after aminolysis with hydroxypropylamine yielding **P1** to **P6**

[b] kg/mol, determined by GPC in THF as solvent for the activated ester polymers **P1R** to **P6R**.

The molar masses of the homopolymers were in the range established for clinically investigated pHPMA-based drug conjugates like PK1 and PK2. [3] The PDI values suggested that these polymers had relatively narrow molar mass distribution, which is characteristic of polymers synthesized by RAFT polymerization (PDI 1.1-1.3). [31] The random copolymers and block copolymers had comparable molar masses and PDI. However, due to their architecture the block copolymers formed micelle-like aggregates in aqueous solutions. These aggregates were spherical and had sizes ranging from about 100 nm to about 200 nm as determined by dynamic and static light scattering as well as by cryo transmission electron microscopy (cryo TEM) imaging experiments. [26]

To verify the concentration-dependent aggregation of the block copolymers **P5** and **P6** and determine the cmc the pyrene fluorescence technique was applied. [39-41] Pyrene has a very low solubility in water and upon formation of the micelles transfers preferentially into their hydrophobic cores. This is accompanied by a red shift in the pyrene fluorescence spectrum and changes in relative peak

intensities of the spectrum's vibrational fine structure. [41] To determine the onset of the micelle formation we analysed the pyrene emission spectra as reported previously by Müller et al. [39] as well as by Winnik [40] and coworkers. Figure 1 shows the dependencies of the intensity ratio I1/I3 vs. concentration of polymer in aqueous solution at pH 7.

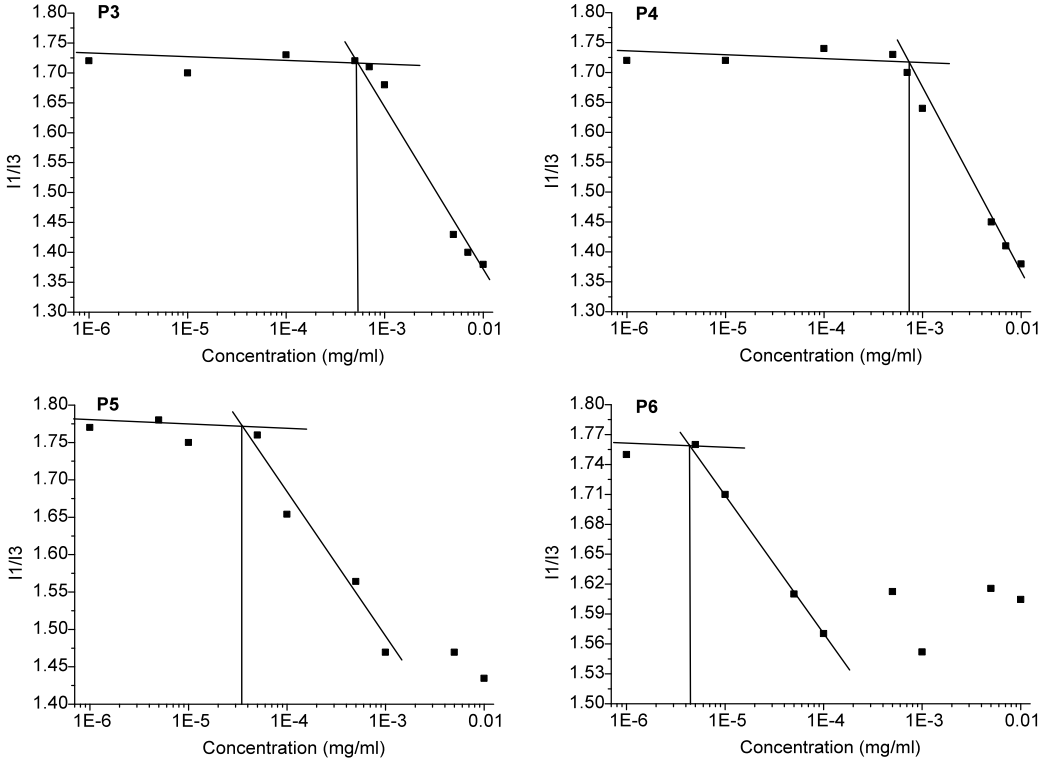

Figure 1. The cmc estimation of random copolymer **P3**, **P4** and block copolymer **P5**, **P6** by pyrene fluorescence spectroscopy in isotonic solution at pH 7

The I1/I3 values remained constant (~1.7-1.8) at the polymer concentrations $c < 6.0\times10^{-5}$ mg/mL ($c < 4.8\times10^{-9}$ mol/L) for **P5** and $c < 5.5\times10^{-6}$ mg/mL ($c < 2.0\times10^{-10}$ mol/L) for **P6**. These I1/I3 values suggest that in the corresponding ranges of the copolymer concentrations pyrene was in aqueous environment and the micelles did not form. At higher concentrations the I1/I3 decreased suggesting that the micelles were formed and pyrene transferred into the hydrophobic environment. The cmc values (table 3) were determined as the intersections between the plateau at I1/I3 ~ 1.7-1.8 and the tangent of the decrease of I1/I3 vs. concentration in figure 1. These values for the block copolymers **P5** and **P6** are rather low, which is attributed to the presence of highly hydrophobic lauryl methacrylate side chains in the hydrophobic blocks. Furthermore the cmc, of **P6** is lower than that of **P5**, which is consistent with the larger hydrophobic block in **P6**.

Table 3. The cmc of the block copolymers (**P3-P6**) in isotonic solution

	Structure	Cmc	
		mg/mL[a]	mol/L[a]
P3	random copolymer	5.3×10^{-4}	3.6×10^{-8}
P4	random copolymer	7.2×10^{-4}	2.2×10^{-8}
P5	block copolymer	2.4×10^{-5}	1.9×10^{-9}
P6	block copolymer	4.1×10^{-6}	1.5×10^{-10}

[a] As determined by pyrene fluorescence spectroscopy

Interestingly, the random copolymers **P3** and **P4** also exhibited a cmc-like behaviour. Specifically, the I1/I3 values for these copolymers decreased above certain concentrations. This suggested aggregation of the copolymers and formation of hydrophobic domains, in which pyrene was incorporated. However, the concentrations corresponding to the onset of the I1/I3 decrease, which for simplicity we will also call "cmc", were considerably higher than the cmc values for **P5** and **P6**.

Table 4. Characterization of aggregates from **P3** to **P6** in hexafluoroisopropanol (HFIP) and aqueous NaBr (1×10^{-3} M) solution

	R_h (nm) in HFIP	c (mg/mL) in aqueous solution	R_h (nm) in aqueous solution	μ_2
P3	3.1 ± 0.15	0.01	37.2	0.11
P4	3.8 ± 0.15	0.01	32.3	0.09
P5	3.0 ± 0.15	0.01	55.7	0.08
P6	3.8 ± 0.15	0.01	112	0.07

Furthermore, the sizes of the aggregates of **P3** and **P4** determined by dynamic light scattering practically did not depend on the copolymer molecular masses, while the sizes of the **P5** and **P6** micelles increased as the copolymer mass increased (table 4). Previous work suggests that the aggregates of the amphiphilic random copolymers in selective solvents are essentially indistinguishable from micelles. [42-45] Such aggregates in aqueous dispersions often consist of dense hydrophobic cores surrounded by a corona of swollen loops formed by the hydrophilic parts of the polymer (figure 2). The formation of the loops leads also to smaller hydrophilic corona as well as less defined and less stable aggregates, which in case of **P3** and **P4** is reflected in a slightly higher m_2 value and higher cmc. Furthermore a certain number of accessible lauryl side chains in the hydrophilic loop can be expected, because a complete separation of hydrophilic and hydrophobic parts will be precluded by steric hindrance and unfavorable entropy term.

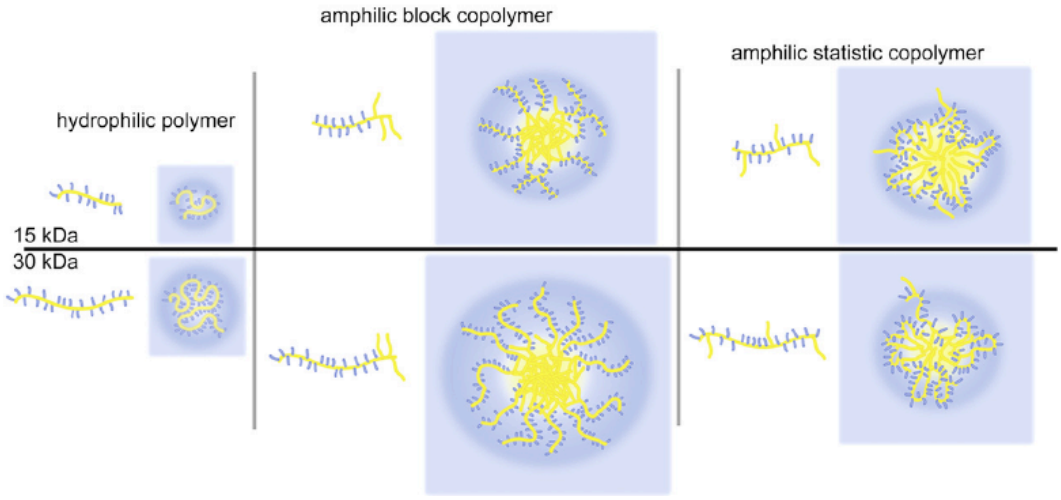

Figure 2. Schematic sketch of self-assembled polymeric structures in aqueous solution (blue parts: hydrophilic, yellow parts: hydrophobic). Homopolymers are present as unimers (left), block copolymers from polymer micelles or micelle like core-shell aggregates (center) while random copolymers can form less stable aggregates through intra- and interchain interactions.

The HPMA homopolymer is well known to be non-toxic and non-immunogenic. Recently we reported that HPMA-lauryl methacrylate block copolymers are also non-toxic to MDCKII cells in concentrations of up to 2 mg/mL. [26] However, we could not exclude that random copolymers were toxic and, therefore, evaluated the cell toxicity of all polymers in MDR breast adenocarcinoma cell line MCF7/ADR using standard 3-(4,5-dimethylthiazol-2-yl)-2,5-diphenyltetrazolium bromide (MTT)

assay. Since we observed no decrease in cell viability following exposure of the cells for 48 h to the random copolymers at concentrations of up to 0.1 mg/mL we concluded that they were safe up to this dose. Next, we investigated the cellular uptake of the fluorescently labelled polymers by flow cytometry. For this purpose the adherent MCF7/ADR cells in 24-well plates were exposed for 60 min to polymer solutions at concentrations ranging from 0.0002 mg/mL to 1 mg/mL. The cells were then suspended and analyzed by flow cytometry to determine the amount of the fluorescence-positive cells (% gated cells) and the mean fluorescence of the cell population. Polymer uptake was time and concentration dependent (exemplarily shown for **P5**, Figure 3A and 3B) as well as temperature-dependent (figure 3C), suggesting that endocytosis was a primary mechanism of the cellular entry. [20]

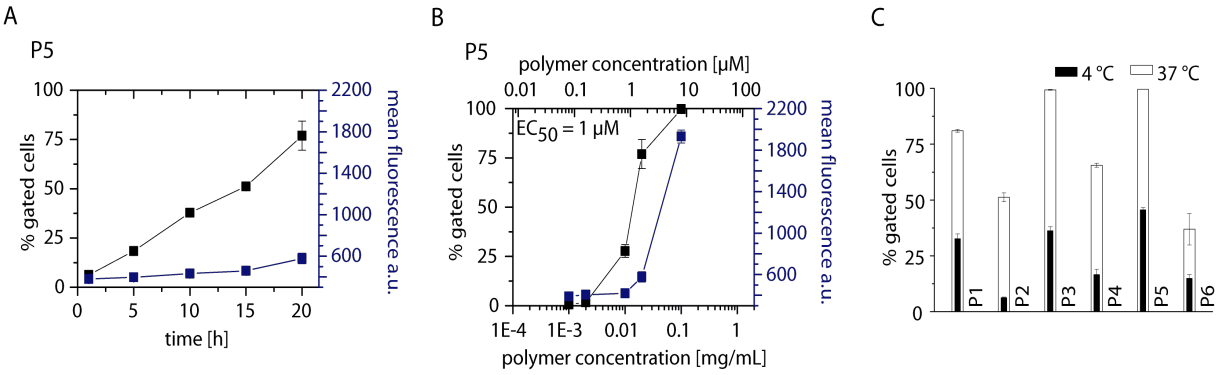

Figure 3. Time (A), concentration (B, 20h incubation) and temperature (C) dependence of cellular uptake of **P5** (A and B) and **P1**-**P6** (C), respectively, as obtained from flow cytometry (% gated cells left; ■ and mean fluorescence per gated event right; ■). EC50 value shows the concentration where 50 % gated cells are observed and were obtained by graphical extraction. Data is represented as mean ± SEM (n=3).

Notably, both the molar mass and structure of the polymers had major effects on the uptake. Specifically, in each pair of the homopolymers, random copolymers or block copolymers the uptake was more pronounced for a smaller polymer in the pair. Furthermore, there were striking differences in the concentration dependences of the uptake between each of the three structure types. To quantify these differences we introduced an effective concentration parameter, EC_{50}, which corresponds to the polymer concentration at which 50 % of cells were gated. It was obvious that the difference in EC_{50} of the smaller and larger homopolymers **P1** and **P2** was negligible (figures 4A and 4B, 33 vs. 35 µM). In contrast, in the case of the random copolymers **P3** and **P4** the smaller copolymer was taken up into the

cells at much lower doses than the larger copolymer (Figures 4C and 4D 0.2 vs. 15 µM). Likewise, in the case of the block copolymers **P5** and **P6** the smaller copolymer was accumulated in cells at lower doses than the larger one (figures 4E and 4F, 7 vs. > 55 µM). We posit that observed differences in the cellular uptake of the homopolymers, random and block copolymers may be related to different mechanisms of cellular entry of the polymers with different architecture.

Figure 4. Concentration dependent endocytosis of fluorescently labelled polymer samples **P1-P6** (A-D). MCF7/ADR cells were incubated for 60 min at 37°C and subsequently analyzed by flow cytometry. In each diagram, the concentration (upper x-axis molar concentration; lower x-axis mass concentration b, is plotted against % gated cells (left, ■) and mean fluorescence per gated event (right, ■). EC_{50} values show the concentration where 50 % gated cells are observed and were obtained by graphical extraction. Data is represented as mean ± SEM (n=3).

As shown for **P5** the cellular uptake was relatively slow and increased almost linearly as the time of incubation increased for at least 20 h (figure 3A). Interestingly, we did not find a pronounced

difference in the concentration dependent behaviour of uptake even if we incubated the cells with the polymer for 20 h. (figure 3B). For example, in the case of **P5**, the EC_{50} after 20 h incubation was 1 μM, which was fairly close to 7 μM observed after 60 min incubation (figure 4E). It is important to keep in mind that at the investigated concentrations the block copolymers **P5** and **P6** aggregated into micelle-like structures with a diameter of approx. 112 nm and 224 nm as reported earlier (table 4). These structures were significantly larger than e.g. the micelles of Pluronic P85 (approx. 15 nm in diameter) that were recently shown to enter mammalian cells through a clathrin-mediated endocytosis. [20]

However, DeSimone and co-workers reported that polymer particles of 100 nm, 150 nm and even as large as several micrometers can be taken up in HeLa cells. [16] As discussed above, **P6** formed considerably larger aggregates (approx. 224 nm diameter) than those formed by **P5** (approx. 112 nm diameter). Such aggregates formed by **P6** also had a hydrophilic corona of longer HPMA chains, which likely hindered interaction of the particles with the membranes. In contrast, the aggregates formed by **P5** had considerably smaller HPMA chains, which could permit limited interactions of the particles with the cellular membranes and increased the cellular uptake.

In contrast to the block copolymers, the random copolymers **P3** and **P4** form aggregates, which are likely to be slightly more loosed and less stable than the block copolymer micelles. These structures are likely to have only small hydrophilic loops, which stabilize the aggregates' particle in aqueous solution. [45] As discussed, the loops will also contain some hydrophobic lauryl groups. Such more accessible hydrophobic groups in the corona of the aggregates can be expected to serve as anchors for unspecific adhesion to the random copolymers in cell membranes. In contrast the hydrophobic lauryl groups are not present in the corona of the block copolymer micelle.

This difference may explain why the onsets of the cellular uptake of the random copolymers were observed at very low concentrations - around 1 mg/L for **P3** (0.03 μM) and **P4** (0.1 μM). These concentrations were one to two orders of magnitude lower than in the case of the homopolymer **P1** or block copolymer **P5** that were most efficiently taken up into cells in their structure classes. Interestingly, while the onset of the uptake of the random copolymers **P3** and **P4** was observed at comparable concentrations, their concentration dependence profiles were quite distinct. Specifically, the uptake of a larger copolymer **P4** increased only slightly as the concentration increased. In contrast, the smaller copolymer **P3** exhibited a sharp increase of the uptake. As a result, the EC_{50} values for **P3** and **P4** differed by two orders of magnitude. We attribute this difference to the differences in the molar mass and sizes of the copolymer chains. As already mentioned above, we hypothesize that aggregated random copolymers can bind with the membrane via the hydrophobic anchor groups - lauryl moieties in the hydrophilic loops of the micelle. These groups are possibly more accessible than in the block copolymer micelles due to the smaller hydrophilic corona of the random copolymer aggregates. Even though the hydrodynamic radii of both random copolymers is comparable, the cmc

value of **P3** is double compared to **P4**, indicating less stable aggregates. In addition, **P3** has a higher relative amount of hydrophobic units in the polymer and therefore can be expected to have a larger number of lauryl chains in the hydrophilic loops of the aggregates. Thus, an increase in the cellular uptake of **P3** compared to **P4** is reasonable.

It is also interesting to note that while **P3** entered the cells at considerably lower concentrations than **P5**, the amount of internalized polymer increased only slowly and reached a plateau at a concentration of around 30 µM, indicating a saturation effect (figure 4C). In contrast, **P5** uptake showed no signs of saturation resulting in greater fluorescence intensity levels than for **P3** at polymer concentrations of 1 mg/mL (figure 4E). A laser scanning confocal microscopy study using these two polymer samples suggested a substantial difference in the sub-cellular localization of these polymers (figure 5).

Figure 5. Confocal microscopy images taken from live MCF7/ADR cells after incubation with 1 mg/mL **P3** (A) or **P5** (B) for 60 min. Nuclei were stained using DRAQ5 (Biostatus Limited, UK), polymers were labelled with oregon green 488. Pictures showing from top left to bottom right DRAQ5, polymer, DIC and merge respectively.

Interestingly, **P3** showed a relatively homogenous distribution within the cytosol and the nucleoplasm (figure 5A). However, much to our surprise, more pronounced fluorescence intensity was found in the nucleoli. In contrast, the confocal micrograph of cells incubated with **P5** revealed a relatively even distribution of fluorescence throughout the cytosol, no appreciable fluorescence in the nucleoplasm

and little fluorescence in the nucleoli. In both cases, however, it was clear that the polymers were not membrane bound but were taken up into the cells and clearly were not punctuate, i.e. not restricted to vesicles within the cytosol. This is an important finding for the projected use of the HPMA-based polymers for drug delivery since it suggests that such polymers can reach various intracellular compartments.

Further investigations are necessary to understand the mechanism of endocytosis involved and the distribution of the polymeric structures within the cell. The novel synthetic approach to obtain well-defined HPMA based polymers of different polymer microstructures by RAFT is important to allow the determination of these complex structure-property relationships.

4. Conclusion

In this work we present the synthesis of well-defined HPMA based homopolymers, random and block copolymers, which allowed us to study the structural effects on the endocytosis in MDR breast cancer cells over a wide range of concentrations. At non-toxic doses of polymers we observed that the amount of polymers taken up by the cells after 60 min of incubation strongly depended on the polymer structure and the molar mass of the samples. For HPMA homopolymers the amount of cellular uptake was relatively low while for the 15 kDa (P5) block copolymers the uptake was higher and occurred at lower concentrations. The random copolymer of 15 kDa (P3) was taken up to a similar extent. However, in contrast to a block copolymer the uptake of P3 began at lower concentrations and reached saturation at higher concentrations. We propose that the molar mass and the polymer architecture are important determinants for the endocytosis and that our new synthetic approach towards defined HPMA based copolymers allows tailoring the cellular uptake of synthetic, biocompatible polymers. More detailed investigations regarding the uptake mechanism and the suitability of these polymers for drug delivery are warranted and are currently performed in our laboratories.

5. Acknowledgements

We gratefully acknowledge the financial support from the United States National Institutes of Health (2RO1 CA89225) and Department of Defence (USAMRMC 06108004) awarded to AVK. We also

acknowledge the Confocal Laser Scanning Microscope and Cell Analysis Core Facility at UNMC for their skillful assistance and the Graduate School of Excellence (MAINZ) for financial support. We would like to thank Mrs. Xia Li for assistance during polymer synthesis, Mrs. Anita Schulz for assistance in cell culture experiments, Dr. K. Fischer and Prof M. Schmidt for light scattering experiments and Prof. H. Ringsdorf for stimulating discussions.

6. References

[1] Ferrari M. Cancer nanotechnology: opportunities and challenges. Nat Rev Cancer 2005;5:161-71.

[2] Ringsdorf H. Structure and properties of pharmacologically active polymers. J Polymer Sci Polym Symp 1975;51:135-53.

[3] Duncan R. Polymer conjugates as anticancer nanomedicines. Nat Rev Cancer 2006;6:688-701.

[4] Haag R, Kratz F. Polymer Therapeutics: Concepts and Applications Angew Chem Int Ed 2006;45:1198-215.

[5] Duncan R. Polymer conjugates for tumor targeting and intracytoplasmic delivery. The EPR effect as a commom gateway? Pharm Sci Technol Today 1999;2:441-9.

[6] Matsumura Y, Maeda H. A new concept for macromolecular therapeutics in cancer chemotherapy: mechanism of tumoritropic accumulation of proteins and the antitumor agent SMANCS. Cancer Res 1986;46:6387-92.

[7] Duncan R. The dawning era of polymer therapeutics. Nat. Rev. Drug Discovery 2003;2:347-60.

[8] Maeda H, Wu J, Sawa Y, Matsumura Y, Hori K. Tumor vascular permeability and the EPR effect in macromolecular therapeutics: a review. J. Controlled Release 2000;65:271-84.

[9] Kwon GS, Kataoka K. Block copolymer micelles as long-circulating drug vehicles. Adv Drug Delivery Rev 1995;16:295-309.

[10] Harris JM, Chess RB. Effect of pegylation on pharmaceuticals. Nat Rev Drug Discovery 2003;2:214-21.

[11] Greish K, Fang J, Inutsuka T, Nagamitsu A, Maeda H. Macromolecular Therapeutics: Advantages and Prospects with Special Emphasis on Solid Tumour Targeting. Clin Pharmacokinet 2003;42:1089-105.

[12] Lee Y, Ishii T, Cabral H, Kim HJ, Seo JH, Nishiyama N et al. Charge-Conversional Polyionic Complex Micelles-Efficient Nanocarriers for Protein Delivery into Cytoplasm. Angew. Chem. 2009 DOI: 10.1002/ange.200900064.

[13] Kabanov AV, Batrokova EV, Alakhov VY. Pluronic® block copolymers as novel polymer therapeutics for drug and gene delivery. J. Controlled Release 2002;82:189-212.

[14] Maeda H. SMANCS and polymer-conjugated macromolecular drugs: advantages in cancer chemotherapy. Adv Drug Deliv Rev 1991;6:181-202.

[15]Jiang W, Kim BYS, Rutka JT, Chan WCW. Nanoparticle-mediated cellular response is size-dependent. Nat Nanotechnol 2008;3:145-50.

[16] Gratton SEA, Ropp PA, Pohlhaus PD, Luft JC, Madden VJ, Napier ME et al. The effect of particle design on cellular internalization pathways. Proc Natl Acad Sci USA 2008;105:11613-8.

[17] Gratton SEA, Napier ME, Ropp PA, Tian S, DeSimone JM. Microfabricated Particles for Engineered Drug Therapies: Elucidation into the Mechanisms of Cellular Internalization of PRINT Particles. Pharm Res 2008;25:2845-52.

[18] Verma A, Uzun O, Hu Y, Hu Y, Han HS, Watson N et al. Surface-structure-regulated cell-membrane penetration by monolayer-protected nanoparticles. Nat Mater 2008;7:588-95.

[19] Batrakova EV, Li S, Alakhov VY, Miller DW, Kabanov AV. Optimal Structure Requirements for Pluronic Block Copolymers in Modifying P-glycoprotein Drug Efflux Transporter Activity in Bovine Brain Microvessel Endothelial Cells. J Pharmacol Exp Ther 2003;304:845-54.

[20] Sahay G, Batrakova EV, Kabanov AV. Different Internalization Pathways of Polymeric Micelles and Unimers and Their Effects on Vesicular Transport. Bioconjugate Chem 2008;19:2023-29.

[21] Kissel M, Peschke P, Šubr V, Ulbrich K, Schuhmacher J, Debus J et al. Synthetic macromolecular drug carriers: biodistribution of poly[(N-2-hydroxypropyl)methacrylamide] and its accumulation in solid rat tumors. PDA J Pharm Sci Tech 2001;55:191-201.

[22] Duncan R, Cable HC, Lloyd JB, Rejmanová P, Kopecek J. Polymers containing enzymatically degradable bonds, 7. Design of oligopeptide side-chains in poly[N-(2-hydroxypropyl)methacrylamide] copolymers to promote efficient degradation by lysosomal enzymes. Makromol Chem 1983;184:1997-2008.

[23] Kopecek J. Kopeková P, Minko T, Lu ZR. HPMA copolymer–anticancer drug conjugates: design, activity, and mechanism of action. Eur J Pharm Biopharm 2000;50:61-81.

[24] Vicent MJ, Greco F, Nicholson RI, Paul A, Griffiths PC, Duncan R. Polymer Therapeutics Designed for a Combination Therapy of Hormone-Dependent Cancer. Angew Chem Int Ed 2005;44:4061-66.

[25] Konak C, Matyjaszewski K, Kopeckova P, Kopecek J. Poly[N-(2-hydroxypropyl)methacrylamide-block-n-butyl acrylate] micelles in water/DMF mixed solvents. Polymer 2002;43:3735-41.

[26] Barz M, Tarantola M, Fischer K, Schmidt M, Luxenhofer R, Janshoff A et al. From Defined Reactive Diblock Copolymers to Functional HPMA-Based Self-Assembled Nanoaggregates. Biomacromolecules 2008;9:3114-18.

[27] Herth M, Barz M, Moderegger D, Allmeroth M, Jahn M, Thews O et al. Radioactive Labeling of Defined HPMA-Based Polymeric Structures Using [18F]FETos for In Vivo Imaging by Positron Emission Tomography. Biomacromolecules 2009; *accepted*.

[28] Matyjaszewski K, Xia J. Atom Transfer Radical Polymerization. Chem Rev 2001;101:2921-90.

[29] Matyjaszewski K, Gnanou Y, Leibler L. Macromolecular Engineering Vol. 1. Weinheim: Wiley-VCH; 2007.

[30] Tsarevsky NV, Matyjaszewski K. "Green" Atom Transfer Radical Polymerization: From Process Design to Preparation of Well-Defined Environmentally Friendly Polymeric Materials. Chem Rev 2007;107:2270-99.

[31] Barner-Kowollik C. Handbook of RAFT Polymerization. Weinheim: Wiley-VCH; Germany; 2008.

[32] Moad G, Rizzardo E, Thang SH. Living Radical Polymerization by the RAFT Process. Aust J Chem 2005;58:379-410.

[33] Moad G, Rizzardo E, Thang SH. Radical addition–fragmentation chemistry in polymer synthesis. Polymer 2008;49:1079-131.

[34] Batz HG, Franzmann G, Ringsdorf H. Model Reactions for Synthesis of Pharmacologically Active Polymers by Way of Monomeric and Polymeric Reactive Esters. Angew Chem Int Ed 1972;11:1103-04.

[35] Ferruti A, Bettelli A, Fere A. High polymers of acrylic and methacrylic esters of N-hydroxysuccinimide as polyacrylamide and polymethacrylamide precursors. Polymer 1972;13:462-4.

[36] Eberhardt M, Mruk R, Zentel R, Theato P. New precursor polymers for the synthesis of multifunctional materials. Eur Polym J 2005;41:1569-75.

[37] Theato P. Synthesis of well-defined polymeric activated esters. J Polym Sci Part A: Polym Chem 2008;

46:6677-87.

[38] Perrier S, Takolpuckdee P, Mars CA. Reversible Addition−Fragmentation Chain Transfer Polymerization: End Group Modification for Functionalized Polymers and Chain Transfer Agent Recovery. Macromolecules 2005;38:2033-6.

[39] Colombani O, Ruppel M, Schubert F, Zettl H, Pergushov DV, Müller AHE. Synthesis of Poly(n-butyl acrylate)-block-poly(acrylic acid) Diblock Copolymers by ATRP and Their Micellization in Water. Macromolecules 2007;40:4338-50.

[40] Wilhelm M, Zhao CL, Wang Y, Xu R, Winnik MA, Mura JL et al. Poly(styrene-ethylene oxide) block copolymer micelle formation in water: a fluorescence probe study. Macromolecules 1991;24:1033-40.

[41] Kalyanasundaram K, Thomas JK. Environmental effects on vibronic band intensities in pyrene monomer fluorescence and their application in studies of micellar systems. J Am Chem Soc 1977;99:2039-44.

[42] Borisov OV, Halperin A. Extending polysoaps in the presence of free amphiphiles. Physical Review E 1998;57:812-22.

[43] Liu RCW, Pallier A, Brestaz M, Pantoustier N, Tribet C. Impact of Polymer Microstructure on the Self-Assembly of Amphiphilic Polymers in Aqueous Solutions. Macromolecules 2007;40:4276-86.

[44] Noda T, Hashidzume A, Morishima Y. Micelle Formation of Random Copolymers of Sodium 2-(Acrylamido)-2-methylpropanesulfonate and a Nonionic Surfactant Macromonomer in Water As Studied by Fluorescence and Dynamic Light Scattering. Macromolecules 2000;33:3694-704.

[45] Borisov OV, Halperin A. Micelles of Polysoaps: The Role of Bridging Interactions. Macromolecules 1996;29:2612-7.

[46] Herzlinger DA, Easton TG, Ojakian GK. The MDCK epithelial cell line expresses a cell surface antigen of the kidney distal tubule. J Cell Biol 1982;93:269-77.

2.4 Langmuir-Blodgett films of biocompatible poly(HPMA)-block-poly(lauryl methacrylate) and poly(HPMA)-random-poly(lauryl methacrylate): Influence of polymer structure on membrane formation and stability

Langmuir, submitted 2009

Authors: Matthias Barz[#], Patrick Scheibe[#], Mirjam Hemmelmann, Rudolf Zentel

Address: Institute of Organic Chemistry, Johannes Gutenberg-University Mainz, Duesbergweg 10-14, 55099 Mainz, Germany

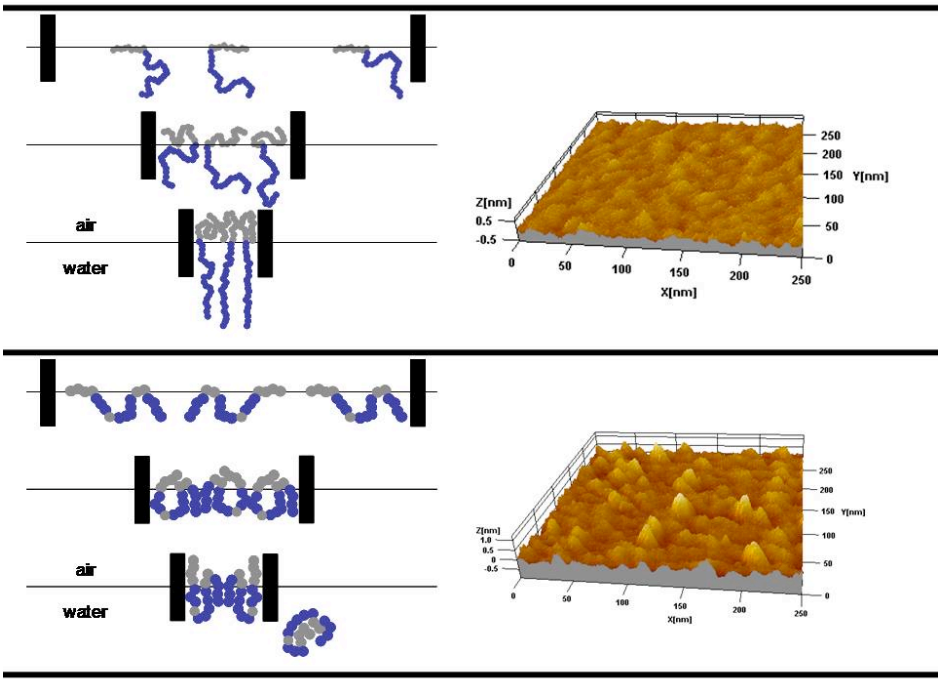

[#] both authors have equally contributed

Abstract

Membranes based on functional biocompatible polymers can be regarded as a useful model system to study biological interactions, e.g. antibody-antigen interactions or protein polymer interactions. These model systems may give a better insight into these processes and may help to find suitable polymeric structures offering biocompatibility as well as reduced polymer protein interaction. In this respect, Langmuir-Blodgett layer formation at the air/water interface is studied in respect to polymer architecture in this article. For this purpose narrowly distributed N-(2-hydroxypropyl)-methacrylamide (HPMA) random and block copolymers have been prepared by the RAFT polymerization method. For random copolymers different molecular weights were prepared. As for the block copolymers also the ratio of hydrophilic and hydrophobic units was varied in order to study the influence of hydrophobic block length on collapse pressure and area. The molecular weights of all polymers were around 15 kDa and 30 kDa. In the case of block copolymers we found a direct correlation of the length of the hydrophobic block to the collapse area. Furthermore hysteresis experiments clearly point out that block copolymers form stable LB layers. No remarkable changes in collapse pressure or area could be observed. In contrast the area occupied by random copolymers changes at each hysteresis cycle indicating a loss of polymer to the aqueous subphase. In addition the LB layers were transferred onto MICA substrates. The block copolymers formed stable and defect free membranes over an area of 10 mm² with a roughness of 2.5 Å. On the contrary, membranes based on random copolymers turned out to have a higher surface roughness. Our findings clearly underline the influence of polymer structure on the LB layer formation at the A/W interface.

2.1 Introduction

Poly(N-(2-hydroxypropyl)-methacrylamide) (HPMA) is well established as a water soluble, nontoxic and non immunogenic polymeric material in the field of polymer therapeutics. [1-6] In the last years HPMA based block copolymer have been synthesized [7] and tested for biological application. [8-10] Beside *in vitro* experiments ensuring the biocompatibility preliminary *in vivo* experiments have been carried out. [10] Furthermore the polymers are well defined due to the use of the RAFT polymerization method. Compared to ATRP [11-13] the RAFT [14-16] polymerization has the advantage that it does not require metal catalysts.

Beside *in vivo* and *in vitro* evaluations it is desirable to have a reliable model system to study the interactions of polymers and targeting molecules attached to them with their counterparts, e.g. antibody-antigen interactions. In this respect, a ligand receptor pair in model systems is the 2,4-dinitrophenyl (DNP)/anti-DNP immunoglobuline system and the biotin / anti-biotin-IgG System. The receptor FceRI for anti-DNP-IgE plays a major role in the allergic response and serves in addition as a modell for several types of immune receptors. The receptor-ligand recognition from membranes is complicated by the cell membrane interface. Therefore, model systems as e.g. LB-films are needed to study the influence of ligand density, accessibility of the ligand within the membrane and lipophilicity of the ligand amongst others. [17,18] In addition, the transferred LB films can be applied to study precisely the interactions with proteins or even cells. [19-21] The Langmuir-Blodgett technique can be applied to create stable block copolymer films from amphiphilic or surface-adsorbing polymers at the air/water (A/W) interface. In these films the interactions of molecules attached to the block copolymer can be precisely studied. The self-assembled structure at the A/W interface can be also transferred to a solid substrate using either the Langmuir-Blodgett (LB) or Langmuir-Schaefer (LS) transfer technique. [22-31]

Examples of amphiphilic block copolymers extensively studied at the A/W interface include polystyrene-*b*-poly(ethylene oxide), polybutadiene-*b*-poly(ethylene oxide), and polystyrene-*b*-polyacrylate. [32-34] A wide range of experimental techniques has also been used for morphology investigation of the monolayers directly on the water surface or after transfer on solid substrates, including neutron and X-ray reflectivity, surface pressure and potential measurements, Brewster angle microscopy (BAM), atomic force microscopy (AFM), transmission electron microscopy (TEM), and ellipsometry. [35-38] With a view toward guest encapsulation and cell uptake, we have recently reported the synthesis of HPMA based random and block copolymers, the characterization of their aggregates in solution as well as their pronounced biocompatibility. [10,12] We observed differences in superstructure formation leading to differences in microstructure of the aggregates, which were directly related to polymer architecture. The differences influenced the cellular uptake. [12]

In the present paper, we study the behavior of poly(HPMA)-block-poly(Lauryl methacrylate) as well as random poly(HPMA)-co-poly(Lauryl methacrylate) at the A/W interface. Furthermore we investigate the influence of polymer composition and architecture on the formation, stability and uniformity of membranes. The derived Langmuir monolayers were characterized by surface pressure measurements, such as isotherms and compression-expansion hysteresis. In addition, the morphologies were monitored by AFM measurements. For these measurements the LB transfer was applied to transfer the polymer films onto mica substrates.

2. Experimental Section

2.1 Materials.

All chemicals were reagent grade and obtained from Aldrich. The chemicals were used without further purification unless otherwise indicated. The pentafluoro-phenol was obtained from fluorochem (Great Britain, UK) and distilled before use. Dioxane used in the synthesis was freshly distilled from a sodium/potassium mixture. 2,2'-Azobis(isobutyronitrile) (AIBN) was recrystallized from diethyl ether and stored at -7°C. Lauryl methacrylate was distilled and kept at -7°C.

2.2 Characterization

^{1}H-, ^{13}C- and ^{19}F-NMR spectra were obtained at 300 or 400 MHz using a FT-spectrometer from Bruker and analyzed using the ACDLabs 6.0 software. The polymers were dried at 40 °C over night under vacuum and afterwards submitted to gel permeation chromatography (GPC). GPC was performed in tetrahydrofurane (THF) as solvent and with following parts: pump PU 1580, auto sampler AS 1555, UV-detector UV 1575, RI-detector RI 1530 from Jasco and miniDAWN Tristar light scattering detector from Wyatt. Columns were used from MZ-Analysentechnik: MZ-Gel SDplus 10^2 Å, MZ-Gel SDplus 10^4 Å and MZ-Gel SDplus 10^6 Å. The elution diagrams were analysed using the ASTRA 4.73.04 software from Wyatt Technology. Calibration was done using polystyrene standards. The flow rate was 1 mL/min at a temperature of 25 °C.

2.3 Synthesis

2.3.1 Synthesis of 4-cyano-4-((thiobenzoyl)sulfanyl)pentanoic acid

The 4-cyano-4-((thiobenzoyl) sulfanyl)pentanoic acid was used as the CTA and synthesized according to the literature. [39]

2.3.2 Synthesis of pentafluoro-phenyl methacrylate (PFMA)

PFMA was prepared according to the literature. [40]

2.3.3 General synthesis of the macro-CTA

The macro-CTA was prepared according to the literature. [40] The RAFT polymerizations of the PFMA using 4-cyano-4-((thiobenzoyl) sulfanyl) pentanoic acid were performed in a schlenk tube. The reaction vessel was loaded with 2,2'-azobis(isobutyronitrile (AIBN), 4-cyano-4-((thiobenzoyl)sulfanyl)pentanoic acid (CTA) (molar ratio of AIBN/CTA = 1:8) and 15 g of PFMA in 20 mL of dioxane. Following three freeze–vaccum–thaw cycles, the tube was immersed in an oil bath at 70 °C. Afterwards the polymer poly(PFMA) was 3 times precipitated into hexane, isolated by centrifugation and dried for 12 hours at 30 °C under vacuum. In the end a slightly red powder was obtained. Yield: (59 %). ^{1}H NMR ($CDCl_3$): 1.6-2.2 (br), 0.9-1.5 (br) δ [ppm] ^{19}F NMR ($CDCl_3$): δ [ppm] -165.1 (br), -159.8 (br), -154.4 (br), -153.1 (br).

2.3.4 General synthesis of the random copolymers

The RAFT polymerizations of the PFMA and lauryl methacrylate using CTA were performed according to the literature. [12] The reaction vessel was loaded with AIBN, CTA (molar ratio of AIBN/CTA (1:8), PFMA and lauryl methacrylate in 20 mL of dioxane. Following three freeze–vacuum–thaw cycles, the tube was immersed in an oil bath at 70 °C. Afterwards the poly(PFMA)-co-poly(lauryl methacrylate) was 3 times precipitated into hexane, isolated by centrifugation and dried for 12 h at 30 °C under vacuum. In the end a slightly red powder was obtained. Yield: (67%). ^{1}H NMR ($CDCl_3$): δ [ppm] 1.6–2.2 (br), 0.9–1.5 (br), 0.8–0.9 (br t). ^{19}F NMR ($CDCl_3$): δ [ppm] -165.1 (br), -159.8 (br), -154.4 (br), -153.1 (br).

2.3.4 General synthesis of block copolymers

The block copolymer was prepared according to the literature. [10] The macro-CTA obtained in the above-mentioned polymerization was dissolved in dioxane and AIBN was added. Nitrogen was bubbled through the solution and three freeze-vacuum-thaw cycles were applied. Afterwards the tube was immersed in an oil bath at 70 °C. After polymerization time of 12 h, the solution was slightly concentrated and precipitated twice in ethanol and diethyl ether, removed by centrifugation, and dried overnight at 30 °C in vacuum. A slightly red powder was obtained. Yield: (89 %). ^{1}H NMR ($CDCl_3$): δ [ppm] 1.6-2.2 (br), 0.9-1.5 (br), 0.8-0.9 (br t) ^{19}F NMR ($CDCl_3$): δ [ppm] -165.1 (br), -159.8 (br), -154.4 (br), -153.1 (br).

2.3.5 Removal of dithioester endgroups

The dithiobenzoate end group was removed according to the procedure reported by Perrier et al. [41] Typically 200 mg of polymer, (Mn = 25.000 g/mol), and 50 mg of AIBN (30 times excess in relation

to the polymer endgroup) were dissolved in 3 mL of anhydrous dioxane/DMSO (4:1). The solution was heated at 80 °C for 2 h. Finally the copolymer was precipitated 3 times in 100 mL of diethyl ether and collected by centrifugation. In the case of the block copolymer the crude product was first precipitated in EtOH 2 times and than 1 time in diethyl ether. The copolymer was dried under vacuum for a period of 24 h and a colourless product was obtained (yield: 92 %). The absence of the dithiobenzoate end group was confirmed by UV-Vis spectroscopy.

2.3.6 Polymer analogous reactions of random copolymers

The polymer analogous reaction was performed according to the literature. [12] In a typical reaction 300 mg of poly(PFMA)-co-poly(lauryl methacrylate) without dithioester end group were dissolved in 4 mL abs. dioxane and 1 mL abs. DMSO. A colorless solution was obtained. In a typical reaction 2.5 mg for the 50 000 g/mol precursor and 5 mg for the 25 000 g/mol precursor of Oregon green 488 cadaverine and 20 mg of triethylamine were added. The mixture was kept at 25 °C for 4 h and finally 200 mg of hydroxypropylamine and 200 mg triethylamine were added. The reaction was allowed to proceed under the above-mentioned conditions overnight. The solution was concentrated in vacuum and introduced to a column filtration using Sephadex^{TM} LH-20 in dioxane and precipitated in diethyl ether, removed by centrifugation and dried in vacuum at 30 °C for 14 h. Yield: (79%). ^{1}H NMR (DMSO-d_6): δ [ppm] 3.4–3.9 (br), 2.6–3.0 (br), 0.9–1.5 (br), 0.8–0.9 (br t).

2.3.7 Polymer analogous reactions of block copolymers

The polymer analogous reaction was performed according to the literature. [10] In a typical reaction 300 mg of poly(PFMA)-block-poly(lauryl methacrylate) were dissolved in 4 ml abs. dioxane and 1 ml abs. DMSO. A colourless solution was obtained. In a typical reaction 5 mg of Oregon green 488 cadaverin and 20 mg of triethylamine were added. The mixture was kept at 25 °C for 4 hours. In the end 200 mg of hydroxypropylamine and 200 mg triethylamine were added. The reaction was allowed to go on under the above-mentioned conditions over night. The solution was concentrated in vacuum and introduced to a column filtration using Sephadex^{TM} LH-20 in dioxane/DMSO (4:1) and precipitated in diethyl ether, removed by centrifugation and dried in vacuum at 30 °C for 14 hours. Yield: (81%). ^{1}H NMR (DMSO-*d*6): δ [ppm] 3.4-3.9 (br), 2.6-3.0 (br), 0.9-1.5 (br), 0.8-0.9 (br t)

2.4 Surface Pressure-Area (p-A) Isotherms and Langmuir-Blodgett Film Transfer

2.4.1 Isotherms of Langmuir Films

Surface pressure-area (p-A) isotherms were obtained using a Nima Langmuir-Blodgett trough (Nima, Coventry, type 611) secured inside an acrylic glass box (Bayer) as dust shield. The total trough surface area was 200 mm × 100 mm and the total trough volume was around 150 mL. The effective trough area was controlled by two hydrophobic barriers that compressed the spread film symmetrically and bilaterally at a rate of 5 cm^2/min. Hysteresis measurements were carried out without any delay

between each compression and expansion step. Deionized water purified with a Milli-Q system (Millipore Corp.) to 18.2 MW-cm resistivity was used as subphase in all trials. For all experiments, the subphase temperature was 25 ± 0.1 °C (15 min delay after the water was filled in and the copolymer solution was spread). Prior to each trial, the water surface was cleaned by aspirating off any residue, such that the measured surface pressure remained <0.1 mN/m over a full compression. The LB components were cleaned daily with absolute chloroform, and the deionized water subphase was replaced regularly. Surface pressure measurements were made from a Wilhemly plate (perimeter of 20 × 10 mm) made out of chromatography paper, which was washed several times with absolute Chloroform prior to each trial to ensure cleanliness. Solutions of the block copolymer in chloroform were spread on the subphase by using a microsyringe (Kloehn). In a typical experiment 20-30 mL of the polymer solution were spread in small portions on the water surface, so that a constant mass of copolymer was deposited for each trial. The spreading solution was deposited dropwise (around 2 mL drop volume) at regularly spaced locations on the trough. In all trials, a 15 min evaporation period between the last deposited drop of solution and the beginning of compression was employed to ensure complete solvent evaporation.

2.4.2 Langmuir-Blodgett Films

Langmuir films were prepared as described above for isotherm measurements. After solvent evaporation (15 min) the barriers were compressed at a constant rate (5 cm^2/min) and the p-A isotherm was recorded. For a Langmuir-Blodgett transfer a 2 cm × 1 cm MICA plate, freshly cleaved, was used. The clean substrate was then immersed into the subphase before the polymer solution was spread. After the desired surface pressure was reached, the substrate was slowly removed from the subphase, passing vertically through the interface and transferring the polymer layer at the air-water interface to the solid substrate while maintaining the surface pressure. The substrate withdrawal rate was typically 1 mm/min. All transferred thin films were imaged within a maximum of two hours after the transfer.

2.4.3 Atomic Force Microscopy

All AFM imaging was conducted on a NanoScope III multimode AFM in tapping mode (Digital Instruments) using a silicon cantilever (thickness = 4.6 mm, resonance frequency = 311.8-339.5 kHz, and spring constant = 47.6-61.8 N/m, Olympus). The AFM probe was housed within a vibration-resistant case on a vibration isolation platform. Each sample was imaged several times at different locations on the substrate to ensure reproducibility. In all cases, the imaging of Langmuir-Blodgett films was performed far from the edge of the MICA substrate to minimize any local effects caused by turbulent water flow at the boundary and meniscus effects during transfer.

3. Results and Discussion

3.1 Polymer synthesis

The random as well as the block copolymers have been synthesized according to the previously reported method. [10,12] Various copolymers have been produced by the RAFT polymerization technique yielding the block copolymer structures **P1R-P3R** and random copolymers **P4R, P5R** (see scheme 1).

Scheme 1. Stepwise synthesis of block (**P1**, **P2** and **P3**) and random copolymers (**P4** and **P5**) by RAFT polymerization and polymer analogous reactions.

The reactive polymer precursors have molecular weights in the range of 25000-60000 g/mol and polydispersity index in the range of 1.2-1.3. The ratio between PFMA and lauryl methacrylate was set in the case of **P1R** to 90:10 whereas for **P2R** to **P5R** it was around 80:20 (see table 1). Afterwards these reactive polymers were transferred into HPMA based block copolymers **P1, P2, P3** and random copolymers **P4, P5** by aminolysis of the activated ester with 2-hydropropylamine. The purified copolymers have been carefully characterized by ^{1}H- as well as ^{19}F-NMR ensuring full conversion of the activated ester. The molecular weight of the polymer **P1**, **P2** and **P4** turned out to be around 15000 g/mol and for **P3** and **P5** around 30000 g/mol. The values of polydispersity were for all systems in the range of 1.2 to 1.3 ensuring well-defined polymers. All characteristics of the synthesized HPMA based polymers are listed in table 1 and table 2.

Table 1. Characteristics of reactive precursor block copolymers (**P1R**, **P2R**, **P3R**) and random copolymers (**P4R**, **P5R**).

polymers	structure	Calc. PFMA/LMA unit ratio[a]	M_n[b]	M_w[b]	PDI[b]
P1R	block copolymer	90:10	24720	28620	1.20
P2R	block copolymer	80:20	22680	27100	1.19
P3R	block copolymer	90:10	54840	64440	1.28
P4R	random copolymer	80:20	22270	27400	1.23
P5R	random copolymer	80:20	49020	59800	1.22

[a] mol ratio of monomers in the polymerization

[b] g/mol, determined by GPC in THF as solvent for the activated ester polymers **P1R** to **P6R**.

Table 2. Characteristics of HPMA based block (**P1**, **P2**, **P3**) and random copolymers (**P4**, **P5**)

polymers	structure	HPMA/LMA unit ratio[a]	M_n[b]	M_w[b]	PDI[b]	$M_{n,block\ lipo}$[a]	$N_{block\ lipo}$[a]
P1	block copolymer	88:12	13590	15740	1.20	2970	12
P2	block copolymer	79:21	12810	15240	1.19	5190	20
P3	block copolymer	87:13	28170	36060	1.28	6790	27
P4	random copolymer	78:22	14600	20200	1.23	-	-
P5	random copolymer	81:19	32800	39300	1.22	-	-

[a] As determined by ^{1}H NMR spectroscopy after aminolysis with 2-hydroxypropylamine yielding **P1** to **P6**

[b] g/mol, determined by GPC in THF as solvent for the activated ester polymers **P1R** to **P6R**.

3.2 Membrane formation and characterization in respect to polymer architecture

The synthesized polymers with different structures and different hydrophobic or hydrophilic block length have been investigated with regard to their behaviour at the A/W interface. Concerning their structures block copolymers **P1** and **P2** differ only in the length of the hydrophobic block. The hydrophobic block of **P2** is almost double in length. The hydrophobic block of **P3** is larger then the hydrophobic block of **P2** (around ~ 25 %) but the hydrophilic block of **P3** is more than twice as big as in **P2**. These structure variations offer the chance to investigate their influence on membrane characteristics (see table 2).

The other group of investigated polymers are random copolymers. Our previous research [12] suggested the formation of inter-intrachain micells of random copolymers in water. The random copolymer **P5** has the double molecular weight of **P4**, but the ratio of hydrophilic to hydrophobic parts is constant (see table 2). We assume that in these systems the hydrophobic parts are stabilized by loops of the hydrophilic parts in the copolymer. In this respect we also expect these polymers to form LB monolayers at the A/W interface, which may be less stable than block copolymer membranes.

3.2.1 Behavior at the Air-Water Interface

Surface pressure-area isotherms were obtained compressing the Langmuir monolayers of the block copolymers **P1**, **P2** and **P3** and of the random polymers **P4** and **P5** formed on the surface of a water subphase (see figure 1).

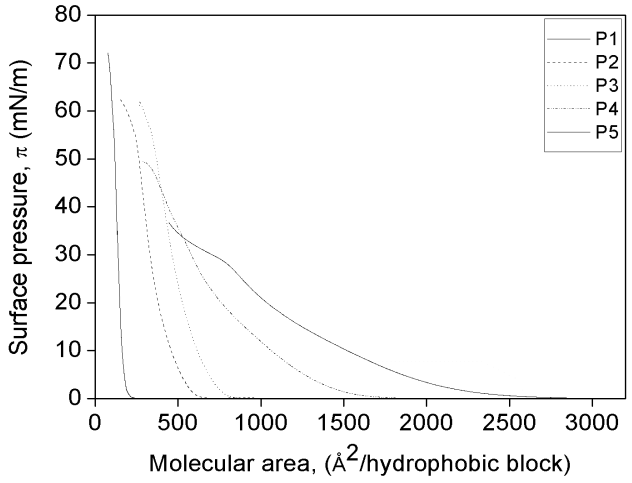

Figure 1. Isotherms of the block copolymers (**P1**, **P2** and **P3**) at 25°C

The three block copolymers **P1**, **P2** und **P3** showed rather similar compression isotherms. In case of the 3 polymers a slow increase of surface pressure at large molecular areas followed by a steeper increase in the smaller molecular area regime at surface pressures higher than 25 mN/m was observed. At surface pressures of 55 mN/m and higher the curve declines, which indicates that the monolayer is collapsing. However there is a difference between these three polymers. The molecular area at which the collaps of the film occurs increases from **P1** (116 $Å^2$ per hydrophobic block) to **P2** (251 $Å^2$ per hydrophobic block) and **P3** (341$Å^2$ per hydrophobic block) indicating a strong correlation to the length of the hydrophobic block (lipoblock). The hydrophobic block consists in the case of **P1** of 12 lauryl methacrylate units. It is therefore smaller than the lipoblock of **P2** (20) and **P3** (27), so their required space is bigger. These findings underline the expected coil formation of the hydrophobic part of the block copolymer during the compression progress like it is schematically shown in Scheme 2.

Scheme 2. Sketch of the Langmuir Blodgett layer formation at the air/water interface for a) block copolymers and b) random copolymers

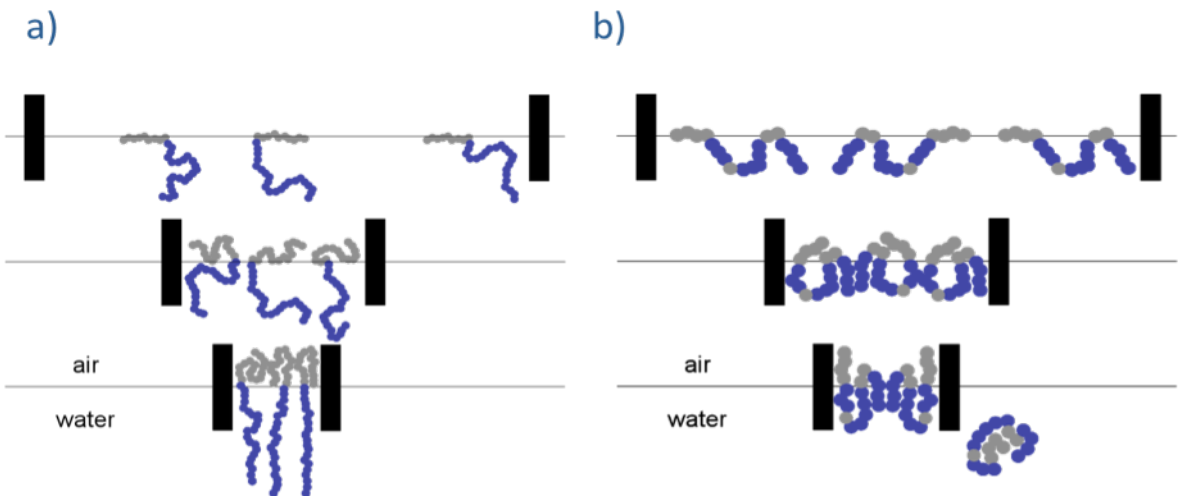

Most likely the area occupied by the hydrophilic part of the polymer strongly depends on the size of the lipophilic moiety as observed by Y. Park et al. [42] Furthermore the Langmuir films show a good stability. To test the stability of the monolayer several compression-expansion cycles were done (see figure 2). For the block copolymer the repetition of the compression-expansion cycle resulted in similar isotherms without a remarkable shift in collaps pressure as well as collapse area. These findings clearly indicate that no loss of material into the subphase occurres during the cycles. In case

of block copolymer **P1** slight shifts in the isotherms could be observed. The reason for this effect might be attributed to the smaller lipoblock of **P1**.

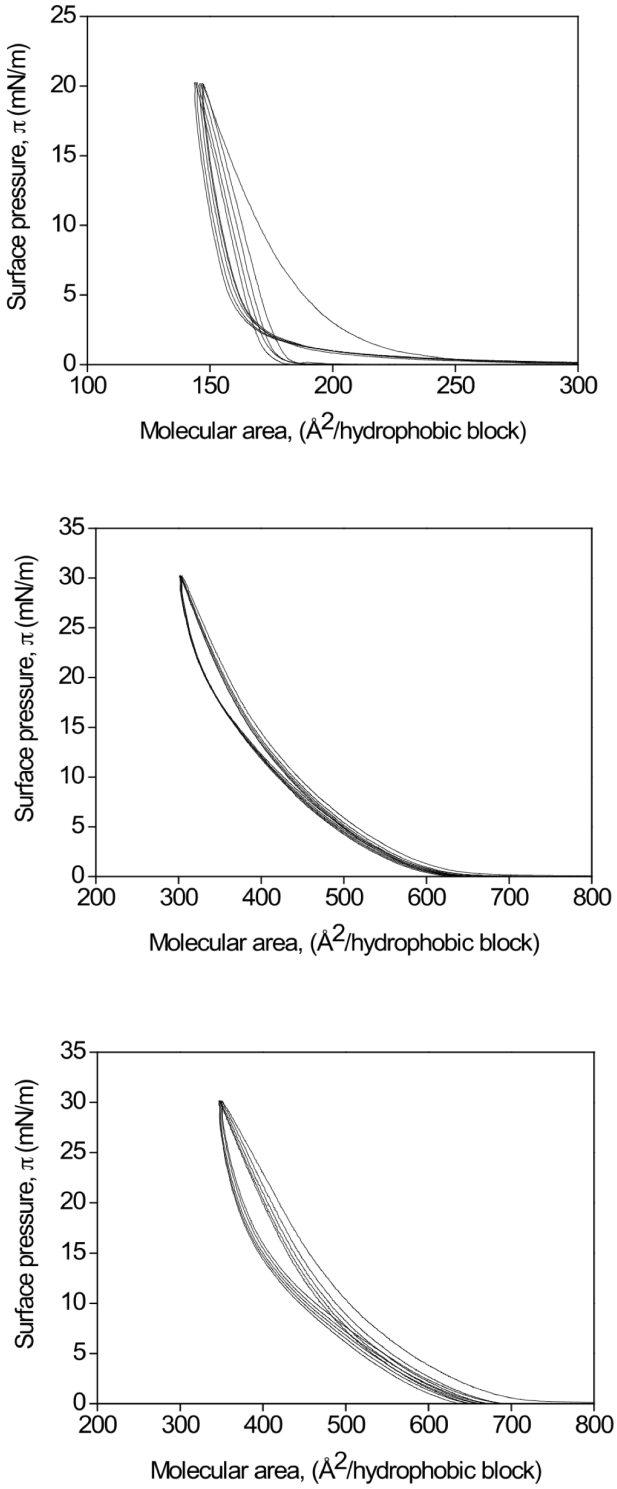

Figure 2. Compression-expansion hysteresis plot of **P1**, **P2** and **P3** at 25°C

In comparison to **P2** it is half the size and in comparison to **P3** it is only one third of the size. In this respect, the hydrophobic part is obviously not able to ensure the formation of a stable film at the A/W interface when it is too small.

In contrast to the block copolymers the random copolymers **P4** and **P5** showed remarkable differences. The isotherms of **P4** and **P5** showed an increase in surface pressure already at very large areas per lipoblock and a shallow increase during compression. The liquid expanded phase begins for **P4** at 1750 $Å^2$ and for **P5** at 2750 $Å^2$. Thus the random copolymers cover a larger area at low surface pressure, but have a much higher compressibility than the block copolymers. Obviously they change the packing at the gas-water interface more easily. At a surface pressure of 25 mN/m the random copolymer **P4** shows a phase transition and at a surface pressure of 30 mN/m **P5** shows one. For **P4** the collaps point is at around only 47 mN/m and in case of **P5** the collaps point is at around only 30 mN/m. All differences are most likely related to a different film formation process (see scheme 2).

In addition the stability of the build LB films is less than for the block copolymers **P2** and **P3**. Figure 3 shows the results of compression-expansion hysteresis experiment.

Figure 3. Compression-expansion hysteresis plot of **P4** and **P5** at 25°C

During each cycle of compression and expansion the area occupied by the random copolymer decreases, indicating a loss of material into the water subphase. Only if the polymer has a defined hydrophobic block, like in the case of **P1**, **P2** and **P3**, the polymer can form stable Langmuir-Blodgett films. Without a defined hydrophobic part the polymers can be easily forced into the subphase when the surface pressure is increased. All discussed results are summarized in table 3.

In order to get information about the differences in film morphology of block and random copolymers, AFM images of the polymers **P2**, **P3**, **P4** and **P5** transferred at a defined surface pressure were performed.

3.2.2 Langmuir-Blodgett Film Morphology

Indirect visualization of the block copolymer self-assembly was achieved by Langmuir-Blodgett film transfer and subsequent imaging of the structures on solid substrates by tapping mode AFM. Figure 4 shows the AFM images of the LB films of **P2** and **P3** transferred at 40 mN/m.

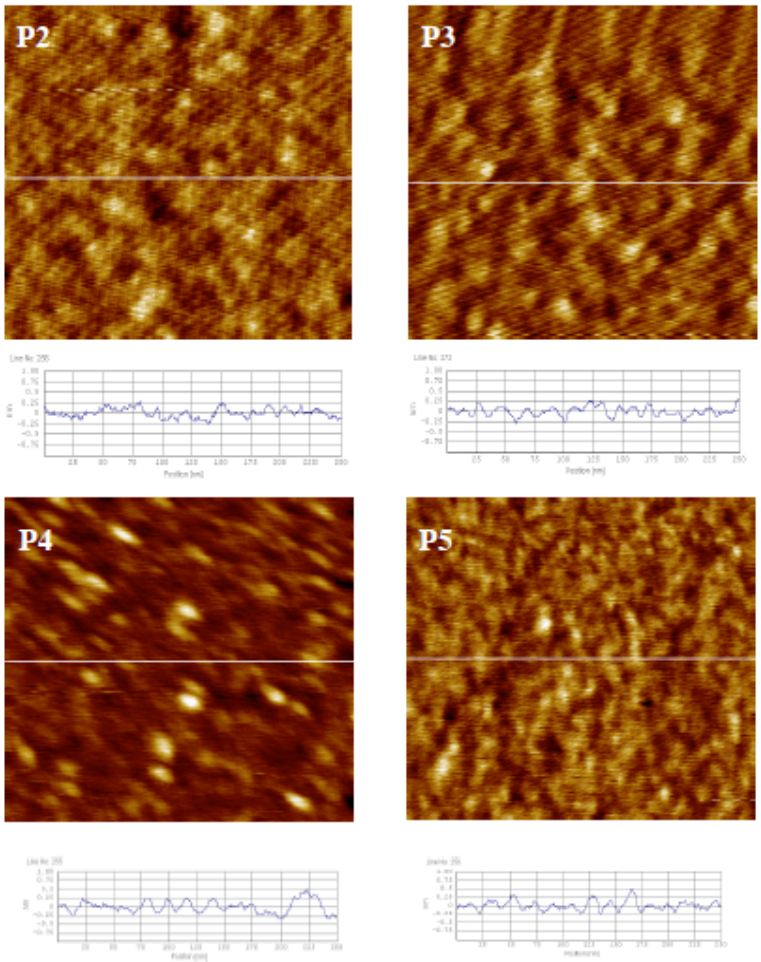

Figure 4. AFM image of LB films transferred at 40 mN/m for the two block copolymers **P2** and **P3**. The LB films of the random copolymers **P4** and **P5** were transferred at 35 mN/m and at 25 mN/m. In all cases the horizontal and the vertical scales are 250 nm

These images show a very smooth film. The roughness of the surface is with ±2.5 Å around surface zero very low (see table 3).

Table 3. Characteristics of the Langmuir Blodgett layer at the air/water interface and after transfer on a MICA substrate

Polymers	structure	collaps presure (mN/m)	area/ polymer mN/m / Å^2	area (hysteresis) mN/m / Å^2	transfer pressure mN/m	roughness (AFM) ±Å
P1	block copolymer	55	55/116	20/147	-	-
P2	block copolymer	55	55/251	30/304	40	2.5
P3	block copolymer	55	55/341	30/351	40	2.5
P4	random copolymer	47.5	47.5/347	20/537-482	35	7.5
P5	random copolymer	(28.5)	(28.5/779)	25/773-580	25	5.0

According to the isotherms the block copolymers can be expected to be in a liquid condensed phase state. In this pressure range, the block copolymers are compressed so that the hydrophobic chains come very close together. In this respect, a complete transfer of the block copolymer monolayer on the MICA substrate is most likely, yielding smooth and defect free membranes over a large area. Figure 5 shows images of 10×10 μm. These films show the same smooth surface structure than the smaller scale images indicating indeed a complete transfer of the LB layer.

In contrast to that result the random copolymers **P4** and **P5** show a slightly different surface architecture as can be seen also in figure 4. The membranes of the random copolymers are rougher and throughout the observed area defect regions can be found. These defects are regions were the detected hight difference is larger than 7.5 Å, which is by 2.5 Å larger than in case of the two block copolymers. That observation could also be made for larger areas as shown in figure 5 with an area of

2×2 µm². We conclude that **P4** and **P5**, due to the lack of any defined structure, are not able to form smooth and stable membranes (figure 3) and therefore the transferred membranes are not as smooth as those of **P2** and **P3**.

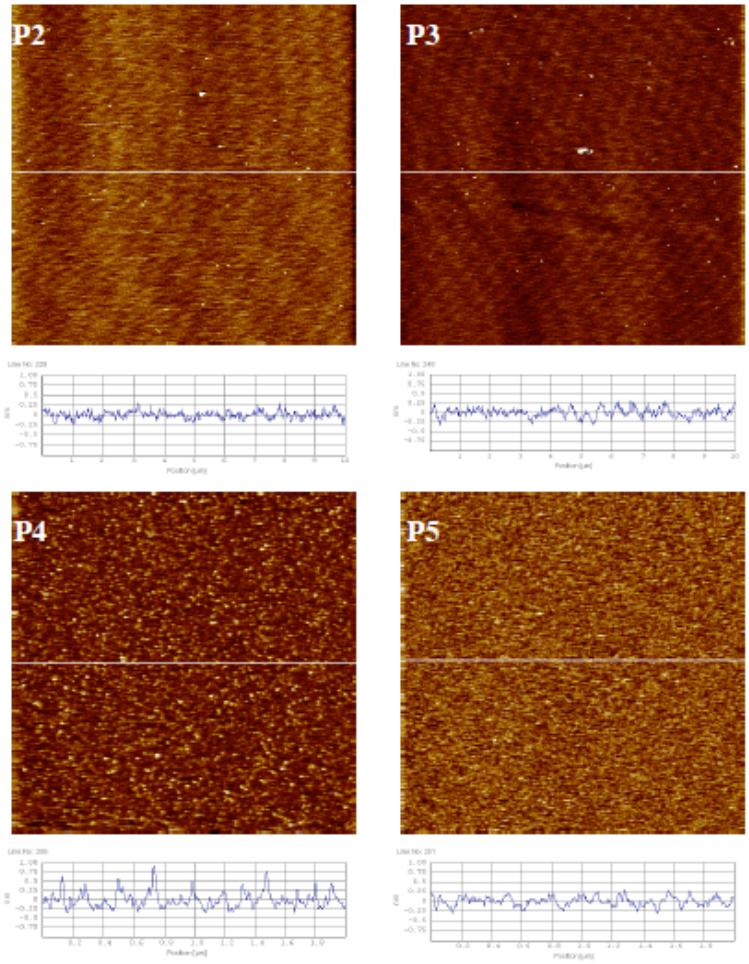

Figure 5. AFM image of LB films transferred at 40 mN/m for **P2** and **P3**. Both, the horizontal and the vertical, scales are 10 µm**.** The LB films of **P4** and **P5** were transferred at 30 mN/m and 25 mN/m. Both scales are 2 µm.

4. Conclusion

In this work we have demonstrated the influence of polymer structure in terms of molecular weight as well as polymeric architecture on the formation and stability of LB layers at the A/W interface. These findings were only possible by the use of the RAFT polymerization enabling the synthesis of defined block and random copolymers. We could demonstrate the influence of hydrophilic block length of block copolymers on the collapse area of their isotherms. Thus, a larger hydrophobic block occupies a larger area at the A/W interface. But even more interesting we found pronounced differences between polymers having the same monomer HPMA/LMA ratio but different architectures. Block copolymers formed stable LB layers, which did not show changes in hysteresis experiments. In contrast random copolymers showed a remarkable loss of polymer into the water sub phase. These findings may also give us some indication of the aggregate stability formed by each polymeric structure. In addition, by AFM we could nicely monitor influences of the polymer architecture on membrane properties. Whereas, block copolymers formed smooth and defect free membranes over an area of 100 μm^2, random copolymers formed less smooth membranes including defects.

Further investigations regarding the incorporation of specific recognition structures and protein polymer membrane interactions are warranted and are currently investigated in our laboratories.

5. Acknowledgment

The authors would like to thank Ms Romina Forst for assistance during the synthesis of polymers. Furthermore the authors would like to thank Ms Sandra Muth and the group of Prof. Schmidt (University of Mainz) for providing the AFM. The authors want to thank the graduate school of excellence MAINZ, COMATT and SAMT for support and funding.

6. References

[1] Duncan, R. *Nature Reviews Cancer*, **2006**, 6(9), 688-701

[2] Duncan, R. *Nat. Rev. Drug Discovery*, **2003**, 2, 347-360

[3] Cuchelkar, V.; Kopeček,J. Polymers in Drug Delivery: Polymer–Drug Conjugates, CRC Press: Boca Raton, FL, 2006, Vol. 1, 155-182

[4] Kopeček, J.; Rejmanova, P. *Controlled Drug Delivery*; CRC Press: Boca Raton, FL, 1983; Vol. 1, 81-124

[5] Ringsdorf, H. *J. Polym. Sci. Polym. Symp*. **1975**, 51, 135-153

[6] Vicent, M. J.; Greco, F.; Nicholson, R. I.; Paul, A.; Griffiths P. C.; Duncan, R. *Angew Chem Int Ed,* **2005**, 44, 4061-4066

[7] Konak, C.; Matyjaszewski, K.; Kopeckova, P.; Kopecek, J. *Polymer,* **2002**, 43, 3735-3741

[8] Barz, M.; Tarantola, M.; Fischer, K.; Schmidt, M.; Luxenhofer, R.; Janshoff, A.; Theato, P.; Zentel, R.. *Biomacromolecules* **2008**, 9, 3114-3118

[9] Herth, M.; Barz, M.; Moderegger, D.; Allmeroth, M.; Jahn, M.; Thews, O.; Zentel, R.; Rösch, F. *Biomacromolecules*, **2009**, 10, 1697-1703

[10] Barz, M.; Luxenhofer, R.; Zentel, R.; Kabanov, A. V. *Biomaterials*, **2009**, 30 (29), 5682-5690

[11] Matyjaszewski, K.; Xia, J. *Chem Rev*, **2001**, 101, 2921–2990

[12] Matyjaszewski, K.; Gnanou, Y.; Leibler, L. *Macromolecular engineering*, vol. 1.,Weinheim: Wiley-VCH, **2007**.

[13] Tsarevsky, N. V.; Matyjaszewski, K. *Chem Rev*, **2007**, 107, 2270–2299

[14] Barner-Kowollik, C. *Handbook of RAFT polymerization*. Weinheim, Germany: Wiley-VCH, **2008**

[15] Moad, G.; Rizzardo, E.; Thang, S. H. *Polymer*, **2008**, 49, 1079–1131

[16] Stenzel, M. H. RAFT polymerization: an avenue to functional polymeric micelles for drug delivery. Chem Commun 2008, 30, 3486-3503

[17] Jung, H.; Yang, T.; Lasagna, M. D.; Shi, J.; Reinhardt, G. D.; Cremer, P. S. *Biophysical Journal*, **2008**, 94, 3094-3103

[18] Moore, N. W.; Kuhl, T. L. *Langmuir*, **2006**, 22, 8485-8491

[19] Ulbricht, M. *Polymer*, **2006**, 47, 2217–2262

[20] Kishida, A.; Mishima, K.; Corretge, E.; Konishi, H.; Ikad, Y. *Biomaterials*, Volume 13, Issue 2, **1992**, 13(2), 113-118

[21] Wang, C.-C.; Lu, J.-N.; Young, T.-H. *Biomaterials*, **2007**, 28(4), 625-631

[22] Blodgett, K. B. *Journal of Physical Chemistry*, **1937**, 41, 975-984.

[23] A. Ulman, An Introduction to Ultrathin Organic Films, Academic Press, Boston, MA, **1991**.

[24] Talham, D. R. *Chemical Reviews*, **2004**, 104(11), 5479-5501.

[25] Ravindranath, R.; Ajikumar, P. K.; Advincula, R. C.; Knoll, W.; Valiyaveettil, S. *Langmuir*, **2006**, 22(21), 9002-9008.

[26] Joncheray, T. J.; Denoncourt, K. M.; Mathieu, C.; Meier, M. A. R.; Schubert, U. S.; Duran, R. S. *Langmuir*, **2006**, 22(22), 9264-9271.

[27] Chen, X.; Lenhert, S.; Hirtz, M.; Lu, N.; Fuchs, H.; Chi, L. F. *Acc. Chem. Res.*, **2007**, *40*, 393-401

[28] Jung, S. Y.; Yoshida, H. *Journal of Thermal Analysis and Calorimetry*, **2007**, 89(3), 681-686

[29] Baker, S. M.; Leach, K. A.; Devereaux, C. E.; Gragson, D. E. *Macromolecules*, **2000**, 33(15), 5432-5436

[30] Rehfeldt, F.; Steitz, R; Armes, S. P.; Gast, A.P.; Tanaka, M. *J. Phys. Chem*, **2006,** *110,* 9177-9182

[31] Hodges, C. S.; Neville, F.; Konovalov, O.; Hammond, R. B.; Gidalevitz, D.; Hamley, I. W. *Langmuir*, **2006**, 22(21), 8821-8825

[32] Cheyne, Robert B.; Moffiitt Matthew G. *Langmuir* **2006**, 22, 8387-8396

[33] Matmour, R.; Joncheray, T. J.; Gnanou, Y.; Duran, R. S. *Langmuir*, **2007**, 23(2), 649-658

[34] Li, S.; Clarke, C. J.; Eisenberg, A.; Lennox, R. B. *Thin Solid Films*, **1999**, 354(1,2), 136-141

[35] Haefele, T.; Kita-Tokarczyk K.; Meier W. *Langmuir*, **2006**, 22, 1164-1172

[36] Joncheray T.J.; Denoncourt K.M.; Meier M.A.R.; Schubert U.S.; Duran R.S. *Langmuir*, **2007**, 23, 2423-2429

[37] Tsai, H.-J.; Lee, Y.-L. *Soft Matter*, **2009**, 5(15), 2962-2970

[38] Kang, J.S.P., Eun J.; Kim, J. H.; Han, M. J. *Materials Science & Engineering, C: Biomimetic and Supramolecular Systems*, **2004**, C24(1-2), 281-284

[39] Eberhardt, M.; Mruk, R.; Zentel, R.; Theato, P. *Eur Polym J*, **2005**, 41, 1569–1575

[40] Eberhardt, M.; Theato, P. *Macromol. Rapid. Commun,.* **2005**, *26*, 1488-1493

[41] Perrier, S.; Takolpuckdee, P.; Mars, C. A. *Macromolecules*, **2005**, 38, 2033–2036

[42] Park, Y.; Choi, Y.-W.; Park, S.; Cho, C. S.; Fasolka, M. J.; Sohn, D. *Journal of Colloid and Interface Science*, **2005**, 283, 322-328

2.5 Synthesis and *in vitro* evaluation of defined HPMA folate conjugates: Influence of aggregation on folate receptor (FR) mediated cellular uptake

Biomaterials 2009, submitted

Authors: Matthias Barz[1#], Fabiana Canal[2#], Kaloian Koynov,[3] R. Zentel[1], Maria J. Vicent[2]

Address: 1) Institute of Organic Chemistry, Johannes Gutenberg-University Mainz, Duesbergweg 10-14, 55099 Mainz, Germany

2) Centro de Investigación Príncipe Felipe, Polymer Therapeutics Lab., Medicinal Chemistry Dpt., Avda Autopista El Saler 16/3, 46012 Valencia, Spain

3) MPI for Polymer Research, Ackermannweg 10, 55128 Mainz, Germany

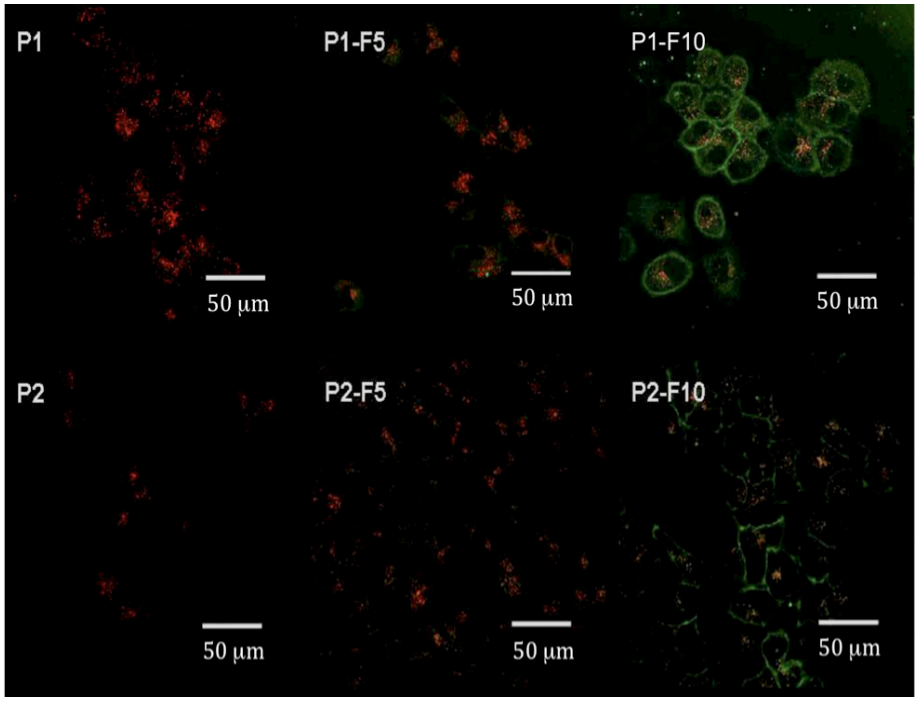

[#] Both authors have equally contributed

Abstract

In this article we report the synthesis and in vitro evaluation of well defined, folate functionalized and fluorescently labeled polymers based on the clinically approved N-(2-hydroxypropyl)-methacrylamide (HPMA). The polymers were prepared applying the RAFT polymerization method as well as the reactive ester approach. The molecular weights of the polymers synthesized were around 15 kDa and 30 kDa. The total content of conjugated folate was varied from 0, 5 to 10 mol %. The cellular uptake of these polymers was investigated in the folate receptor (FR)-positive human nasopharyngeal epidermal carcinoma (KB-3-1) and FR-negative human lung epithelial carcinoma (A549) cancer cell lines. In FR-positive cells the cellular uptake of polymers depended strongly on the folate content. The conjugates with the highest folate content lead to the highest level of cell associated fluorescence. Regarding influence of molecular weigth, non-significant differences were observed when total cell uptake was analyzed. The cellular uptake is related to the aggregate formation of the polymer conjugates, which were studied by fluorescence correlation spectroscopy (FCS). For the conjugates we found aggregates with a diameter in the range from 11-18 nm. Much to our surprise, for the 30 kDa polymer bearing 5 mol % folate and the 15 kDa and the 30 kDa conjugates with a folate content of 10 mol %, we found aggregates of the same size, which were independent from either molecular weight or folate content. Consequently, a different conformation in solution for the different conjugates was expected. By live cell confocal fluorescence microscopy the receptor mediated endocytosis process was demonstrated, as co-localization with lysosomal markers was achieved. In addition, cellular uptake was not observed in FR-negative cells (A549) or can be dramatically reduced by blocking the FR with free folic acid. Our findings clearly underline the need of a minimum amount of accessible folate units in order to target the FR that triggers specific cellular uptake. Furthermore, it has been nicely demonstrated that the targeting vector itself strongly influences the aggregation behavior in solution and therefore, determines the interaction with cells regarding cellular uptake as well as intra cellular localization.

1. Introduction

Although scientific research lead to important findings in the field of Polymer Therapeutics, such as long-circulating carriers or enhanced permeability and retention (EPR) effect, there is still an urgent need for specific drug accumulation, e.g. in solid tumors. [1-5] Folic acid has become an useful ligand due it has a high affinity (Kd ~ 10^{-10} M) to the folate receptor (FR) [6] and its ability to transport even larger molecules into the cell. [7] Folic acid itself belongs to the group of vitamins. [8] It is essential for eukaryotic cells for one carbon transfer reactions used in the biosynthesis of nucleotide bases. [9,10] In this respect, cell survival and proliferation do strongly depend on cell ability to acquire the folic acid or its derivatives. The cellular uptake of folates can follow by either a low affinity reduced folate carrier (Km ~ 1 μM [11]), which is present at virtually any cell in the human body, or a high affinity glycosylphosphatidylinositol-linked FR (Kd ~ 10^{-10} M [12,13]). This receptor (FR) is highly limited in its appearance among cells inside the human organism. Furthermore, FR has the ability to transport folic acid as well as various folate conjugates (i.e. chemotherapeutics, proteins, liposomes, nanoparticles, etc.). [7] The uptake takes place in two steps. First, the folate binds to the receptor and is, in a second step, transferred into the cell by a process called receptor mediated endocytosis [14,15] allowing even larger particles to enter the cell. An additional benefit is offered by the fact that the folate receptor exhibits limited expression on healthy cells but is highly expressed in many tumor types, such as ovarian, lung, breast, brain, colon and kidney cancers. [16-20]

Taking these two points into account, it is rather obvious to use the folate receptor to achieve a fast and selective cell uptake of nanoparticles like micelles [21-24], dendrimers [25,26], coated inorganic nanoparticles [27-29] or liposomes [30-33] into tumor cells. But only little work has been done regarding the *in vivo* application of folate functionalized nanoparticles for therapy as well as molecular imaging. [34-36]

Most of the polymer-based nanoparticles known in literature, which folic acid was conjugated to, are based on polyethylene oxide (PEG). [21-24] But, on the other hand, 2-N-hydroxymethylacrylamide (HPMA) is another clinically approved and carefully investigated polymer. [1,2] HPMA is polymerized by radical polymerization techniques leading to broad molecular weight distributions (MW) and undefined end groups. In order to achieve more defined polymers, fractionation techniques had to be applied with, consequently, a tremendous loss of product. This problem could be successfully solved by the use of the modern controlled radical polymerization techniques such as Nitroxide Mediated Polymerization (NMP), Atom Transfer Radical Polymerization (ATRP) and Reversible Addition Fragmentation Chain Transfer (RAFT) polymerization. [37-43] Applying these techniques, the well-known HPMA can be used to create various well-defined polymer architectures. But more important it is possible to precisely control the MW and polydispersity (PDI) of the compound, which is one of the key requirements for successful structure-property correlation as well as pharmaceutical applications on the field of nanomedicine. [44] But not only polymerization

techniques have improved, furthermore, the armory of functional monomers has been tremendously improved. [45] Especially activated esters appear again as useful tools in the synthesis of functional copolymers based on acryl- or methacrylamides. [46] But the activated ester approach can be also used to synthesize reactive homopolymers, which can be precisely characterized by Nuclear Magnetic Resonance (NMR) and Gel Permeation Chromatography (GPC) and afterwards, transferred into multifunctional random copolymers in a polymer analogous reaction. [47-49] This approach offers the great opportunity to vary the content of a certain functionality such as folic acid (targeting moiety), yielding polymers only differing in the content of folic acid but having the same degree of polymerization.

Here, we investigated the influence of MW and folate content and the aggregation behavior of defined HPMA based polymers by fluorescence correlation spectroscopy (FCS) [50], which will most likely determine the cellular uptake as well as intracellular localization in FR positive KB-3-1 cells (human nasopharyngeal epidermal carcinoma) as well as FR negative A549 cells (human lung epithelial carcinoma). Thus, this work can be considered the base for further in vivo studies on polymer biodistribution applying positron emission tomography (PET) by following our recently published procedure. [47]

2. Experimental Section

2.1 Materials

All chemicals were reagent grade and obtained from Aldrich. The chemicals were used without further purification unless otherwise indicated. The Oregon green (OG) 488 cadaverine was obtained from Invitrogen. The pentafluoro-phenol was obtained from Fluorochem (Great Britain, UK) and distilled before use. Dioxane used in the synthesis was freshly distilled from a sodium/potassium mixture. 2,2'-Azobis(isobutyronitrile) (AIBN) was recrystallized from diethyl ether and stored at -7°C. Dialysis was performed using Spectra/Por® 3 membranes obtained from Carl Roth GmbH + Co. KG (Germany).

The A549 human lung epithelial carcinoma and the KB-3-1 human nasopharyngeal epidermal carcinoma cell lines were obtained from the American Type Culture Collection (ATCC) (Rockville, MD). Tissue culture grade dimethylsulfoxide (DMSO), folate-depleted Dulbecco's Modified Eagle's Medium (FDMEM), L-glutamine, 3-(4,5-dimethyiltiazol-2-yl)-2,5-diphenyl-tetrazolium bromide (MTT) and Trypan-blue were from Sigma-Aldrich Co. (St Louis, MO, USA). Dextran-Texas Red 40000MW was from Invitrogen (Carlsbad, CA, USA). 0.25% trypsin-EDTA was from Gibco BRL Life Technologies (Paisley, UK). Heat-inactivated fetal bovine serum was from Seromed GmbH (Wien, Austria).

2.2 Equipment

^{1}H-, ^{13}C- and ^{19}F-NMR spectra were obtained at 300 or 400 MHz using a FT-spectrometer from Bruker and analyzed using the ACDLabs 6.0 software. The polymers were dried at 40°C overnight under vacuum and afterwards submitted to gel permeation chromatography (GPC). GPC was performed in tetrahydrofurane (THF) as solvent and with following parts: pump PU 1580, auto sampler AS 1555, UV-detector UV 1575, RI-detector RI 1530 from Jasco and miniDAWN Tristar light scattering detector from Wyatt. Columns were used from MZ-Analysentechnik: MZ-Gel SDplus 10^2 Å, MZ-Gel SDplus 10^4 Å and MZ-Gel SDplus 10^6 Å. The elution diagrams were analyzed using the ASTRA 4.73.04 software from Wyatt Technology. Calibration was done using polystyrene standards. The flow rate was 1 mL/min at a temperature of 25°C.

MTT assay measurements were performed using a Victor^2 Wallac 1420 Multilabel HTS Counter Perkin Elmer plate reader (Northwolk, CT, USA). FACS analysis was carried out using Cytomics FC500 Beckman Coulter Inc. (Fullerton, CA, USA). Live cell confocal fluorescence microscopy studies were carried out at the confocal microscopy service at CIPF (Valencia, Spain) and were performed using a Leica confocal microscope from Leica Microsystems GmbH (Wetzlar, D) equiped with a l-blue 63 oil immersion objective and handled with a TCS SP2 system, equipped with an acoustic optical beam splitter (AOBS). Excitation was with an argon laser (548, 476, 488, 496 and 514 nm) and blue diode (405 nm). Images were captured at an 8-bit gray scale and processed with LCS software Version 2.5.1347 (Leica, Germany) containing multicolor, macro and 3D components.

2.3 Synthesis of 4-cyano-4-((thiobenzoyl)sulfanyl)pentanoic acid

The 4-cyano-4-((thiobenzoyl)sulfanyl)pentanoic acid was used as the CTA and synthesized according to the literature in a 3 step reaction. [51]

2.4 Synthesis of pentafluoro-phenyl methacrylate (PFMA)

PFMA was prepared according to the literature.[52]

2.5 General synthesis of poly(pentafluoro-phenyl methacrylate) (PPFMA)

The macro-CTA was prepared according to the literature.[53] The RAFT polymerizations of the PFMA using 4-cyano-4-((thiobenzoyl)sulfanyl)pentanoic acid were performed in a schlenk tube. The reaction vessel was loaded with 2,2'-azobis(isobutyronitrile) (AIBN), 4-cyano-4-((thiobenzoyl)sulfanyl)pentanoic acid (CTA) (molar ratio of AIBN/CTA = 1:8) and 15 g of PFMA (59 mmol) in 20 mL of dioxane. Following three freeze–vacuum–thaw cycles, the tube was immersed in an oil bath at 70°C. Afterwards the polymer poly(PFMA) was 3 times precipitated into hexane, isolated by centrifugation and dried for 12 h at 30°C under vacuum. In the end a slightly red powder was obtained. (Yield: 59 %). ^{1}H NMR ($CDCl_3$): δ [ppm] 1.6-2.2 (br), 0.9-1.5 (br) ^{19}F NMR ($CDCl_3$): δ [ppm] -165.1 (br), -159.8 (br), -154.4 (br), -153.1 (br).

2.6 Removal of dithioester endgroups

The dithiobenzoate endgroup was removed according to the procedure reported by Perrier et al.[54] Typically 200 mg (0,008 mmol) of polymer (Mn = 25.000 g/mol) and 50 mg (30 mmol) of AIBN

(30 times excess in relation to the polymer endgroups) were dissolved in 3 mL of anhydrous dioxane:DMSO (4:1). The solution was heated at 80°C for 2 h. Finally, the copolymer was precipitated (3x) in 100 mL of diethyl ether and collected by centrifugation. In the case of the block copolymer the crude product was first precipitated in EtOH (2x) and then in diethyl ether (1x). The copolymer was dried under vacuum for a period of 24 h and a colorless product was obtained (yield: 92 %). The absence of the dithiobenzoate endgroup (302 nm) was confirmed by UV-Vis spectroscopy.

2.7 Synthesis of 2,2-(ethylendioxy)bis(ethylamine) folate (folate spacer conjugate)

441 mg of folic acid (1 mmol) were dissolved in 30 mL DMSO, 248 mg dicyclohexylcarbodiimide (DCC) (1.2 mmol) and 115 mg (1 mmol) of N-hydroxysuccinimide (NHS) were added to the solution. The solution was kept at 40°C for 6 h. The resulting activated folate-NHS was added dropwise to a solution of 1501 mg of 2,2-(ethylendioxy)bis(ethylamine) (10 mmol) and 101 mg of triethylamine (1 mmol) in 20 mL DMSO. The reaction was allowed to proceed overnight at 30°C. The crude product was precipitated by addition of a large excess of diethyl ether, filtered and washed with diethyl ether (3x) before drying under vacuum. The dried product was purified using preparative HPLC. Preparative HPLC: Rt = 58.4 min (prep. Luna C18, Grad: acetonitrile/water + 0.1% v/v TFA (5:95)->(20:80), 60 min, λ = 274 nm). The fraction containing the 2,2-(ethylendioxy)bis(ethylamine) folate was lyophilized and a yellow product was yielded. (Yield: 54 %). ^{1}H NMR (300 MHz, DMSO-d_6): δ [ppm] 8.65 (s, 1H), 7.65 (d, 2H), 6.63 (d, 2H), 4.49 (s, 2H), 4.34 (dd, 1H, C19-H), 3.75–3.10 (m, 10 H), 2.96 (m, 2H), 2.26 (m, 2H, C21-H2), 2.15-1.85 (m, 2H). ESI-MS: calc.: 571.2, found: 572.3 ($M+H^+$)

2.8 Polymer analogous reactions yielding dye labeled homopolymers

In a typical reaction, 300 mg (6 mmol for 50000 g/mol precursor, 12 mmol for the 25000 g/mol precursor) of PPFMA without dithioester endgroups were dissolved in 4 mL abs. dioxane and 1 mL abs. DMSO. A colorless solution was obtained. In a typical reaction, 2.5 mg (0.006 mmol) for the 50000 g/mol precursor and 5 mg (0.012 mmol) for the 25000 g/mol precursor of OG 488 cadaverine and 10 mg (0.1 mmol) of triethylamine were added. The mixture was kept at 25°C for 4 h and finally 200 mg (2.66 mmol) of 2-hydroxypropylamine and 300 mg (3 mmol) triethylamine were added. The reaction was allowed to proceed under the above-mentioned conditions overnight. The solution was concentrated in vacuum, carefully mixed with water (Millipore) and dialyzed using Spectra/Por® membranes with a MW cutoff (MWCO) of 3500 g/mol overnight. The solution of the purified product was lyophilized yielding a slightly orange polymer. (Yield: 86 %). ^{1}H NMR (DMSO-*d6*): δ [ppm] 3.4-3.9 (br), 2.6-3.0, 0.9-1.5 (br)

2.9 Polymer analogous reactions yielding dye labeled folate conjugates

In a typical reaction 300 mg (6 mmol for 50000 g/mol precursor, 12 mmol for the 25000 g/mol precursor) of PPFMA without dithioester endgroups were dissolved in 4 mL abs. dioxane and 1 mL abs. DMSO. A colorless solution was obtained. In a typical reaction, 2.5 mg (0.006 mmol) for the **P1R** precursor and 5 mg (0.012 mmol) for the **P2R** precursor of OG 488 cadaverine and 10 mg (0.1 mmol)

of triethylamine were added. The mixture was kept at 25°C for 4 h followed by the addition of 32 mg (0.06 mmol) of 2,2-(ethylendioxy) bis(ethylamine) folate for **P1-F5/P2-F5** and 64 mg (0.12 mmol) for **P1-F10/P2-F10**. The polymer analogous reaction was allowed to proceed for another 4 h. Finally, 200 mg (2.66 mmol) of 2-hydroxypropylamine and 300 mg (3 mmol) triethylamine were added. The reaction was allowed to proceed under the above-mentioned conditions until full conversion could be ensured by ^{19}F NMR. The solution was concentrated in vacuum, mixed with Millipore water and dialyzed against Millipore water for 24 h using Spectra/Por® membranes (MWCO 3500 g/mol). The purified solution was lyophilized and a yellowish polymer was obtained. (Yield: 75 %). ^{1}H NMR (DMSO-*d*6): δ [ppm] 8.6 (s), 7.6-6.6 (br), 4.49 (s), 3.1-3.9 (br), 2.6-3.0, 0.9-1.5 (br)

2.10 Characterization of block copolymers in solution by fluorescence correlation spectroscopy (FCS)

Fluorescence correlation spectroscopy (FCS) experiments were performed using a commercial FCS setup (Zeiss, Germany) consisting of the module ConfoCor 2 and an inverted microscope model Axiovert 200 with a Zeiss C-Apochromat 40 ×/1.2 W water immersion objective. The fluorophores were excited by an Argon laser (λ = 488 nm) and the emission was collected after filtering with a LP505 long pass filter. For detection, an avalanche photodiode that enables single-photon counting was used. Eight-well, polystyrene-chambered coverglass (Laboratory-Tek, Nalge Nunc International) was used as a sample cell. The dye labeled polymer conjugates **P1-F5**, **P2-F5**, **P1-F10** and **P2-F10** were dissolved in DMSO (c = 20 mg/mL) and PBS buffer (pH = 7.2) was slowly added until a final concentration of 0.1 mg/mL was reached. The solutions were kept at room temperature (RT) over 24 h prior to the measurements. For each solution, 10 measurements with total duration 5 min were performed.

The time-dependent fluctuations of the fluorescent intensity $\delta I(t)$ were recorded and analyzed by an autocorrelation function $G(t)=1+\langle \delta I(t') \, \delta I(t'+t)\rangle / \langle I(t')\rangle^2$. As it has been shown theoretically for an ensemble of m different types of freely diffusing fluorescence species, $G(t)$ has the following analytical form: [k1]

$$G(t) = 1 + \left[1 + \frac{f_T}{1 - f_T} e^{-t/\tau_T}\right] \frac{1}{N} \sum_{i=1}^{m} \frac{f_i}{\left[1 + \frac{t}{\tau_{Di}}\right] \sqrt{1 + \frac{t}{S^2 \tau_{Di}}}} \qquad (1)$$

Here, N is the average number of diffusing fluorescence species in the observation volume, f_T and τ_T are the fraction and the decay time of the triplet state, τ_{Di} is the diffusion time of the *i-th* species, f_i is the fraction of component i, and S is the so-called structure parameter, $S = z_0/r_0$, where z_0 and r_0 represent the axial and radial dimensions of the confocal volume, respectively. Furthermore the diffusion time, τ_{Di}, is related to the respective diffusion coefficient, D_i, through [k1] $D_i = r_0^2/4 \, \tau_{Di.}$ The experimentally obtained $G(t)$ can be fitted with eq. 1 yielding the corresponding diffusion times and

subsequently the diffusion coefficients of the fluorescent species. Finally, the hydrodynamic radii R_h can be calculated (assuming spherical particles) using the Stokes-Einstein relation: $R_h = k_B T/6\pi\eta D$, where k_B is the Boltzmann constant, T is the temperature, and η is the viscosity of the solution. As the value of r_0 depends strongly on the specific characteristics of the optical setup a calibration was done using a reference standard with known diffusion coefficient, i.e. Rhodamine 6G.

2.11 Cell cultures

A549 (human lung epithelial carcinoma cells) and KB-3-1 (human nasopharyngeal epidermal carcinoma cells) were grown in FDMEM, folate-depleted medium, supplemented with 10% (v/v) heat-inactivated fetal bovine serum (FBS). Cells were maintained at 37°C in an atmosphere of 5% carbon dioxide and 95% air and underwent passage twice weekly.

2.12 Cell viability assay

The cytotoxicity of the conjugates synthesized was evaluated using the MTT (3-(4,5-dimethyltiazol-2-yl)-2,5-diphenyl-tetrazolium bromide) cell viability assay (72 h incubation) with A549 and KB-3-1 cells. Cell lines were seeded into sterile 96-well microtitre plates ($2x10^4$ cell/mL for A549 and $2.5x10^4$ cell/mL for KB-3-1 cells). Cells were allowed to settle for 24 h before the unlabeled polymers **P1-F5/P2-F5** and **P1-F10/P2-F10** (0.2 μm filter-sterilized) were added. A series of stock solutions of conjugates dissolved in DMSO, with different concentrations ranging from 1 mg/mL to 300 mg/mL, were prepared and the cells were treated with 1 μL of each stock solution, in such a manner that the final polymer concentrations range from 0,01 mg/mL to 3 mg/mL with a final DMSO concentration of 1% (v/v). As control, cells were treated with the same percentage of DMSO, in absence of conjugates to evaluate solvent toxicity. 100% cell viability was assigned to control cells with 1% DMSO. After a further 68 h incubation, MTT (20 μL of a 5 mg/mL solution in PBS) was added to each well, and the cells were incubated for 4 h. After removal of the medium, the precipitated formazan crystals were dissolved in optical grade DMSO (100 μL), and the plates were read spectrophotometrically at 570 nm after 30 min using a Victor^2 Wallac plate reader.

Cytotoxicity data were expressed as IC_{50} values, *i.e.*, the concentrations of the test agent inducing 50% reduction in cell viability compared with control cultures.

2.13 Cellular uptake by fluorescence activated cell sorting (FACS)

Cells were seeded at a density of $3x10^5$ cells/mL in a sterile 6-well plate. After 48 h incubation, cells were treated with 10 μL of OG-labeled conjugate solution. The experiments were carried out by triplicate, some wells were untreated and used as control. After previously set incubation times of 0, 5, 30 min, 1, 2 and 5 h at 37°C, the plates were put in ice, the medium was removed and cells were washed trice with 1 mL of cold PBS and scraped. Cell associated fluorescence was then analyzed using a Cytomics FC 500 (Beckman Coulter Inc.) equipped with an argon laser (405 nm) and an emission filter for 455 nm. Data collection involved 15000 counts per sample and was analyzed with Beckman Coulter CXP software.

The experiments were carried out also at 4°C, placing the plates at 4°C 30 min before the experiment

started and then following the same procedure described above.

In free folate competition studies, 1 mM folic acid solution was added 1 h before cell treatment with the selected conjugates.

2.14 Live cell confocal fluorescence microscopy

Cells were seeded on a glass slide placed into 10 cm^2 Petri plates at a density of $2.5x10^5$ cell/mL. After 24 h incubation, cells were treated with 10 μL of OG-labeled conjugate solution. The final polymer concentration was in the range of 0.5-1 mg/mL, in such a manner that dye equivalents were the same in all cases.

Pulse and chase experiments were performed: after 5, 15 min or 1 h of incubation at 37°C, the medium was removed and replaced with fresh one. Cells were then incubated at 37°C for further 5, 30 min or 1, 2 and 5 h, respectively. At the same time, cells were also treated with Dextran-Texas Red, used as lysosomal marker, at a final concentration of 0.25 mg/mL. Then, cells were washed trice with PBS supplemented with 10% (v/v) of FBS (3 mL), the glass was removed and finally set on the microscope. Images were captured with a confocal Leica microscope.

2.15 Statistical Analysis

All results are given as means ± SD ($n \geq 3$). When only two groups were compared, the Student's t test for small sample size was used to estimate statistical significance. If more than two groups were compared evaluation of significance was performed using one way-Analysis Of Variance (ANOVA) followed by Bonferroni post hoc test. Graph pad Instant software (Graph Pad Software Inc. CA, USA) was used. In all cases, statistical significance was set at $p < 0.05$**.**

3. Results and discussion

3.1 Synthesis of HPMA folate conjugates

In order to determine the influence of MW as well as the amount of folate moieties we have synthesized various reactive precursors **P1R**-**P2R** by applying the RAFT polymerization method as well as the activated ester approach (see scheme 1). The reactive polymers had MW from 25 kDa to 60 kDa and a PDI around 1.2 ensuring well defined polymers (see table 1). In the next step the reactive precursor polymers were aminolyzed yielding the Oregon Green 488 (OG)-containing HPMA based polymers (**P1** and **P2**), as well as the folate conjugates (**P1-F5**, **P2-F5**, **P1-F10** and **P2-F10**) (see table 2). The folate conjugates were synthesized with slight variations according to the method of Lee et al. [23]

Scheme 1. Synthetic pathway to poly(HPMA) folate conjugates using a reactive ester approach.

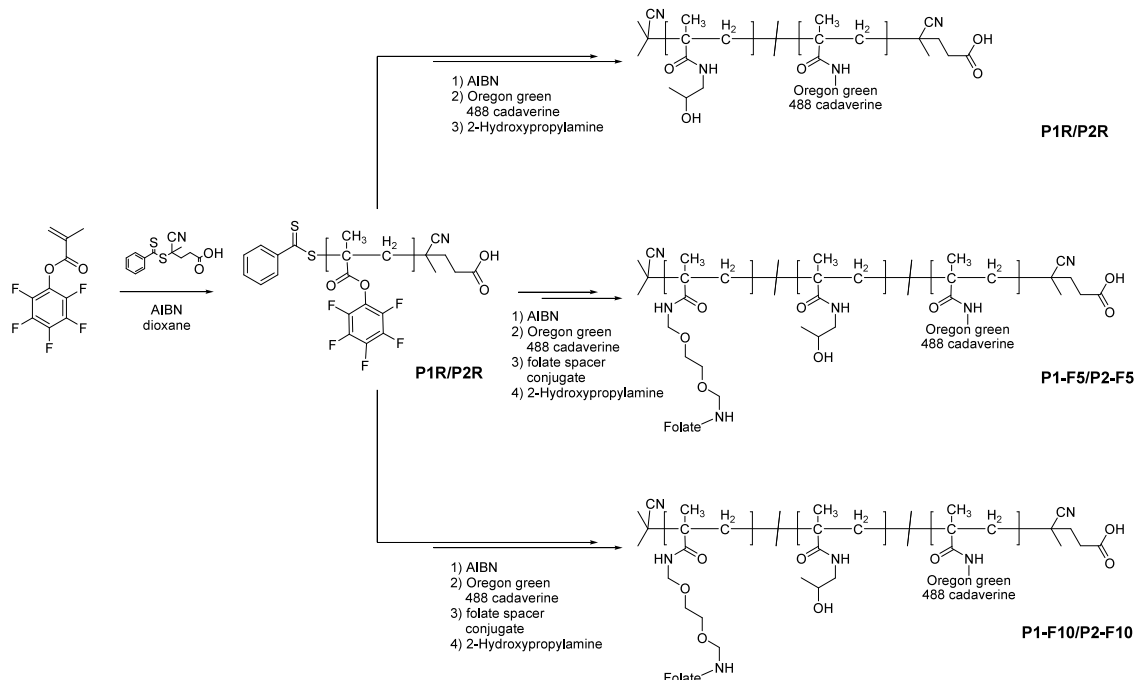

The spacer itself was a diamino functionalized oligo PEG (2-(aminomethoxy)-ethoxy)methanamine) and the final purification was performed by RP-HPLC (see supporting information) yielding a pure product, which can be seen either in NMR as well as in electron spray ionization mass spectroscopy (ESI-MS) (see supporting information).

The final polymer conjugates (**P1**, **P2**, **P1-F5**, **P2-F5**, **P1-F10** and **P2-F10**) have been purified by dialysis, size exclusion chromatography (SEC) (Sephadex G-25), lyophilized and analyzed by NMR and UV ensuring successful conjugation as well as purification. The fluorescence output of polymer solutions was determined by fluorescence measurements and normalized. The conjugates synthesized were then applied to the *in vitro* studies using a FR negative (A549) and a FR positive (KB-3-1) cell lines.

Table 1. Characteristics of reactive homopolymers (**P1R**, **P2R**)

Polymers	Calculated g/mol	M_nM_n[a,b] g/mol	M_w[a,c] g/mol	PDI[a,d]
P1R	25000	21100	25100	1.19
P2R	60000	50200	60800	1.21

a) determined by GPC in THF solvent

b) $M_n = \sum_i \frac{n_i m_i}{n_i}$ number average molecular weight

c) $M_w = \sum_i \frac{n_i^2 m_i}{n_i m_i}$ mass average molecular weight

d) $PDI = \frac{M_w}{M_n}$ polydispersity index

Table 2. Characteristics of folate-poly(HPMA) conjugates (**P1**, **P2, P1-F5, P2-F5, P1-F10 and P2-F10**)

Polymer	M_n[a,d] g/mol	MW[a,e] g/mol	PDI[a,f]	Folate content[b]	OG content[c]
P1	12200	14600	1.19	0 %	1 %
P2	29200	35300	1.21	0 %	1 %
P1-F5	16500	19600	1.19	5 %	1 %
P2-F5	28500	34400	1.21	5 %	0.5 %
P1-F10	18500	22000	1.19	10 %	1 %
P2-F10	32500	39300	1.21	10 %	0.5 %

a) calculated from the MW of the activated ester polymers P1R and P2R, determined by GPC in THF as solvent

b) determined by ^{1}H-NMR in DMSO-d_6

c) determined by fluorescence measurements

d) $M_n = \sum_i \frac{n_i m_i}{n_i}$ number average molecular weight

e) $M_w = \sum_i \frac{n_i^2 m_i}{n_i m_i}$ mass average molecular weight

f) $PDI = \frac{M_w}{M_n}$ polydispersity index

3.2 Aggregation behavior of polymer conjugates in solution by fluorescence correlation spectroscopy (FCS)

The synthesized dye labeled HPMA folate conjugates (**P1-F5**, **P2-F5**, **P1-F10** and **P2-F10**) have been applied to FCS in order to investigate the super structures formed under *in vitro* conditions. In this respect, all samples were prepared micmicking those conditions used in the cell experiments. The measurements were carried out in PBS buffer (pH = 7.2). For the HPMA homopolymers **P1** and **P2** random coil structures with a hydrodynamic diameter of around 5 nm could be expected. However, for the random copolymers containing the only slightly water-soluble folate the situation will be -in all probability- different. We have recently reported the aggregate formation of poly(HPMA)-random-poly(lauryl methacrylate) copolymers that yielded aggregates with hydrodynamic radii in the range of ~30 nm, which was very surprisingly, independent from the polymer MW used to form the particle. [48] Taking these finding into account, we applied FCS to determine the diffusion coefficient and, by applying the Stokes-Einstein equation, the hydrodynamic radius of each conjugate (see table 3). In all studied solutions, in addition to the slowly diffusing aggregates, we also found a faster diffusing component reflecting the contribution of the small residual amounts of free dye molecules and non-aggregated polymer chains. This is the reason for the selection of the two component model (m=2) in order to fit the experimental autocorrelation curves.

Table 3. Characterization of fluorescently labeled (OG) polymer-folate conjugates (**P1-F5**, **P2-F5**, **P1-F10** and **P2-F10**) in PBS buffer (pH = 7.2) by fluorescence correlation spectroscopy (FCS)

Polymer	Concentration mg/mL	Diffusion coefficient m^2/s	Hydrodynamic diameter nm[a)]
P1-F5	0.1	3,93E-11	11
P2-F5	0.1	2,40E-11	18
P1-F10	0.1	2,70E-11	16
P2-F10	0.1	2,40E-11	18

a) Calculated using the Stokes-Einstein equation: $$D = \frac{k_B T}{6\pi\eta r}$$

In this way we found aggregates with a diameter of ~11 nm for conjugate **P1-F5**. Interestingly, polymers **P2-F5**, **P1-F10** and **P2-F10** formed structures of comparable size (see table 3). These aggregates were found to have a hydrodynamic diameter of around 17 nm, which clearly indicates the formation of agglomerates. Furthermore it is most likely, that the aggregates of the low MW polymer contain a higher amount of polymer chain assuming a comparable density. These results are comparable to those derived from the poly(HPMA)-random-poly(lauryl methacrylate) copolymers even so the aggregates are smaller. This smaller size, however, can be attributed to the more hydrophilic character of the folic acid compared to the lauryl methacrylate. It is important to consider all these findings in order to understand the interaction of the conjugates with the membrane bound folate receptor (FR).

3.3 In vitro evaluation of polymer-folic acid conjugates

3.3.1 Cell viability assay

The cytotoxic activity of the conjugates **P1-F5** to **P2-F10** was studied in A549 and KB-3-1 cell lines. The conjugates did not show any cytotoxicity after 72 h treatment up to 3 mg/mL concentration in both cell lines tested (IC_{50} > 3 mg/mL) (see supporting information). Furthermore, no difference in cell toxicity related to folate content or polymer MW was observed.

3.3.2 Cellular uptake by fluorescence activated cell sorting (FACS)

Cellular uptake of OG-labeled conjugates was studied by FACS in the two cell lines above described. From literature [7] it is well known that folate-containing particles enter the cell by receptor-mediated endocytosis. In order to prove this internalization pathway for our conjugates, we performed internalization studies at 37ºC and at 4°C. In fact, at 4ºC all energy-dependent mechanisms, e.g. endocytosis, are minimized and only simple diffusion through the more rigid cell membrane would lead to remarkable cell associated fluorescence.

Considering FR positive cells KB-3-1, conjugates **P1-F10** and **P2-F10** with 10 mol % folate content showed the highest cell associated fluorescence level, suggesting a good cellular uptake, significantly different ($p<0.001$) from conjugates **P1-F5** and **P2-F5**, with only 5 mol % folate content, and with cell internalization profiles similar to those shown by the non-targeted conjugates (**P1** and **P2**) used as control (see figure 1).

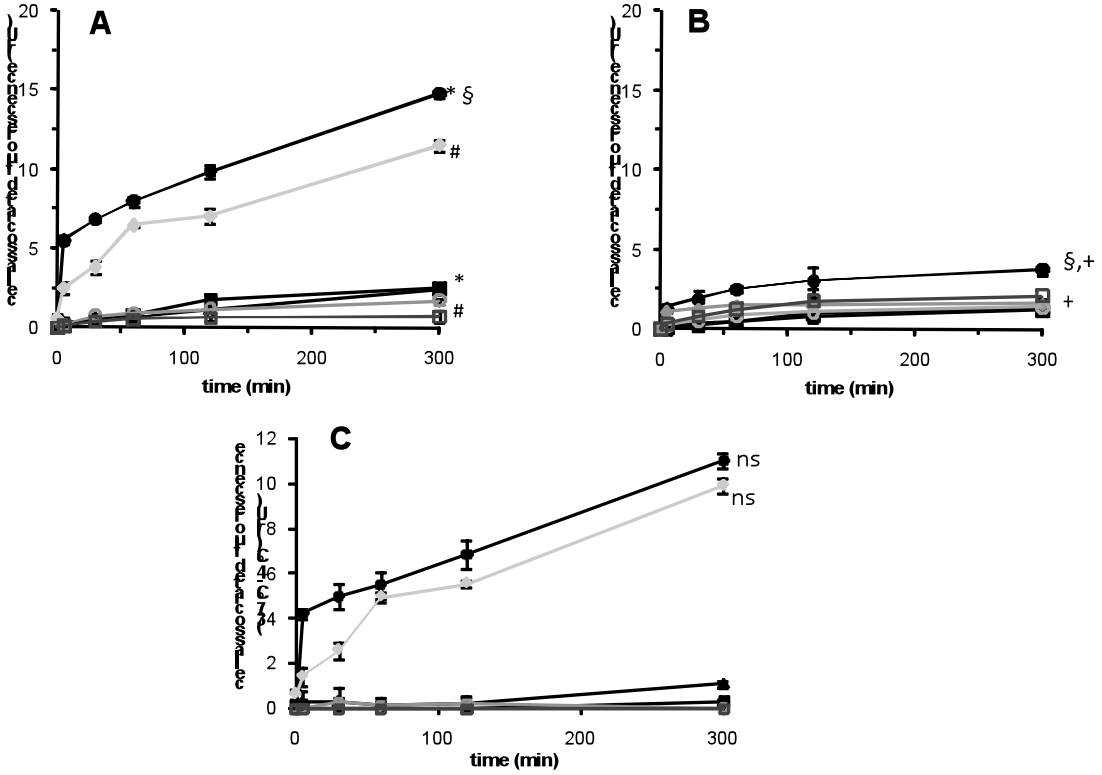

Figure 1. Cellular internalization of **P1** □, **P2** □, **P1-F5** □, **P2-F5** □, **P1-F10** □ and **P2-F10** ♦ measured at 37°C (A), 4°C (B) and total cell uptake (cell associated fluorescence at 37ºC minus at 4ºC) in KB-3-1 cells. Data are represented as mean ± SEM (n = 3). (* p<0,0001 for **P1-F10** vs **P1-F5** and **P1-F10** vs **P1**; # p<0,0001 for **P2-F10** vs **P2-F5** and **P2-F10** vs **P2**; § p<0,0001 for **P1-F10** at 37°C vs 4°C; + p<0,001 for **P1-F10** vs **P2-F10** at 4°C; ns: non-significant).

It has to be kept in mind that the synthesized copolymers are completely different from the well-known PEG-folate conjugates. In our systems, the functionalities are randomly distributed among to the polymer backbone. Thus, the above-mentioned observations of aggregate formation are most likely attributed to the nonpolar character of the folate residues. The solubility of folic acid in water is 0.0016 mg/mL indicating a partially hydrophobic character. In these aggregates, the folate moieties try to avoid contact with its hydrophilic surrounding. This leads to a reduced amount of folate in the hydrophilic particle corona. In order to achieve an efficient receptor mediated endocytosis, a "minimum" amount of accessible folic acid units are required to allow interaction with FRs at cell membrane. For this reason, the increase of folate loading is expected to enhance polymer cell internalization.

In the experiments carried out at 4°C, all conjugates showed a very low uptake level (figure 1B).

These results clearly underline that all conjugates enter the cell following an energy dependent mechanism, such as endocytosis. The difference in the internalization level at 37°C and at 4°C was particularly evident with conjugates **P1-F10** and **P2-F10** ($p<0.0001$) (see figure 1A-B). On the other hand, cell associated fluorescence of the polymer **P1-F10** at 4ºC was slightly but significantly higher ($p<0.05$) compared to **P2-F10** (see figure 1B) indicating an enhanced cell binding prior to the internalization process for the smaller polymer. This result can be explained by differences in the aggregates of **P1-F10** and **P2-F10** although having comparable hydrodynamic diameters. But assuming a comparable super structure density, an aggregate of **P1-F10** would include more single chains and therefore greater accessibility for the folate moieties found on the polymer carrier that induced to a greater conjugate membrane binding effect (figures 1A-B). Quantification of total cell uptake (cell associated fluorescence at 37ºC minus at 4ºC) (figure 1C) showed onlysmall non-significant differences on polymer trafficking kinetics when MW influence was evaluated.

A further proof of FR mediated endocytosis was derived from the experiments carried out in A549 cell line, which is FR negative. In that cells, the associated fluorescence for all conjugates was very low, suggesting that only slight unspecific cell uptake took place. This unspecific uptake may be due to electrostatic interactions of the pteroinic acid part of the folate with the phospholipids in the cell membrane leading –in all properbility- to "adsorptive" pinocytosis. Even so the charge density is much lower than in the case of polyamines such as polyethylenamine and comparable effects cannot be excluded.

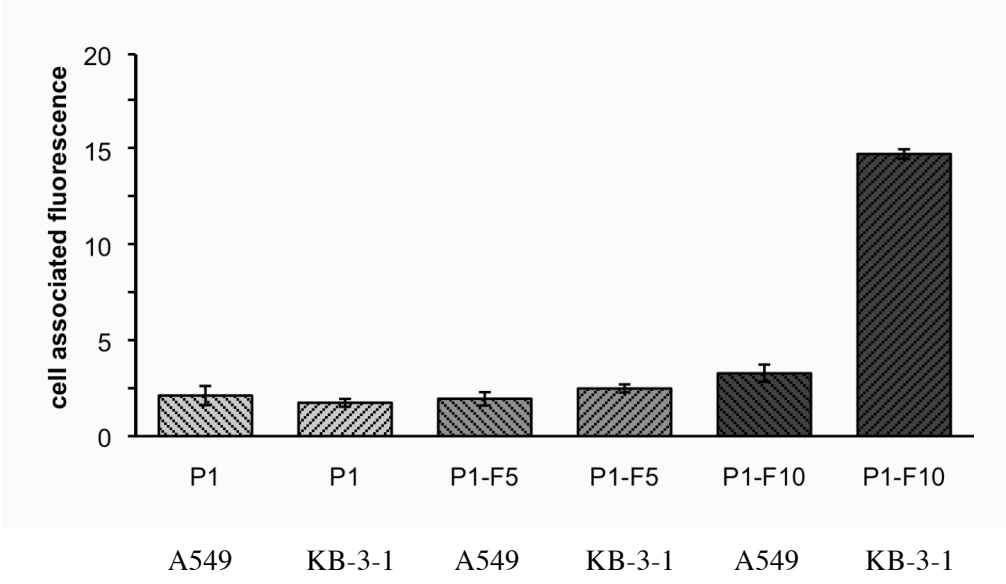

Figure 2. Comparison of cell uptake of the polymers **P1**, **P1-F5** and **P1-F10** in KB-3-1 cells (FR positive) and A549 cells (FR negative) at 37°C at time 5h. Data are represented as mean ± SEM (n = 3) (* p< 0,0001)

But the differences in cell associated fluorescence in KB-3-1 (see figure 2) and A549 are remarkable ($p<0.0001$ for **P-F10**, and $p<0.05$ for **P-F5**). In order to confirm the key role that folate units played in the internalization mechanism in KB-3-1 cell line itself, a competition assay with an excess of free folic acid was also carried out with **P1-F10** and **P2-F10**. In presence of free folic acid, cell associated fluorescence decreased 5-6 fold (see figure 3) ($p<0.0001$).

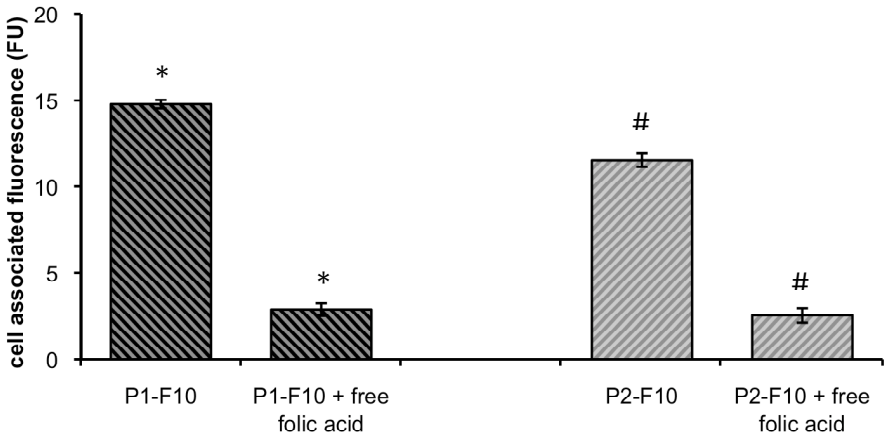

Figure 3. Influence of free folic acid on the polymer uptake of **P1-F10** and **P2-F10** in KB-3-1 cells (FR positive) after 5h of incubation. The free folic acid (1mM) competes with the conjugate for the interaction with the folate receptor (FR) and inhibits its internalization by receptor mediated endocytosis. Data are represented as mean ± SEM (n = 3) (* $p < 0.0001$; # $p < 0.001$).

These results lead to the reasonable assumption that the free folic acid is competing with the conjugates in interacting with FR as already reported in literature. [6] Due to the higher diffusion rates and the excess of folic acid, the FR is blocked and the polymer uptake by receptor-mediated endocytosis is minimized. The cell associated fluorescence for **P1-F10** and **P2-F10** in presence of free folic acid was comparable to the unspecific uptake in A549 cells shown by these conjugates or to **P1** and **P2** without folic acid molecules. These findings clearly underline the key role of the FR in pronounced uptake of the conjugates into living tumor cells.

3.3.3 Live cell confocal fluorescence microscopy

Confocal fluorescence microscopy experiments complement FACS studies and were performed to determine the specific cellular localization of our conjugates. Again, the fluorescence output of all the conjugates was normalized and the cells were treated with the same dye equivalents to allow data comparison. Green fluorescence, due to OG conjugated polymers, was present only when KB-3-1 cells were incubated with conjugates **P1-F10** and **P2-F10** (figure 4), both of them with a folic acid content of 10 mol %.

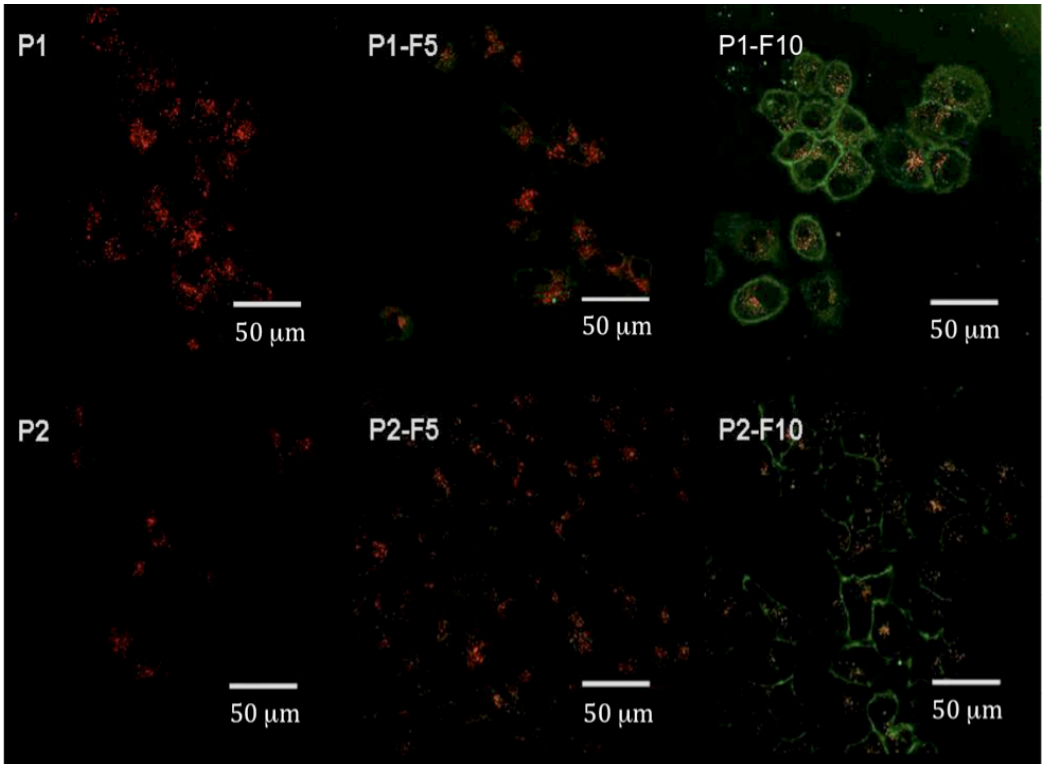

Figure 4. Confocal microscopy images were taken from live KB-3-1 cells after 5 h of incubation with the polymers **P1-F10** and **P2-F10**. Dextran-Texas Red was employed as lysosomal marker (in red in the figure) and polymers were labeled with OG (in green).

In these cases, the fluorescence was detected at the level of the cell membrane already after 30 min incubation. This membrane associated fluorescence nicely monitors the interaction of the folic acid with the membrane bound FR (figure 5).

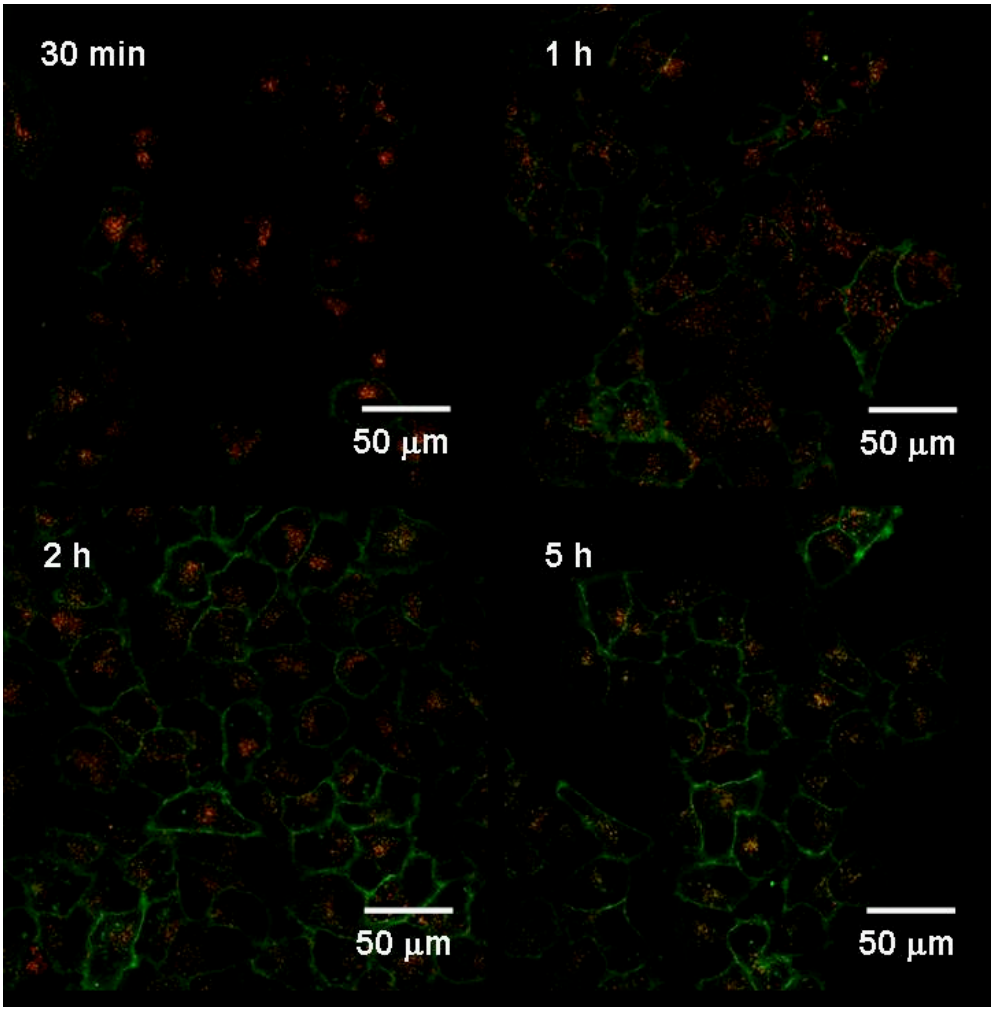

Figure 5. Confocal microscopy images were taken from live KB-3-1 cells after 30 min, 1h, 2h, and 5 h of incubation with the polymers **P2-F10**. Dextran-Texas Red was employed as lysosomal marker (in red in the figure) and polymers were labeled with OG (in green).

At longer incubation times, the fluorescence was detected also inside the cells even at lysosomal level, as demonstrated by co-localization with lysosomal marker Dextran-Texas Red. These results corroborate the expected uptake mechanism of FR mediated endocytosis. With conjugate **P1-F5** and **P2-F5** (lower folate modification degree) almost no fluorescence was registered neither on the cell membrane nor inside the cells, at any time considered, even using different polymer concentration. No

fluorescence was present when cells were treated with control polymers **P1** and **P2**.

As expected, all conjugates when incubated in A549 cells, gave no detectable cell associated fluorescence at any time considered. These results are in good agreement with FACS data. The absence of fluorescence in A549 cells could be attributed to the absence of FRs in their cell membrane. Thus, receptor mediated endocytosis could not take place and the rate of normal endocytosis with our systems was inefficient to achieve a remarkable amount of polymer inside the cell.

These findings suggested that the presence of FR in the cell membrane of KB-3-1 cells allowed the conjugates with a higher folate content to first interact with the cell membrane and then to enter the cells through a receptor mediated process. But most importantly, our findings clearly underline that the aggregate formation has to be investigated carefully to understand the kinetics of cellular uptake. In many cases it is most likely that the interaction of polymers with cells is based on aggregate-cell interactions.

4. Conclusion

We have shown here the synthesis of a family of well-defined HPMA folate conjugates, which allowed us to study the influence of folate content and MW on cellular uptake in FR positive KB-3-1 cells as well as in FR negative A549 cells. By applying the RAFT polymerization method we were able to precisely control the MW and achieved low PDI of ~1.2 for all polymers synthesized. At non-toxic doses, we observed that the amount of polymer taken up by FR positive cells (KB-3-1) after 5 h incubation strongly depended on folate content in the polymer conjugate. On the other hand, the effect of MW was almost negligible regarding total cell uptake. However, a different internalization process could be detected. In the molar mass range of the synthesized polymers from 15 kDa to 30 kDa significant differences could be observed regarding cell binding that indicate a greater polymer-FR interaction, possibly due to the conformation adopted in solution by the lower MW conjugate that leads to a greater exposure of its folic acid residues. For HPMA homopolymers as well as conjugates with 5 mol % folate content, cell associated fluorescence was relatively low pointing out that a minimum amount of folic acid is mandatory for efficient cell uptake. We assume that this finding is due to the aggregation of conjugates in solution, which was investigated by FCS. For the conjugates taken up into the FR positive cells we observed aggregates of comparable size of around 16 -18 nm. In these aggregates the less hydrophilic folate tries to avoid contact with water and is mostly located in the core of the particle. Keeping in mind that these aggregates are based on random copolymers, which can only form micellar structures by the formation of loops, it is most likely that a certain

amount of folate is still located in the hydrophilic corona of the particle. These units could then interact with the FR and induce a receptor-mediated endocytosis. In FR negative cells (A549) the polymers synthesized did not show any significant cell uptake, even after 5 h incubation. More importantly, the uptake of conjugates was drastically reduced by addition of an excess of free folic acid, which is understandable taking into account that also free folic acid has a high affinity to the FR. This data clearly showed the high affinity/selectivity of our systems for FR.

In addition, we were able to nicely monitor the uptake process by live cell confocal microscopy. After 30 min the folate bearing conjugates were only localized at the cell membrane, whereas after 5h the fluorescently labeled polymers were also present inside the cells. The co-localization of polymers with the lysosomal marker (Dextran Texas Red) indicated the presence of the conjugates in the lysosomes and therefore, the participation of an endocytic pathway.
More detailed investigations regarding the uptake mechanism are warranted and currently being investigated in our laboratories. Furthermore, we are applying the recently published radioactive labeling method [46] and others to the folate polymer conjugates in order to use them as a polymeric imaging agent in positron emission tomography (PET).

But nevertheless, our findings clearly underline the key role of aggregate formation, which has to be considered carefully whenever interactions of polymers with cells are discussed.

5. Acknowledgment

The authors would like to thank Ms Xia Li and Ms Lydia Braun for assistance during the synthesis of conjugates, Mr Anton Kaiser for skillful assistance during HPLC workup of the folate linker conjugate and H. Ringsdorf for his helpful advice. We also gratefully acknowledge the Flow Cell Analysis Facility and the Confocal Microscopy Service of the Centro de Investigación Príncipe Felipe (Valencia, Spain) for their skillful assistance. The authors want to thank the graduate school of excellence MAINZ, COMATT, SAMT and the Spanish Ministry Grant (CTQ2007-60601) for support and funding.

6. References

[1] Duncan R. The dawning era of polymer therapeutics. Nat Rev Drug Discov 2003;2:347–60.

[2] Duncan R. Polymer conjugates as anticancer nanomedicines. Nat Rev Cancer 2006;6:688-701.

[3] Ferrari M. Cancer nanotechnology: opportunities and challenges. Nat Rev Cancer 2005;5:161-71.

[4] Gu, F., Karnik, R., Wang, A., Alexis, F., Levy-Nissenbaum, E., Seungpyo, H., Langer, R., Farokhzad, O., Targeted nanoparticles for cancer therapy, Nano Today 2007;2:14-21

[5] Haag R, Kratz F. Polymer Therapeutics: Concepts and Applications Angew Chem Int Ed 2006;45:1198-215.

[6] Kamen BA, Capdevila A. Receptor-mediated folate accumulation is regulated by the cellular folate content. Proc Natl Acad Sci USA 1986;83:5983-5987

[7] Leamon CP, Low PS. Delivery of macromolecules into living cells: A method that exploits folate receptor endocytosis. Proc Natl Acad Sci USA 1991;88:5572-5576

[8] Hoffbrand AV, Weir DG The history of folic acid. Br J Haematol 2001;113:579-589

[9] Duthie SJ. Folic acid defiency and cancer: mechanisms of DNA instability, British Medical Bulletin 1999;55:578-592

[10] Shane B. Folate chemistry and metabolism. Folate in health and disease (L.B. Baily ed.), Marcel Dekker, New York, 1995;1:1-21

[11] Elnakat H, Ratnam M. Distribution, functionality and gene regulation of folate receptor isofroms: implications in targeted therapy. Adv Drug Deliv Rev 2004;56:1067-1084

[12] Rothberg KG, Ying Y, Kolhouse JF, Kamen BA, Anderson RGW. The glycophospholipid-linked folate receptor internalizes folate without entering the clathrin-coated pit endocytic pathway. J Cell Biol 1990; 110: 637-649

[13] Antony AC, Kane MA, Portillo RM, Elwood PC, Kolhouse JF. Studies of the role of a particulate folate-binding protein in the uptake of 5-methyltetrahydrofolate by cultured human KB cells. J Biol Chem 1985;260:14911–14917.

[14] Conner SD, Schmid SL. Regulated portals of entry into the cell, Nature 2003;422:37- 44

[15] Sabharanjak S, Mayor S. Folate receptor endocytosis and trafficking, Adv Drug Deliv Rev 2004;56:1099-1109

[16] Mattes MJ, Major PP, Goldenberg DM, Dion AS, Hutter RV, Klein KM. Patterns of antigen distribution in human carcinomas. Cancer Res 1990;50:880–884.

[17] Weitman SD, Lark RH, Coney LR, Fort DW, Frasca V, Zurawski VR, Jr., Kamen BA. Distribution of the folate receptor GP38 in normal and malignant cell lines and tissues. Cancer Res 1992;52:3396–3401

[18] Ross JF, Chaudhuri PK, Ratnam M. Differential regulation of folate receptor isoforms in normal and malignant tissues in vivo and in established cell lines. Physiologic and clinical implications. Cancer 1994;73:2432–2443.

[19] Weitman SD, Frazier KM, Kamen BA. The folate receptor in central nervous system malignancies of childhood. J Neurooncol 1994;21:107–112.

[20] Toffoli G, Cernigoi C, Russo A, Gallo A, Bagnoli M, Boiocchi M. Overexpression of folate binding protein in ovarian cancers. Int J Cancer 1997;74:193–198.

[21] Lu Y, Low PS. Folate-mediated delivery of macromolecular anticancer therapeutic agents. Adv Drug Del Rev 2002;54:675-693

[22] Lee ES, Na K, Bae YH. Polymeric micelle for tumor pH and folate-mediated targeting. J. Control. Rel 2003;91:103-113

[23] Yoo HS, Park TG. Folate receptor targeted biodegradable polymeric doxorubicin micelles. J Control Rel 2004;96:273-283

[24] Pasut G, Canal F, Dalla Via L, Arpicco S, Veronese FM, Schiavon O. Antitumoral activity of PEG-gemcitabine prodrugs targeted by folic acid. J Control Rel 2008;127:239-248

[25] Quintana A, Raczka E, Piehler L, Lee I, Myc A, Majoros I, Patri AK, Thomas T, Mule J, Baker JR. Design and function of a dendrimer-based therapeutic nanodevice targeted to tumor cells through the folate receptor. Pharm Res 2002;19:1310-1316

[26] Chandrasekara D, Sistlaa R, Ahmadb FJ, Kharb RK, Diwan PV. The development of folate-PAMAM dendrimer conjugates for targeted delivery of anti-arthritic drugs and their pharmacokinetics and biodistribution in arthritic rats. Biomaterials 2007;28:504–512.

[27] Pan D, Turner JL, Wooley KL. Folic acid conjugated nanostructured materials designed for cancer cell targeting. Chem Commun 2003;2400–2401.

[28] Choi H, Choi SR, Zhou R, Kung HF, Chen I.. Iron oxide nanoparticles as magnetic resonance contrast agent for tumor imaging via folate receptor-targeted delivery. Acad Radiol 2004;11:996–1004.

[29] Sonvico F, Mornet S, Vasseur S, Dubernet C, Jaillard D, Degrouard J, Hoebeke J, Duguet E, Colombo P, Couvreur P. Folate-Conjugated Iron Oxide Nanoparticles for Solid Tumor Targeting as Potential Specific Magnetic Hyperthermia Mediators: Synthesis, Physicochemical Characterization, and *in Vitro* Experiments. Bioconj Chem 2005;16:1181–1188

[30] Anderson KE, Eliot LA, Stevenson BR, Rogers JA. Furmulation and evaluation of a folic acid receptor-targeted oral vancomycin liposomal dosage form. Pharm Res 2001;18:316-322.

[31] Lee RJ, Low PS. Delivery of liposomes into cultured KB cells via folate receptor-mediated endocytosis. J Biol Chem 1994;269:3198-3204.

[32] Lee RJ, Low PS. Folate-mediated tumor cell targeting of liposome-entrapped doxorubicin in vitro. Biochim Acta 1995;1233:134-144.

[33] Gabizon A, Shmeeda H, Horowitz AT, Zalipsky S. Tumor cell targeting of liposome-entrapped drugs with phospholipid-anchored folic acid-PEG conjugates. Adv Drug Deliv Rev 2004;56:1177-1192.

[34] Fernandes JC, Wang H, Jreyssaty C, Benderdour M, Lavigne P, Qiu X, Winnik FM, Zhang X, Dai K, Shi Q. Bone-protective Effects of Nonviral Gene Therapy With Folate-Chitosan DNA Nanoparticle Containing Interleukin-1 Receptor Antagonist Gene in Rats With Adjuvant-induced Arthritis. Mol Ther 2008;16;1243-1251

[35] Shi X, Wang SH, Swanson SD, Ge S, Cao Z, Van Antwerp ME, Landmark KJ, Baker JR. Dendrimer-functionalized shell-crosslinked iron oxide nanoparticles for in-vivo magnetic resonance imaging of tumors. Adv. Mat. 2008;20:1671-1678

[36] Leamon CP, Cooper SR, Hardee GE. Folate-Liposome-Mediated Antisense Oligodeoxynucleotide Targeting to Cancer Cells: Evaluation in Vitro and in Vivo. Bioconj Chem. 2003;14:738–747

[37] Hawker CJ, Bosman AW, Harth E. New Polymer Synthesis by Nitroxide Mediated Living Radical Polymerizations. Chem Rev 2001;101:3661-3688.

[38] Matyjaszewski K, Xia J. Atom transfer radical polymerization. Chem Rev 2001;101:2921–90.

[39] Matyjaszewski K, Gnanou Y, Leibler L. Macromolecular engineering, vol. 1. Weinheim: Wiley-VCH; 2007.

[40] Tsarevsky NV, Matyjaszewski K. ‘‘Green’’ atom transfer radical polymerization: from process design to preparation of well-defined environmentally friendly polymeric materials. Chem Rev 2007;107:2270–99.

[41] Barner-Kowollik C. Handbook of RAFT polymerization. Weinheim, Germany: Wiley-VCH; 2008.

[42] Moad G, Rizzardo E, Thang SH. Radical addition–fragmentation chemistry in polymer synthesis. Polymer 2008;49:1079–131.

[43] Stenzel MH. RAFT polymerization: an avenue to functional polymeric micelles for drug delivery, Chem. Commun. 2008;30:3486-503.

[44] Godwin A, Hartenstein M, Müller AHE, Brocchini S. Narrow Molecular Weight Distribution Precursors for Polymer-Drug Conjugates. Angew. Chem. Int. Ed. 2001;40:594-597.

[45] Gauthier MA, Gibson MI, Klok H-A. Synthesis of Functional Polymers by Post-Polymerization Modification. Angew. Chem. Int. Ed. 2009;48:48–58

[46] Theato P. Synthesis of well-defined polymeric activated esters. J Polym Sci Part A Polym Chem 2008;46:6677–87.

[47] Herth M, Barz M, Moderegger D, Allmeroth M, Jahn M, Thews O, et al. Radioactive labeling of defined HPMA-based polymeric structures using [18F]FETos for in vivo imaging by positron emission tomography. Biomacromolecules 2009;10,1697–1703

[48] Barz M, Luxenhofer R, Zentel R, Kabanov AV. The uptake of N-(2-hydorxypropyl)methacryl-amide based homo, random and block copolymers by human multi-drug resistant breast adenocarcinoma cells. Biomaterials 2009;30:5682-5690

[49] Gibson MI, Fröhlich E, Klok H-A, Postpolymerization Modification of Poly(Pentafluorophenyl methacrylate): Synthesis of a Diverse Water-Soluble Polymer Library. Journal of Polymer Science: Part A: Polymer Chemistry 2009; 47:4332–4345

[50] Rigler R, Elson ES. Fluorescence Correlation Spectroscopy. Springer-Verlag: New York, 2001.

[51] Chong YK, Moad G, Rizzardo E, Tang SH. A More Versatile Route to Block Copolymers and other Polymers of Complex Architecture by Living Radical Polymerization: The RAFT Process. Macromolecules 1999;*32*:2071-2074.

[52] Eberhardt M, Mruk R, Zentel R, Theato P. New precursor polymers for the synthesis of multifunctional materials. Eur Polym J 2005;41:1569–75.

[53] Eberhardt M, Theato P. RAFT polymerization of pentafluorophenyl methacrylate: Preparation of reactive linear diblock copolymers. Macromol Rapid Commun 2005; 26:1488-93.

[54] Perrier S, Takolpuckdee P, Mars CA. Reversible addition–fragmentation chain transfer polymerization: end group modification for functionalized polymers and chain transfer agent recovery. Macromolecules 2005;38:2033–6.

2.6 Synthesis, Characterization and Evaluation of P(HPMA)-*block*-P(LLA) Copolymers: A New Type of Functional Biocompatible Block Copolymer

Journal: Macromolecules 2009, submitted

Authors: Matthias Barz[1], Florian Wolf[1], Fabiana Canal[2], Kaloian Koynov[3], Maria J. Vicent[2], Holger Frey[1] and Rudolf Zentel[1,*]

Address: [1] Institute of Organic Chemistry, Johannes Gutenberg-University Mainz, Duesbergweg 10-14, D-55099 Mainz, Germany

[2] Centro de Investigacion Principe Felipe, Avda Autopista el Saler 16/3, 46012 Valencia, Spain

[3] Max-Planck-Institute for Polymer Research, 55128 Mainz, Germany

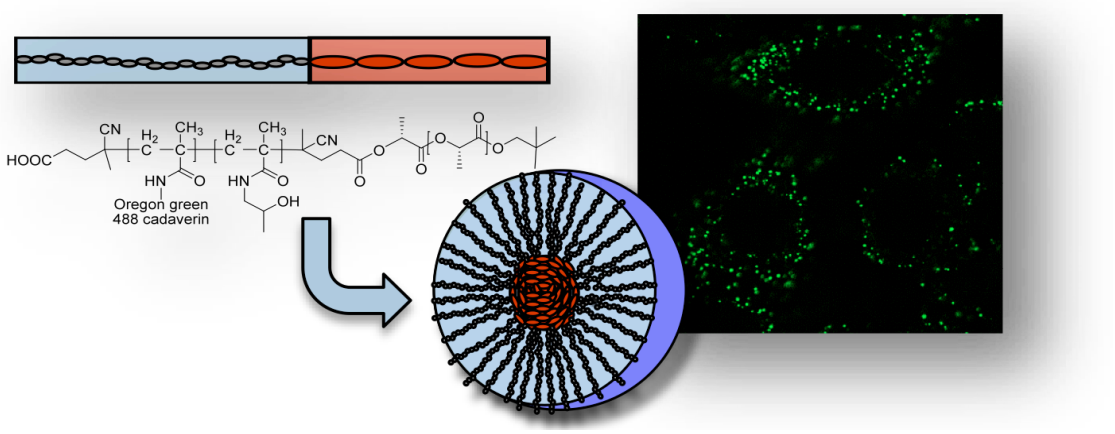

Abstract

We describe a synthetic pathway to functional poly(N-(2-hydroxypropyl)-methacrylamide)-*block*-poly(L-lactide) block copolymers (P(HPMA)-*block*-P(LLA)) in 4 steps. The synthesis relies on a combination of ring-opening polymerization of L-lactide, conversion into a macroinitiator for controlled radical polymerization via end-group modification with a dithioester and subsequent RAFT polymerization of pentafluorophenyl methacrylate. A series of well-defined reactive ester block copolymers have been prepared and characterized. The materials exhibited molecular weights M_n ranging from 7,600 g/mol to 34,300 g/mol with moderate polydispersities M_w/M_n between 1.3 and 1.45. These reactive precursor polymers have been transformed into biocompatible P(HPMA)-*block*-P(LLA) copolymers with additional, covalently linked fluorescence marker units by facile replacement of the pentafluorophenyl groups in a polymer modification reaction. The fluorescence label was used in lieu of a drug for detailed cellular uptake studies. The aggregation behavior of this new type of partially degradable amphiphilic block copolymers was studied for the sample $P(HPMA)_{77}$-*block*-$P(LLA)_{42}$ in aqueous solution, employing fluorescence correlation spectroscopy (FCS). For this fluorescently labeled block copolymer aggregates with a hydrodynamic diameter of 17.6 nm (0.1 mg/mL in PBS buffer, pH 7.2) were observed. These micellar structures have been used for explorative *in vitro* studies and exhibited pronounced cellular uptake as well as nontoxic behavior of the block copolymer up to a concentration of 3 mg/mL in HeLa cells (human cervix adenocarcinoma). The partially degradable, functional P(HPMA)-*block*-P(LLA) block copolymers represent promising drug delivery vehicles for both *in vitro* and *in vivo* applications.

1. Introduction

Since publication of the seminal concept for polymers as therapeutic agents in the 1970ies by Ringsdorf et al. [1] there has been tremendous progress in polymer based nanomedicine. [2-6] In recent decades, polymers have been widely investigated as carrier systems for drugs. In the ideal case, the drug is selectively and exclusively transported to the desired site of action, increasing the drug efficacy and minimizing undesired side effects. Masking the active agent for circulation in healthy tissue and organs can either be achieved by polarity driven encapsulation in a polymer based aggregate/physical matrix or by covalent attachment to the polymer structure. The first polymers designed to fulfill these demands entered clinical trials approximately a decade ago and have been subjected to extensive research ever since. [7-9] A pioneering step for a synthetic polymer in clinical approval was achieved by a drug conjugate based on the N-(2-hydroxypropyl)-methacrylamide (HPMA) in the 1980ies. [7] Most other systems with clinical approval are based on poly(ethylene glycol) (PEG), e.g., protein polymer conjugates [10,11] antibody polymer conjugates [12,13] as well as polymeric micelles with a drug encapsulated or covalently attached to the hydrophobic part of the block copolymer. [14-17]

In contrast to the difunctional PEG based systems, acrylate and acrylamide based polymers provide access to a plethora of different functionalities and reactive groups at the polymer backbone, e.g., activated esters or alkyne side chains, since they are readily obtained by straightforward synthetic chemistry. [18-21] Particularly in biological or medical applications multifunctional systems are desired, as they offer control of functionality, hydrophilicity, pH-induced phase behavior and charge density. However, the major drawback of all systems obtained previously by free radical polymerization is their lack of controlled molecular weights and considerable polydispersity. Currently, the modern controlled radical polymerization techniques, e.g. ATRP, RAFT or NMP [22-27], provide means to tackle this issue and can also be employed to generate unprecedented block copolymer structures. In this respect, various multifunctional systems have been used for biological or medical application. [28-33]

The synthesis of amphiphilic block copolymers is often challenging, especially when the expected window for common solvents for both blocks is narrow. Successful approaches to this problem either rely on the cleavage of silane [34] or acetal [35] based protecting groups, the oxidation of vinyl functionalities, hydrolysis of epoxides and the methylation/protonation of pendant amines and salt formation in general. In this respect the activated ester approach [45] offers a useful tool in the synthesis of multifunctional and amphiphilic block copolymers. In addition, the transformation of fluorinated activated ester groups, such as pentafluorophenol esters can be precisely monitored by ^{19}F NMR spectroscopy. The block copolymer systems explored at present are based on non-degradable

backbone structures, which is expected to represent a drawback for long-term therapeutic applications. Therefore it is highly desirable to combine both a degradable and a functional segment in one block copolymer. This concept is particularly attractive, if eventual degradation of one block leads to well-known building blocks, like it would be the case for a combination of P(HPMA) with the biodegradable poly(L-lactide) (PLLA).

In this context, we have developed functional P(HPMA)-*block*-P(LLA) copolymers by combining ring-opening polymerization (ROP) and subsequent RAFT polymerization. PLLA is well-known to be degradable under *in vivo* conditions and is widely used in biomedical polymer technology, compromising applications in drug delivery [36], tissue engineering [37], surgical sutures, etc. [38,39] However, one of the most interesting properties reported for PEG-*block*-PLLA block copolymers is their stability in blood described by Kataoka et al. in 2001. [36] This is a crucial prerequisite that renders PLLA-based block copolymer systems a promising platform for *in vivo* transport. Particularly the stereoregular P(LLA) blocks retain their integrity due to their thermodynamic and kinetic stability and hence should allow for a targeted delivery prior to their excretion or degradation.

Surprisingly, only few examples combining ROP with a controlled radical polymerization technique are known in literature. [40-43] To date, none of them has capitalized on the activated ester approach to generate reactive precursor block copolymers, which can be precisely characterized and afterwards transformed into functional P(HPMA) based block copolymers. In the approach presented here, well-defined poly(lactide)s bearing a chain transfer agent (CTA) enable a chain extension with pentafluorophenol methacrylates via the RAFT polymerization method.

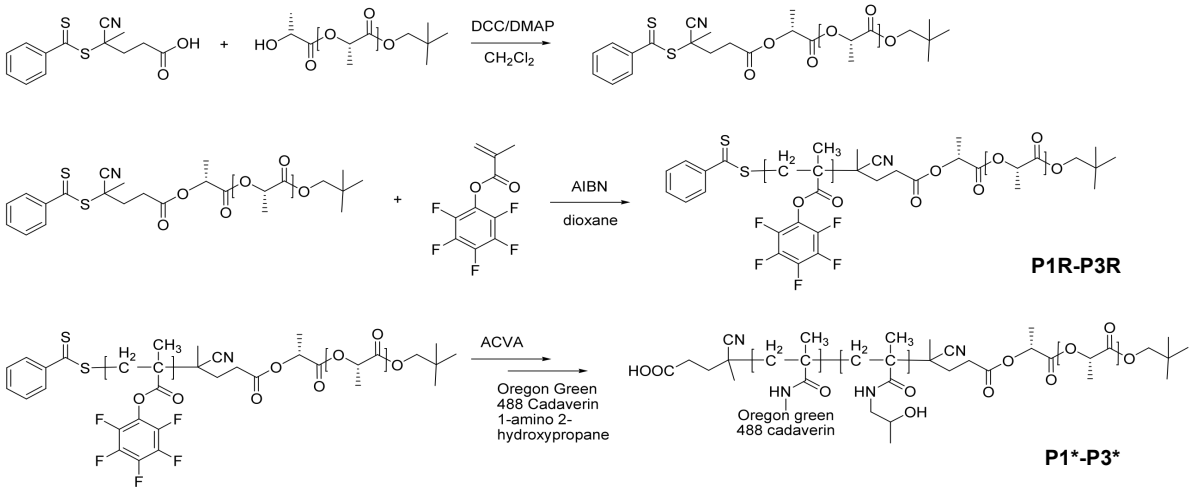

Scheme 1. Synthesis of functional poly(HPMA)-*block*-poly(L-lactide) copolymers by a combination of ROP and RAFT polymerization, using the activated ester approach.

In the next step the reactive precursor was reacted with Oregon Green 488 cadaverine and 2-hydroxypropylamine, yielding a dye-labeled HPMA block copolymer, in analogy to a recently reported method [33] for structurally different materials. Additionally, in this work we have studied micelle formation in solution (PBS buffer pH = 7.2) by fluorescence correlation spectroscopy (FCS) and present a first biological evaluation regarding cellular uptake and toxicity.

2. Materials and Methods

2.1 Materials

All chemicals were reagent grade, obtained from Aldrich and used without further purification, unless indicated otherwise. All solvents were of analytical grade. Pentafluorophenol was obtained from Fluorochem (Great Britain, UK) and distilled prior to use. Dioxane, dimethylsulfoxide (DMSO) and dichloromethane were dried and freshly destilled. 2,2'-Azobis(isobutyronitrile) (AIBN) was recrystallized from diethyl ether and stored at -7°C. DBU (1,8-Diazabicyclo[5.4.0]undec-7-ene) (99%) was purchased from Acros and distilled from calcium hydride. Deuterated chloroform-d_1 was purchased from Deutero GmbH, dried and stored over molecular sieves. L-lactide was purchased from Purac/Gorinchem (Netherlands), recrystallized three times from dry toluene and stored under vacuum prior to use. Dialysis of block copolymers was performed with Cellu SepH1® membranes (Membrane Filtration Products, Inc.) with a molecular weight cutoff of 1000 g/mol and Spectra/Por® membranes (Roth) with a molecular weight cutoff of 3,500 g/mol.

2.2 Characterization

^{1}H-, ^{13}C- and ^{19}F-NMR spectra were obtained at 300 or 400 MHz using a FT-spectrometer from Bruker and analyzed using the ACDLabs 6.0 software. The polymers were dried at 40 °C over night under vacuum and afterwards characterized by gel permeation chromatography (SEC).

For SEC measurements in DMF (containing 1 g/L of lithium bromide as an additive) at 30°C, an Agilent 1100 series system was used as an integrated instrument including three HEMA-based-columns ($10^5/10^3/10^2$ Å porosity) from MZ-Analysentechnik GmbH, a UV (275 nm) and a RI detector. Calibration was achieved with poly(styrene) standards provided by Polymer Standards Service (PSS). Size-exclusion chromatography with THF as an eluent was performed at 25°C and at a flow rate of 1 mL min^{-1} with an instrument consisting of a Waters 717 plus autosampler, a TSP Spectra Series P 100 pump, and a set of three PSS-SDV 5-l columns with porosities of 100, 1000, and 10,000 Å, respectively.

2.3 Synthesis of 4-Cyano-4-((thiobenzoyl)sulfanyl)pentanoic Acid

The 4-cyano-4-((thiobenzoyl) sulfanyl)pentanoic acid was used as the chain transfer agent (CTA) and synthesized according to literature in a 3-step reaction. [44]

2.4 Synthesis of Pentafluorophenyl Methacrylate (PFMA)

PFMA was prepared according to the literature. [45]

2.5 Poly(L-lactide) Synthesis

Neopentyl alcohol and lactide were charged into a Schlenk-tube at predetermined molar ratio. The tube was sealed with a rubber septum and repeatedly flashed with argon after evacuation. Freshly distilled dichloromethane (4 mL/g dilactide) was added via a syringe. Polymerization was initiated by injecting a 10% solution of DBU in dry dichloromethane corresponding to 1% of the total amount of monomer after 2 minutes. The polymerization was quenched after 15 minutes by injecting a 10% dichloromethane solution of benzoic acid, corresponding to a twofold excess of the catalyst. An aliquot of the sample was harvested for conversion analysis prior to the precipitation in excess methanol. The polymer was collected by centrifugation or filtration and taken up in CH_2Cl_2 for a second precipitation in diethyl ether. ^{1}H-NMR ($CDCl_3$, 400MHz): δ [ppm] 0.92 (s, C(CH_3)$_3$; 1.57 (d, ^3J =7.0 Hz CHCH_3, poly(lactide) chain); 3.78-3.89 (m, -OCH_2C(CH$_3$)$_3$); 4.34 (q, ^3J =7.0 Hz HOCH(CH$_3$)); 5,15 (q, ^3J =7.0 Hz CH(CH$_3$), poly(lactide) chain).

^{1}H-NMR (DMSO-d$_6$, 400MHz): δ [ppm] 0.89 (s, C(CH_3)$_3$; 1.27 (d, ^3J =7.0 Hz HOCH(CH_3)1.47 (d, ^3J =7.0 Hz CHCH_3, poly(lactide) chain); 3.76-3.86 (m, -OCH_2C(CH$_3$)$_3$); 4.20 (m HOCH(CH$_3$)); 5,20 (q, ^3J =7.0 Hz CH(CH$_3$), poly(lactide) chain).

2.6 End group modification of PLLA to w-CTA macroinitiator for RAFT polymerization

1.0 g 4-Cyano-4-((thiobenzoyl) sulfanyl)pentanoic acid was dissolved under nitrogen in 100mL CH_2Cl_2. The solution was cooled in an ice bath and 0.5 g of dicyclohexylcarbodiimide (DCC) were added. After 10 minutes a solution of 0,02 g 4-(dimethylamino)-pyridin (DMAP) in 5 mL CH_2Cl_2 was slowly added. 3.3 g of the poly(L-lactide) in 20 mL CH_2Cl_2 were added to the activated acid. The reaction was allowed to proceed over night. Finally the solution was concentrated and the functionalized polymer was precipitated twice in cold methanol, once in diethyl ether, dried in high vacuum and a reddish powder was obtained. Yield: 3.06 g, 91%, 69 % functionalization (NMR).

^{1}H NMR (300 MHz, CDCl-d$_1$): δ [ppm] 0.92 (s, C(CH_3)$_3$; 1.57 (d, ^3J =7.0 Hz CHCH_3, PLLA chain); 1.92 (s, CR$_2$CH_3, CTA); 2.50 2.75 (m, -CH$_2$CH$_2$, CTA); 3.78-3.89 (m, -OCH_2C(CH$_3$)$_3$); 4.34 (q, ^3J =7.0 Hz HOCH(CH$_3$)); 5,15 (q, ^3J =7.0 Hz CH(CH$_3$), poly(lactide) chain); 7.38 (t, J =1.0 Hz CH=CH, CTA); 7.56 (t, J =1.0 Hz CH=CH, CTA); 7.89 (d, J =1.0 Hz CH=CH, CTA).

2.7 Synthesis of P(PFMA)-*block*-P(LLA)

RAFT polymerization of PFMA using the poly(L-lactide) macroinitiator was performed in a Schlenk tube. The reaction vessel was loaded with 3.5 mg 2,2'-azobis(isobutyronitrile (AIBN) (0.02 mmol), 0.2 g poly(D-lactide) macroinitiator and 1.58 g of PFMA (12 mmol) (example for P2R) in 5 mL of dioxane. Following three freeze–vacuum–thaw cycles, the tube was immersed in an oil bath at 80 °C for 12 h. Subsequently, the block copolymer was once precipitated in ethanol and twice in hexane, isolated by centrifugation and dried at 30 °C under high vacuum for 12 hours. The block copolymer was obtained as a slightly red powder. Yield: (59 %).

^{1}H-NMR ($CDCl3$-d_1, 400MHz): δ [ppm] 0.92 (s, C(CH_3)$_3$; 1.42 (s, CRCH_3, poly(PFMA) chain); 1.57 (d, ^{3}J =7.0 Hz CHCH_3, poly(lactide) chain); 2.07 (s, -CH_2- poly(PFMA) chain) 3.78-3.89 (m, -OCH_2C(CH_3)$_3$); 4.34 (q, ^{3}J =7.0 Hz HOCH(CH_3)); 5,15 (q, ^{3}J =7.0 Hz CH(CH_3), poly(lactide) chain). ^{19}F NMR ($CDCl_3$): -165.1 (br), -159.8 (br), -154.4 (br), -153.1 (br).

2.8 Removal of the dithioester endgroup.

The dithiobenzoate end group was removed according to the procedure reported by Perrier et al.[46] Typically 200 mg of polymer, (M_n = 23.000 g/mol), and 80 mg of 4,4'-azobis(4-cyanovaleric acid) (~30 times excess in relation to the polymer end group) were dissolved in 3 mL of anhydrous dioxane. The solution was heated to 80 °C for 3 h. Finally the copolymer was precipitated 3 times in 100 mL of diethyl ether and collected by centrifugation. In the case of the block copolymer, the crude product was first precipitated in ethanol twice and than once in diethyl ether. The copolymer was dried in vacuo for a period of 24 h and a colorless product was obtained (yield: 90 %). The absence of the dithiobenzoate end group was confirmed by UV-Vis spectroscopy with the absence of the peak at 302 nm wavelength.

2.9 Synthesis of P(HPMA)-*block*-P(LLA) block copolymers

In a typical reaction 100 mg of **P(HPMA)-*block*-P(LLA)** without ditihioester end group was dissolved in 2 mL abs. dioxane and 0.5 mL dried DMSO. A colorless solution was obtained. Subsequently 20 mg of triethylamine (TEA) and 15 mg of hydroxypropylamine were added. The mixture was kept at 30 °C for 24 h and finally additional 15 mg of hydroxypropylamine and 20 mg triethylamine were added. The reaction was allowed to proceed under the above-mentioned conditions for 4 h. The solution was concentrated in vacuum, precipitated twice in diethyl ether, mixed with water and dialyzed against water using Spectra/Por® membranes with a molecular weight cutoff of 3,500 g/mol. In a last purification step a preparative SEC (Sephadex G-25) was used to purify the final product. The solution of the product was lyophilized, yielding 30 mg of a colorless polymer. ^{1}H NMR (DMSO-d_6): δ [ppm] 0.92 (s, C(CH_3)$_3$; 0.7-1.42 (CR_3CH_3, C$H3$CHOH poly(HPMA) chain); 1.57 (d, ^{3}J =7.0 Hz CHCH_3, poly(lactide) chain); 1.2-2.1 (s, -CH_2- poly(HPMA) chain); 2.6-3.2(CHOH,

poly(HPMA) chain); 3.72 (CH_2NH, poly(HPMA) chain); 5.15 (q, ^3J =7.0 Hz CH(CH_3), poly(lactide) chain).

2.10 Synthesis of dye labeled P(HPMA)-*block*-P(LLA) block copolymers

The polymer modification reaction was carried out under the same conditions as mentioned above, but a small fraction of Oregon Green 488 cadaverin dye was used in addition (cf. Table 2). In a typical reaction 150 mg of P(PFMA)-block-P(LLA) (Mn = 25,000 g/mol) without ditihioester end group were dissolved in 2 mL abs. dioxane and 0.5 mL dried DMSO. A colorless solution was obtained. In a typical reaction 2.5 mg Oregon Green 488 cadaverin and 20 mg triethylamine were added and the reaction was allowed to proceed at 30 °C for 4 h. In the next step 40 mg of TEA and 25 mg of hydroxypropylamine were added. The mixture was kept at 30 °C for 24 h, and finally additional 25 mg of hydroxypropylamine and 30 mg TEA were added. The reaction was allowed to proceed for another 4 h. The solution was concentrated in vacuum, precipitated twice in diethyl ether, carefully mixed with water and dialyzed against water using Spectra/Por® membranes with a molecular weight cutoff of 3,500 g/mol.

In a last purification step a preparative SEC (HiTrap™ Desalting Column, Sephadex G-25 superfine) was used to purify the final product. The solution of the purified product was lyophilized, yielding a yellowish polymer. Yield: 30 mg. ^{1}H NMR (DMSO-*d*6): δ [ppm] 0.92 (s, C(CH_3)$_3$; 0.7-1.42 (CR_3CH_3, C*H3*CHOH poly(HPMA) chain); 1.57 (d, ^3J =7.0 Hz CHCH_3, PLLA chain); 1.2-2.1 (s, -CH_2-poly(HPMA) chain); 2.6-3.2(C*H*OH, poly(HPMA) chain); 3.72 (CH_2NH, poly(HPMA) chain); 5.15 (q, ^3J =7.0 Hz CH(CH_3), poly(lactide) chain).

2.11 Characterization of block copolymers in solution by fluorescence correlation spectroscopy (FCS)

Fluorescence correlation spectroscopy experiments were performed using a commercial FCS setup (Zeiss, Germany) consisting of the module ConfoCor 2 and an inverted microscope model Axiovert 200 with a Zeiss C-Apochromat 40 /1.2 W water immersion objective. The fluorophores were excited by an Argon laser (l = 488 nm) and the emission was collected after filtering with a LP505 long pass filter. For detection, an avalanche photodiode that enables single-photon counting was used. Eight-well, polystyrene-chambered cover glass (Laboratory-Tek, Nalge Nunc International) was used as sample cell. The dye-labeled P(HPMA)-*block*-P(LLA) block copolymer was dissolved in DMSO (c = 20 mg/mL) and PBS buffer (pH = 7.2) was slowly added to obtain a final concentration of 0.1 mg/mL. The solution was kept at room temperature over 24 h prior to the measurements. For each solution, 10 measurements with a total duration of 5 min were performed. The time-dependent fluctuations of the fluorescence intensity *dI(t)* were recorded and analyzed by an autocorrelation function $G(t)=1+< dI(t') dI(t'+t)>/<I(t')>^2$. As has been shown theoretically for an ensemble of *m* different types of freely diffusing fluorescence species, $G(t)$ has the following analytical form: [51]

$$G(t) = 1 + \left[1 + \frac{f_T}{1 - f_T} e^{-t/\tau_T}\right] \frac{1}{N} \sum_{i=1}^{m} \frac{f_i}{\left[1 + \frac{t}{\tau_{Di}}\right] \sqrt{1 + \frac{t}{S^2 \tau_{Di}}}} \quad (1)$$

Here, N is the average number of diffusing fluorescence species in the observation volume, f_T and t_T are the fraction and the decay time of the triplet state, t_{Di} is the diffusion time of the *i-th* species, f_i is the fraction of component i, and S is the so-called structure parameter, $S = z_0/r_0$, where z_0 and r_0 represent the axial and radial dimensions of the confocal volume, respectively. Furthermore the diffusion time, t_{Di}, is related to the respective diffusion coefficient, D_i, through [k1] $D_i = r_0^2/4\ t_{Di.}$ The experimentally obtained $G(t)$ can be fitted with eq. 1, yielding the corresponding diffusion times and subsequently the diffusion coefficients of the fluorescent species. Finally, the hydrodynamic radii R_h can be calculated (assuming spherical particles) using the Stokes-Einstein relation: $R_h = k_B T/6\text{ph}D$, where k_B is the Boltzmann constant, T is the temperature, and h is the viscosity of the solution. As the value of r_0 depends strongly on the specific characteristics of the optical setup a calibration was done using a reference standard with known diffusion coefficient, i.e., Rhodamine 6G.

2.12 Cell cultures

HeLa (human cervix adenocarcinoma cells) were grown in DMEM medium supplemented with 10% v/v of heat-inactivated fetal bovine serum (FBS). Cells were maintained at 37°C in an atmosphere of 5% carbon dioxide and 95% air and underwent passage twice weekly.

2.13 Cells viability assay

The cytotoxicity of the conjugates synthesized was evaluated using the MTT (3-(4,5-dimethyltiazol-2-yl)-2,5-diphenyl-tetrazolium bromide) cell viability assay (72 h incubation) with HeLA cells. Cells were seeded into sterile 96-well microtitre plates (seeding density $2.2\text{x}10^4$ cell/mL). Cells were allowed to settle for 24 h before the unlabeled polymer P1 (0.2 µm filter-sterilized) was added. A series of stock solutions of conjugates dissolved in DMSO, with different concentrations ranging from 1 mg/mL to 300 mg/mL, were prepared and the cells were treated with 1 µL of each stock solution, in such a manner that the final polymer concentrations range from 0,01 mg/mL to 3 mg/mL with a final DMSO concentration of 1% (v/v). As control, cells were treated with the same percentage of DMSO, in absence of conjugates to evaluate solvent toxicity. 100% cell viability was assigned to control cells with 1% DMSO. After a further 68 h incubation, MTT (20 µL of a 5 mg/mL solution in PBS) was added to each well, and the cells were incubated for 4 h. After removal of the medium, the precipitated formazan crystals were dissolved in optical grade DMSO (100 µL), and the plates were read spectrophotometrically at 570 nm after 30 min using a Victor^2 Wallac plate reader.

2.14 Live cell confocal fluorescence microscopy

Cells were seeded on a glass placed into 10 cm^2 Petri plates at density of $2\text{x}10^5$ cell/mL. After 24 h of

incubation the cells were treated with 10 µL of Oregon Green-labeled conjugate solution. The final polymer concentration was 0.1 mg/mL. Pulse and chase experiments were performed: after 1 h or 2 h of incubation at 37°C, the medium was removed and replaced with fresh one and cells were incubated at 37°C for further 1 h or 2 h. Then cells were washed trice with PBS supplemented with 10% (v/v) of fetal bovine serum (3 mL) and the glass was removed and set on the microscope. Images were captured with a confocal Leica microscope equipped with a l-blue 63 oil immersion objective and handled with a TCS SP2 system, equipped with an acoustic optical beam splitter (AOBS). Excitation was with an argon laser (548, 476, 488, 496 and 514 nm) and blue diode (405 nm). Images were captured at an 8-bit gray scale and processed with LCS software Version 2.5.1347 (Leica, Germany) containing multicolor, macro and 3D components.

3. Results and Discussion

A. Synthesis of P(HPMA)-*block*-P(LLA) Block Copolymers

The synthesis of the P(HPMA)-*block*-PLLA block copolymers was carried out in 4 steps (see Scheme 1), combining the ring opening polymerization of L-lactide with the RAFT technique. The strategy chosen is governed by the idea to create a reactive ester block copolymer that can be used as a versatile platform for subsequent polymer modification, e.g., by attachment of a drug or/and fluorescence labels, as well as eventually the 2-hydroxypropylamide side chains. Further functionalization would of course be impossible with a P(LLA)-*block*-P(HPMA) block copolymer prepared directly.

In the initial step, PLLA was prepared by controlled ring-opening polymerization (ROP) with the organo-base 1,8-diazabicyclo-[5.4.0]undec-7-ene (DBU), which has been introduced recently as highly efficient transesterification catalyst by Hedrick and coworkers. [47,48] The use of Sn-based catalysts, which is common in P(LLA) synthesis was avoided in view of the eventual biomedical use of the block copolymers. Polymerization time and temperature could be kept low (< 20 min at room temperature) for catalyst loadings of 1% of the monomer concentration. Polymerization of the L-lactide resulted in full conversion. It is important to mention that further extension of the reaction time leads to undesired transesterification side reactions, resulting in broadening of the molecular weight distribution. This was confirmed by MALDI-ToF spectrometry (not shown) and was visible in the appearance of a second sub-distribution with an odd number of lactic acid units, which increased with polymerization time. Neopentyl alcohol was chosen as an initiator with a primary OH-group, since its nine protons of identical chemical shift facilitate molecular weight determination via ^{1}H-NMR (Figure

1). The molecular weight of the rather short PLLA-block (DP_n=42) was chosen to be sufficient for proper stabilization of the desired aggregates, but low enough to be readily degraded intracellularly.
In a second step the hydroxyl end group of the P(LLA) block was coupled with the well known chain transfer agent 4-cyano-4-((thiobenzoyl)sulfanyl)pentanoic acid by DCC-mediated esterification. An overall degree of functionalization of 69 % (NMR) was achieved by applying a 2-fold excess of the activated acid.
The ensuing RAFT polymerization was carried out under the recently reported conditions for the controlled radical polymerization of PFMA. [30,32,49] It is reasonable to assume that the polymerization kinetics is comparable to the kinetics for PFMA homopolymerization reported by Theato et al. [49] and Klok et al. [32], because the reactivity of the chain transfer agent remains unaltered.

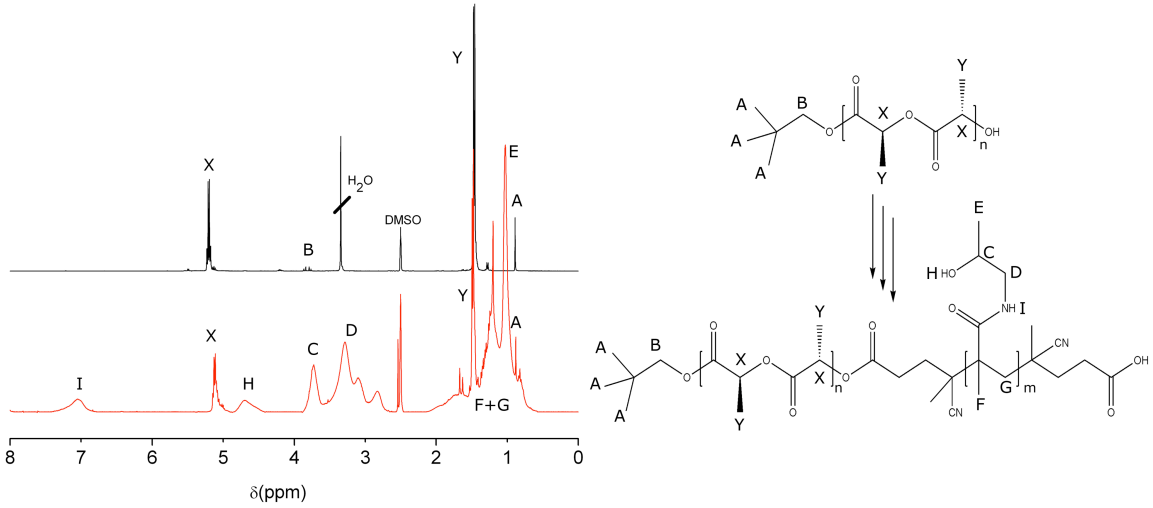

Figure 1. ^{1}H NMR spectra of PLLA (top) and final P(HPMA)-*block*-P(LLA) copolymer (**P2***, bottom**)** in DMSO-d_6. Strong line broadening for the block copolymer is due to micellar association.

Following this procedure we were able to prepare a series of block copolymers differing in the block length of the P(PFMA) block (see Table 1). These reactive block copolymers possess molecular weights in the range of 7,600 g/mol to 34,300 g/mol (M_n) and moderate PDIs from 1.3 to 1.45, confirming well-defined block structures. The degree of polymerization of the P(PFMA) block was varied from 10 up to 117 in order to systematically vary the amphiphilic behavior of the materials.

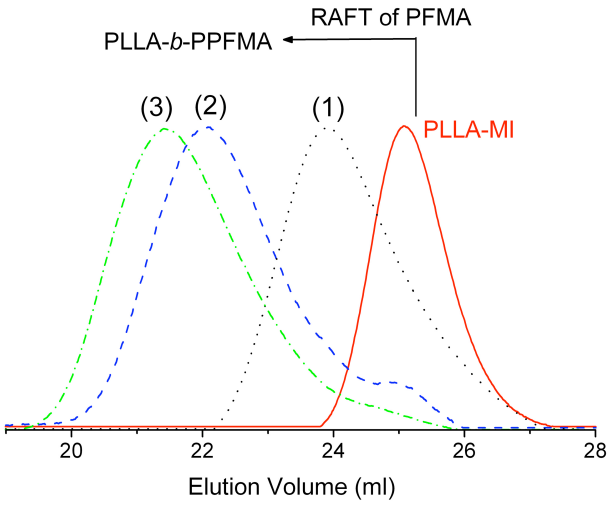

Figure 2. a) SEC elugrams of the P(LLA)-macroinitiator (GPC_{THF}/polystyrene based calibration, M_n = 4,600 g/mol, M_n (NMR) = 3,000 g/mol; PDI = 1.08) and the respective P(PFMA)-*block*-P(LLA) block copolymers **P1, P2** and **P3** prepared in THF (RI-detection).

In Figure 2 the SEC elugrams (solvent THF; RI-detection) of the $P(LLA)_{42}$ macroinitiator as well as the P(PFMA)-*block*-P(LLA) reactive ester block copolymer derived thereof are shown. The obvious shift towards lower elution volumes in SEC indicates an increase in hydrodynamic volume of the sample and thus successful chain extension. The small shoulder for the block copolymer is most probably related to residual P(LLA) homopolymer, which is consistent with NMR-measurements, from which a degree of functionalization with the CTA of 69 % was observed. However, the contamination with homopolymer can easily be removed during work-up of the subsequent reaction step.

Table 1. Characteristics of reactive ester P(PFMA)-*block*-P(LLA) block copolymer precursors **P1R**, **P2R** and **P3R**

polymers	$M_{n,P(LLA)\ block}$	$M_{n,P(LLA)\ block}$	$PDI_{P(LLA)\ block}$	$M_{n,calc}$ kg/mol	M_n kg/mol	M_w kg/mol	PDI kg/mol
P1R	3.0	3.2	1.08	10.0	7.6	9.9	1.31
P2R	3.0	3.2	1.08	30.0	22.8	33.1	1.45
P3R	3.0	3.2	1.08	50.0	34.3	49.1	1.43

In order to avoid undesired side reactions of the dithiobenzyl ester end group, for instance disulfide or thiolactone formation, the method of Perrier et al. was employed for its modification, using 4,4′-azobis(4-cyanovaleric acid). [46] In this approach a 20-fold excess of initiator is used, converting the dithiobenzyl ester end group into a 4-cyanovaleric acid end group by a radical substitution reaction. The initiator was chosen due to its hydrophilic character, which is favorable for the end group of the water soluble PHPMA-block. Full conversion of this reaction was confirmed by UV spectroscopy.

In the final step the activated ester units of the precursor block copolymer were aminolysed in a polymer modification reaction, using 2-hydroxypropylamine. In contrast to the already published procedures [30,32,45], it was not possible to work with an excess of amine in this case, due to the possible, concurrent aminolysis side reaction of the PLLA block. In this respect, the polymer modification reaction was carried out at a stoichiometric ratio of PFMA units in the polymer to amine, which was found to be tolerable for the polyester structure, since amide formation of the activated ester structures proceded significantly faster than ester aminolysis of the P(LLA) block, which was not observed. After 24 h reaction time, the remaining reactive ester groups were quenched at 40º C with a small amount of amine, until full conversion was confirmed by ^{19}F-NMR. Following this procedure, aminolysis of the P(LLA) could be avoided, which is confirmed by the ratio of the signal intensity of the methine proton in PLLA at 5.1 ppm to the intensity of the tertiary proton of the HPMA units at 3.7 ppm (cf. Figure 1, bottom). According to the determined molecular weights this ratio has to be 0.54 for P2, and a ratio of 0.53 was observed by ^{1}H-NMR. The slight differences between calculated and experimentally derived values are in the range of measuring accuracy. The absence of signals from P(LLA) degradation products and the constant ratio of P(LLA) to acrylate based signals confirm the stability of the P(LLA) block during the transformation of the P(PFMA) block to P(PHPMA). Although not integratable due to signal overlap with the polymer backbone, the singulet (A) at 0.89 ppm originating from the neopentyl initator at the a-chain end is still clearly visible. Integration of Lactide (X) and HPMA signals (C and D) allowed the validation of the achieved block length ratios via proton NMR.

Furthermore, the SEC elugram (eluent: DMF), showed a shift to higher molecular weights, which is most likely due to aggregate formation of the block copolymers in DMF. Prior to the aminolysis using 2-hydroxypropylamine, a small fraction of Oregon green cadaverine dye was coupled with the activated ester in order to label the block copolymers with a fluorescence marker. Subsequently the abovementioned polymer modification procedure was applied to obtain the P(HPMA) block.

The final block copolymers were first precipitated from diethyl ether (1x) and EtOH (2x). Afterwards, dialysis against water and preparative SEC (Sephadex G-25) were applied to remove all side products of the polymer modification. After the last step the aqueous polymer solution was lyophilized yielding the final block copolymer. A pure product is of crucial importance for both fluorescence correlation spectroscopy and for biological evaluation. In this respect, yields of approx. 60 % after purification for the polymer modification reaction are more than acceptable. The block copolymers prepared are listed

in Table 2 with the respective characterization data. Similar like the precursor materials, also the P(HPMA) block copolymers showed narrow polydispersity in the range of 1.3 to 1.45, evidencing that chain scission of the PLLA block had not occurred. In the dye-labeled series of block copolymers, the dye content of the hydrophilic block was varied between 0.8 and 10 mol%.

Table 2. Characteristics of poly(HPMA)-*block*-poly(L-lactide) block copolymer (**P1**, **P2** and **P3**) and fluorescently labeled derivatives (**P1***, **P2*** and **P3***)

polymers	Average block ratio (HPMA/L-lactide)	Dye content in the hydrophilic block % (Oregon Green 488)	M_n kg/mol	M_w kg/mol	PDI
P1	10/42	-	5.4	7.0	1.30
P2	78/42	-	14.2	20.5	1.45
P3	124/42	-	20.7	29.6	1.43
P1*	9/42	10	5.8	7.5	1.30
P2*	77/42	1.3	15.9	23.1	1.45
P3*	123/42	0.8	22.1	31.6	1.43

B. P(HPMA)-*block*-P(LLA) Block Copolymers: Aggregation, Cellular Uptake and Toxicity

Aiming at applications for drug transport or molecular imaging, the study of the aggregates formed by the amphiphilic block copolymer structures in buffer solutions and a first evaluation in cell cultures represents an important issue of this work. Due to the amphiphilic character of the block copolymers, the formation of various aggregates in aqueous solution is expected (e.g., micelles, compound micelles or polymersomes). Particularly for biological studies regarding cellular uptake and intracellular distribution, the aggregation behavior is highly important. For example Sahay et al. recently reported that the uptake route of Pluronic P85 switches from caveolae mediated endocytosis to uptake through clathrin coated pits, when the concentration of the copolymer is increased from below to above the critical micelle concentration (cmc). [50] In this respect, we have investigated the superstructure formation in isotonic aqueous solution, applying fluorescence correlation spectroscopy (FCS) to the polymer **P2***, which has in addition been biologically evaluated with respect to cell uptake and cell

toxicity. [51] The DP_n of the non-degradable P(HPMA) block within block copolymer **P2*** is still below the renal exclusion value, which ensure elimination from the body. This design principle is fundamental whenever therapeutic applications are targeted. In contrast to light scattering, where absorption of the laser light by the particles studied is undesirable, the FCS technique measures and correlates fluctuations of the fluorescence signal in order to determine diffusion coefficients. Thus, fluorescently labeled compounds have to be used. Since the diffusion of the labeled polymer is the primary variable of interest in FCS, it is possible to work under the same conditions as employed in cellular biology. Hence it is possible to work in an environment more suitable for biologically relevant issues, as long as the absorption maximum of the dye is different from the surrounding medium. [51]

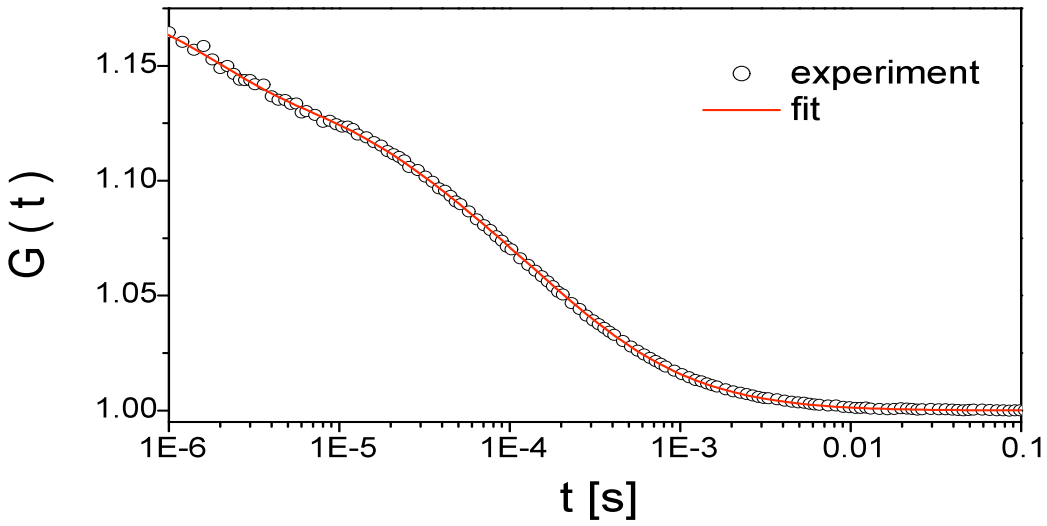

Figure 3. Experimental autocorrelation curve determined by fluorescence correlation spectroscopy (FCS) for fluorescently labeled P(HPMA)-*block*-P(LLA) **P2*** (c = 0.1 mg/ml in PBS buffer (pH = 7.2)) and the corresponding fit with eq.1.

For the FCS measurements the block copolymer **P2*** ($P(HPMA)_{77}$-*block*-$P(LLA)_{42}$) was dissolved in DMSO at a concentration of 10 mg/mL. This solution was slowly mixed with PBS buffer (pH = 7.2) to obtain a concentration of 1 mg/mL. For the final measurements the solution was further diluted, resulting in a concentration of 0.1 mg/mL. We assume that this concentration significantly exceeds the critical micelle concentration (CMC) of the block copolymer, as is observed for other lactide based amphiphilic block structures. [52] Furthermore, this concentration turned out to be suitable for further cell studies that will be described in the following paragraph. Typical autocorrelation curves and the corresponding representation using eq. 1 are shown in Fig. 3.

We had to apply a two component fit (m=2 in eq.1) for the experimental autocorrelation curve. This means that in addition to the slowly diffusing aggregates also fast diffusing species, such as residual amounts of free dye molecules were present in the solution. From the diffusion time of the slow component we evaluated a hydrodynamic radius (R_H) of around 8.5 nm. Thus, block copolymer micelles with an average diameter of 17 nm and nonpolar PLLA core were present in neutral PBS buffer, which is in line with expectation.

These findings are comparable to the results of Saeed et al., who very recently observed aggregates of around 20-30 nm for related P(EGMA)-*block*-P(PLGA) block copolymers. [52] We have also studied solutions with lower concentrations of **P2***. The results, summarized in Table 3, show that aggregates with slightly lower hydrodynamic diameter form at concentrations as low as 0.001 mg/mL. This ensures that at 0.1 mg/mL one works definitely above the CMC. This fact is crucial for the ensuing cellular uptake studies.

Table 3. Characterization of fluorescently labeled (Oregon green 488 cadaverine) P(HPMA)-*block*-P(LLA) block copolymer in PBS buffer (pH = 7.2) by fluorescence correlation spectroscopy (FCS)

Concentration of Polymer **P2***		Fluorescence Correlation Spectroscopy Data		
mg/mL	mol/L	τ_D / µs	D / m^2/s	D_h / nm
0.1	6.5E-6	221	2.67E-11	17.0
0.01	6.5E-7	172	3.42E-11	13.2
0.001	6.5E-8	152	3.87E-11	11.6

The synthesized P(HPMA)-*block*-P(LLA) block copolymers are designed for *in vitro* as well for *in vivo* applications. Even though both polymeric parts of the block copolymer have already been approved to be non toxic at suitable concentrations as well as highly biocompatible, it has to be proven that the new block copolymer itself is also non toxic. To this end, we carried out MTT tests on the block copolymers. The MTT assay is a standard colorimetric assay for the evaluation of the cell viability by evaluating the mitochondrial activity.

C. Cell toxicity assay and intracellular localization of P(HPMA)-*block*-P(LLA) copolymers in human cancer cells (HeLa)

We investigated the concentration dependent influence of the block copolymer **P2** on cell viability over a period of 24 as well as 72 h. At both times very high cell viability levels with respect to the control samples was observed, which was close to 100%. These findings strongly suggested very low toxicity of the block copolymers for concentrations up to 3 mg/mL.

Of course the data derived from MTT test could also be explained by an inefficient or non-existent cellular uptake. In order to lend further support to cellular uptake of block copolymer micelles, live cell confocal fluorescence microscopy was employed. Preliminary uptake studies were performed at a block copolymer concentration of 0.1 mg/mL. This concentration exceeds the CMC, as mentioned above. Thus, we can expect micelles interacting with the cell membrane. The confocal microscopy image shown in Figure 4 was taken after 1h incubation time.

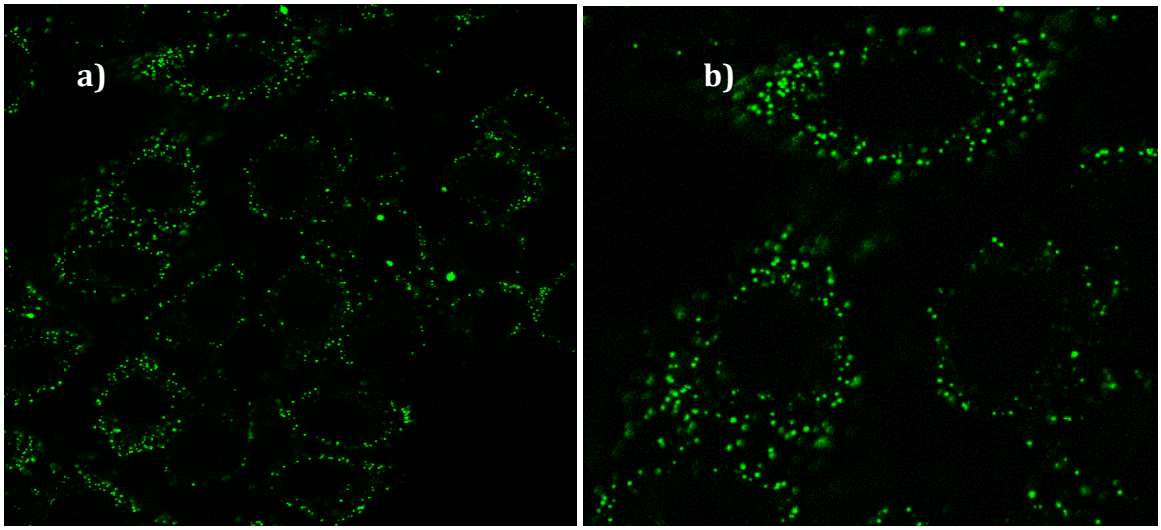

Figure 4. Confocal microscopy images taken from live HeLa cells after 1 h of incubation with the Oregon green 488 cadaverine labeled P(HPMA)-*block*-P(LLA) copolymer at a polymer concentration of 0.1 mg/mL. (scale bar = 50 mm (a) and 25 mm (b)).

Both images show a uniform distribution of fluorescently labeled aggregates within the cells. In addition, the aggregates were well separated from each other and no agglomeration was observed.

These findings are promising and warrant further biological evaluation. From the confocal microscopy results it can be concluded that pronounced cellular uptake of the block copolymers took place. Thus, we could ensure non toxic behavior for the sample **P2***, leading to the reasonable assumption, that this new type of polymer is generally non toxic for imaging purposes as well as therapeutic applications. This is promising, since HPMA and PLLA are both well-established for biomedical use. Further studies regarding the uptake kinetics, intracellular location and degradation studies are warranted and currently under investigation in our laboratories. In addition, we are studying the encapsulation capability of these block copolymer micelles for in vitro as well as in vivo applications.

In summary, these first results on cellular uptake and toxicity clearly underline the potential of P(HPMA)-*block*-P(LLA) copolymers for further application in biological systems.

4. Conclusion

To the best of our knowledge, the highly biocompatible, polar P(HPMA) and the biodegradable P(LLA) structures have not been combined in block-like structures to date, which is most probably due to the entirely different mechanisms for the controlled polymerization of the respective monomers. In this work we have established a combination of these building blocks by ring opening of LLA and successive RAFT-polymerization of pentafluorophenyl methacrylate P(PFMA), resulting in reactive ester precursor block copolymers. The molecular weight (M_n) of the block copolymers could be controlled in the range of 7,600 g/mol to 34,300 g/mol, and well-defined (PDI = 1.30-1.45) reactive block copolymers were obtained. These materials represent a versatile platform for further functionalization via attachment of drugs, target moieties and labels due to the activated ester block of P(PFMA) by polymer modification reaction. The functionalization reactions were shown to proceed without any apparent degradation and side reactions to the basic polyester structure as evidenced by proton NMR with all modified polymers achieving the desired block ratios. This remarkable selectivity – cleavage of side chain ester bonds in one block and no degradation of main chain ester bonds in the other – confirms the high reactivity difference of the reactive ester and the poly(lactide) backbone. This principle is of general value and can be exploited for several other polyester block copolymers.

The synthetic pathway established here resulted in the formation of amphiphilic P(HPMA)-*block*-P(LLA) copolymers that represent an intriguing type of polymeric drug delivery vesicles. The aggregation behavior of a carefully purified block copolymer sample ($P(HPMA)_{77}$-*block*-$P(LLA)_{42}$) was studied by fluorescence correlation spectroscopy, demonstrating the formation of micellar structures with a hydrodynamic diameter of 17 nm at a concentration of 0.1 mg/mL. We have also

been able to confirm the expected non toxic behavior of this new type of block copolymers at concentrations up to 3 mg/mL for $P(HPMA)_{77}$-*block*-$P(LLA)_{42}$. Furthermore, by confocal fluorescence microscopy we have shown that the block copolymers are taken up by human cervix adenocarcinoma cells (HeLa). These findings demonstrated that the novel P(HPMA)-*block*-P(LLA) copolymers are a versatile platform for micellar drug-delivery applications, as long as the degree of polymerization of the P(HPMA) block is kept below the molecular weight threshold for elimination from the body by renal clearance. Further experiments regarding the detailed uptake mechanism as well as detailed intracellular distribution for the whole series of block copolymers are currently carried out in our laboratories. In addition we are studying the encapsulation properties as well as the *in vivo* fate of the micellar block copolymer particles.

5. Acknowledgment

The authors would like to thank Ms Romina Forst for assistance during the synthesis of conjugates and Prof. Helmut Ringsdorf for his helpful advice. We also gratefully acknowledge the Confocal Microscopy Service of the Centro de Investigación Príncipe Felipe (Valencia, Spain) for their skillful assistance. The authors also thank the graduate school of excellence MAINZ, COMATT, IMPRS, the Spanish Ministry Grant (CTQ2007-60601) and particularly the cluster of excellence SAMT of Rhineland-Palatina for support and funding.

6. References

[1] Ringsdorf, H. *J. Polym. Sci. Polym. Symp.* **1975**, *51*, 135-153.

[2] Ferrari, M. *Nat. Rev. Cancer* **2005**, *5*, 161-171.

[3] Duncan, R. *Nat. Rev. Cancer* **2006**, *6*, 688-701.

[4] a) Haag, R.; Kratz, F. *Angew. Chem. Int. Ed.* **2006**, *45*, 198-215; b) Liu, S.; Maheshwari, R.; Kiick, K. L. *Macromolecules* **2009**, *42*, 3-13.

[5] Duncan, R. *Pharm. Sci. Technol. Today* **1999**, *2*, 441-449.

[6] Duncan, R. *Nat. Rev. Drug Discovery* **2003**, *2*, 347-360.

[7] Duncan, R.; Coatsworth, J. K.; Burtles, S. *Hum. Exp. Toxicol.* **1998**, *17*, 93-104.

[8] Vasey, P.A,; Kaye, S. B.; Morrison, R.; Twelves, C.; Wilson, P.; Duncan, R.; Thomson, A. H.; Murray, L. S.; Hilditch, T. E.; Murray, T.; Burtles, S.; Fraier, D.; Frigerio, E.; Cassidy, J. and on behalf of the Cancer Research Campaign Phase I/II Committee. *Clin. Cancer Res.* **1999**, *5*, 83-94.

[9] Hopewell, J.W.; Duncan, R.; Wilding, D.; Chakrabarti, K. *Hum. Exp. Toxicol.* **2001**, *20*, 461-470.

[10] Matsumura, Y.; Maeda, H. *Cancer Res.* **1986**, *46*, 6387-92.

[11] Veronese, F. M.; Pasut, G. *DDT* **2005**, *10*, 1451-1458.

[12] Baka, S.; Clamp, A. P.; Jayson, G. C. *Expert Opin. Ther. Targets* **2006**, *10*, 867-876.

[13] Kaushik, V. V.; Moots, R. J. Expert *Opin. Biol. Ther.* **2005**, *5*, 601-606.

[14] Matsumura, Y.; Kataoka, K. *Cancer Sci.* **2009**, *100*, 572-579.

[15] Nishiyama, N.; Kataoka, K. Pharmacol. Ther. **2006**, 112, 630-648.

[16] E.V. Batrakova, A.V. Kabanov. *J. Control. Release* **2008**, *130*, 98–106.

[17] Kabanov, A. V.; Alakhov, V. *Crit. Rev. Ther. Drug. Carr. Syst.* **2002**, *19*, 1-72.

[18] Gauthier, M. A.; Gibson, M.I.; Klok, H.-A. *Angew. Chem. Int. Ed.* **2009**, *48*, 48–58.

[19] Theato, P. *J. Polym. Sci. Part A: Polym. Chem.* **2008**, *46*, 6677-6687.

[20] Binder, W.H.; Sachsenhofer, R. *Macromol. Rapid Commun.* **2008**, *29*, 952-981.

[21] Batz, H. G.; Franzmann, G.; Ringsdorf, H. *Angew. Chem. Int. Ed.* **1972**, *11*, 1103-1104.

[22] Matyjaszewski, K.; Gnanou, Y.; Leibler, L. Macromolecular Engineering Vol. 1. WILEY-VCH Verlag GmbH & Co, Weinheim, **2007**.

[23] Tsarevsky, N. V.; Matyjaszewski, K. *Chem. Rev.* **2007**, *107*, 2270-99.

[24] Moad, G.; Rizzardo, E. L.; Thang, S. H. *Polymer* **2008**, *49*, 1079-1131.

[25] Stenzel, M. *Chem. Commun.* **2008**, 3486-3503.

[26] Boyer, C.; Bulmus, V.; Davis, T. P.; Ladmiral, V.; Liu, J.; Perrier, S. *Chem. Rev.* **2009**, DOI: 10.1021/cr9001403.

[27] Hawker, C. J.; Bosman, A. W.; Harth, E. *Chem. Rev.* **2001**, *101*, 3661-3688.

[28] York, A. W.; Scales, C. W.; Huang, F.; McCormick, C. L. *Biomacromolecules* **2007**, *8*, 2337-2341

[29] Konak, C.; Matyjaszewski, K.; Kopeckova, P.; Kopecek, J. *Polymer* **2002**, *43*, 3735-3741.

[30] Barz, M.; Tarantola, M.; Fischer, K.; Schmidt, M.; Luxenhofer, R.; Janshoff, A.; Theato, P.; Zentel, R. *Biomacromolecules* **2008**, *9*, 3114-3118.

[31] Herth, M.; Barz, M.; Moderegger, D.; Allmeroth, M.; Jahn, M.; Thews, O.; Zentel, R.; Rösch, F. *Biomacromolecules* **2009**, *10*, 1697–1703.

[32] Gibson, M. I.; Fröhlich, E.; Klok, H.-A. *J. Polym. Sci. Part A: Polym. Chem.* **2009**, *47*, 4332–4345.

[33] Barz, M.; Luxenhofer, R.; Zentel, R.; Kabanov, A. V. *Biomaterials* **2009**, *30*, 5682-5690.

[34] Du, J.; Chen, Y. *Macromolecules* **2004,** *37,* 6322-6328.

[35] Mori, H.; Hirao, A.; Nakahama, S. *Macromolecules* **1994**, *27*, 35-39.

[36] Yamamoto, Y.; Nagasaki, Y.; Kato, Y.; Sugiyama, Y.; Kataoka, K. *J. Control. Release* **2001**, *77*, 27-38.

[37] Murphy, W. L.; Peters, M.C; , Kohn, D. H.; Mooney, D. J. *Biomaterials* **2000**, *21*, 2521-2527.

[38] Jain, R. A. *Biomaterials* **2000**, *21*, 2475-2490.

[39] Gupta, B.; Revagade, N.; Hilborn, J. *Prog.Polym. Sci.*, **2007,** *32*, 455-482.

[40] Hales, M.; Barner-Kowollik, C.; Davis, T. P.; Stenzel, M. H. *Langmuir* **2004**, *20*, 10809-10817.

[41] You, Y.; Hong, C.; Wang, W.; Lu, W.; Pan, C. *Macromolecules* **2004**, *37*, 9761-9767.

[42] Messman, J. M.; Scheuer, A. D.; Storey, R. F. *Polymer* **2005**, *46*, 3628–3638.

[43] Wolf, F. F.; Friedemann, N.; Frey, H. *Macromolecules* **2009**, *42*, 5622–5628.

[44] Chong, Y. K.; Moad, G.; Rizzardo, E.; Tang, S. H. *Macromolecules*, **1999**, *32*, 2071-2073.

[45] Eberhardt, M.; Mruk, R.; Zentel, R.; Theato, P. *Eur Polym J* **2005**, *41*, 1569–1575.

[46] Perrier, S.; Takolpuckdee, P.; Mars, C. A. *Macromolecules* **2005**, *38*, 2033–2036.

[47] Dve, A. P.; Pratt, R. C.; Lohmeijer, B. G. G.; Waymouth, R. M.; Hedrick, J. L. *J. Am. Chem. Soc.* **2005**, *127*, 13798–13799.

[48] Pratt, R. C.; Lohmeijer, B. G. G.; Long, D. A.; Lundberg, P. N. P.; Dove, A. P.; Li, H. B.; Wade, C. G.; Waymouth, R.; Hedrick, J. L. *Macromolecules* **2006**, *39*, 7863–7871.

[49] Eberhardt, M.; Theato, P. *Macromol. Rapid Commun.* **2005**, *26*, 1488-1493.

[50] Sahay, G.; Batrakova, E. V.; Kabanov. A. V. *Bioconjugate Chem* **2008**, *19*, 2023-2029.

[51] Rigler, R.; Elson, E. S. Fluorescence Correlation Spectroscopy. Springer-Verlag: New York, **2001**.

[52] Saeed, A. O.; Dey, S.; Howdle, S. M.; Thurecht, K. J.; Alexander, C. *J. Mater. Chem.* **2009**, *19*, 4529-4535.

2.7. Synthesis, Characterization and Evaluation of P(HPMA)-*block*-P(LLA) and P(HPMA)-*block*-P(DLLA) Copolymers: Influence of Lactide Tacticity on Micellization, Cellular Uptake Kinetics and Intracellular Localization in HeLa cells

Biomaterials 2009, submitted

Author: Matthias Barz[1], Fabiana Canal[2], Florian Wolf[1], Kaloian Koynov[3], Holger Frey[1], Maria J. Vicent[2] and Rudolf Zentel[1,*]

Address: [1] Institute of Organic Chemistry, Johannes Gutenberg-University Mainz, Duesbergweg 10-14, D-55099 Mainz, Germany

[2] Centro de Investigacion Principe Felipe, Avda Autopista el Saler 16/3, 46012 Valencia, Spain

[3] Max-Planck-Institute for Polymer Research, 55128 Mainz, Germany

Abstract

In this work we describe the synthesis, micellization and biological evaluation of fluorescently labeled poly(N-(2-hydroxypropyl)-methacrylamide)-*block*-poly(L-lactide) (PHPMA-*block*-PLLA) and poly(N-(2-hydroxypropyl)-methacrylamide)-*block*-poly(DL-lactide) block copolymers (PHPMA-*block*-PDLLA). We introduce block copolymers of comparable molecular weights and block length ratios, differing in the tacticity of the hydrophobic poly lactide block, which were prepared applying the activated ester approach. In this respect, pure P(HPMA)-block-P(Lactide) block copolymers and fluorescently labeled analogues were synthesized exhibiting molecular weights M_n around 20,000 g/mol with moderate polydispersities M_w/M_n of 1.4.

In addition, the aggregation behavior of this new type of partially degradable amphiphilic block copolymers was studied for the dye labeled systems in aqueous solution, employing fluorescence correlation spectroscopy (FCS). We observed differences in the hydrodynamic diameter of the labeled block copolymer P(HPMA)-*block*-P(Lactide) aggregates. We observed micellar structures with a hydrodynamic diameter of 17.0 nm for the (PHPMA-*block*-PLLA) block copolymer and 20.4 nm for (PHPMA-*block*-PDLLA) block copolymer (0.1 mg/mL in PBS buffer (pH 7.2)).

Furthermore, the block copolymer micelles have been applied to in vitro studies in HeLa (human cervix adenocarcinoma) cells. We observed for both systems a pronounced cellular uptake as well as non-toxic behavior up to a concentration of 3 mg/mL. Interestingly, we observed significant differences in the cellular uptake of the block copolymers. (PHPMA-*block*-PDLLA) block copolymers entered the cells more pronounced than PLLA based systems. The uptake process itself is energy depended indicating the expected endocytosis. Furthermore, we applied a lysosomal marker (Dextrane Texas Red) to investigate the intracellular localization. In the case of both block copolymers colocalization of marker and polymer was not observed during the experiments, which could be a first hint of an endosomal escape. Therefore, we expect this new type of HPMA/lactide based functional block copolymers to be a promising candidate for further *in vitro* and *in vivo* applications. Our findings underline that small changes of the polymer structure have a major influence on aggregation, cellur uptake and intracellular localization.

1. Introduction

In the last decades the main ideas of polymer-based therapeutics have moved from fundamental science into clinical practice. [1-5] Beside protein-, antibody-polymer and polymer-drug conjugates polymeric micelles and polymersomes have been evaluated as drug carrier systems leading to first clinical trails. [6] Especially block copolymer micelles with a hydrophilic, non-immunogenic and functional corona have attracted growing interest due to their enormous potential as long-circulating drug carrier systems. [7-14] The circulation time is greatly influenced by the hydrophilic corona, which can encapsulate a hydrophobic drug [15-18], oligonuclide [19-21] or peptide [22,23] to avoid adsorption and subsequent uptake by the reticuloendothelial system (RES) or enzymatic degradation. A long circulating time enables passive tumor targeting, which could be further improved by the incorporation of a targeting moiety on the outer sphere of the micelle.

In addition, a stimuli responsive or degradable hydrophobic block is desirable in combination within a functional amphiphilic block copolymer. This concept is particularly attractive, if eventual degradation of one part leads to well-known building blocks, like it would be the case for a combination of N-(2-hydroxypropyl)-methacrylamide P(HPMA) with the biodegradable poly(L-lactide) (PLLA). P(HPMA) is beside polyethylenglycol (PEG) the most carefully investigated polymeric systems for drug delivery. [24-26] Furthermore, it was the first polymer-drug conjugate entering clinical trails. [27-29] Furthermore, PLLA has proved its biocompatible as well as biodegradable character through the development of medical devices and controlled release formulations. Indeed, extensive investigations have been carried out to evaluate the potential of PEG-PLA block copolymers as a drug delivery vehicle in cancer therapy. [30-38] Additionally Y. Yamamoto et al. published a study in 2001 indicating that PEG-PDLLA micelles with an appropriate particle size and a narrow size distribution have great potential as a stealth and long-circulating carrier system with a minimal uptake into the liver and spleen. The stealth property could be improved by introducing a weak anionic charge on the micelle surface, achieving essentially negligible liver and spleen uptake. [39]

In this respect, we have recently published the synthesis of functional P(HPMA)-*block*-P(LLA) copolymers bearing acidic end groups by a combination of ring opening polymerization (ROP) and reversible addition fragmentation chain transfer (RAFT) polymerization. [40] In addition to its excellent biocompatiblitiy and degradability into naturally occurring metabolites, poly(lactide)s physical properties by adjusting the degree of crystallization via the chain tacticity. The latter is readily tunable via the lactides stereochemistry. [41] Crystallization of atactic Poly(D,L-lactide) prepared from a 1:1 mixture of D- and L- Lactide shows not tendency to crystallize, neither in bulk nor in a micellar core. Variations of the poly(lactide)s tacticity in the micellar core can been used to influence the kinetic stability and thus the release profile of the encapsulated therapeutic agent in drug

delivery applications. [42] The tacticity of the hydrophobic block may also influence the, cellular uptake and intracellular localization. We have recently reported the tremendous influence of polymer architecture on the super structure formation in solution as well as on kinetics of cellular uptake and intracellular fate of HPMA based copolymers. [43] These investigations of structure-property relationships are essential to understand polymer-cell interactions, which determine any therapeutic approach.

In this work we report the synthesis of either P(HPMA)-*block*-P(LLA) as well as P(HPMA)-*block*-P(DLLA) copolymers combining ROP, RAFT polymerization as well as the activated ester approach based on our recently published strategy. [40] The polymer end group of the poly(lactide) was functionalized with an chain transfer agent enabling the RAFT polymerization [44-47] of pentafluorophenyl methacrylate block onto the lactide chain. The activated ester offers the great advantage that the hydrophilic reactive block copolymer can be first precisely characterized in organic solvents and afterwards it can be easily transferred into a functional HPMA based amphiphilic block copolymer by postpolymerization modification. [48,49] Furthermore we carried out fluorescence correlation spectroscopy (FCS) [50,51] experiments to determine the hydrodynamic diameter (D_h) of P(HPMA)-*block*-P(LLA) as well as P(HPMA)-*block*-P(DLLA) copolymer aggregates in PBS buffer. In the FCS studies conditions comparable to the cell experiments were applied. We report on cell toxicity, kinetics of cellular uptake studied by fluorescence activated cell sorting (FACS) as well as the investigation of intracellular localization by confocal fluorescence microscopy of either PLLA and PDLA based micelles. In order to point out the intracellular position of both types of aggregates a lysosomal marker (Dextran Texas Red) was applied in confocal microscopy.

In summary, in the following article we investigate the influence of poly(lactide) tacticity on micellization and endocytosis of HPMA based block copolymers in a human cervix adenocarcinoma (HeLa) cell line.

2. Materials and Methods

2.1 Materials

All chemicals were reagent grade, obtained from Aldrich and used without further purification, unless indicated otherwise. All solvents were of analytical grade. Pentafluorophenol was obtained from Fluorochem (Great Britain, UK) and distilled prior to use. Dioxane, dimethylsulfoxide (DMSO) and dichloromethane were dried and freshly destilled. 2,2'-Azobis(isobutyronitrile) (AIBN) was

recrystallized from diethyl ether and stored at -7°C. DBU (1,8-Diazabicyclo[5.4.0]undec-7-ene) (99%) was purchased from Acros and distilled from calcium hydride. Deuterated chloroform-d_1 was purchased from Deutero GmbH, dried and stored over molecular sieves. L-lactide was purchased from Purac/Gorinchem (Netherlands), recrystallized three times from dry toluene and stored under vacuum prior to use. Dialysis of block copolymers was performed with Cellu SepH1® membranes (Membrane Filtration Products, Inc.) with a molecular weight cutoff of 1000 g/mol and Spectra/Por® membranes (Roth) with a molecular weight cutoff of 3,500 g/mol.

2.2 Characterization

^{1}H-, ^{13}C- and ^{19}F-NMR spectra were obtained at 300 or 400 MHz using a FT-spectrometer from Bruker and analyzed using the ACDLabs 6.0 software. The polymers were dried at 40 °C over night under vacuum and afterwards characterized by gel permeation chromatography (SEC).

For SEC measurements in DMF (containing 1 g/L of lithium bromide as an additive) at 30°C, an Agilent 1100 series system was used as an integrated instrument including three HEMA-based-columns ($10^5/10^3/10^2$ Å porosity) from MZ-Analysentechnik GmbH, a UV (275 nm) and a RI detector. Calibration was achieved with poly(styrene) standards provided by Polymer Standards Service (PSS). Size-exclusion chromatography with THF as an eluent was performed at 25°C and at a flow rate of 1 mL min^{-1} with an instrument consisting of a Waters 717 plus autosampler, a TSP Spectra Series P 100 pump, and a set of three PSS-SDV 5-l columns with porosities of 100, 1000, and 10,000 Å, respectively.

2.3 Synthesis of 4-Cyano-4-((thiobenzoyl)sulfanyl)pentanoic Acid

The 4-cyano-4-((thiobenzoyl) sulfanyl)pentanoic acid was used as the chain transfer agent (CTA) and synthesized according to literature in a 3-step reaction. [52]

2.4 Synthesis of Pentafluorophenyl Methacrylate (PFMA)

PFMA was prepared according to the literature. [53]

2.5 Poly(L-lactide) Synthesis

Neopentyl alcohol and lactide were charged into a Schlenk-tube at predetermined molar ratio. The tube was sealed with a rubber septum and repeatedly flashed with argon after evacuation. Freshly distilled dichloromethane (4 mL/g dilactide) was added via a syringe. Polymerization was initiated by injecting a 10% solution of DBU in dry dichloromethane corresponding to 1% of the total amount of monomer after 2 minutes. The polymerization was quenched after 15 minutes by injecting a 10% dichloromethane solution of benzoic acid, corresponding to a twofold excess of the catalyst. An aliquot of the sample was harvested for conversion analysis prior to the precipitation in excess methanol. The polymer was collected by centrifugation or filtration and taken up in CH_2Cl_2 for a

second precipitation in diethyl ether. ^{1}H-NMR ($CDCl_3$, 400MHz): δ [ppm]: 0.92 (s, C(CH_3)$_3$; 1.57 (d, ^{3}J =7.0 Hz CHCH_3, poly(lactide) chain); 3.78-3.89 (m, -OCH_2C(CH_3)$_3$); 4.34 (q, ^{3}J =7.0 Hz HOCH(CH_3)); 5,15 (q, ^{3}J =7.0 Hz CH(CH_3), poly(lactide) chain).

^{1}H-NMR (DMSO-d_6, 400MHz): δ [ppm]: 0.89 (s, C(CH_3)$_3$; 1.27 (d, ^{3}J =7.0 Hz HOCH(CH_3)1.47 (d, ^{3}J =7.0 Hz CHCH_3, poly(lactide) chain); 3.76-3.86 (m, -OCH_2C(CH_3)$_3$); 4.20 (m HOCH(CH_3)); 5,20 (q, ^{3}J =7.0 Hz CH(CH_3), poly(lactide) chain).

2.6 Poly(D,L-lactide) Synthesis

The synthesis was carried out as described above (2.5). Due to the amorphous character of poly(D,L-Lactide) the sample was precipitated repeatedly (3x) in cold (-25°C) diethylether after quenching with an equimolar amount of benzoic acid. ^{1}H-NMR ($CDCl_3$, 400MHz) δ(/ppm): 0.92 (s, C(CH_3)$_3$; 1.50-1.60 (m, CHCH_3, poly(lactide) chain); 3.78-3.89 (m, -OCH_2C(CH_3)$_3$); 4.34 (q, ^{3}J =7.0 Hz HOCH(CH_3)); 5.11-5.21 (m CH(CH_3), poly(lactide) chain).

2.7 End group modification of PLLA and PDLLA to ω-CTA macroinitiator for RAFT polymerization

1.0 g 4-Cyano-4-((thiobenzoyl) sulfanyl)pentanoic acid was dissolved under nitrogen in 100mL CH_2Cl_2. The solution was cooled in an ice bath and 0.5 g of dicyclohexylcarbodiimide (DCC) were added. After 10 minutes a solution of 0,02 g 4-(dimethylamino)-pyridin (DMAP) in 5 mL CH_2Cl_2 was slowly added. 3.3 g of the poly(lactide) in 20 mL CH_2Cl_2 were added to the activated acid. The reaction was allowed to proceed over night. Finally the solution was concentrated and the functionalized polymer was precipitated twice in cold methanol, once in diethyl ether, dried in high vacuum and a reddish powder was obtained. Yield (PLLA-CTA: 3.06 g, 91%, 69 % functionalization (NMR), Yield (PLLA-CTA: 2.7 g, 82%, 75 % functionalization (NMR).

^{1}H NMR (PLLA-CTA) (300 MHz, CDCl-d_1): δ [ppm] 0.92 (s, C(CH_3)$_3$; 1.57 (d, ^{3}J =7.0 Hz CHCH_3, PLLA chain); 1.92 (s, CR_2CH_3, CTA); 2.50 2.75 (m, -CH_2CH_2, CTA); 3.78-3.89 (m, -OCH_2C(CH_3)$_3$); 4.34 (q, ^{3}J =7.0 Hz HOCH(CH_3)); 5,15 (q, ^{3}J =7.0 Hz CH(CH_3), poly(lactide) chain); 7.38 (t, J =1.0 Hz CH=CH, CTA); 7.56 (t, J =1.0 Hz CH=CH, CTA); 7.89 (d, J =1.0 Hz CH=CH, CTA).

^{1}H NMR (PDLLA-CTA) (300 MHz, CDCl-d_1): δ [ppm] 0.92 (s, C(CH_3)$_3$; 1.50-1.60 (m, CHCH_3, poly(lactide) chain); 1.92 (s, CR_2CH_3, CTA); 2.50 2.75 (m, -CH_2CH_2, CTA); 3.78-3.89 (m, -OCH_2C(CH_3)$_3$); 4.34 (q, ^{3}J =7.0 Hz HOCH(CH_3)); 5.11-5.21 (m CH(CH_3), poly(lactide) chain); 7.38 (t, J =1.0 Hz CH=CH, CTA); 7.56 (t, J =1.0 Hz CH=CH, CTA); 7.89 (d, J =1.0 Hz CH=CH, CTA).

2.8 Synthesis of P(PFMA)-*block*-P(LLA)

RAFT polymerization of PFMA using the poly(L-lactide) macroinitiator was performed in a Schlenk tube according to our recently published method [40]. The reaction vessel was loaded with 3.5 mg 2,2'-azobis(isobutyronitrile (AIBN) (0.02 mmol), 0.2 g poly(D-lactide) macroinitiator and 1.58 g of PFMA (12 mmol) (example for P2R) in 5 mL of dioxane. Following three freeze–vacuum–thaw cycles, the tube was immersed in an oil bath at 80 °C for 12 h. Subsequently, the block copolymer was once precipitated in ethanol and twice in hexane, isolated by centrifugation and dried at 30 °C under high vacuum for 12 hours. The block copolymer was obtained as a slightly red powder. Yield: (59 %).

^{1}H-NMR ($CDCl3$-d_1, 400MHz): δ [ppm]: 0.92 (s, C(CH_3)$_3$; 1.42 (s, CRCH_3, poly(PFMA) chain); 1.57 (d, ^{3}J =7.0 Hz CHCH_3, poly(lactide) chain); 2.07 (s, -CH_2- poly(PFMA) chain) 3.78-3.89 (m, -OCH_2C(CH_3)$_3$); 4.34 (q, ^{3}J =7.0 Hz HOCH(CH_3)); 5,15 (q, ^{3}J =7.0 Hz CH(CH_3), poly(lactide) chain). ^{19}F NMR ($CDCl_3$): δ [ppm] -165.1 (br), -159.8 (br), -154.4 (br), -153.1 (br).

2.9 Synthesis of P(PFMA)-*block*-P(DLLA)

RAFT polymerization of PFMA using the poly(DL-lactide) macroinitiator was performed in a Schlenk tube according to our recently published method [40]. The reaction vessel was loaded with 3.5 mg 2,2'-azobis(isobutyronitrile (AIBN) (0.02 mmol), 0.2 g poly(D-lactide) macroinitiator and 1.58 g of PFMA (12 mmol) (example for P2R) in 5 mL of dioxane. Following three freeze–vacuum–thaw cycles, the tube was immersed in an oil bath at 80 °C for 12 h. Subsequently, the block copolymer was once precipitated in ethanol and twice in hexane, isolated by centrifugation and dried at 30 °C under high vacuum for 12 hours. The block copolymer was obtained as a slightly red powder. Yield: (51 %).

^{1}H-NMR ($CDCl_3$, 400MHz): 0.92 (s, C(CH_3)$_3$; 1.42 (s, CRCH_3, poly(PFMA) chain); 1.50-1.60 (m, CHCH_3, poly(lactide) chain); 2.07 (s, -CH_2- poly(PFMA) chain) 3.78-3.89 (m, -OCH_2C(CH_3)$_3$); 4.34 (q, ^{3}J =7.0 Hz HOCH(CH_3)); . ^{19}F NMR ($CDCl_3$): δ [ppm] -165.1 (br), -159.8 (br), -154.4 (br), -153.1 (br).

2.10 Removal of the dithioester end group

The dithiobenzoate end group was removed according to the procedure reported by Perrier et al.. [54] Typically 200 mg of polymer, (M_n = 23.000 g/mol), and 80 mg of 4,4'-azobis(4-cyanovaleric acid) (~30 times excess in relation to the polymer end group) were dissolved in 3 mL of anhydrous dioxane. The solution was heated to 80 °C for 3 h. Finally the copolymer was precipitated 3 times in 100 mL of diethyl ether and collected by centrifugation. In the case of the block copolymer, the crude product was first precipitated in ethanol twice and than once in diethyl ether. The copolymer was dried in vacuo for a period of 24 h and a colorless product was obtained (yield: 90 %). The absence of the

dithiobenzoate end group was confirmed by UV-Vis spectroscopy with the absence of the peak at a wavelength of 302 nm.

2.11 Synthesis of P(HPMA)-*block*-P(LLA) block copolymers

In a typical reaction 100 mg of P(HPMA)-*block*-P(LLA) without ditihioester end group was dissolved in 2 mL abs. dioxane and 0.5 mL dried DMSO. A colorless solution was obtained. Subsequently 20 mg of triethylamine (TEA) and 15 mg of hydroxypropylamine were added. The mixture was kept at 30 °C for 24 h and finally additional 15 mg of hydroxypropylamine and 20 mg triethylamine were added. The reaction was allowed to proceed under the above-mentioned conditions for 4 h. The solution was concentrated in vacuum, precipitated twice in diethyl ether, mixed with water and dialyzed against water using Spectra/Por® membranes with a molecular weight cutoff of 3,500 g/mol. In a last purification step a preparative SEC (Sephadex G-25) was used to purify the final product. The solution of the product was lyophilized, yielding 35 mg of a colorless polymer. ^{1}H NMR (DMSO-d_6): δ [ppm] 0.92 (s, C(CH_3)$_3$; 0.7-1.42 (CR$_3$CH_3, C*H3*CHOH poly(HPMA) chain); 1.57 (d, ^3J =7.0 Hz CHCH_3, poly(lactide) chain); 1.2-2.1 (s, -CH$_2$- poly(HPMA) chain); 2.6-3.2(C*H*OH, poly(HPMA) chain); 3.72 (CH_2NH, poly(HPMA) chain); 5.15 (q, ^3J =7.0 Hz C*H*(CH$_3$), poly(lactide) chain).

2.12 Synthesis of P(HPMA)-*block*-P(DLLA) block copolymers

In a typical reaction 100 mg of **P(HPMA)-*block*-P(DLLA)** without ditihioester end group was dissolved in 2 mL abs. dioxane and 0.5 mL dried DMSO. A colorless solution was obtained. Subsequently 20 mg of triethylamine (TEA) and 15 mg of hydroxypropylamine were added. The mixture was kept at 30 °C for 24 h and finally additional 15 mg of hydroxypropylamine and 20 mg triethylamine were added. The reaction was allowed to proceed under the above-mentioned conditions for 4 h. The solution was concentrated in vacuum, precipitated twice in diethyl ether, mixed with water and dialyzed against water using Spectra/Por® membranes with a molecular weight cutoff of 3,500 g/mol. In a last purification step a preparative SEC (Sephadex G-25) was used to purify the final product. The solution of the product was lyophilized, yielding 33 mg of a colorless polymer. ^{1}H NMR (DMSO-d_6): δ [ppm] 0.92 (s, C(CH_3)$_3$; 0.7-1.42 (CR$_3$CH_3, CH_3CHOH poly(HPMA) chain); 1.50-1.60 (m, CHCH_3, poly(lactide) chain)); 1.2-2.1 (s, -CH$_2$- poly(HPMA) chain); 2.6-3.2(C*H*OH, poly(HPMA) chain); 3.72 (CH_2NH, poly(HPMA) chain); 5.11-5.21 (m C*H*(CH$_3$), poly(lactide) chain).

2.13 Synthesis of dye labeled P(HPMA)-*block*-P(LLA) block copolymers

The polymer modification reaction was carried out under the same conditions as mentioned above, but a small fraction of Oregon Green 488 cadaverin dye was used in addition (cf. Table 2). In a typical reaction 150 mg of P(PFMA)-block-P(LLA) (Mn = 25,000 g/mol) without ditihioester end group were dissolved in 2 mL abs. dioxane and 0.5 mL dried DMSO. A colorless solution was obtained. In a typical reaction 2.5 mg Oregon Green 488 cadaverin and 20 mg triethylamine were added and the

reaction was allowed to proceed at 30 °C for 4 h. In the next step 40 mg of TEA and 25 mg of hydroxypropylamine were added. The mixture was kept at 30 °C for 24 h, and finally additional 25 mg of hydroxypropylamine and 30 mg TEA were added. The reaction was allowed to proceed for another 4 h. The solution was concentrated in vacuum, precipitated twice in diethyl ether, carefully mixed with water and dialyzed against water using Spectra/Por® membranes with a molecular weight cutoff of 3,500 g/mol.

In a last purification step a preparative SEC (HiTrap™ Desalting Column, Sephadex G-25 superfine) was used to purify the final product. The solution of the purified product was lyophilized, yielding a yellowish polymer. Yield: 35 mg. ^{1}H NMR (DMSO-*d*6): δ [ppm] 0.92 (s, C(C*H*$_3$)$_3$; 0.7-1.42 (CR$_3$C*H*$_3$, C*H3*CHOH poly(HPMA) chain); 1.57 (d, ^3J =7.0 Hz CHC*H*$_3$, PLLA chain); 1.2-2.1 (s, -CH$_2$- poly(HPMA) chain); 2.6-3.2(C*H*OH, poly(HPMA) chain); 3.72 (C*H*$_2$NH, poly(HPMA) chain); 5.15 (q, ^3J =7.0 Hz C*H*(CH$_3$), poly(lactide) chain).

2.14 Synthesis of dye labeled P(HPMA)-*block*-P(DLLA) block copolymers

The polymer modification reaction was carried out under the same conditions as mentioned above, but a small fraction of Oregon Green 488 cadaverin dye was used in addition (cf. Table 2). In a typical reaction 150 mg of P(PFMA)-block-P(DLLA) (Mn = 25,000 g/mol) without ditihioester end group were dissolved in 2 mL abs. dioxane and 0.5 mL dried DMSO. A colorless solution was obtained. In a typical reaction 2.5 mg Oregon Green 488 cadaverin and 20 mg triethylamine were added and the reaction was allowed to proceed at 30 °C for 4 h. In the next step 40 mg of TEA and 25 mg of hydroxypropylamine were added. The mixture was kept at 30 °C for 24 h, and finally additional 25 mg of hydroxypropylamine and 30 mg TEA were added. The reaction was allowed to proceed for another 4 h. The solution was concentrated in vacuum, precipitated twice in diethyl ether, carefully mixed with water and dialyzed against water using Spectra/Por® membranes with a molecular weight cutoff of 3,500 g/mol.

In a last purification step a preparative SEC (HiTrap™ Desalting Column, Sephadex G-25 superfine) was used to purify the final product. The solution of the purified product was lyophilized, yielding a yellowish polymer. Yield: 32 mg. ^{1}H NMR (DMSO-*d*6): δ [ppm] 0.92 (s, C(C*H*$_3$)$_3$; 0.7-1.42 (CR$_3$C*H*$_3$, C*H3*CHOH poly(HPMA) chain); 1.50-1.60 (m, CHC*H*$_3$, poly(lactide) chain); 1.2-2.1 (s, -CH$_2$- poly(HPMA) chain); 2.6-3.2(C*H*OH, poly(HPMA) chain); 3.72 (C*H*$_2$NH, poly(HPMA) chain);5.11-5.21 (m C*H*(CH$_3$), poly(lactide) chain).

2.15 Characterization of block copolymers by fluorescence correlation spectroscopy (FCS)

Fluorescence correlation spectroscopy experiments were performed using a commercial FCS setup (Zeiss, Germany) consisting of the module ConfoCor 2 and an inverted microscope model Axiovert 200 with a Zeiss C-Apochromat 40 ×/1.2 W water immersion objective. The fluorophores were

excited by an Argon laser (λ = 488 nm) and the emission was collected after filtering with a LP505 long pass filter. For detection, an avalanche photodiode that enables single-photon counting was used. Eight-well, polystyrene-chambered cover glass (Lab-Tek, Nalge Nunc International) was used as sample cell. The dye-labeled P(HPMA)-*block*-P(LLA) and P(HPMA)-*block*-P(DLLA) block copolymers were dissolved in DMSO (c = 20 mg/mL) and PBS buffer (pH = 7.2) was slowly added to obtain a final concentration of 0.1 mg/mL. The solution was kept at room temperature over 24 h prior to the measurements. For each solution, 10 measurements with a total duration of 5 min were performed. The time-dependent fluctuations of the fluorescence intensity *dI(t)* were recorded and analyzed by an autocorrelation function $G(t)=1+< dI(t') dI(t'+t)>/<I(t')>^2$. As has been shown theoretically for an ensemble of *m* different types of freely diffusing fluorescence species, $G(t)$ has the following analytical form [50]:

$$G(t) = 1 + \left[1 + \frac{f_T}{1 - f_T} e^{-t/\tau_T}\right] \frac{1}{N} \sum_{i=1}^{m} \frac{f_i}{\left[1 + \frac{t}{\tau_{Di}}\right] \sqrt{1 + \frac{t}{S^2 \tau_{Di}}}} \qquad (1)$$

Here, N is the average number of diffusing fluorescence species in the observation volume, f_T and t_T are the fraction and the decay time of the triplet state, t_{Di} is the diffusion time of the *i-th* species, f_i is the fraction of component *i*, and S is the so-called structure parameter, $S = z_0/r_0$, where z_0 and r_0 represent the axial and radial dimensions of the confocal volume, respectively. Furthermore the diffusion time, t_{Di}, is related to the respective diffusion coefficient, D_i, through [50] $D_i = r_0^2/4\ t_{Di.}$ The experimentally obtained *G(t)* can be fitted with eq. 1, yielding the corresponding diffusion times and subsequently the diffusion coefficients of the fluorescent species. Finally, the hydrodynamic radii R_h can be calculated (assuming spherical particles) using the Stokes-Einstein relation: $R_h = k_B T/6\pi\eta D$, where k_B is the Boltzmann constant, T is the temperature, and η is the viscosity of the solution. As the value of r_0 depends strongly on the specific characteristics of the optical setup a calibration was done using a reference standard with known diffusion coefficient, i.e., Rhodamine 6G.

2.16 Cell cultures

HeLa (human cervix adenocarcinoma cells) were grown in DMEM medium supplemented with 10% v/v of heat-inactivated fetal bovine serum (FBS). Cells were maintained at 37°C in an atmosphere of 5% carbon dioxide and 95% air and underwent passage twice weekly.

2.17 Cells viability assay

The cytotoxicity of the conjugates synthesized was evaluated using the MTT (3-(4,5-dimethyltiazol-2-yl)-2,5-diphenyl-tetrazolium bromide) cell viability assay (72 h incubation) with HeLa cells. Cells were seeded into sterile 96-well microtitre plates (seeding density 2.2×10^4 cell/mL). Cells were allowed to settle for 24 h before the unlabeled polymers **P1** and **P2** (0.2 μm filter-sterilized) was

added. A series of stock solutions of conjugates dissolved in DMSO, with different concentrations ranging from 1 mg/mL to 300 mg/mL, were prepared and the cells were treated with 1 µL of each stock solution, in such a manner that the final polymer concentrations range from 0,01 mg/mL to 3 mg/mL with a final DMSO concentration of 1% (v/v). As control, cells were treated with the same percentage of DMSO, in absence of polymers to evaluate solvent toxicity. 100% cell viability was assigned to control cells with 1% DMSO. After 68 h incubation, MTT (20 µL of a 5 mg/mL solution in PBS) was added to each well, and the cells were incubated for further 4 h. After removal of the medium, the precipitated formazan crystals were dissolved in optical grade DMSO (100 µL), and the plates were read spectrophotometrically at 570 nm after 30 min using a Victor^2 Wallac plate reader.

2.18 Cellular uptake by fluorescent activated cell sorting (FACS)

Cells were seeded at a density of 2x10^5 cells/mL in a sterile 6-well plate. After 48 h incubation, cells were treated with 10 µL of OG-labeled polymers **P1*** and **P2*** solution in PBS with 10% v/v of DMSO. In the time-dependent experiment the final polymer concentration was 0.1 mg/mL, while in the concentration-dependent experiments the polymer concentration range from 1,E-06 to 1 mg/mL.

The experiments were carried out by triplicate, some wells were untreated and used as control. In the time-dependent experiments, cells were incubated for times of 0, 5, 30 min, 1, 2 and 5 h at 37°C, afterwards the plates were put in ice, the medium was removed and cells were washed trice with 1 mL of cold PBS and scraped. Cell associated fluorescence was then analyzed using a Cytomics FC 500 (Beckman Coulter Inc.) equipped with an argon laser (405 nm) and an emission filter for 455 nm. Data collection involved 15000 counts per sample and was analyzed with Beckman Coulter CXP software. The experiments were carried out also at 4°C, placing the plates at 4°C 30 min before the experiment started and then following the same procedure described above.

The concentration-dependent experiments were carried out incubating the cells for 1 h at 37°C with different polymer concentrations and then following the same procedure above reported.

2.19 Live cell confocal fluorescence microscopy

Cells were seeded on a glass placed into 10 cm^2 Petri plates at density of 2x10^5 cell/mL. After 24 h of incubation the cells were treated with 10 µL of Oregon Green-labeled polymers **P1*** and **P2*** solution. The final polymer concentration was 0.1 mg/mL. Pulse and chase experiments were performed: after 5, 15 min, 1, 2 or 5 h of incubation at 37°C, the medium was removed and replaced with fresh one and cells were incubated at 37°C for further 5 or 30 min, 1, 2 or 5 h. Then cells were washed trice with PBS supplemented with 10% (v/v) of fetal bovine serum (3 mL) and the glass was removed and set on the microscope. Images were captured with a confocal Leica microscope equipped with a l-blue 63 oil immersion objective and handled with a TCS SP2 system, equipped with an acoustic optical beam splitter (AOBS). Excitation was done with an argon laser (458, 476, 488, 496 and 514 nm) and blue

diode (405 nm). Images were captured at an 8-bit gray scale and processed with LCS software Version 2.5.1347 (Leica, Germany) containing multicolor, macro and 3D components.

3. Results and Discussion

3.1 Synthesis of P(HPMA)-*block*-P(LLA) and P(HPMA)-*block*-P(DLLA) copolymers

In order to investigate the influence of poly(lactide) stereochemistry on the aggregation in solution as well as on biological properties we have synthesized P(HPMA)-*block*-P(LLA) (see scheme 1) and P(HPMA)-*block*-P(DLLA) (see scheme 2) copolymers and their fluorescently labeled analogous in different molecular weights.

Scheme 1. Synthesis P(HPMA)-*block*-P(LLA) copolymers

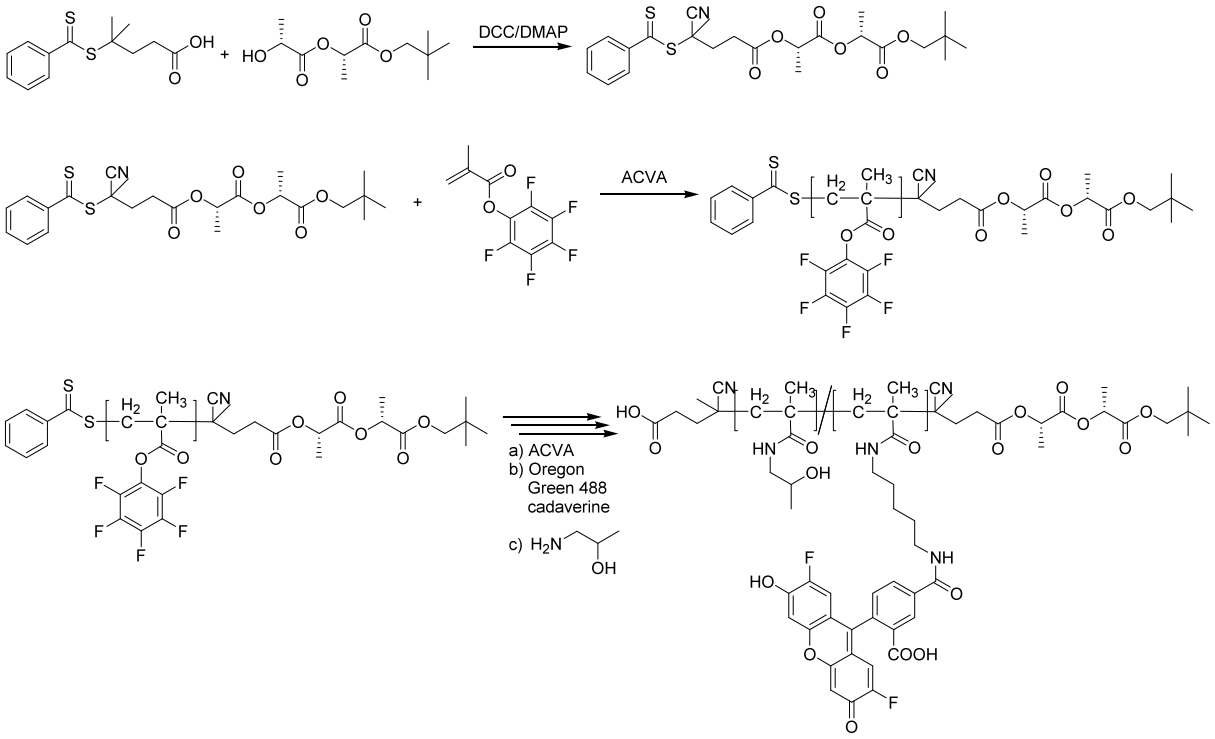

The synthesis in 4 steps is shown in detail in both schemes. It is based on our recently published method. [40]

Scheme 2. Synthesis P(HPMA)-*block*-P(LLA) copolymers

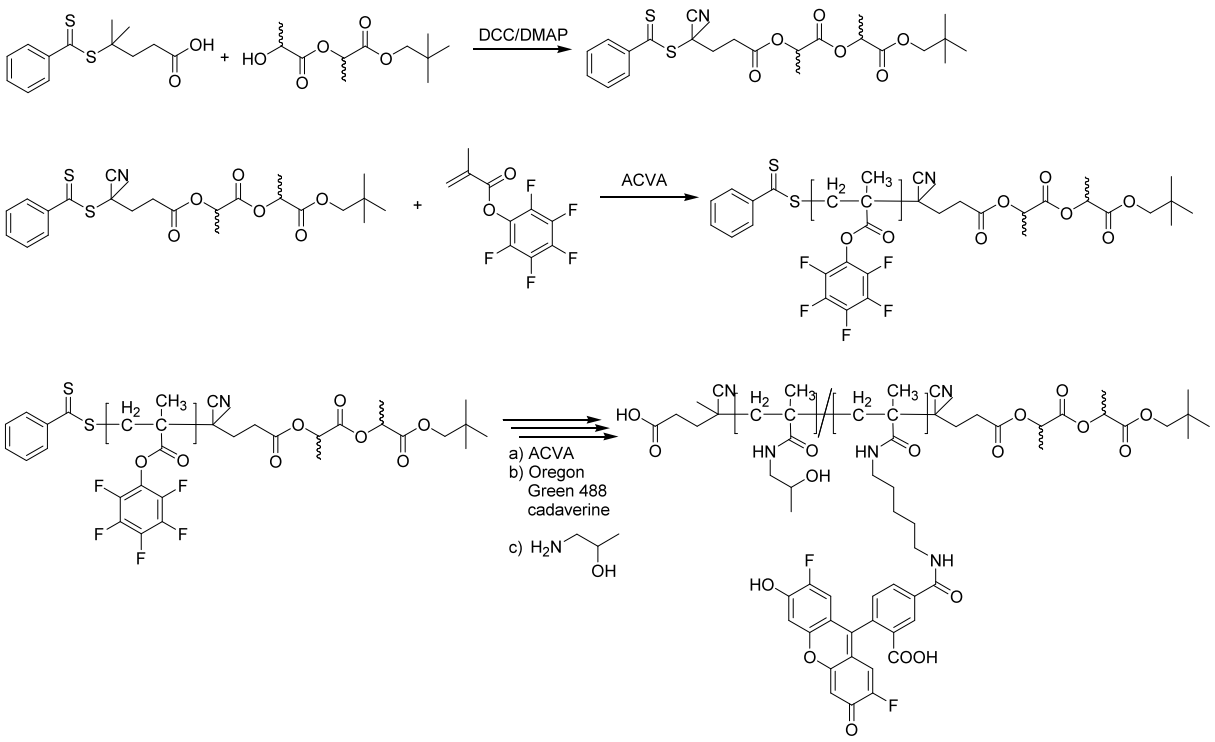

In a first step the PLLA and PDLLA homopolymers were synthesized by controlled ring opening polymerization (ROP) with the organo-base 1,8-diazabicyclo[5.4.0]undec-7-ene (DBU), which is well-known to be a highly efficient transesterification catalyst introduced by Hedrick and coworkers. [55,56]

Well defined polymers (M_N 3000g/mol: PDI: 1.07-1.08) were obtained for stereoregular PLLA as well as atactic PDLLA which exhibit a free ω-hydroxyl end group wich was used for further functionalization with a chain transfer agent (CTA) –in our case 4-cyano-4-((thiobenzoyl) sulfanyl)pentanoic acid under Steglich conditions.. A total end group functionalization of 69 % for PLLA and 75 % of PDLLA was achieved. The degree of functionalization in both cases is more then acceptable for an end group functionalization of polymers. And it has to be kept in mind that during the synthetic process and the related purification steps, remaining unfunctionalized polylactide was removed.

In the next step the derived macro initiator was used to perform the RAFT polymerization of pentafluorophenyl methacrylate yielding P(PFMA)-*block*-P(LLA) **P1R** as well as P(PFMA)-*block*-P(DLLA) **P2R** copolymers. In figure 1 the SEC elugrams of both lactide precursors as well of both reactive block copolymers clearly indicate the chain extension during the RAFT polymerization process. The small shoulder of remaining polylactide is in good accordance with the degree of functionalization. However, the contamination with homopolymer can be easily removed during the work-up of the subsequent reaction steps.

The RAFT polymerization using the poly(lactide) macroinitiators was performed under the same conditions reported in literature. [57-59] Thus, we were able to synthesize reactive P(PFMA)-*block*-P(LLA) **P1R** as well as P(PFMA)-*block*-P(DLLA) **P2R** copolymers of the same molecular weight and block length ratio (see table 1) of around 25 kDa.

Table 1. Characteristics of reactive ester P(PFMA)-*block*-P(LLA) block copolymer precursors **P1R**, **P2R**

Polymers	$M_{n,P(LLA)\ block}$	$M_{n,P(LLA)\ block}$	$PDI_{P(LLA)\ block}$	M_n	M_w	PDI
	kg/mol	kg/mol	kg/mol	kg/mol	kg/mol	kg/mol
P1R	3.0	3.2	1.08	22.8	31.9	1.4
P2R	3.3	3.5	1.07	23.7	30.8	1.3

The HPMA block is kept under the in literature reported renal clearance level reported by Seymour et al. [60] The polymers showed moderate polydispersity of around 1.4 conforming well-defined block copolymers. No influence of the tacticity of the poly(lactide)on the RAFT polymerization could be detected.

The end group remaining from the RAFT polymerization was in both cases removed by the method of Perrier et al.. An excess of 4,4'-azobis(4-cyanovaleric acid) was used to produce a hydrophilic end group. Full conversion could be nicely monitored by the disappearance of the dithiobenzyl ester absorption in the UV spectra.

In the final step the reactive block copolymers were transferred into HMPA based block copolymers. In addition fluorescently labeled polymers we prepared from the same reactive precursor systems. The HPMA based block copolymers have been derived by aminolysis of the activated esters among the

polymer backbone. The same conditions previously reported by our group have been applied during the synthesis [40]. In the same step an amino functionalized fluorescence label (Oregon Green 488 cadaverine) can be easily attached to the polymer. The aminolysis of the activated reactive ester was monitored by ^{19}F-NMR until full conversion was observed. The final polymers first precipitated from diethyl ether (1x) and EtOH (2x). Afterwards, dialysis against water and preparative SEC (Sephadex G-25) were applied to remove all side products of the postpolymerization modification. After the last step the aqueous polymer solution was lyophilized yielding the final block copolymer. A pure product is mandatory for both fluorescence correlation spectroscopy as well as for further biological evaluations. In this respect, yields of approx. 60 % after purification for the both polymers are more than acceptable. The block copolymers prepared are listed in Table 2 with the respective characterization data. The P(HPMA) block copolymers showed narrow polydispersity in the range of 1.3 to 1.45 ensuring well-defined block copolymers.

Table 2. Characteristics of poly(HPMA)-*block*-poly(PLLA) **P1** and poly(HPMA)-*block*-poly(PDLLA) **P2** copolymers and fluorescently labeled derivatives (**P1*** and **P2***)

Polymers	Average block ratio (HPMA/lactide)	Dye content in the hydrophilic block % (Oregon Green 488)	M_n kg/mol	M_w kg/mol	PDI
P1	78/42	-	14.2	20.5	1.4
P2	80/46	-	14.8	19.3	1.3
P1*	77/42	1.3	14.9	22.1	1.4
P2*	79/46	1.3	15.3	20.0	1.3

In addition, for both polymeric systems a degradation of the polylactide was avoided during the aminolysis, which is confirmed by the ratio of the signal intensity of the methine proton in PLLA at 5.1 ppm to the intensity of the tertiary proton of the HPMA units at 3.7 ppm. According to the determined molecular weights this ratio has to be 0.54 for P2, and a ratio of 0.53 was observed by ^{1}H-NMR. In the case of the PDLLA block copolymer a ratio of 0.48 was detected by ^{1}H-NMR, which is in good accordance to the ratio 0.52 calculated from the SEC data. The slight differences between calculated and experimentally derived values are in the range of measuring accuracy. The final P(HPMA)-*block*-P(LLA) **P1,P1*** and P(HPMA)-*block*-P(LLA) **P2, P2*** are characterized in table 2.

In the next step the new type of degradable block copolymers were applied to FCS measurements and cellular biology in order to study the influence of stereochemistry of the hydrophobic lactide block on aggregation as well as on cellular uptake and intracellular localization.

For a possible application for drug or protein delivery structure property relationships are mandatory to tune the block copolymer properties.

3.2. Micellization of P(HPMA)-*block*-P(LLA) and P(HPMA)-*block*-P(DLLA) Copolymers monitored by Flourescence Correlation Spectroscopy (FCS)

With a view towards an application as drug carrier or molecular imaging agent, a detailed study of the aggregates formed by the amphiphilic block copolymer structures in isotonic solutions is an important issue. Due to the amphiphilic character of the block copolymers, the formation of various aggregates in aqueous solution is expected (e.g., micelles, compound micelles or polymersomes). Especially for biomedical studies regarding cellular uptake and intracellular distribution, the aggregation behavior is highly important. Sahay et al. recently reported that the uptake route of Pluronic P85 switches from caveolae mediated endocytosis to uptake through clathrin coated pits, when the concentration of the copolymer is increased from below to above the critical micelle concentration (CMC). [61] In addition, we could nicely demonstrate that the cellular uptake as well as the intracellular localization is strongly influenced by the polymer architecture. [40]

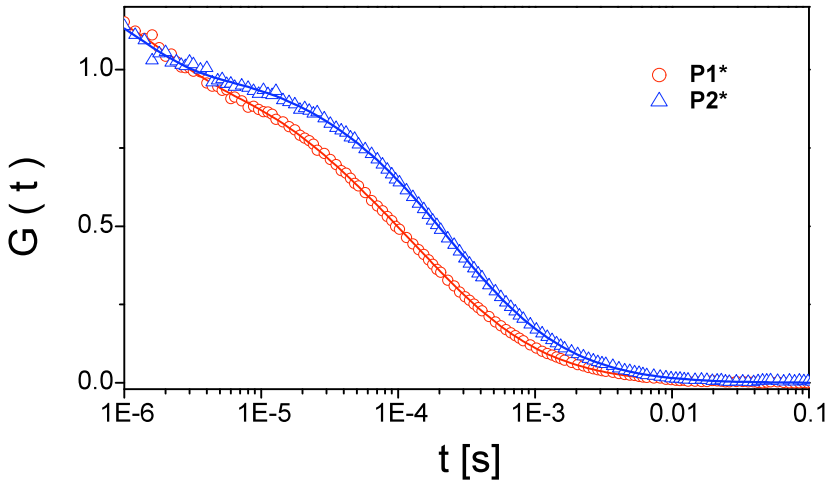

Figure 2. Normalized autocorrelation curves determined by fluorescence correlation spectroscopy for P(HPMA)-block-P(LLA) **P1*** (○) and P(HPMA)-block-P(DLLA) **P2*** (△)**.** The solid lines represent the corresponding fits with eq.1.

This clearly underlines the importance of super structure formation in solution which was investigated for P(HPMA)-block-P(LLA) **P1*** and P(HPMA)-block-P(DLLA) **P2*** copolymers in isotonic aqueous solution, applying fluorescence correlation spectroscopy (FCS). [51] The normalized autocorrelation curves measured for 0.1 mg/mL PBS buffer solutions of **P1*** and **P2*** and the corresponding representation with eq. 1 are shown in Figure 2. A two component fit (m=2 in eq.1) was applied in order to fit the experimental autocorrelation curves. This means that in addition to the slowly diffusing aggregates also fast diffusing species e.g. residual amounts of free dye molecules were present in the solutions. From the diffusion time of the slow component we evaluated a hydrodynamic radius (R_H) of around 8.5 nm and 10.2 nm for **P1*** and **P2*** respectively (see Table 3). As these values are significantly higher than the single polymer chain hydrodynamic radius we conclude that micelles with average diameters of 17 nm and 20.4 nm have been formed in neutral PBS buffer.

Table 3. Characterization of fluorescently labeled (Oregon green 488 cadaverine) P(HPMA)-*block*-P(LLA) **P1*** and P(HPMA)-*block*-P(LLA) **P2*** copolymers in PBS buffer (pH = 7.2) by fluorescence correlation spectroscopy (FCS)

Polymer	Concentration of Polymer		Fluorescence Correlation Spectroscopy Data		
	mg/mL	mol/L	τ_D / μs	D / m^2/s	D_h / nm
P1*	0.1	6.5E-6	221	2.67E-11	17.0
P2*	0.1	6.5E-6	268	2.20E-11	20.4

3.3 Cell Toxicity Assay, Uptake Kinetics and Intracellular Localization of P(HPMA) *block*-P(LLA) and of P(HPMA)-*block*-P(DLLA) copolymers in human cancer cells (HeLa)

In order to determine the influence of the tacticity of the poly(lactide) block on the biological behavior of the synthesized polymers, the cytotoxicity, the cellular uptake and intracellular localization in human cervix adenocarcinoma cell line (HeLa) were studied.

Both P(HPMA)-*block*-P(LLA) and P(HPMA)-*block*-P(DLLA) copolymers did not show any toxicity in HeLa cells, neither after 24 h nor after 72 h of incubation, up to 3 mg/mL concentration. Furthermore no difference in cell toxicity related to tacticity of the poly(lactide) block was observed. The absence of toxicity is a very important proof if we consider a possible application of these polymers as drug or protein delivery systems.

Once ensured the non-toxic character of both systems, the time-dependent as well as the concentration-dependent cellular uptake was investigated in HeLa cells. The time-dependent experiments were carried out at two different temperatures, at 37°C and at 4°C, in order to prove the energy-dependent mechanism of internalization. In figure 3 the internalization profiles of **P1*** and **P2*** after 1 h of incubation at 37°C at different concentrations are reported. In both cases the cellular internalization increased with the increasing of the concentration. A minimum polymer concentration of 0,1 mg/mL was needed to measure the cellular uptake, due to the dye loading of the systems and the limits of detection. The increasing of the uptake was higher for **P1*** than for **P2***, reaching the value of 67 FU at 1 mg/mL, significantly different ($p<0,05$) from the maximum uptake at 1 mg/mL of 54 FU registered for **P2***.

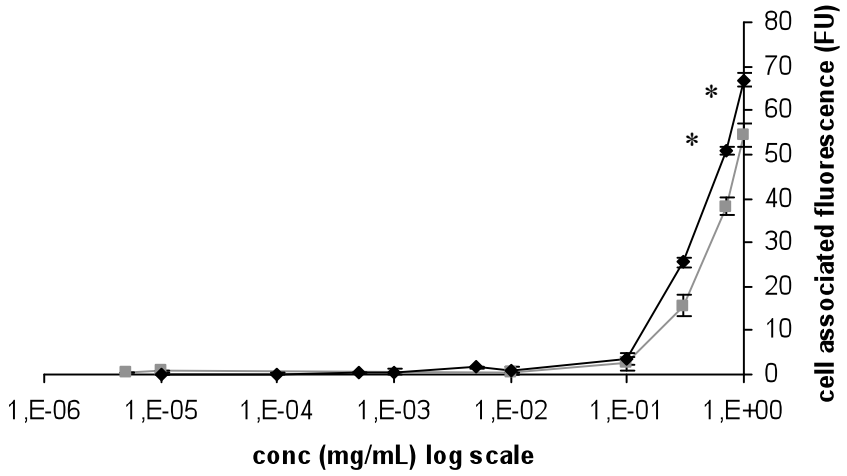

Figure 3. Concentration-dependent cellular uptake of **P1*** (♦) and **P2*** (■) after 1 h of incubation at 37°C. Data are expressed as mean ± SD. (* = $p<0,05$).

In the time-dependent experiments, cells were treated for different time ranging from 5 min to 5 h with 0,1 mg/mL polymer solution at 37°C. As shown in figure 4 the cellular internalization profile of **P1***

increased with the increasing of the incubation time, with a maximum at 5 h. Indeed in the case of **P2***, the maximum uptake was registered after 1 h of incubation, followed by a decreasing after 2 and 5 h. This kind of uptake could be due to a exocytosis process or a quenching phenomenon, due to the high accumulation of the fluorescent polymer inside the cells. Maybe also a degradation of the P(DLLA) block takes place effecting the endosomal department. But this hypothesis has to be proven in further experiments. In any case, **P2*** showed a higher degree of internalization than **P1***, at all times considered. When the experiments was carried out at 4°C, both systems showed a low cellular uptake, indicating that the internalization mechanism is energy-dependent, maybe following the endocytosis pathway, which is most likely for block copolymer aggregates. A possible explanation of the higher cellular uptake of the P(DLLA) block copolymer can be the amorphous character of the atactic polylactide block leading to a higher critical micelle concentration (cmc) as well as to less stable block copolymer micelles. In addition, the aggregates of **P2*** are with 20.4 nm in diameter larger than the ones observed for **P1***, which have a size of 17 nm.

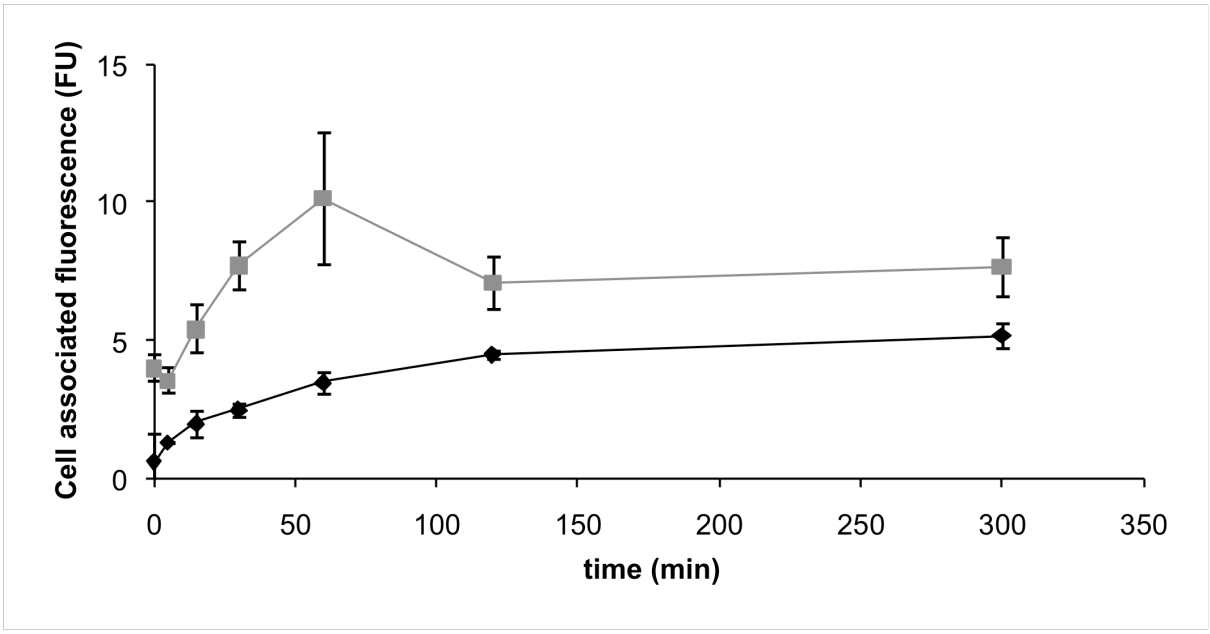

Figure 4. Time-dependent cellular uptake of **P1*** (♦) and **P2*** (■) at 37°C.

But interestingly the uptake kinetics of P(HPMA)-*block*-P(DLLA) are comparable to the ones of P(DLLA) spheres prepared by emulsion polymerization. [62] These systems do also shown a local minimum in the time depended cellular uptake before the cell associated fluorescence remains constant.

The localization of the polymers inside the cells was proved by live cell confocal fluorescence microscopy, incubating the cells with 0,1 mg/mL polymer solutions at different times. The highest internalization was detected after 1h to 2 h of incubation in both cases, as reported in figure 5. In order to determine if the polymers followed the endocytosis pathway, cells were treated also with dextran-Texas Red, employed as lysosomal marker (in red in the pictures). We have chosen the 2 h incubation time for the colocalization times after applying the lysosomal marker, because 2 h can be expected to a suitable time for determining the cellular fate of the aggregates.

Figure 5. Representative image of the intracellular localization of a) P(HPMA)-*block*-P(LLA) **P1*** and b) P(HPMA)-*block*-P(DLLA) **P2*** in the human cervix adenocarcinoma (HeLa) cell line. The images are: 1) Green polymer associated fluorescence (covalently linked Oregon Green 488) 2) Red lysosomal marker attributed fluorescence (dextran-Texas Red) 3) Overlay of both fluorescence images 4) Optical microscopy image

Most interesting for both block copolymers we could not observe colocalization of the polymer associated fluorescence with the lysosomal marker, which could be a first hind for an endosomal escape of the block copolymers. But on the other hand the absence of colocalization can be also due to a slower intracellular delivery, which means that the block copolymer aggregates may need surprisingly longer than 2 hours to arrive in the lysosomes. So further studies involving longer time

frames have to be carried out. But never the less, a degradation of the lactide leads to a release of lactic acid, which may lead to a tremendous change in the endosomal compartment pH. The effect is comparable to the well-known proton sponge effect for polyamines. [63-65] But further investigations have to be carried out, because for PEG based PLA block copolymers no endosomal escape was reported in literature. Degradation has been studied on intracellular and extracellular level. Furthermore the ability as transport vehicle has to be evaluated. But so far all reported findings a very promising and worth to undergo more detailed investigations.

4. Conclusion

In this work we have reported the synthesis of P(HPMA)-*block*-P(LLA) and P(HPMA)-*block*-P(DLLA) based on our recently published method. The synthetic procedure combines the RAFT polymerization technique with the activated ester approach. The synthesized polymers differ only in the tacticity of the polylactide block. All other parameters, e.g. block length and degree of polymerization, are kept constant for the synthesized block copolymers. In this respect we were able to investigate the influence of the polylactide tacticity on the micellization as well as on the biological fate of formed micells.

We have first data indicating a direct influence of the polymer tacticity of the polylactide block on cellular uptake as well as on intracellular localization. In the confocal laser scanning microscopy images no colocalization of the polymer with a lysosomal marker (Dextrane Texas Red) could be observed even after 5 h incubation. These findings could be a first indication of an endosomal escape. But further studies are needed to verify the uptake kinetics as well as the endosomal escape hypothesis. In this respect, additional biological studies are mandatory and will be carried out in close future.

5. Acknowledgement

The authors would like to thank Ms Romina Forst for assistance during the synthesis of conjugates and Prof. Helmut Ringsdorf for his helpful advice. We also gratefully acknowledge the Confocal Microscopy Service of the Centro de Investigación Príncipe Felipe (Valencia, Spain) for their skillful

assistance. The authors also thank the graduate school of excellence MAINZ, COMATT, IMPRS, the Spanish Ministry Grant (CTQ2007-60601) and particularly the cluster of excellence SAMT of Rhineland-Palatinafor support and funding.

6. References

[1] Ringsdorf H. Structure and properties of pharmacologically active polymers. J Polymer Sci Polym Symp 1975;51:135-153.

[2] Ferrari M. Cancer nanotechnology: opportunities and challenges. Nat Rev Cancer 2005;5:161-171.

[3] Duncan R. Polymer conjugates as anticancer nanomedicines. Nat Rev Cancer 2006;6:688-701.

[4] Haag R, Kratz F. Polymer Therapeutics: Concepts and Applications Angew Chem Int Ed 2006;45:1198-1215.

[5] Harris JM, Chess RB. Effect of pegylation on pharmaceuticals. Nat Rev Drug Discovery 2003;2:214-221.

[6] Matsumura Y, Kataoka K, Preclinical and clinical studies of anticancer agent-incorporating polymer micelles. Cancer Sci. 2009;100(4):572-579.

[7] Kabanov AV, Chekhonin VP, Alakhov YV, Batrakova EV, Lebedev AS, Melik-Nubarov NS, Arzhakov SA, Levashov AV, Morozov GV, Severin ES, Kabanov VA. The neuroleptic activity of haloperidol increases after its solubilization in surfactant micelles: micelles as microcontainers for drug targeting. FEBS Lett. 1989;258:343-345.

[8] Yokoyama M, Miyauchi M, Yamada N, Okano T, Sakurai Y, Kataoka K, Inoue S. Characterization and anticancer activity of the micelle-forming polymeric anticancer drug adriamycin-conjugated poly(ethylene glycol)–poly(aspartic acid) block copolymer. Cancer Res. 1990;50:1693-1700.

[9] Yokoyama M, Okano T, Sakurai Y, Ekimoto H, Shibazaki C, Kataoka K. Toxicity and antitumor activity against solid tumors of micelle-forming polymeric drug and its extremely long circulation in blood. Cancer Res. 1991;51:3229-3236.

[10] Kataoka K, Kwon GS, Yokoyama M, Okano T, Sakurai Y. Block copolymer micelles as vehicles for drug delivery. J. Control. Release 1993;29:119-132.

[11] Kwon GS, Yokoyama M, Okano T, Sakurai Y, Kataoka K. Biodistribution of micelle-forming polymer-drug conjugate, Pharm. Res. 1993;10:970-974.

[12] Kwon GS, Yokoyama M, Okano T, Sakurai Y, Kataoka K. Enhanced tumor accumulation and prolonged circulation times of micelle-forming poly(ethylene oxide –aspartate) block copolymer-adriamycin conjugate. J. Control. Release 1994;29:17-23.

[13] Yokoyama M, Okano T, Sakurai Y, Fukushima S, Kataoka K. Selective delivery of adriamycin to a solid tumor using a polymeric micelle carrier system. J. Drug Target. 1999;7:171-86.

[14] Kataoka K, Harada A, Nagasaki Y. Block copolymer micelles for drug delivery: design, characterization and biological significance, Adv. Drug Deliv. Rev. 2001;47:113-31.

[15] Kwon GS, Kataoka K. Block copolymer micelles as long-circulating drug vehicles. Adv. Drug. Delivery Rev. 1995;16:295-309.

[16] Jones M-C, Leroux J-C. Polymeric micelles- a new generation of colloidal drug carriers. Eur. J. Pharm. Biopharm. 1999;268:101-111.

[17] Torchilin VP,. Structure and design of polymeric surfactant-based drug delivery systems. J. Control. Release 2001;73:137-172

[18] Nagarajan R, Ganesh K. Block copolymer self-assembly in selective solvents:theory of solubilization in spherical micelles. Macromolecules 1989;22:4312-4325.

[19] Kabanov AV, Batrakova EV, Alakhov VY. Pluronic block copolymers as novel polymer therapeutics for drug and gene delivery. J. Control. Release 2002;82:189-212.

[20] Slepnev VP, DeCamilli P, Endocytosis: an overview, in: Kabanov AV, Felgner PL, Seymour LW. Self-Assembling Complexes for Gene Delivery: From Laboratory to Clinical Trial, Wiley, Chichester, UK, 1998

[21] Lee Y, Miyata K, Oba M, Ishii T, Fukushima S, Han M, Koyama H, Nishiyama N, Kataoka K. Charge-conversion ternary polyplex with endosome disruption moiety: A technique for efficient and safe gene delivery. Angew. Chem. Int. Ed. 2008;47(28):5163-5166.

[22] Lee Y, Ishii T, Cabral H, Kim H-J, Seo J-H, Nishiyama N, Oshima H, Osada K, Kataoka K. Charge-conversional polyionic complex micelles-efficient nanocarriers for protein delivery into cytoplasm. Angew. Chem. Int. Ed. 2009;48(29):5309-5312.

[23] Kim SH, Jeong JH, Joe CO, Park TG. Folate receptor mediated intracellular protein delivery using PLL–PEG–FOL conjugate. J. Control. Release 2005;103(3): 625-634.

[24] Duncan R. The dawning era of polymer therapeutics. Nat. Rev. Drug Discovery 2003;2:347-360.

[25] Kopecek J, Kopeková P, Minko T, Lu ZR. HPMA copolymer–anticancer drug conjugates: design, activity, and mechanism of action. Eur J Pharm Biopharm 2000;50:61-81.

[26] Noria A, Jensena KD, Tijerinaa M, Kopecková P, Kopecek J. Subcellular trafficking of HPMA copolymer–Tat conjugates in human ovarian carcinoma cells. J. Control. Release 2003;91(1-2):53-59.

[27] Duncan R, Coatsworth JK, Burtles S. Preclinical toxicology of a novel polymeric antitumour agent: HPMA copolymer-Doxorubicin (PK1). Hum. Exp. Toxicol. 1998;17(2):93-104.

[28] Vasey PA, Kaye SB, Morrison R, Twelves C, Wilson P, Duncan R, Thomson AH, Murray LS, Hilditch TE, Murray T, Burtles S, Fraier D, Frigerio E, Cassidy J and on behalf of the Cancer Research Campaign Phase I/II Committee. Phase I clinical and pharmacokinetic study of PK1 [N-(2-hydroxypropyl)metharylamide copolymer Doxorubicin]: first member of a new class of chemotherapeutic agents-drug-polymer conjugates, Cancer Research Campaign I/II Committee. Clin. Cancer Res. 1999;5(1):83-94.

[29] Hopewell JW, Duncan R, Wilding D, Chakrabarti K. Preclinical evaluation of the cardiotoxicity of PK2: A novel HPMA copolymer–doxorubicin–galactosamine conjugate antitumour agent. Hum. Exp. Toxicol. 2001;20(9):461-470

[30] Li Y, Kissel T. Synthesis and properties of biodegradable ABA triblock copolymers consisting of poly(L-lactic acid) or poly(L-lactic-co-glycolic acid) A-blocks attached to central poly(oxyethylene) B-blocks. J. Control. Release 1993;27:247-257.

[31] Piskin E, Kaitian X, Denkbas EB, Kucukyavuz Z. Novel PDLLA/PEG copolymer micelles as drug carriers, J. Biomater. Sci. Polym. Ed. 1995;7:359-373.

[32] Vittaz M, Bazile D, Spenlehauer G, Verrechia T, Veillard M, Puisieux F, Labarre D. Effect of PEO surface density on long-circulating PLA-PEO nanoparticles which are very low complement activators. Biomaterials 1996;17:1575-1581.

[33] Zhang X, Jackson JK, Burt HM. Development of amphiphilic diblock copolymers as micellar carriers of taxol. Int. J. Pharm. 1996;132:195-206.

[34] Peracchia MT, Gref R, Mianamitake Y, Domb A, Lotan N, Langer R. PEG-coated nanospheres from amphiphilic diblock and multiblock copolymers: investigation of their drug encapsulation

and release characteristics, J. Control. Release 1997;46:223-231.

[35] Tanodekaew S, Pannu R, Heatley F, Attwood D, Booth C. Association and surface properties of diblock copolymers of ethylene oxide and DL-lactide in aqueous solution, Macromol. Chem. Phys. 1997;198:927-944.

[36] Matsumoto J, Nakada Y, Sakurai K, Nakamura T, Takahashi Y. Preparation of nanoparticles consisted of poly(L-lactide)-poly(ethylene glycol)-poly(L-lactide) and their evaluation in vitro. Int. J. Pharm. 1999;185:93-101.

[37] Riley T, Govender T, Stonik S, Xiong CD, Garnett MC, Illum L, Davis SS. Colloidal stability and drug incorporation aspects of micellar-like PLA-PEG nanoparticles. Colloids Surfaces B: Biointerfaces 1999;16:147-159.

[38] Yasugi K, Nagasaki Y, Kato M, Kataoka K. Preparation and characterization of polymer micelles from poly(ethylene glycol)-poly(D,L-lactide) block polymers as potential drug carrier. J. Control. Release 1999;62:89-100.

[39] Yamamoto Y, Nagasaki Y, Kato Y, Sugiyama Y, Kataoka K. Long-circulating poly(ethylene glycol)–poly(D,L-lactide) block copolymer micelles with modulated surface charge. J. Control. Release 2001;77:27–38.

[40] Barz M, Wolf F, Canal F, Vicent MJ, Frey H, Zentel R, Synthesis, Characterization and Evaluation of poly(HPMA)-*block*-poly(L-Lactide) copolymers: A new type of functional biocompatible block copolymers. Macromolecules submitted.

[41] Slager J, Domb AJ. Biopolymer Stereocomplexes. Adv. Drug Del. Rev., 2003 55, 549–583

[42] Burt HM, Zhang X, Toleikis P, Embree L, Hunter WL. Development of copolymers of poly(D,L-lactide) and methoxypoly- ethylene glycol as micellar carriers of paclitaxel. Colloids Surf. B 1999;16:161-171.

[43] Barz M, Luxenhofer R, Zentel R, Kabanov AV. The uptake of N-(2-hydorxypropyl)methacryl-amide based homo, random and block copolymers by human multi-drug resistant breast adenocarcinoma cells. Biomaterials 2009;30:5682-5690.

[44] Moad G, Rizzardo E, Thang SH. Living Radical Polymerization by the RAFT Process. Aust J Chem 2005;58:379-410.

[45] Moad G, Rizzardo E, Thang SH. Radical addition–fragmentation chemistry in polymer synthesis. Polymer 2008;49:1079-1131.

[46] Stenzel M. RAFT polymerization: an avenue to functional polymeric micelles for drug delivery. Chem. Commun. 2008: 3486-3503.

[47] Boyer C, Bulmus V, Davis TP, Ladmiral V, Liu J, Perrier S. Bioapplications of RAFT Polymerization. Chem. Rev. 2009;109:5402–5436.

[48] Gauthier MA, Gibson MI, Klok H-A. Synthesis of Functional Polymers by Post-Polymerization Modification. Angew. Chem. Int. Ed. 2009;48:48–58.

[49] Theato P. Synthesis of well-defined polymeric activated esters. Journal of Polymer Science Part A: Polymer Chemistry 2008;46(20):6677-6687.

[50] Rigler R, Elson ES. Fluorescence Correlation Spectroscopy. Springer-Verlag: New York, 2001.

[51] Bonne TB, Ludtke K, Jordan R, Stepanek P, Papadakis CM Aggregation behavior of amphiphilic poly(2-alkyl-2-oxazoline) diblock copolymers in aqueous solution studied by fluorescence correlation spectroscopy, Colloid And Polymer Science 2004;282:833-843.

[52] Y. K. Chong, G. Moad, E. Rizzardo, S. H. Tang. A More Versatile Route to Block Copolymers and Other Polymers of Complex Architecture by Living Radical Polymerization: The RAFT Process. Macromolecules 1999;32:2071-2073.

[53] Eberhardt M, Mruk R, Zentel R, Theato P. New precursor polymers for the synthesis of multifunctional materials. Eur Polym J 2005;41:1569-1575.

[54] Perrier S, Takolpuckdee P, Mars CA. Reversible Addition−Fragmentation Chain Transfer Polymerization: End Group Modification for Functionalized Polymers and Chain Transfer Agent Recovery. Macromolecules 2005;38:2033-2036.

[55] Dve AP, Pratt RC, Lohmeijer BGG, Waymouth RM, Hedrick JL. Thiourea-Based Bifunctional Organocatalysis: Supramolecular Recognition for Living Polymerization. J. Am. Chem. Soc. 2005;127:13798–13799.

[56] Pratt RC, Lohmeijer BGG, Long DA, Lundberg PNP, Dove AP, Li HB et al. Exploration, Optimization, and Application of Supramolecular Thiourea−Amine Catalysts for the Synthesis of Lactide (Co)polymers. Macromolecules 2006;39:7863–7871.

[57] Eberhardt M, Theato P. RAFT Polymerization of Pentafluorophenyl Methacrylate: Preparation of Reactive Linear Diblock Copolymers. Macromol. Rapid Commun. 2005;26:1488-1493.

[58] Barz M, Tarantola M, Fischer K, Schmidt M, Luxenhofer R, Janshoff A et al. From Defined Reactive Diblock Copolymers to Functional HPMA-Based Self-Assembled Nanoaggregates. Biomacromolecules 2008;9:3114-3118.

[59] Gibson MI, Fröhlich E, Klok H-A, Postpolymerization Modification of Poly(Pentafluorophenyl methacrylate): Synthesis of a Diverse Water-Soluble Polymer Library. Journal of Polymer Science: Part A: Polymer Chemistry 2009; 47:4332–4345.

[60] Seymour LW, Duncan R, Strohalm J, Kopecek J. Effect of molecular weight of (2-hydroxypropyl)methacrylamide copolymers on body distribution and rate of excretion after subcutaneous, intraperitoneal, and intravenous administration to rats. J. Biomed. Mat. Res. 1987;21(11):1341-1358.

[61] Sahay G, Batrakova EV, Kabanov AV. Different Internalization Pathways of Polymeric Micelles and Unimers and Their Effects on Vesicular Transport. Bioconjugate Chem 2008;19:2023-2029.

[62] Mailänder V, Landfester K. Interaction of Nanoparticles with Cells. Biomacromolecules 2009;10:2379–2400.

[63] Behr J-P. The proton sponge: a trick to enter cells the viruses did not exploit. Chimica 1997;51:34–36.

[64] Boussif O, Lezoualch F, Zanta M A, Mergny M D, Scherman D, Demeneix B, Behr J-P A versatile vector for gene and oligonucleotide transfer into cells in culture and in vivo: polyethylenimine. Proc. Natl. Acad. Sci. 1995;92:7297–7301.

[65] Pack D, Putnam D, Langer R. Design of imidazole-containing endosomolytic biopolymers for gene delivery. Biotechnol. Bioeng. 2000;67:217–223.

2.8 Radioactive Labeling of Defined HPMA-Based Polymeric Structures Using [^{18}F]FETos for In Vivo Imaging by PositronEmission Tomography

Biomacromolecules **2009,** *10, 1697–1703*

Authors: Matthias M. Herth,[†,2] Matthias Barz,[†,1] Dorothea Moderegger,[2] Mareli Allmeroth,[1] Markus Jahn,[2] Oliver Thews,[3] Rudolf Zentel,[*,1] and Frank Rösch[*,2]

Address: [1]Institute of Nuclear Chemistry, Johannes Gutenberg-University Mainz, Fritz-Strassmann-Weg 2, 55128 Mainz, Germany,,

[2]Institute of Organic Chemistry, Johannes Gutenberg-University Mainz, Duesbergweg 10-14, 55099 Mainz, Germany

[3] Institute of Pathophysiology, Johannes Gutenberg-University Mainz, Duesbergweg 6, 55128 Mainz, Germany

Abstract

During the last decades polymer-based nanomedicine has turned out to be a promising tool in modern pharmaceutics. The following article describes the synthesis of well-defined random and block copolymers by RAFT polymerization with potential medical application. The polymers have been labeled with the positron-emitting nuclide fluorine-18. The polymeric structures are based on the biocompatible *N*-(2-hydroxypropyl)-methacrylamide (HPMA). To achieve these structures, functional reactive ester polymers with a molecular weight within the range of 25000-110000 g/mol were aminolyzed by 2-hydroxypropylamine and tyramine (3%) to form ^{18}F-labelable HPMA polymer precursors. The labeling procedure of the phenolic tyramine moieties via the secondary labeling synthon 2-[^{18}F]fluoroethyl-1-tosylate ([^{18}F]FETos) provided radiochemical fluoroalkylation yields of ~80% for block copolymers and >50% for random polymer architectures within a synthesis time of 10 min and a reaction temperature of 120 °C. Total synthesis time including synthon synthesis, ^{18}F-labeling, and final purification via size exclusion chromatography took less than 90 min and yielded stable ^{18}F-labeled HPMA structures in isotonic buffer solution. Any decomposition could be detected within 2 h. To determine the in vivo fate of ^{18}F-labeled HPMA polymers, preliminary small animal positron emission tomography (PET) experiments were performed in healthy rats, demonstrating the renal clearance of low molecular weight polymers. Furthermore, low metabolism rates could be detected in urine as well as in the blood. Thus, we expect this new strategy for radioactive labelling of polymers as a promising approach for in *vivo* PET studies.

1. Introduction

Polymer-based therapeutics are of increasing interest in the development of nanomedical tools for medical diagnosis and treatment. [1-3] For example, micelles [4-11] and polymer drug conjugates [12-15], containing various functionalities among a single molecule, have been applied to drug delivery applications. In this respect, polymers can interact with different biological targets selectively, carrying drugs or fulfilling biological tasks.

Functionalities can be introduced in a polymeric system either by polymerizing a mixture of monomers leading to random copolymers or by synthesizing reactive polymer structures that can be transferred into functional structures by a polymer analogous reaction afterward. The reactive ester approach offers two major advantages: On one hand only homopolymers need to be synthesized which can be precisely characterized; on the other hand copolymerization parameters can be disregarded. Copolymers based on N-(2-hydroxypropyl)-methacrylamide (HPMA) and active ester methacrylates have been applied to various medical *in vivo* applications. [1,4,16,17]

However, to optimize medical application detailed knowledge about the biodistribution of polymers in the living organism is necessary. It provides insights in pharmacokinetics of the medical substance or metabolism pathways within the target tissue or other organs. The nonspecific interaction between proteins and polymer surfaces determines the in vivo fate of drug carriers. [18-20] Therefore, particle-sizes, compositions, physical properties, and surface chemistry influence the behavior of nanomaterials *in vivo*. [21]

To understand and finally fine-tune these parameters for in vivo therapies or diagnostics, appropriate imaging strategies are needed. In this respect, noninvasive, quantitative, and repetitive whole body molecular imaging techniques such as positron emission tomography (PET) and single photon emission computed tomography (SPECT) using adequate radiolabeled derivatives would provide a significant advance in the understanding of the mentioned interactions. Compared with other imaging methods, PET and SPECT bear the advantages of high sensitivity (the level of detection approaches 10^{-12} M of tracer) and isotropism (i.e., ability to detect organ accumulation accurately, regardless of tissue depth, whereas fluorescence emission is limited by a low penetration depth), which provide reliability for *in vivo* quantitative imaging analysis. For macromolecules, most frequently used radioactive nuclides for *in vivo* imaging are chelated metals, such as ^{111}In or ^{99m}Tc for SPECT and ^{64}Cu for PET. [22-24] Nevertheless, PET offers the more precise and detailed imaging technique due to higher spatial and temporal resolution as well as quantification. [25]

Recent research has demonstrated the use of chelators (e.g., DOTA derivatives) for the attachment of metallic PET radionuclides. [24] This strategy may have a major drawback. Typically, the chelating

agent itself is rather large, bulky and charged and as a result may strongly influence the particle structure and consequently its biological behavior. This work introduces a new approach for ^{18}F-labeling polymers with a rather small synthon 2-[^{18}F]fluoroethyl-1-tosylate ([18F]FETos) that should not influence the structural properties of the self-assembled nanoobject itself.

The imaging time frame of polymer-based therapeutics differs regarding their biological targeting. Due to this fact, long-term and short-term imaging is needed. An example for long-time imaging is passive polymer accumulation in tumor tissue. In contrast, there is a need for short-term in blood pool imaging. All these mentioned applications are of major interest in clinical research, for example, in tumor diagnostics [25] and therapy [3], in certain heart dysfunctions [26,27], or tissue perfusion. [28] In this context, ^{18}F-labeled HPMA polymers should allow precise imaging of short-term pharmacokinetics of nanostructures.

2. Materials and Methods

2.1 Materials

All chemicals were reagent grade and obtained from Aldrich. The chemicals were used without further purification unless otherwise indicated. Dioxane used in the synthesis was freshly destilled from a sodium/potassium mixture. 2,2'-Azobis(isobutyronitrile) (AIBN) was recrystallized from diethyl ether and stored at -7°C. Lauryl methacrylate was distilled and kept at -7°C.

2.2 Characterization

^{1}H-, ^{13}C- and ^{19}F-NMR spectra were obtained at 300 or 400 MHz using a FT-spectrometer from Bruker and analyzed using the ACDLabs 6.0 software. The polymers were dried at 40 °C over night under vacuum and afterwards submitted to gel permeation chromatography (GPC). GPC was performed in tetrahydrofurane (THF) as solvent and with following parts: pump PU 1580, auto sampler AS 1555, UV-detector UV 1575, RI-detector RI 1530 from Jasco and miniDAWN Tristar light scattering detector from Wyatt. Columns were used from MZ-Analysentechnik: MZ-Gel SDplus 10^2 Å, MZ-Gel SDplus 10^4 Å and MZ-Gel SDplus 10^6 Å. The elution diagrams were analysed using the ASTRA 4.73.04 software from Wyatt Technology. Calibration was done using polystyrene standards. The flow rate was 1 mL/min at a temperature of 25 °C. Radio-TLC`s (thin layer chromatography) were analyzed via an Instand Imager (Canberra Packard). HPLC was performed with a Sykam S 1100 pump and a Knauer UV-detector (K-2501), whereas SEC was performed with a

waters pump (1500 Series),a Waters UV-detector (2487 λ Absorbence Detector) and a Berthold LB 509 radiodetector. μPET studies were performed with a Siemens MicroPET Focus 120 camera.

2.3 Animals

Male Wistar rats (150-300 g) housed in the animal care facility of the University of Mainz were used in this study. All experiments had previously been approved by the regional animal ethics committee and were conducted in accordance with the German Law for Animal Protection

2.4 Synthesis of 4-cyano-4-((thiobenzoyl)sulfanyl)pentanoic acid

The 4-cyano-4-((thiobenzoyl) sulfanyl)pentanoic acid was used as the chain transfer agent (CTA) and synthesized according to the literature. [29]

2.5 Synthesis of pentafluoro-phenyl methacrylate (PFMA)

Pentafluorophenyl methacrylate (PFMA) was prepared according to the literature. [30]

2.6 General synthesis of the macro-chain transfer agents (CTA)

The macro CTA was prepared according to the literature. [31] RAFT polymerizations of PFMA using 4-cyano-4-((thiobenzoyl) sulfanyl)pentanoic acid were performed in a schlenk tube. The reaction vessel was loaded with 2,2'-azobis(isobutyronitrile (AIBN), 4-cyano-4-((thiobenzoyl)sulfanyl) pentanoic acid (CTA) (molar ratio of AIBN/CTA = 1:8) and 15 g of PFMA in 20 mL of dioxane. Following three freeze–vaccum–thaw cycles, the tube was immersed in an oil bath at 70 °C. Afterwards the polymer poly(PFMA) was 3 times precipitated into hexane, isolated by centrifugation and dried for 12 hours at 30 °C under vacuum. In the end a slightly red powder was obtained. Yield: (59 %). ^{1}H NMR ($CDCl_3$): δ [ppm] 1.6-2.2 (br), 0.9-1.5 (br) ^{19}F NMR ($CDCl_3$): δ [ppm] -165.1 (br), -159.8 (br), -154.4 (br), -153.1 (br).

2.7 General synthesis of block copolymers

The block copolymer was prepared according to the literature. [32]

2.8 Removal of dithioester end groups

The dithiobenzoate end group was removed according to the procedure reported by Perrier et al.. [33] Typically 200 mg of polymer, (Mn = 25.000 g/mol), and 40 mg of AIBN (20 times higher than copolymer, mol/mol) were dissolved in 3 mL of anhydrous dioxane/DMSO (4:1). The solution was heated at 80 °C for 2 h. Finally the copolymer was precipitated 3 times in 100 mL of diethyl ether and collected by centrifugation. In the case of the block copolymer the crude product was first precipitated in EtOH 2 times and than 1 time in diethyl ether. The copolymer was dried under vacuum for a period

of 24 h (yield: 92 %). The absence of the dithiobenzoate end group was confirmed by UV-Vis spectroscopy.

2.9 Polymer analogous reactions of homopolymers

In a typical reaction 300 mg of PPFMA without ditihioester endgroup were dissolved in 4 mL abs. dioxane and 1 mL abs. dimethylsulfoxide (DMSO). A colorless solution was obtained. In a typical reaction 8 mg of tyramin and 20 mg of triethylamine were added. The mixture was kept at 25 °C for 4 hours and finally 200 mg of hydroxypropylamine and 200 mg triethylamine were added. The reaction was allowed to proceed under the above-mentioned conditions over night. The solution was concentrated in vacuum and introduced to a column filtration using Sephadex^{TM} LH-20 in dioxane and precipitated in diethyl ether, removed by centrifugation and dried in vacuum at 30 °C for 14 hours. Yield: 85%. ^{1}H NMR (DMSO-*d*6): δ [ppm]) 6.6-7.2 (br), 4.5-4.8 (br), 3.4-3.9 (br), 2.6-3.0 (br), 0.9-1.3 (br)

2.10 Polymer analogous reactions of block copolymers

In a typical reaction 300 mg of poly(PFMA)-block-poly(Lauryl methacrylate) were dissolved in 4 ml abs. dioxane and 1 ml abs. dimethylsulfoxide (DMSO). A colourless solution was obtained. In a typical reaction 8 mg of tyramin and 20 mg of triethylamine were added. The mixture was kept at 25 °C for 4 hours. In the end 200 mg of hydroxypropylamine and 200 mg triethylamine were added. The reaction was allowed to go on under the above-mentioned conditions over night. The solution was concentrated in vacuum and introduced to a column filtration using Sephadex^{TM} LH-20 in dioxane and precipitated in diethyl ether, removed by centrifugation and dried in vacuum at 30 °C for 14 hours. Yield: 82%. ^{1}H NMR (DMSO-*d*6): δ [ppm]) 6.6-7.2 (br), 4.5-4.8 (br), 3.4-3.9 (br), 2.6-3.0 (br), 0.9-1.5 (br), 0.8-0.9 (br t)

2.11 Synthesis of 2-[^{18}F]fluoroethyl-1-tosylate [^{18}F]FETos

To a dried Kryptofix®2.2.2./[^{18}F]fluoride complex, 4 mg ethyleneglycol-1,2-ditosylate in 1 mL acetonitrile was added and heated under stirring in a sealed vial for 3 min. Purification of the crude product was accomplished using HPLC (Lichrosphere RP18-EC5, 250×10mm, acetonitrile/water 50:50, flow rate: 5 mL/min, R_f: 8 min). After diluting the HPLC fraction containing the [^{18}F]FETos with water (HPLC fraction/water 1:4) the product was loaded on a C18-Sepac cartridge, dried with a nitrogen stream and eluted with 1.2 mL of DMSO. The whole preparation time was about 40 min and the overall radiochemical yield was between 60 and 80%. [34]

2.12 Radioactive labeling of polymers using [^{18}F]FETos

In a typical reaction, 3 mg of polymer was dissolved in 1 mL DMSO. A clear solution with a concentration of 3 mg/mL was obtained. To this solution 1 µL of 5N sodium hydroxide solution and

[^{18}F]FETos solution were added. The clear solution was kept at temperatures from 80-150 °C for 20 min. For kinetic measurements samples were taken from the solution every 5 min. The decay-corrected radiochemical yield (RCY) was check by TLC (Merck 60 F_{254}) and SEC (HiTrap™ Desalting Column, Sephadex™ G-25 Superfine , column volume 5 mL; flowrate: 1 mL PBS-buffer solution)) leading to comparable results.

2.13 Proove of Stability

In a typical test, labeled polymers were reinjected into a SEC column (HiTrap™ Desalting Column, Sephadex™ G-25 Superfine , column volume 5 mL; flowrate: 1 mL PBS-buffer solution) and checked for impurities.

2.14 *In Vitro* Binding of Polymers to Human Serum Albumine

Solutions with a concentration of 40 mg/mL of human serum albumine (HSA; **S1**), 1 mg/mL of polymer **P2** (**S2**) as well as a mixture of 0.2 mg **P2** and 40 mg HSA in 1 mL of **S3** were prepared. A TLC in MeOH/H2O (4:1) using RP-18F(254s) TLC plates was performed by spotting the prepared isotonic solutions. *Rf* values (**S1**, 0.8; **S2**, 0; **S3**, 0.8 and 0).

2.15. *Ex Vivo* Metabolism Studies of ^{18}F-Labeled Particles

Male Wistar rats were anaesthetized with pentobarbital (40 mg/kg, i.p., Narcoren, Merial, Hallbergmoos, Germany) and a catheter was inserted into the left jugular vein for radiotracer application, a second catheter was inserted into the left carotic artery and a tube was placed in the trachea. The radiotracer was injected i.v. at a dose of ~10 MBq of the labeled ^{18}F-polymer. At 5, 10, 20, 30, and 60 min post-injection, blood samples were collected and analyzed. Whole blood was centrifuged at 7500 rpm for 5 min at 4 °C to separate plasma and blood cells. Plasma and blood cell fractions were obtained and radioactivity was measured with an automatic γ-counter (2470 Wizard; Perkin-Elmer). The percentage of radioactivity bound to plasma and blood cells was calculated thereafter. In addition, at 60 min p.i. samples of the urine were obtained from puncture of the animal's bladder. For metabolic studies the blood plasma and urine fractions were analyzed via reverse phase thin layer chromatography applying the same conditions described in section 2.14.

2.16. Initial *In Vivo* PET Studies of ^{18}F-Labeled HPMA Polymers

Positron emission tomography scans were performed with a Siemens/Concorde Microsystems microPET Focus 120 small animal PET (μPET) scanner. Animals were anaesthetized with pentobarbital (40 mg/kg, i.p., Narcoren, Merial, Hallbergmoos, Germany) and a catheter was inserted into the left jugular vein for radiotracer application and a tube was placed in the trachea. During PET measurements the animals were placed in supine position and breathed room air spontaneously through a tracheal tube. Listmode acquisition was started with the tracer injection of 15-25 MBq

(specific activity: 1.5-2.5 × 10-3 GBq/μmol). The ^{18}F labelled tracers were applied via i.v. injection into the jugular vein catheter. The tracer distribution was followed for up to 4 h after injection. Thereafter, a whole body scan of the rat was performed.

3. Results and Discussion

The synthesis and ^{18}F-labeling of functional HPMAcopolymers and block copolymers is based on precisely characterized active ester polymers [30], which can be easily modified using primary amines. The synthetic route to functional block copolymers based on the clinically approved *N*-(2-hydroxypropyl) methacrylamide (HPMA) was recently described by Barz and coworkers. [32] Random and block copolymers based on HPMA with phenolic hydroxyl groups in the polymer backbone (scheme 1) were synthesized using the active ester approach.

Scheme 1. Synthetic pathway to functional precursor polymers via RAFT polymerization

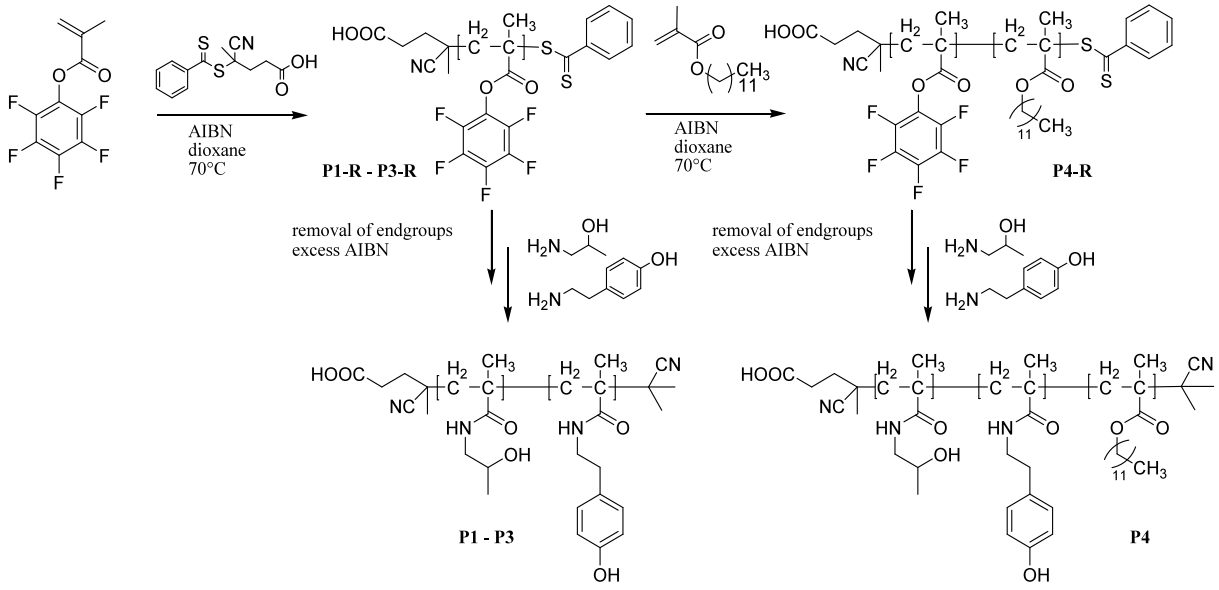

The reactive ester homopolymers and block copolymers have been synthesized by the RAFT polymerization method [29] leading to well-defined polymers with narrow molecular weight distributions. In general, the obtained polymers exhibit a polydispersity index (PDI) of 1.2-1.3 (Table 1) and have been characterized by NMR and GPC (Figure 1). The reactive polymers have been transferred to HPMA based polymeric structures as previously reported. [32]

Table 1. Synthesized reactive and functional polymers as precursors for radioactive labeling

polymer	block ratio	ratio of tyramin units at the polymer %	M_n number average of molecular weight	M_w weight average of molecular weight	PDI
P1-R	-	-	21090[b]	25090[b]	1.19[b]
P2-R	-	-	50260[b]	60840[b]	1.21[b]
P3-R	-	-	103900[b]	134100[b]	1.29[b]
P4-R	87:13[a]	-	22680[b]	27920[b]	1.25[b]
P1	-	3[a]	10980[c]	13050[c]	1.19
P2	-	3[a]	26140[c]	31640[c]	1.21
P3	-	3[a]	54030[c]	69730[c]	1.29
P4	87:13[a]	3[a]	12570[c]	15880[c]	1.25

a) As determined by ^{1}H NMR after aminolysis with hydroxypropylamine yielding **P1** and **P2**

b) As determined by GPC in THF as solvent for the activated ester polymers **P1-R** and **P2-R**. The value for **P1** and **P2** is recalculated from the molecular structure

c) Calculated from the block ratio obtained by ^{1}H NMR and GPC data of **P1-R** and **P2-R**

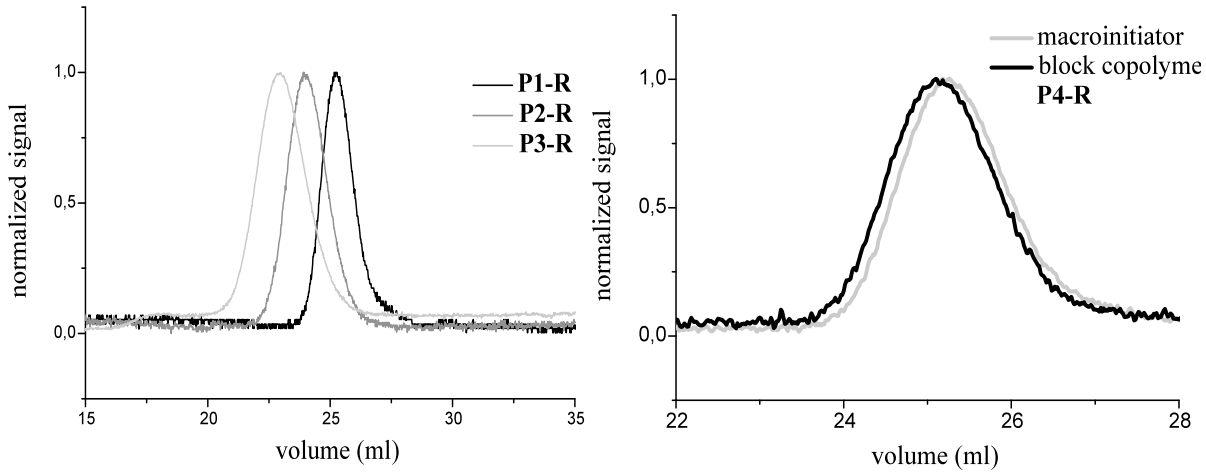

Figure 1. a) GPC elugram of a reactive homopolymers **P1-R**, **P2-R** and **P3-R** and b) GPC elugram of the macro initiator and final block copolymer **P4-R**

To achieve regio-selective introduction of an ^{18}F-label, the reactive polymers have been reacted with 2-hydroxy-1-aminopropane and besides with a rather small amount (3%) of tyramine (4-(2-aminoethyl) phenol) to the hydrophilic block to minimize the influence on the polymer's structure. For ^{18}Flabeling purposes, the phenolic tyramine moieties were first deprotonated using a smaller amount of base compared to the introduced phenolic hydroxy groups and subsequently labeled using [^{18}F]FETos (Scheme 2).

Scheme 2. Radioactive labeling of polymers using [^{18}F]FETos

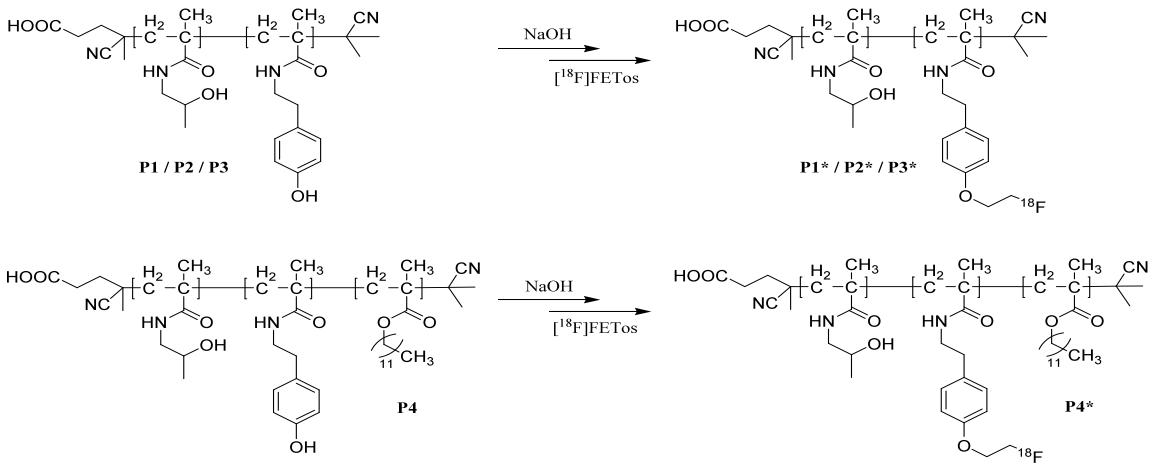

The radioactive labeling kinetics for 4 different polymers (**P1**-**P4**) have been evaluated and optimized. A clear dependence of the molecular weight on the decay-corrected radiochemical yield (RCY) at constant temperature could be observed. Higher molecular weight of the polymer led to minor RCY (Figure 2).

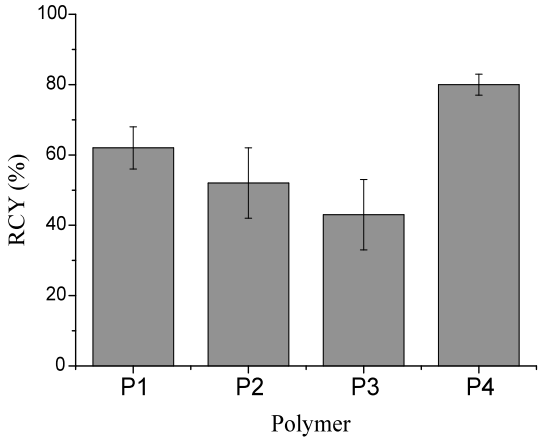

Figure 2. Corrected radioactive labeling yields (RCY) of statistic copolymers **P1**, **P2**, **P3** and block copolymer **P4** after 20 min at 100°C using 3 mg of each precursor polymer.

This expected effect could be explained by the decrease in the surface-volume ratio. Less phenolic moieties should therefore be able to better interact with [^{18}F]FETos. This effect is obvious at all temperatures.

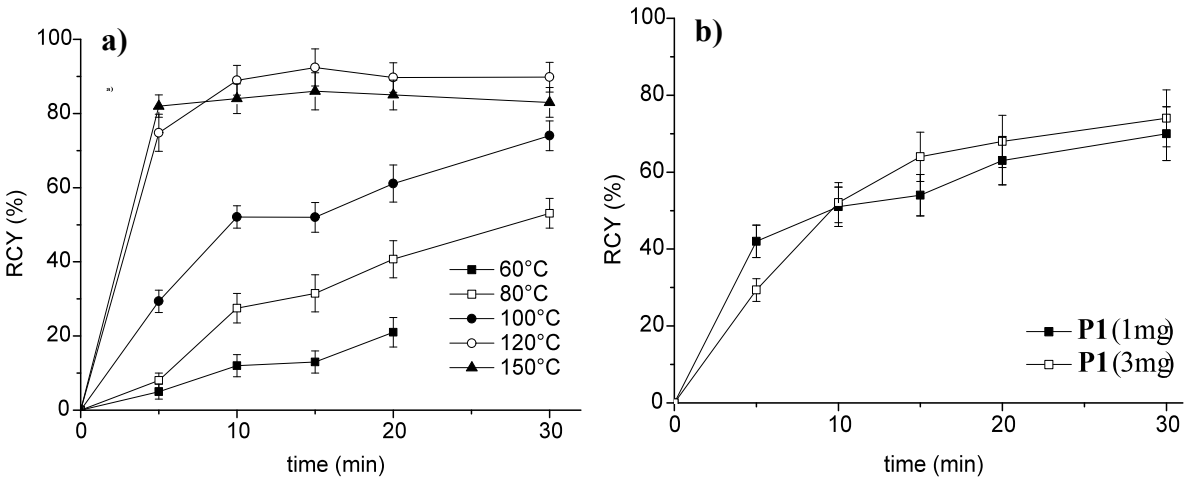

Figure 3. Corrected radioactive labeling yields (RCY) of **P1** dependency on a) temperature and b) amount of precursor at 100 °C.

Five different temperatures from 60 up to 150 °C were studied and resulted in the expected tendency of increasing RCY with rising temperature until a maximum yield at ~120 °C reached. At all temperatures, the polymer itself is stable and does not decompose. The results are plotted in Figure 3.

The optimal RCY could be obtained at 120 °C in a reaction time of 10 min. However, even at 60 °C a suitable RCY of ~20% was observed after 15-20 min. This offers the possibility of labeling at ambient temperatures, which is necessary for incorporating temperature sensitive molecules into the polymer. The impact of sample mass of the polymer samples turned out to be rather small due to the fact that the amount of labeling agent [^{18}F]FETos is 10^4 to 10^7 times lower compared to the amount of polymer used. This leads to quasifirst order reaction kinetics, explaining the results.

Purification was carried out by size exclusion chromatography (SEC) workup in PBS-buffer leading to a pure, labeled polymer and took ~10 min. The highest RCYs of 50% for random and ~80% for block copolymers have been obtained for the block copolymer **P4**. An explanation can be micellization in polar DMSO. Tyramine units are trapped in the hydrophilic part of the superstructure. Therefore, the local concentration of phenolic hydroxyl groups is higher compared to the random coil structures. This may result in high labeling yields. The specific radioactivity (*A*s) of the polymers was found to be 30 $MBq/g_{polymer}$.

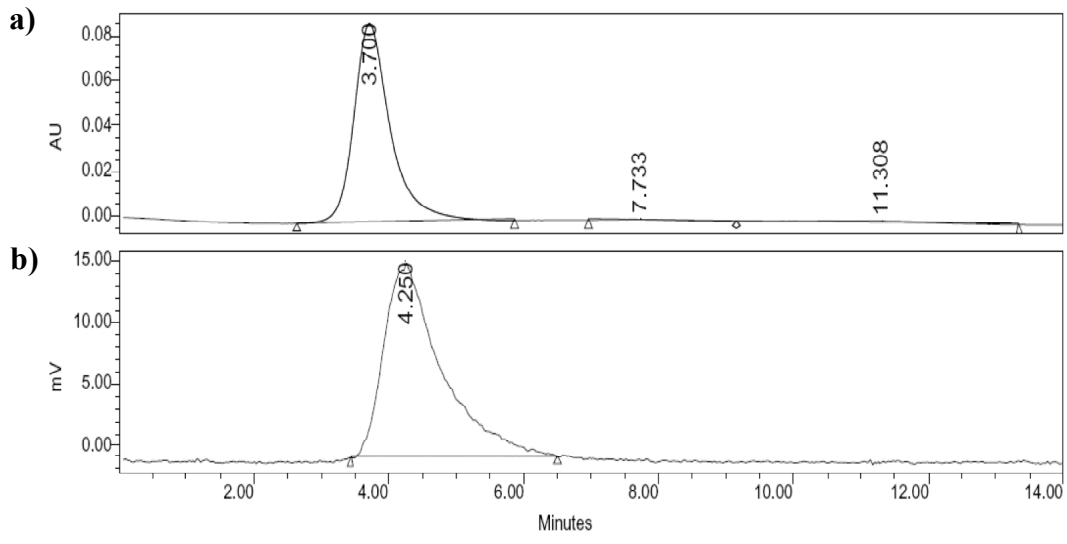

Figure 4. SEC elugram of the ^{18}F-labeled polymer **P2*** proofing stability 2 h after the initial purification in isotonic solution: UV detector signal a) and gamma counter signal b) did not show any low molecular weight contamination due to decomposition

The stability of the polymer was tested 2 h after initial purification and no decomposition occurred (see Figure 4).

A metabolism study demonstrated the *in vivo* stability of the labeled HPMA-particles. Only a maximum content of ~20% radioactive metabolites could be detected in the blood. Interestingly, this amount does not change during 1 h hour of investigation hinting on a stable ^{18}F-labeled polymer after initial metabolism. *In vitro*, the labeled polymer was not bound to human serum albumine (Figure 5a), indicating that the synthesized polymer does not show physical interaction with proteins. However, *in vivo* analysis of the metabolism showed that approximately 20-30% of the radioactivity was found bound to plasma proteins (Figure 6b, "radioactivity bound to metabolites"), indicating that the polymer undergoes some kind of metabolism and the ^{18}F-label may detach from the polymer. A more detailed study has to be carried out to investigate the stability of the O-fluoro-ethyl label and the influence of structural diverse polymers on *in vivo* metabolism.

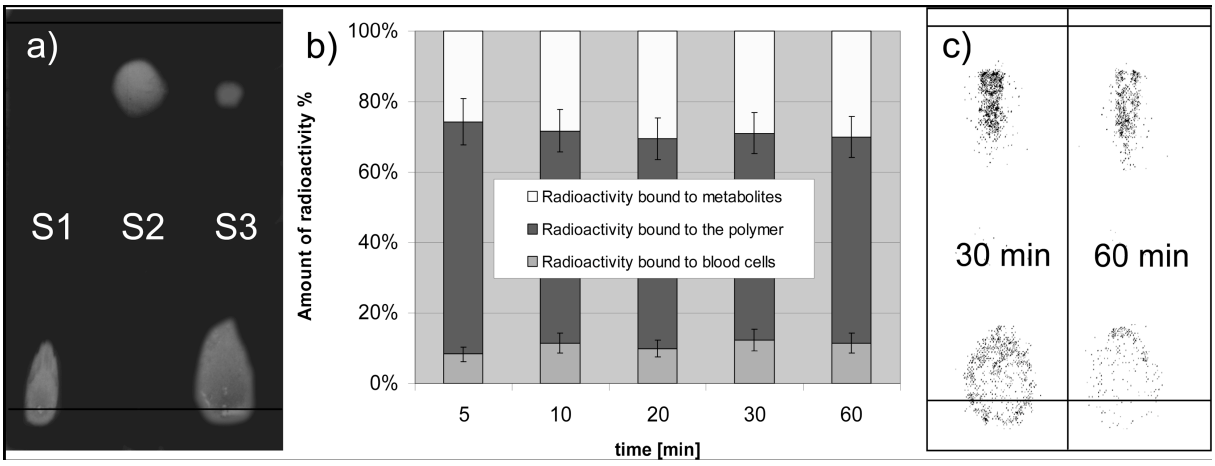

Figure 5. Metabolic analyses of 18F-labeled HPMA. (a) RP-TLC in MeOH/H2O (4:1) of isotonic solutions: 40 mg/mL of human serum albumine (HSA; **S1**), 1 mg/mL of polymer **P2** (**S2**), as well as a mixture of 0.2 mg **P2** and 40 mg HSA in 1 mL of **S3**. Staining was performed using Seebach Reagent. (b) Distribution of radioactivity among blood cells, proteins, and free polymer 18F-labeled **P2*** in plasma water from 5 to 60 min p.i. determined by radio RP-TLC and automatic γ-counter. (c) Comparison of metabolism of polymer 18F-labeled **P2*** in blood 30 and 60 min p.i. monitored by radio RP-TLC in MeOH/H2O (4:1), ensuring a small amount of metabolite.

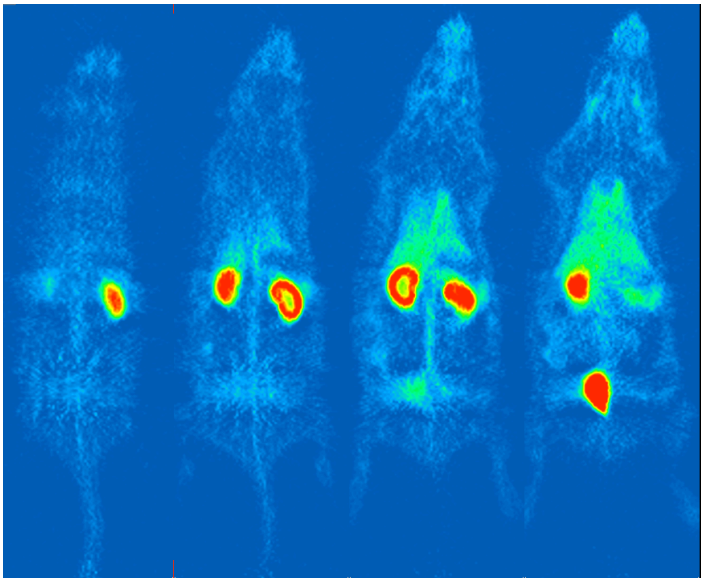

Figure 6. A representative whole body image 150 min p.i. of the ^{18}F-labeled polymer **P2*** proofing the renal clearance. A heavy accumulation could only be observed in the kidneys and the bladder.

These promising results enabled initial PET experiments to determine the *in vivo* fate of these polymers in healthy rats. PET scans with polymer **P2*** were performed. As expected for slightly negative charged low molecular weight HPMA based polymers [35], a strong accumulation was observed in the kidneys and in the bladder. Figure 6 shows a representative whole body μPET image of the 18F-labeled polymer **P2***.

The accumulation of radioactivity in the kidneys and the bladder in the PET study can be explained by the renal clearance of the ^{18}F-labeled HPMA-polymers. A metabolism study of the urine demonstrated only the existence of ^{18}F-labeled macromolecules within the bladder indicating the polymer per se is not metabolized in the organsim.

Altogether, total ^{18}F-fluorination including [^{18}F]FETos synthesis, polymer labeling, and polymer purification via SEC took no longer than 90 min and resulted in an ^{18}F-labeled polymer which can now be used for PET imaging over a period from 5–10 h. This time scale appears reasonable to study the particle distribution and accumulation regarding short-term pharmacokinetics.

4. Conclusion

A new versatile ^{18}F-labeling strategy for polymeric particles has been introduced. Defined and functional HPMA-based random and block copolymers have been synthesized by RAFT polymerization and labeled in high RCY of >50% using [^{18}F]FETos in a reaction time of ~ 10 min. Overall synthesis, including [^{18}F]FETos synthesis, polymer labeling, and polymer purification via SEC, was carried out in less than 90 min. The labeled polymer showed no decomposition. First metabolism and μPET experiments showed promising results concerning the *in vivo* behavior of the ^{18}F-labeled polymer **P2***. The accumulation of radioactivity in kidneys and bladder is due to the renal clearance of the intact compound. Slight metabolism was observed in the blood. However, after initial metabolism, no further degradation could be detected.

In summary, a new method to label polymer precursors by ^{18}F-fluorine has been carried out enabling biological evaluation of polymeric systems in vivo via μPET in the close future. This approach will provide the possibility of precise in vivo imaging of polymeric nanoparticles over a period of 5-10 h. Furthermore, this approach may lead to a detailed understanding in which way alterations in physical properties of the nanostructures such as size, surface chemistry or core material will influence the fate of nanoparticles in living systems.

5. Acknowledgement

The authors wish to thank Sabine Höhnemann and Vasko Kramer for the synthesis of [^{18}F]FETos as well as Nicole Bausbacher and Hans-Georg Buchholz for assistance during PET measurements. We also want to thank Prof. Dr. Helmut Ringsdorf for excellent and fruitful discussion. Financial support by Friedrich-Naumann-Stiftung, the European Network of Excellence (EMIL), and Polymat Graduate School of Excellence is gratefully acknowledged.

6. References

[1] Jemal, A.; Murray, T.; Ward, E.; Samuels, A.; Tiwari, R. C.; Ghafoor, A.; Feuer, E. J.; Thun, M. J. Cancer statistics. *CA Cancer J. Clin.* **2005**, *55*, 10.

[2] Thompson, J. F.; Scolyer, R. A.; Kefford, R. F. *Lancet* **2005**, *365*, 687.

[3] Duncan, R. *Nat. Re*V. *Cancer* **2006**, *6* (9), 688.

[4] Ringsdorf, H. *J. Polym. Sci., Polym. Symp.* **1975**, *51*, 135.

[5] Adams, M. L.; Lavasanifar, A.; Kwon, G. S. *J. Pharm. Sci.* **2003**, *92*, 1343.

[6] Bae, Y.; Fukushima, S.; Harada, A.; Kataoka, K. *Angew. Chem., Int. Ed.* **2003**, *42*, 4640.

[7] Kakizawa, Y.; Harada, A.; Kataoka, K. *Biomacromolecules* **2001**, *2*, 491.

[8] Kim, S. Y.; Shin, I. L. G.; Lee, Y. M.; Cho, C. S.; Sung, Y. K. *J. Controlled Release* **1998**, *51*, 13.

[9] Kwon, G.; Naito, M.; Yokoyama, M.; Okano, T.; Sakurai, Y.; Kataoka, K. *Langmuir* **1993**, *9*, 945.

[10] Nasongkla, N.; Bey, E.; Ren, J.; Ai, H.; Khemtong, C.; Guthi, J. S.; Chin, S. F.; Sherry, A. D.; Boothman, D. A.; Gao, J. *Nano Lett.* **2006**, *6*, 2427.

[11] Torchilin, V. P. *Pharm. Res.* **2007**, *24*, 1.

[12] Hongrapipat, J.; Kope Ková, P.; Prakongpan, S.; Kopecek, J. *Int.J. Pharm.* **2008**, *351*, 259.

[13] Mitra, A.; Nan, A.; Papadimitriou, J. C.; Ghandehari, H.; Line, B. R. *Nucl. Med. Biol.* **2006**, *33*, 43.

[14] Satchi-Fainaro, R.; Puder, M.; Davies, J. W.; Tran, H. T.; Samson, D. A.; Greene, A. K.; Corfas, G.; Folkman, J. *Nat. Med.* **2004**, *10*, 225.

[15] Vicent, M. J.; Greco, F.; Nicholson, R. I.; Paul, A.; Griffiths, P. C.; Duncan, R. *Angew. Chem., Int. Ed.* **2005**, *44*, 2.

[16] Duncan, R. *PSTT* **1999**, *2*, 441.

[17] Konak, C.; Matyjaszewski, K.; Kopeckova, P.; Kopecek, J. *Polymer* **2002**, *43*, 3735.

[18] Ayhan, H.; Tuncel, A.; Bor, N.; Piskin, E. *J. Biomater. Sci., Polym. Ed.* **1995**, *7*, 329.

[19] Norde, W.; Lyklema, J. *J. Biomater. Sci., Polym. Ed.* **1991**, *2*, 183.

[20] Schwendener, R. A.; Lagocki, P. A.; Rahman, Y. E. *Biochim. Biophys. Acta* **1984**, *772*, 93.

[21] Krenning, E. P.; Kwekkeboom, D. J.; Valkema, R.; Pauwels, S.; Kvols, L. K.; De Jong, M. *Ann. N. Y. Acad. Sci.* **2004**, *1014*, 234.

[22] Harrington, K. J.; Rowlinson-Busza, G.; Syrigos, K. N.; Uster, P. S.;Abra, R. M.; JSW Stewart, J. S. W. *Br. J. Cancer* **2000**, *83*, 232.

[23] Wunderlich, G.; Grüning, T.; Paulke, B. R.; Lieske, A.; Kotzerke, J. *Nucl. Med. Biol.* **2003**, *31*, 87.

[24] Nahrendorf, M.; Zhang, H.; Hembrador, S.; Panizzi, P.; Sosnovik, D. E.; Aikawa, E.; Libby, P.; Swirski, F. K.; Weissleder, R. *Circulation* **2008**, *117*, 379.

[25] Wolf, G. L. *Targeted Deli*V*ery of Imaging Agents*; CRC Ress: Boca Raton, FL, 1995; Vol. 3.

[26] Stein, P. D. *Curr. Opin. Pulm. Med.* **1999**, *2*, 295.

[27] Rubin, G. D. *J. Thorac. Imaging* **1997**, *12*, 128–149.

[28] Mathias, C. J.; Green, M. A. *Appl. Radiat. Isot.* **2008**, *66*, 1910–1912.

[29] Moad, G.; Rizzardo, E.; Tang, S. H. *Polymer* **2008**, *49*, 1079–1131.

[30] Eberhardt, M.; Mruk, R.; Zentel, R.; Theato, P. *Eur. Polym. J.* **2005**, *41*, 1569.

[31] Eberhardt, M.; Theato, P. *Macromol. Rapid. Commun.* **2005**, *26*, 1488.

[32] Barz, M.; Tarantola, M.; Fischer, K.; Schmidt, M.; Luxenhofer, R.; Janshoff, A.; Theato, P. Zentel, R. *Biomacromolecules* **2008**,

[33] Perrier, S.; Takolpuckdee, P.; Mars, C. A. *Macromolecules* **2005**, *38*, 2033.

[34] Bauman, A.; Piel, M.; Schirrmacher, R.; Ro¨sch, F. *Tetrahedron Lett.* **2003**, *44*, 9165.

[35] Kissel, M.; Peschke, P.; Subr, V.; Ulbrich, K.; Schumacher, J.; Debus, J.; Friedrich, E. *PDA J. Pharm. Sci. Technol.* **2001**, *55*, 191.

2.9. $^{72/74}$As-labeling of HPMA based polymers for long-term *in vivo* PET imaging

Tetrahedron Letters 2009, submitted

Author: Markus Jahn[1, †], Matthias Barz[2, †], Matthias M. Herth[1], Rudolf Zentel[2] and Frank Rösch[1]

Address: [1]Institute of Nuclear Chemistry, University of Mainz, Fritz-Strassmann-Weg 2, D-55128 Mainz, Germany

[2]Institute of Organic Chemistry, University of Mainz, Duesbergweg 10-14, D-55099 Mainz

[†] Both authors contributed equally.

Abstract

Various clinically approved N-(2-hydroxypropyl)-methacrylamide (HPMA) based polymers were radioactive labelled using the positron emitter $^{72/74}$As (^{72}As $t_{1/2}$ = 26h; ^{74}As $t_{1/2}$ = 17.8d). This approach may lead to the possibility to determine non-invasively the long-term *in vivo* fate of these labelled polymers by PET (positron-emission-tomography). Presumably, the label itself will not strongly influence the polymer structure due to the fact that the used nuclide binds to already existing thiol moieties within the polymer structure. No addition charges or bulks groups are introduced.

Labelled homo polymers, random copolymers as well as block copolymers were synthesized by the RAFT polymerization technique. Furthermore, thiol groups can be either derived by the aminolyisation and reduction of the dithiobenzyl ester polymer end groups or by a postpolymerisation modification. However, the latter approach was only carried in random copolymers. Disulfide bonds among the polymer backbone were introduced, which can be reduced to thiol groups afterwards. Arsenic can interact covalently with those thiol groups and form thioesters. Therefore, $^{72/74}$As-labeling resulted in satisfying RCYs (corrected radiochemical yield). Homo and block copolymers were labelled in around 20 % and random copolymer in ~ 80 %. These findings are clearly attributed to the higher amount (20 times) of thiol groups in the random copolymer system. Preliminary *in vitro* studies demonstrated stability of the radioactive label at least in buffer for 48 h. Summing up, a new synthetic method for $^{72/74}$As-labelling of HPMA-based polymers could be developed which possibly allows medium- and long-term in vivo visualisation of nanoparticles by PET.

1. Manuscript

The field of polymer-based therapeutics has seen a tremendously increasing interest during the last decades. [1-7] Under the term nanomedicine various systems have entered a brought range of clinical research. One reason for this is the promising opportunity to combine various functionalities among one particle. Although the ideas sound promising, further research needs to gain detailed knowledge about short- as well as long-term biodistribution to understand and enhance the particle properties. To date, it is already well known that particle properties such as size, charge and surface characteristics determine the *in vivo* fate as well as cellular uptake and intracellular distribution. [8,9] Thus, these properties of nanoparticles offer the possibility to tune the body distribution e.g. in cancer therapy via the enhanced permability and retention effect (EPR-effect; passive targeting) [6,10] or by the

attachment of various selective targeting vectors (active targeting). [4] In addition, encapsulation of drugs, proteins or oligonuclides within these polymeric structures and controlled release afterwards, bear the possibility to reduce the toxicity. This concept leads to first polymer therapeutics in clinical trails. [11-13]

In this respect, FDA (Food and Drug Administration) approved N-(2-hydroxypropyl)-methacrylamide (HPMA) based polymers play an important role in medical *in vivo* applications. [3,11,12] Various functionalities can be introduced either by polymerizing a mixture of monomers leading to copolymers onto which a drug can be conjugated. A new approach is the synthesis of reactive polymer precursors, which can be transferred into functional HPMA based structures by a post-polymerization modification. These polymer analogous reactions are based on the activated ester approach [14-16], which offers two major advantages: On one hand, only homo polymers or block copolymers of comparable polarity need to be synthesized which can be precisely characterized; on the other hand copolymerization parameters can be disregarded.

A detailed knowledge of the *in vivo* biodistribution of these polymeric structures provides insights in pharmacokinetics or metabolism pathways within the target tissue or other organs. Theses results may be helpful to optimize polymers for specific medical applications in therapy or diagnosis.

Thereby, particle-sizes, compositions, physical properties, and surface chemistry of the polymer influence the *in vivo* behavior. [8] To understand and finally to fine-tune these parameters appropriate imaging strategies are needed. Positron emission tomography (PET) is a non-invasive, quantitative, and repetitive whole body molecular imaging techniques to understand the mentioned interactions. Most frequently used radioactive nuclides for *in vivo* imaging are chelated metals, such as ^{64}Cu. [17,18] This strategy may have a major drawback. Typically, the chelating agent itself is rather large, bulky and charged and therefore, it will change the properties of the polymeric particle itself. As a result the polymeric *in vivo* fate will be strongly influenced by the radioactive marker. Consequently its biological behavior differs from the original nanoparticle. Recently, Herth, Barz et al. [19] described a new ^{18}F-labeling strategy via 2-[^{18}F]fluoroethyl-1-tosylate to image the short-term *in vivo* fate avoiding this disadvantage.

Herein, we want to report the $^{72/74}$As-labeling of HPMA based polymeric structures to image non-invasively long-term biological effects *in vivo* such as the passive polymer accumulation in tumor tissue (EPR-effect). For these investigations a timeframe of weeks to month is mandatory. ^{72}As is a pure β^+-emitter with a $t_{1/2}$ = 26h, whereas ^{74}As decays via β^+-emission (29%) and electron capture (66%) with a $t_{1/2}$ = 17.8d.

As(III) can bind to thiol groups covalently. Due to the mechanism of the reversible addition fragmentation chain transfer (RAFT) polymerisation and the used dithiobenzoic ester as a chain tranfer agent every polymeric chain bears one dithiobenzoate (scheme 1). These endgroups can be converted afterwards into thiols by either an aminolysis or reduction. But this reaction leads to the formation of by-products, e. g. disulfides are formed, which have to be reduced to derive free thiols. Thiols display an adequate precursor moiety for the labelling with $^{72/74}$As. [20] Therefore, this labelling approach should not strongly influence the chemical structure of the nanoparticles.

All together, in comparison to the chelated ^{64}Cu, $^{72/74}As$ bear advantages due their half-life and their binding mode. The modification of the polymeric structure itself is reduced to a minimum by the radioactive label.

Scheme 1. Synthesis of HPMA based polymers bearing thiol end groups for radioactive labelling with $^{72/74}As$

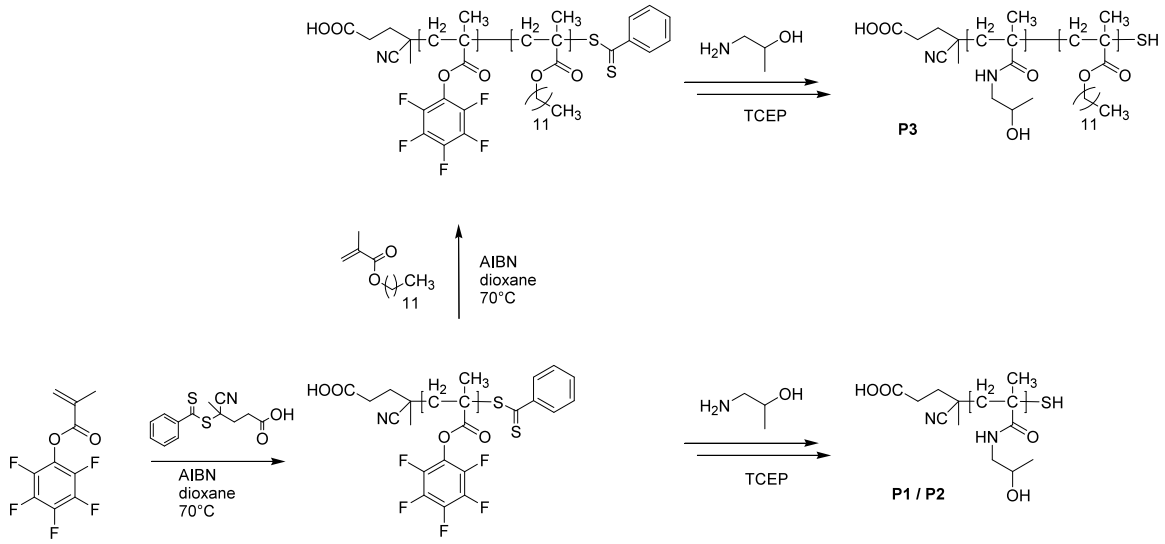

The synthesis of well defined poly(HPMA) homopolymers **P1** and **P2**, poly(HPMA)-block-poly(lauryl methacrylate) block copolymers **P3** and poly(HPMA)-random-poly(Ethylmethyl disulfide acrylamide) **P4** copolymers was performed according to the recently published method of Barz et al.. [21-22]

The synthesized polymers are listed and characterized in table 1.

Table 1. Characteristics of synthesized polymers for labelling with $^{72/74}$As.

polymer	structure	thiol content %[a)]	M_n[a)]	M_w[a)]	PDI[a)]
P1	homo polymer	1.1	12.5	15.7	1.26
P2	homo polymer	0.50	27.1	33.6	1.24
P3	block copolymer	0.48	27.7	32.5	1.26
P4	random copolymer	9.6	27.0	33.5	1.24

[a)] calculated from the degree of polymerization and ^{1}H NMR.

[b)] kg/mol, calculated from the molecular weight of the reactive precursors, which was determined by GPC in THF as solvent

As mentioned above disulfides can be formed during the aminolysis of the dithiobenzoic ester, which have to be reduced to enhance the RCY. Thus, in all polymers were reduced using (tris(2-carboxyethyl)phosphine) (TCEP) yielding polymers bearing free thiol groups, which could be purified from side products of the reduction by SEC and used in the next step for radioactive labeling (figure 1).

$^{72/74}$As were cyclotron produced by (p,n) bombardment of ^{nat}Ge at the (DKFZ) in Heidelberg. The proton beam used had an energy of 15 MeV and a beam currant of up to 30 µA. Thereby, yields of 4 GBq of ^{72}As and 400 MBq of ^{74}As were obtained with a loading of 200 µAh.

The radio-arsenic was separated from bulk amounts of the germanium target material in a multi step separation procedure that is described in detail elsewhere. [23] In a first step the major amount of germanium was separated from the radio-arsenic by distillation of $GeCl_4$ from 10 M HCl at 120 °C while the $^{72/74}$As is not volatile in the oxidation state (V) and stays inside the distillation vessel. In a second step the $^{72/74}$As(V) was purified from remaining traces of germanium by anion exchange chromatography yielding the arsenic in about 500 µL 10 M HCl. Reduction to $^{72/74}$As(III) was carried out by boiling the solution at 60 °C for 1 h after the addition of 10 mg CuCl. The $^{72/74}$As(III) was

extracted into 500 µL CCl_4 followed by back extraction into 500 µL of PBS-buffer at pH 7. This solution was directly used for labeling experiments.

$^{72/74}$As-Labeling of HPMA based polmers (**P1**, **P2** and **P3**) were carried out in H_2O at 70 °C. Thereby, 0.1 mmol (3 mg) of polymer **P2** were solved in 0.5 mL H_2O/DMSO and 10 µmol (3 mg) of TCEP were added to reduce disulfide bonds to the desired thiols. This mixture was allowed to stir for at least 1h before the radioactive nuclides dissolved in 0.5 ml PBS-Buffer were added to the reduced polymers. Radiochemical yields (RCY) were analyzed at different time points via size exclusive chromatography (SEC) (HiTrap Desalting Column, Sephadex G-25 Superfine, column volume 5 mL; flow rate: 0.5 ml 0.9 % NaCl-solution). Figure 2 shows exemplarily an elution profile of the SEC. RCY`s of ~ 20% could be obtained, whereas figure 3 shows the time dependency of the reaction.

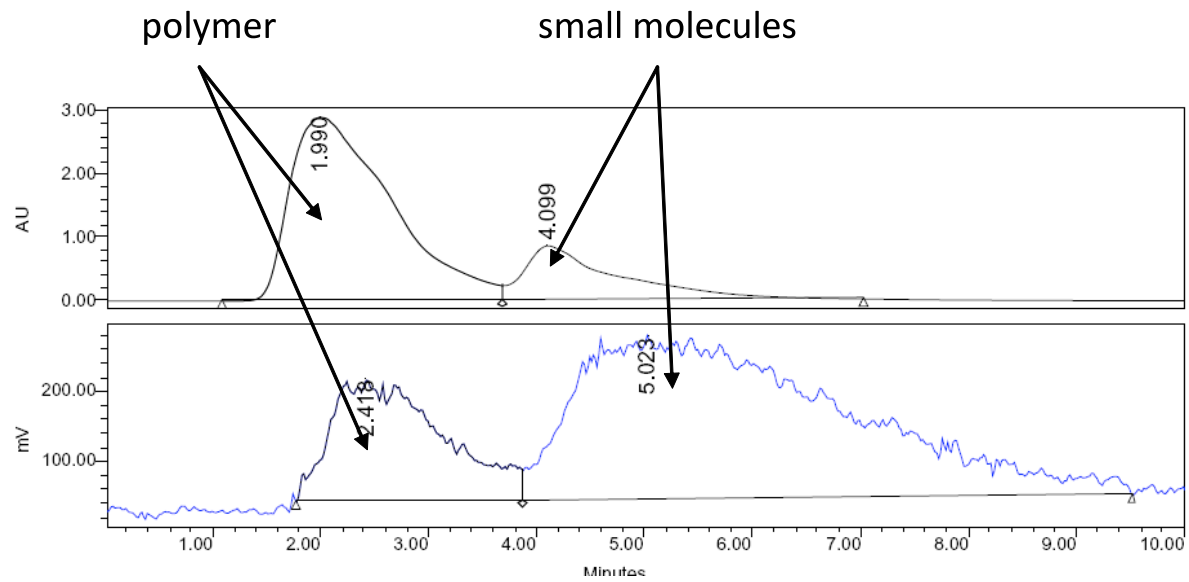

Figure 1. Exemplarily elution profile of the SEC; Channel 1: UV absorption, channel 2: radioactivity detection

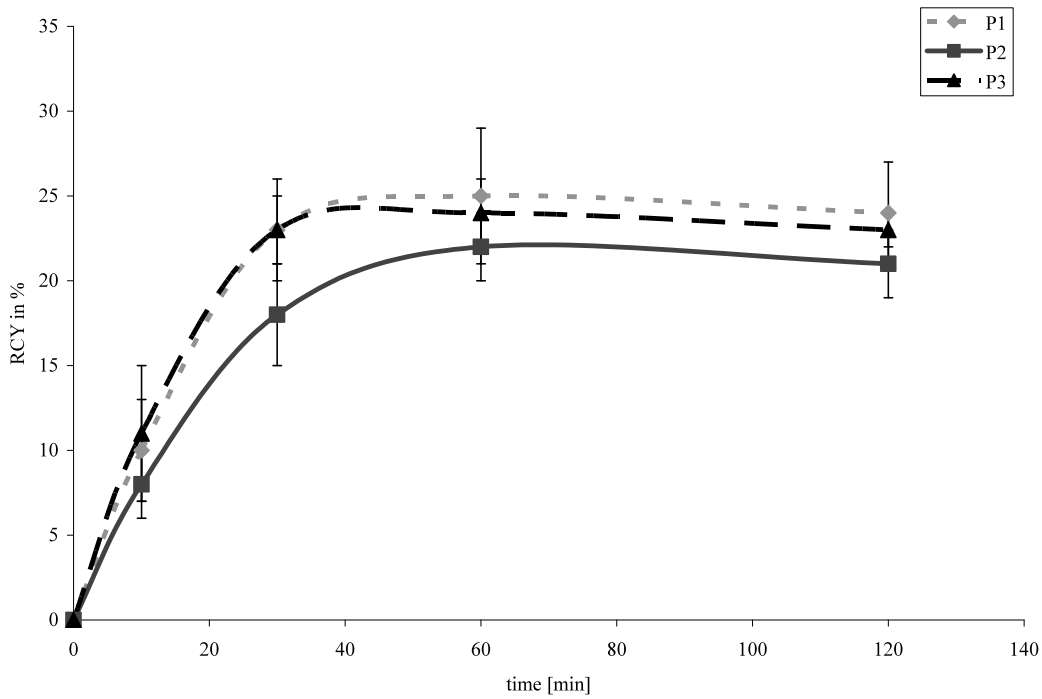

Figure 2. Time dependency of the RCY`s of **P1**, **P2** and **P3** (n =3)

In addition, we also synthesised one polymer (**P4**) bearing a higher number of disulfide side chains, which can be reduced by TCEP resulting in thiol units. A higher number of precursor groups is thereby accessible and should in principle lead to higher RCY`s (figure 2).

Scheme 2. Synthesis of HPMA based polymers with an increased content of free thiol groups among the polymer backbone for radioactive labelling with $^{72/74}$As.

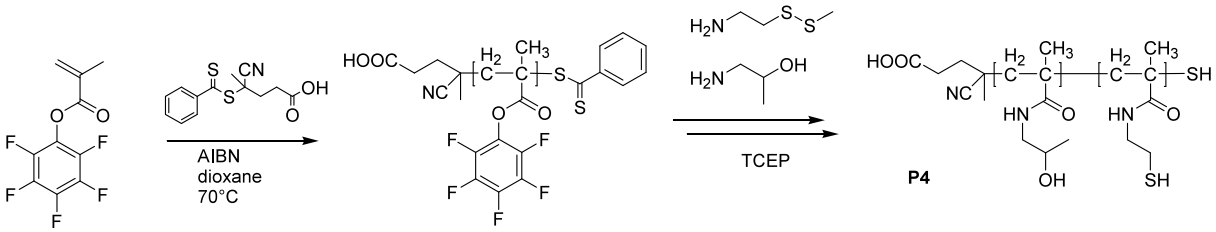

The labelling procedure for **P4** was slightly modified. In a first step 3 mg (0.1 mmol) **P4** was dissolved in 500 µL 0.9 % NaCl-solution and incubated for at least 1 h with 3 mg (10 µmol) TCEP at room temperature. In this time the disulfide bonds were cleaved and mercaptomethane was formed. As the arsenic reacts with all kind of thiol-groups the mercaptomethane was removed before the labelling procedure by SEC (HiTrap Desalting Column, Sephadex G-25 Superfine, column volume 5 mL; flow rate: 0.5 ml 0.9 % NaCl-solution). The purified **P4** in was obtained in 1 mL of 0.9 % NaCl-solution and added directly to the $^{72/74}$As(III) in 500 µL PBS-buffer. To prevent the thiols from reoxidation 10 µL TCEP (410 nmol) was added to the solution. The incubation was carried out at 30 °C and the yield was monitored at various time points via SEC. Figure 3 demonstrates the high RCY`s of ~ 90% in 150 min.

a)

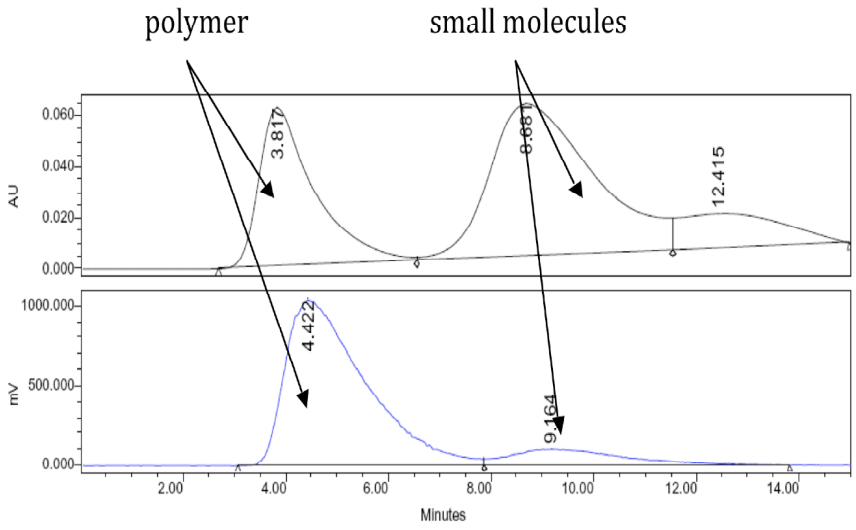

b)

time [min]	RCY of P4 [%]
0	0
10	22 ± 3
30	68 ± 6
60	75 ± 7
120	82 ± 8

Figure 3. ^{72}As-Labeling of 0,1 mmol **P4** at 30 °C using H_2O as a solvent (n =4)

a) Exemplarily elution profile of the SEC; Channel 1: UV absorption, channel 2: radioactivity detection b) Time dependency of the RCY of P4

In addition, we tested the stability of the labelled polymer in water. For this purpose the water stored polymers were reinjected into a SEC column (HiTrap Desalting Column, Sephadex G-25 Superfine,

column volume 5 mL; flow rate: 0.5 mL 0.9 % NaCl-solution) and checked for impurities. Even 48h after initial purification no decomposition occurred.

In conclusion, $^{72/74}$As-labeling of HPMA based polymers was carried out in rather high RCY`s. In combination with a stability of at least 48h in 0.9 % NaCl-solution this will presumably lead to the possibility to perform *in vivo* long-term μPET studies without strongly influencing the polymer structure. Therefore, this approach may lead to a detailed understanding in which way alterations in physical properties of the nanostructures such as size, surface chemistry or core material will influence the fate of nanoparticles in living systems. Detailed studies regarding the in vivo stability as well as initial *in vivo* experiments are warranted and currently under investigation.

2. Acknowledgments

The authors wish to thank H. Hauser and Prof. Dr. M. Eisenhut for the production of $^{72/74}$As at the DKFZ in Heidelberg. We also want to thank Prof. Dr. H. Ringsdorf for excellent and fruitful discussion. Financial support by Friedrich-Naumann-Stiftung, the European Network of Excellence (EMIL), and Polymat Graduate School of Excellence is gratefully acknowledged.

3. References

[1] Ferrari M. Cancer nanotechnology: opportunities and challenges. Nat Rev Cancer 2005;5:161-71.

[2] Ringsdorf H. Structure and properties of pharmacologically active polymers. J Polymer Sci Polym Symp 1975;51:135-53.

[3] Duncan R. Polymer conjugates as anticancer nanomedicines. Nat Rev Cancer 2006;6:688-701.

[4] Haag R, Kratz F. Polymer Therapeutics: Concepts and Applications Angew Chem Int Ed 2006;45:1198-215.

[5] Duncan R. Polymer conjugates for tumor targeting and intracytoplasmic delivery. The EPR effect as a commom gateway? Pharm Sci Technol Today 1999;2:441-9.

[6] Matsumura Y, Maeda H. A new concept for macromolecular therapeutics in cancer chemotherapy: mechanism of tumoritropic accumulation of proteins and the antitumor agent SMANCS. Cancer Res 1986;46:6387-92.

[7] Duncan R. The dawning era of polymer therapeutics. Nat. Rev. Drug Discovery 2003;2:347-60.

[8] Gratton SEA, Ropp PA, Pohlhaus PD, Luft JC, Madden VJ, Napier ME et al. The effect of particle design on cellular internalization pathways. Proc Natl Acad Sci USA 2008;105:11613-8.

[9] Barz M, Luxenhofer R, Zentel R, Kabanov AV. The uptake of hydroxypropyl methacrylamide based homo, random and block copolymers by human multi-drug resistant breast adenocarcinoma cells. Biomaterials 2009; :

[10] Maeda H, Wu J, Sawa Y, Matsumura Y, Hori K. Tumor vascular permeability and the EPR effect in macromolecular therapeutics: a review. J. Controlled Release 2000;65:271-84.

[11] PA, Kaye SB, Morrison R, Twelves C, Wilson P, Duncan R, Thomson AH, Murray LS, Hilditch TE, Murray T, Burtles S, Fraier D, Frigerio E, Cassidy J and on behalf of the Cancer Research Campaign Phase I/II Committee. Phase I clinical and pharmacokinetic study of PK1 [N-(2-hydroxypropyl)metharylamide copolymer Doxorubicin]: first member of a new class of chemotherapeutic agents-drug-polymer conjugates, Cancer Research Campaign I/II Committee. Clin. Cancer Res. 1999;5(1):83-94

[12] Hopewell JW, Duncan R, Wilding D, Chakrabarti K. Preclinical evaluation of the cardiotoxicity of PK2: A novel HPMA copolymer–doxorubicin–galactosamine conjugate antitumour agent. Hum. Exp. Toxicol. 2001;20(9):461-470

[13] Matsumura Y, Kataoka K, Preclinical and clinical studies of anticancer agent-incorporating polymer micelles. Cancer Sci. 2009;100(4):572-579

[14] Batz HG, Franzmann G, Ringsdorf H. Model Reactions for Synthesis of Pharmacologically Active Polymers by Way of Monomeric and Polymeric Reactive Esters. Angew Chem Int Ed 1972;11:1103-04.

[15] Theato P. Synthesis of well-defined polymeric activated esters. Journal of Polymer Science Part A: Polymer Chemistry 2008;46(20):6677-6687

[16] Gauthier MA, Gibson MI, Klok H-A. Synthesis of Functional Polymers by Post-Polymerization Modification. Angew. Chem. Int. Ed. 2009;48:48–58

[17] Rossin R, Muro S, Welch MJ, Muzykantov VR, Schuster DP. In Vivo Imaging of ^{64}Cu-Labeled Polymer Nanoparticles Targeted to the Lung Endothelium, J. NUC. MED. 2008;49(1):103-111

[18] Nahrendorf M, Zhang H, Hembrador S, Panizzi P, Sosnovik DE, Aikawa E, Libby P, Swirski FK, Weissleder R. Nanoparticle PET-CT Imaging of Macrophages in Inflammatory Atherosclerosis. Circulation 2008;117:379-387

[19] Herth M, Barz M, Moderegger D, Allmeroth M, Jahn M, Thews O, et al. Radioactive labeling of defined HPMA-based polymeric structures using [18F]FETos for in vivo imaging by positron emission tomography. Biomacromolecules 2009;10,1697–1703

[20] Jennewein, M., et al., Vascular Imaging of Solid Tumors in Rats with a Radioactive

Arsenic-Labeled Antibody that Binds Exposed Phosphatidylserine. Clin Cancer Res,

2008. 14(5): p. 1377-85.

[21] Barz M, Tarantola M, Fischer K, Schmidt M, Luxenhofer R, Janshoff A et al. From Defined Reactive Diblock Copolymers to Functional HPMA-Based Self-Assembled Nanoaggregates. Biomacromolecules 2008;9:3114-18.

[22] Barz M, Canal F, Koynov K, Zentel R, Vicent MJ. Synthesis and in vitro evaluation of defined HPMA folate conjugates: Influence of aggregation on folate receptor (FR) mediated cellular uptake. Submitted.

[23] Jahn M, Radchenko V, Filosofov D, Hauser H, Eisenhut M, Rösch F, Jennewein M

Separation and purification of no carrier added arsenic from bulk amounts of

germanium being adequate to radiopharmaceutical labeling chemistry Radiochimica Acta – Submitted for publication

[24] The homo and blockcopolymers were synthesized according to [9].

[25] Synthese of homopolymer precursors(1). The RAFT polymerizations of the PFMA using 4-cyano-4-((thiobenzoyl) sulfanyl) pentanoic acid were performed in a schlenk tube. The reaction vessel was loaded with 2,2'-azobis(isobutyronitrile (AIBN), 4-cyano-4-((thiobenzoyl)-sulfanyl)pentanoic acid (CTA) (molar ratio of AIBN/CTA = 1:8) and 15 g of PFMA in 20 mL of dioxane. Following three freeze–vaccum–thaw cycles, the tube was immersed in an oil bath at 70 °C. Afterwards the polymer poly(PFMA) was 3 times precipitated into hexane, isolated by centrifugation and dried for 12 hours at 30 °C under vacuum. In the end a slightly red powder was obtained. Yield: (59 %). ^{1}H NMR ($CDCl_3$): 1.6-2.2 (br), 0.9-1.5 (br) δ [ppm] ^{19}F NMR ($CDCl_3$): δ [ppm] -165.0 (br), -159.7 (br), -154.4 (br), -153.1 (br).

[26] General synthesis of block copolymer precursors(2). The macro CTA obtained in the above-mentioned polymerization was dissolved in dioxane and AIBN was added. Nitrogen was bubbled through the solution and three freeze-vacuum-thaw cycles were applied. Afterwards the tube was immersed in an oil bath at 70 °C. After polymerization time of 12 h, the solution was slightly concentrated and precipitated twice in ethanol and diethyl ether, removed by centrifugation, and

dried overnight at 30 °C in vacuum. A slightly red powder was obtained. Yield: (89 %). ^{1}H NMR ($CDCl_3$): δ [ppm] 1.6-2.2 (br), 0.9-1.5 (br), 0.8-0.9 (br t) ^{19}F NMR ($CDCl_3$): δ [ppm] -165.2 (br), -159.8 (br), -154.4 (br), -153.1 (br).

[27] Postpolymerization modification of homo polymers(3). In a typical reaction 300 mg of PPFMA were dissolved in 4 mL abs. dioxane and 1 mL abs. DMSO. A slightly reddish solution was obtained. In a typical reaction for the 50000 g/mol precursor and 200 mg of 2-hydroxypropylamine and 200 mg triethylamine were added. The reaction was allowed to proceed at 50 °C over night. The solution was concentrated in vacuum and introduced to a column filtration using SephadexTM LH-20 in dioxane and precipitated in diethyl ether, removed by centrifugation and dried in vacuum at 30 °C for 14 hours. Yield: (86 %). 1H NMR (DMSO-d_6): δ [ppm] 3.4-3.9 (br), 2.6-3.0, 0.9-1.5 (br)

[28] Postpolymerization modification of block copolymers(4). In a typical reaction 300 mg of poly(PFMA)-block-poly(lauryl methacrylate) were dissolved in 4 mL abs. dioxane and 1 mL abs. DMSO. A slightly reddish solution was obtained. In a typical reaction 200 mg of 2-hydroxypropylamine and 200 mg triethylamine were added. The reaction was allowed to go on at 50 °C over night. The solution was concentrated in vacuum and introduced to a column filtration using SephadexTM LH-20 in dioxane/DMSO (4:1) and precipitated in diethyl ether, removed by centrifugation and dried in vacuum at 30 °C for 14 hours. Yield: (81%). 1H NMR (DMSO-d_6): δ [ppm] 3.4-3.9 (br), 2.6-3.0 (br), 0.9-1.5 (br), 0.8-0.9 (br t)

[29] Synthesis of random copolymers by postpolymerization modification(5). In a typical reaction 300 mg of PPFMA were dissolved in 3.5 mL abs. dioxane and 1 mL abs. DMSO. A slightly reddish solution was obtained. In a typical reaction for the 50000 g/mol precursor 15 mg methyldisulfanyl cysteamin in 0.5 mL abs. dioxane and 50 mg triethylamine were added. The reaction was allowed to go on for 4 h at 50 °C. Afterwards 300 mg of 2-hydroxypropylamine and 300 mg triethylamine were added. The reaction was allowed to proceed at 50 °C over night. The solution was concentrated in vacuum and introduced to a column filtration using SephadexTM LH-20 in dioxane and precipitated in diethyl ether, removed by centrifugation and dried in vacuum at 30 °C for 14 hours. Yield: (86 %). 1H NMR (DMSO-d_6): δ [ppm] 3.4-3.9 (br), 2.6-3.0, 2.4 (br), 0.9-1.5 (br)

3. Conclusion

In this work new types of biocompatible polymers have been developed by combination of the activated ester approach with modern controlled radical polymerization techniques. Various reactive polymeric architectures have been synthesized and transferred into HPMA-based structures by the aminolysis of the activated ester. Besides PEG, HPMA is one of the most carefully investigated polymeric materials for drug delivery applications. The polymer is known to be non-immunogenic and has very little interactions with intra- as well as extra- cellular macromolecules. The polymer architectures differ in their individual properties, e.g. size, polarity and structure. It was found that these differences in microstructure greatly influence the superstructure formation of amphiphilic random or block copolymers. In addition, these polymers have been functionalized with folic acid, which is known to be a ligand for the tumor-associated antigen the folate receptor (FR). Those conjugates showed enhanced cellular uptake in FR positive cell lines underlining the potential of the synthetic approach.

Besides synthetic approaches, it could be demonstrated impressively that specific or non-specific cellular uptake and intracellular fate of polymeric particles is determined by the formed superstructures in first order and just in second by the single polymer itself. In this respect, the structural changes induced by a targeting moiety have to be considered and investigated carefully, because they will influence the aggregation process and therefore the particle structure directly. These findings clearly point out the need for highly defined polymeric carriers and excipients for future applications in the field of nanomedicine.

The structure-property relationships described on the cellular level will most likely determine the *in vivo* biodistribution of polymers. But in order to investigate these effects standard fluorescence labeling is rather insufficient or at least limited to certain small animal models. Thus, the development of new labeling strategies for precise, fast and non-invasive imaging is of great importance. Therefore the established labeling strategies will offer an ideal tool for short and long term PET imaging.

With a high probability, the combination of all derived approaches will lead to a better understanding of structure-property relationships on cellular as well as on an in vivo level. Furthermore the established synthetic platform may be a useful tool for the development of more efficient nanomedical devices.

4. Outlook

Nanomedicine in general or polymer therapeutics as a special subunit seek to deliver a valuable set of tools for biomedical application, which can be transferred into clinical practice in the close future. Therefore polymer-based devices have to fulfill various requirements. The highest importance has to be their medical activity, meaning they have to monitor or treat diseases to improve health-related quality of life.

Consequently, every newly synthesized polymer therapeutic should be applicable to certain medical issues or should at least be based on biological rational. The author is well aware of the results presented in this work being far away from clinical application, but in this brief outlook some promising field of medical application will be named.

As described, one possible application is definitely the use of radioactive polymers for tumor imaging applications. In first experiments the EPR effect could be used to visualize tumor tissues in a rat model. For imaging applications it would be rather useful to have highly selective markers. Consequently, polymeric systems can be used to combine passive as well as active targeting and a radioactive label among a polymer. So most likely the described folate conjugates can be used as a imaging agent for FR positive tumors. Besides ^{18}F labeling there is need for nuclides with a shorter half-life, as in clinical practice a fast decay of radioactivity is beneficial to reduce the expenditure of time for each imaging process. For a fast selective imaging the EPR effect itself is inefficient, because the related passive accumulation is slow (hours to days). But on the other hand radionuclides with a longer half-life time can offer wonderful insides into long-term pharmacokinetics. If the radioactive label is stable under *in vivo* conditions, the first non-invasive long-term biodistribution of polymeric carriers can be performed, which would tremendously ease the development and approval of new polymer therapeutics.

A second group of applications can be summarized by the well-known term drug delivery. The synthesized systems offer great possibilities to either encapsulate a pharmacological active substance or even covalently conjugate it. As well a wide field of applications is opened up, since many drugs are hardly soluble or degrade in extracellular compartments. In this case even simple encapsulation can be beneficial. If the drug itself is harmful and a local application is desired conjugation is more suitable due to the higher stability of drug attachment. Another interesting field is the influence of polymers on the P-glycoprotein (Pgp), which is extensively distributed and expressed in intestinal epithelium, hepatocytes, renal proximal tubular cells, adrenal gland and capillary endothelial cells comprising the blood-brain and blood-testis barrier. This protein is a member of the MDR/TAP subfamily being involved in multidrug resistance, which aggravate the treatment of tumor cells or the drug delivery across the blood-brain-barrier. Some substances are not harmful to the body and

additionally they would be interesting antipsychotic drugs. However, they are substrates for Pgp and consequently cannot cross the blood-brain barrier. This has already been demonstrated by Kabanov and coworkers, as the ATP-dependent efflux pump can be enabled and drug delivery over the blood-brain-barrier can be achieved by the use of polymeric carriers (Pluronics). These results encourage the development of polymers for the delivery of antipsychotic drugs.

However, the combination of encapsulation with conjugation is of greatest potential for the introduced functional block copolymers is. If the hydrophobic block is exchanged with a positively or negatively charged block oligo-nucleotides or enzymes can be efficiently encapsulated and transported to the individual side of action. This strategy opens promising research areas. For example, it enables the use of polymers in tumor vaccination by stimulating dentritic cells. In this idea, an oligo-nucleotide has to be encapsulated by the cationic block, while the hydrophilic HPMA block bears the immunoadjuvant, a marker and a targeting moiety (antibody) underlining the importance of multifunctional polymeric systems. As for another idea the delivery of proteins (apoptosis proteins) would open new ways in cancer treatment, which may further reduce side effects.

Summering up these ideas may obviously sound more than promising, although it the journey to create the polymeric systems for each individual application is surely long. Predictably many systems will fail. But nevertheless the activated ester approach will be beneficial for the development of polymeric systems, because it will open up an easy access to polymer libraries, which are mandatory for an efficient screening and improvement of carrier properties.

Generally polymer based nanomedicin is a promising tool for medical application. Although the development will be demanding, the benefits will be groundbreaking. Hopefully some decades later polymer therapeutics will become a standard tool in clinical use and improve each single patient`s quality of life.